NUREG-1179
Vol. 2

Rupture of Model 48Y UF_6 Cylinder and Release of Uranium Hexafluoride

Cylinder Overfill, March 12-13, 1986
Investigation of a Failed UF_6 Shipping Container

U.S. Nuclear Regulatory Commission

NUREG-1179
Vol. 2

Rupture of Model 48Y UF_6 Cylinder and Release of Uranium Hexafluoride

Cylinder Overfill, March 12-13, 1986
Investigation of a Failed UF_6 Shipping Container

Manuscript Completed: May 1986
Date Published: June 1986

Augmented Investigation Team

U.S. Nuclear Regulatory Commission
Uranium Recovery Field Office
Region IV
Denver, CO 80225

ABSTRACT

NUREG-1179, Volume 1, reported on the rupture of a Model 48Y uranium hexafluoride (UF_6) cylinder and the subsequent release of UF_6. At the time of publication, a detailed metallurgical examination of the damaged cylinder was under way and results were not available.

Subsequent to the publication of Volume 1, a second incident occurred at the Sequoyah Fuels Corporation facility. On March 13, 1986, a Model 48X cylinder was overfilled during a special one-time draining procedure; however, no release of UF_6 occurred. An Augmented Investigation Team investigated this second incident.

This report, NUREG-1179, Volume 2, presents the findings made by the Augmented Investigation Team of the March 13 incident and the report of the detailed metallurgical examination conducted by Battelle Columbus Division of the cylinder damaged on January 4, 1986.

TABLE OF CONTENTS

APPENDICES

PREFACE

The U.S. Nuclear Regulatory Commission Augmented Investigation Team, which conducted the investigation of the March 13, 1986, incident at the Sequoyah Fuels Corporation facility, consisted of the following members:

R. Dale Smith, Leader
Charles L. Cain
Justin T. Long
Gary F. Sanborn

1 INTRODUCTION

1.1 Background of Events

On January 4, 1986, a filled Model 48Y uranium hexafluoride (UF_6) cylinder ruptured while it was being heated at the Sequoyah Fuels Corporation (the licensee) conversion facility near Gore, Oklahoma. The accident sequence and resulting analysis are described in Volume 1 of NUREG-1179. This report, Volume 2 of NUREG-1179, describes events that occurred on March 12-13, 1986, as the licensee drained UF_6 from process cold traps to shipping cylinders.

1.1.1 Cylinder Overfill

On March 12, 1986, the Sequoyah Fuels Corporation began draining UF_6 from process cold traps to shipping cylinders. This operation was necessary to enable modification of facilities and equipment at the plant, which had been shut down since January 4, 1986. A secondary objective was to attempt to determine, by inventory accountability, the amount of UF_6 in the cylinder that had ruptured on January 4, 1986. (NUREG-1179, Volume 1, presented engineering estimates of the probable amount, but actual data were not yet available.)

During the course of the draindown process on March 13, 1986, a Model 48X cylinder was filled with 26,017 pounds of UF_6, an amount that was 4,987 pounds more than the cylinder's maximum shipping weight specification of 21,030 pounds. This weight exceeded the maximum amount of liquid UF_6 capacity for the cylinder, indicating that some solidification had occurred during the filling process. The draindown process was to have been conducted in accordance with special licensee procedures (Appendix A), which further limited each cylinder to be filled with no more than 20,000 pounds of UF_6.

The causes of the overfill were identified as (1) a malfunctioning scale, (2) failure to include procedures to test the functioning of the scale, and (3) failure to recognize indications of malfunction.

The licensee's procedure prohibited the cylinders from being heated in the steam chests. Because this procedure was followed, the cylinder did not rupture and no material was released. Most of the excess material was evacuated back to the process equipment before the temperature and vacuum equilibrated with the vapor pressure of the material, causing flow to cease. The cylinder is in storage pending future plans for removing the excess UF_6 (172 pounds above the maximum shipping weight specification, and 1,202 pounds over the limit set by the one-time procedures). Reviews by the licensee and NRC concluded that storage of the overfilled cylinder poses no significantly greater risk than storage of properly filled cylinders.

1.1.2 Investigation of a Failed UF_6 Shipping Container

At the time of publication of Volume 1, a detailed metallurgical examination of the damaged cylinder was under way and results were not yet available.

Battelle Columbus Laboratory conducted an investigation of the failed UF_6 shipping container to determine the cause of failure. The investigation consisted of (1) an onsite inspection of the failed vessel, (2) laboratory evaluations of appropriate sections removed from the failed container, and (3) stress analyses to estimate the pressures required to cause failure.

The investigation revealed (Appendix B) that the failure initiated in the region of the valve end stiffener ring. It appears that cracking of the butt weld in that stiffener ring occurred first. Cracking in the vessel wall appeared to be an extension of the stiffener ring crack. Upon rupture, the cracks propagated axially in a shear mode. Stress analyses indicated that the crack in the vessel shell may have initiated at an internal pressure of 1250 psig and that final rupture occurred at an internal pressure of approximately 1800 psig. There was no indication that the failure was related to material deficiencies.

1.2 Investigation of Cylinder Overfill

An Augmented Investigation Team (AIT) was assembled to review the activities relating to the draindown of the cold traps and the resultant overfilling of a Model 48X cylinder that occurred on March 12-13, 1986. The team consisted of the team leader and one investigator from the AIT who had investigated the January 4, 1986, incident, and was supplemented by representatives from Region IV and the Office of Nuclear Material Safety and Safeguards. The investigation was conducted in accordance with the draft "Procedure for AIT Response to Operational Events." Accordingly, the objectives of the investigation were to

- conduct an onsite fact-finding investigation of the March 13, 1986, incident
- identify and communicate any generic and specific safety concerns related to this event
- document the findings and conclusions of the onsite investigation

Furthermore, the scope of this investigation did not include

- an examination of proposed licensee actions to correct the cause of the event
- licensee actions taken or planned to be taken before resumption (or continuation) of draindown operations
- NRC staff review of the licensee's one-time special procedures for draindown.

2 CONDUCT OF THE ONSITE INVESTIGATION

2.1 Personal Interviews

On March 16-17, 1986, members of the AIT conducted personal interviews with Sequoyah Fuels Corporation employees who had firsthand knowledge of the events leading up to, during, and immediately following the incident that occurred on March 12-13. The team also interviewed an employee from the McElhaney Scale Company (Fort Smith, Arkansas) who had serviced the scales on the day after the incident. Seventeen persons were interviewed during this period. All of the interviews were recorded by a certified shorthand reporter, and transcripts were prepared.

The transcripts of these interviews are not presented separately; instead, they form much of the basis for the observations and descriptions contained in the investigation team's report.

2.2 Examination of Scale

On March 17, 1986, the team members examined the scale that had malfunctioned. The team was accompanied by the scale service technician who demonstrated the condition of the scale before and after he had serviced them on March 14, 1986.

3 FACTS SURROUNDING THE INCIDENT

3.1 Background Information

Further background information regarding facility description, management organization, and process description may be found in Section 3 of Volume 1 of NUREG-1179.

3.2 Recent History of Scale Use and Service

Section 2.3 of Volume 1 of NUREG-1179 describes the tests that were performed on the two drain station scales and the final product scale on January 28-29, 1986. These tests were observed by a representative of the National Bureau of Standards (NBS), and the scales were found to perform within expected tolerances. Because no mechanical abnormalities were observed at the south drain station scale, comprehensive testing was not performed on the matching north drain station scale. However, test weights were applied to this scale on January 29, and the scale was found to register accurately after approximately 25,000 pounds were applied.

The testing was performed before any decontamination of the scales occurred to ensure that the decontamination would not disturb in any way the condition of the scales that existed at the time of the accident on January 4, 1986. The scales were then released for decontamination, which was completed on January 31, 1986. The scales were not retested or recalibrated after decontamination.

All three scales had been previously checked and serviced by McElhaney Scale Company on September 17, 1985, and earlier on March 6, 1985. The invoice for the March 1985 service call recorded that one of the scales was found to be sticking and to have a minor weighing error that was corrected by the technician. This is consistent with earlier accounts by employees that the north scale had been sticking and had been repaired. The September 1985 invoice noted only that the scales were calibrated and serviced where necessary. Both invoices advised a regular service inspection every 90 days. Records show that the scales were routinely serviced three times a year over the past 7 years.

After the scale malfunctioned during the filling of the cylinder on March 12-13, 1986, a scale technician was summoned to the site to examine the north drain station scale on the morning of March 14. The invoice for this service stated that the main lever to the nose iron had been moved out of place. This caused the pivot, which is mounted on the lever, to be out of the bearing block, which is supported in the bottom of the scale pit (see Figure 3.1). The invoice further stated that the lever had been realigned, the scale calibration had been checked, and the scale was found to be in good working order.

The AIT interviewed the scale technician during the morning of March 17, 1986, and the technician accompanied the team members to the north drain station scale. The floor grating was removed to gain access to the scale pit midway between the catwalk located near the fill header and the scale platform. The

technician then demonstrated the condition in which he had found the scale on the previous Friday when he entered the scale pit. He then dislodged the lever to demonstrate how it could have been done and replaced it to its normal position. A member of the AIT then entered the pit and repeated these actions. The scale technician rechecked the positioning of the lever. The dislodgement of the lever was noted to take minimal effort. Thus, the lever could have been unnoticeably and unintentionally jarred out of position by decontamination workers working in the pit.

The AIT interviewed employees who had decontaminated the scale on January 31, 1986, to determine if anyone recalled stepping on or otherwise coming in contact with the lever. Although several employees recalled entering the pit to clean it out, none were able to recall whether the lever had been touched during the work. These employees also indicated that this was the only occasion since the January accident that they had observed the grating removed from above the scale pit and, thus, the only task likely to have caused the lever dislodgement. The day shift health physics technician also acknowledged that he had not been aware of any other work involving removal of the scale grating.

AIT interviews of plant employees who had participated in the filling of the cylinder disclosed that some operators had observed that the scale tare poise was in an unusual position during the filling. One employee had notified his supervisor of this condition and was told by the supervisor that the change in scale operation was likely caused by the recent calibration performed on the scale. (An erroneous assumption; no actual calibration of the north scale had occurred.)

3.3 Draindown Procedure Development and Review

After the January 4, 1986, accident, Sequoyah Fuels Corporation wanted to completely empty (drain) the UF_6 remaining in the cold traps to enable modification of facilities and equipment at the plant and to attempt to determine, by inventory accountability, the amount of UF_6 in the cylinder that ruptured during the accident. For this purpose, the licensee had drafted a procedure, "Special One-Time Instructions for Draining Cold Traps," to be followed during the operation (Appendix A).

The procedure was prepared jointly by four managers at Sequoyah Fuels Corporation, none of whom was assigned ultimate responsibility for the task. Final review and approval of the procedure was performed by the plant manager. One of the four managers had recommended that, for convenience and to limit activity in the area, the filling of the cylinders be performed only on the south drain station scales. This recommendation had been rejected by the team preparing the procedures in favor of the greater operating flexibility provided by using both drain stations.

An initial draft of the procedure was sent for approval to NRC's Region IV office (letter from S. D. Emerson, Sequoyah Fuels Corp., to R. D. Martin, NRC, dated February 13, 1986), and NRC responded with recommendations in a memorandum dated February 28, 1986 (memorandum from R. D. Martin, NRC, to S. D. Emerson, Sequoyah Fuels Corp.). The revised procedure was transmitted to Region IV on March 5, 1986 (letter from W. L. Utnage, Sequoyah Fuels Corp., to R. D. Martin, NRC), and the NRC responded with a memorandum dated March 10,

1986 (memorandum from R. D. Martin, NRC, to S. D. Emerson, Sequoyah Fuels Corp.), stating that the revised procedure was approved and that the licensee could proceed with the cold trap draining.

Neither the initial nor final drafts of the procedure contained requirements for testing the scales before beginning the draining operation. The licensee routinely uses two special cylinders of certified weight to test the response of the final product scale, (see Procedure N-280-1, Appendix D, NUREG-1179, Volume 1) but these had not been used in conjunction with either of the drain station scales. The cylinders have been previously certified off site and weigh 4,503 and 25,509 pounds, respectively. The accuracy of these weights was confirmed during the January 28-29, 1986, tests. If these cylinders had been used to test the drain scales before their use, the inaccuracy of the north scale would have been identified.

The NBS report prepared for the scale testing performed at the site during January 1986 (NUREG-1179, Volume 1, Appendix A) recommended that the test cylinders be used after a scale had been serviced. This recommendation was not made by NRC during its review of the licensee's draindown procedures, since the scales were not serviced after the tests performed during January. In its memorandum dated February 28, 1986, NRC recommended that the licensee clearly identify in the procedure that no cylinder was to be heated in the steam chests. The procedure also included a requirement that the filled cylinders undergo weighing on the final product scale before being stored.

3.4 Training of Employees in Regard to the Draindown Procedure

The licensee implemented training for the specific procedures that were to be used for draining the cold traps on Tuesday, March 11, 1986, one day before the draining operation was to begin. According to information gained from interviews of the employees who were involved, the two shift supervisors and four chemical operators who had been selected to perform the draining of the cold traps met in the control room and reviewed in detail not only the one-time draindown procedure but also each of the standard operating procedures referenced in the special procedure. Following this discussion, which took about 3 hours, they went into the process plant to walk through the procedures and check equipment at their respective work stations. Testing of the scales at the drain stations was not discussed during the training session.

The licensee had designed and begun implementing a retraining program that included both orientation and job-related training for all shift supervisors and chemical operators. Among the individuals assigned to the draining operation, only the chemical operators had officially entered this program before the beginning of the cold trap draining. These employees were in the initial stages of the orientation phase of the program when they were withdrawn from training to participate in the draindown operation. The retraining program would not have addressed the special draindown procedures. Therefore, temporary withdrawal of the operators from the program appears to have had no effect on the conduct of the special draindown operations.

3.5 Sequence of Events for the First Day of Draining

The draindown operation began at 6:00 a.m. on Wednesday, March 12. The first shift crew, consisting of a supervisor and two chemical operators, was to work until 2:00 p.m. A similar second shift crew was to arrive at 11:00 a.m. and work until 7:00 p.m. Thus, the two shifts were to overlap by 3 hours.

A simplified flow diagram illustrating the draindown equipment is shown in Figure 3.2.

Cylinder No. 1033 was moved to the north drain station and cylinder No. 637 was placed in the south drain station. Both cylinders had passed quality inspections performed on March 10 separately by a design engineer and an area supervisor. The cylinders were again inspected by the shift supervisor on the morning of March 12. After the cylinders were placed on the scales, the tare poise on each scale was set to cancel exactly the tare weight of each cylinder and its associated cart. It was at this time that one of the operators who noticed the abnormal position of the tare poise informed his supervisor that the north scale tare poise required positioning at a point different from what he was accustomed to encountering. The supervisor stated that he believed that this resulted from the testing and calibration of the scales that had occurred in January. He instructed the operator to continue with the draining procedures.

Tempering (heating to approximately 75°F) of two cold traps began at 6:00 a.m. These traps were identified in the shift log book as #1P (primary trap No. 1) and #1S (secondary trap No. 1). Traps #2P, #4P, #6C (cleanup reactor trap No. 6), and #3S were placed on line with the fluorination towers and were refrigerated to provide vacuum and backup capacity for the contents of the heated cold traps. Traps #1P and #1S were switched to the heat cycle (to allow heating to about 210°F in order to liquify the UF_6) at approximately 7:00 a.m. The #5C trap was switched to temper cycle at 8:45 a.m. The licensee reported that heating of the traps was normal and system pressures were within prescribed parameters.

At 10:30 a.m., trap #1P began to be drained into cylinder No. 1033, which was positioned on the north scale. By 12:15 p.m., the north scale indicated that 13,710 pounds of UF_6 was in the cylinder. The log noted at this time that draining to cylinder No. 1033 had slowed and had therefore been switched to cylinder No. 637 on the south scale. Apparently, cylinder No. 1033 had already been filled almost full at this point, which would explain the reduced flow rate. At the time, however, the shift crew suspected that the filter to the north cylinder had partially clogged, because they were aware that the product being drained was likely to have a high chromium content. (At the time of the January 4 accident, a cylinder with high chromium content was being evacuated back to the cold traps.)

Draining continued into cylinder No. 637 until 2,100 pounds of UF_6 was in the cylinder and trap #1P was empty. Trap #5C was then heated, and the contents of trap #1S began draining into the cylinders, starting with cylinder No. 1033. Cylinder No. 1033 received 980 pounds (indicated), and cylinder No. 637 received 540 pounds. At 3:30 p.m., a second draining of #1S added 480 pounds to cylinder No. 637. At 3:40 p.m., draining of trap #5C began, and the north scale indicated that an additional 1,150 pounds of product was drained into cylinder, No. 1033. Slow flow required changing the flow to the south

cylinder, which received 3,690 pounds before trap #5C was emptied. At 5:15 p.m., traps #1P, #1S, and #5C had been emptied and were returned to a refrigerated state. The operation was then terminated for the day. The north scale indicated that cylinder No. 1033 had a net weight of 15,840 pounds. Cylinder No. 637 on the south scale contained 6,810 pounds for a total of 22,650 pounds of product presumably drained for the day. These summary data were recorded on a "Cold Trap and Product Status" log sheet.

3.6 Sequence of Events for the Second Day of Draining

The second day of the operation began at 6:00 a.m. with the same shift schedules as for the first day. The #2P and #2S traps were started on the tempering cycle. The #1P, #1S, and #5C traps, which were emptied on the first day, were placed on line and refrigerated to provide vacuum and backup trap capacity. Heating was begun on #2P and tempering was begun on #6C at 6:45 a.m. Trap #2S was heated at 7:30 a.m., but the trap was found to be empty, as indicated by the absence of pressure gain. This trap was then cooled and refrigerated. The #3S trap was tempered at 8:30 a.m. and heated at 9:00 a.m.

At 11:00 a.m. draining commenced using trap #2P. The flow stopped after 750 pounds (indicated) were drained into cylinder No. 1033 on the north scale. Draining was diverted to cylinder No. 637, to which 4,890 pounds of UF_6 were added. Draining of trap #3S began at 1:50 p.m., and 3,630 pounds were drained into cylinder No. 637. At this point, the south scale indicated that cylinder No. 637 contained 15,330 pounds. Trap #3S remained heated so that another attempt to drain this trap could be made later in the day.

One of the assigned chemical operators was also the operator who, during the midnight shift of January 4, 1986, had filled the 14-ton cylinder that later ruptured when it was heated in the steam chest. This operator remarked that cylinder No. 1033 was behaving just like the 14-ton cylinder had before. He suggested that No. 1033 be disconnected from the north fill bay and moved to the final product scale for a check weighing. At about 3:20 p.m., the cylinder was transferred to this scale, which indicated that the gross weight (of the cylinder and its contents) was 30,568 pounds. The net weight was determined to be 26,017 pounds after deducting the tare weight of the empty cylinder.

The maximum net shipping weight specification for the Model 48X 10-ton cylinder is 21,030 pounds. However, the special procedure for this operation called for the cylinder to be filled to only 20,000 pounds. Thus, the cylinder was filled to 4,987 pounds in excess of the maximum shipping weight specification and 6,017 pounds in excess of the amount specified in the special procedure. This quantity exceeded, by 1-7% (depending on temperature), the maximum amount of liquid UF_6 capacity for the cylinder, indicating that some solidification had occurred during the filling process.

The shift supervisor notified the acting production manager at 3:30 p.m., who then immediately notified the plant manager. An NRC staff member, who was with the plant manager at the time of the notification, in turn notified NRC regional management. NRC headquarters management was subsequently notified.

The overfilled cylinder remained on the final weigh station scale, where it was connected to a vacuum line for evacuating the UF_6 to the process equipment.

Evacuation of the overfilled cylinder to trap #1P began at 4:10. All other traps were returned to a refrigerated state later that evening.

The production manager moved the 25,509-pound test cylinder onto the north drain station scale. He later recounted to the AIT that the scale indicated only about 13,000 pounds.

Evacuation of the overfilled cylinder continued until Friday afternoon (March 14), at which time the contents had solidified to the extent that no further material could be removed using the plant vacuum (about 14 inches of mercury (Hg)). The net weight of the cylinder was then 21,203 pounds, 173 pounds above the maximum shipping weight specification of 21,030 and 1,203 pounds over the limit established by the one-time procedures.

Subsequently, the overfilled cylinder was disconnected and placed into storage pending future NRC approval of plans to further reduce the amount of the contained UF_6.

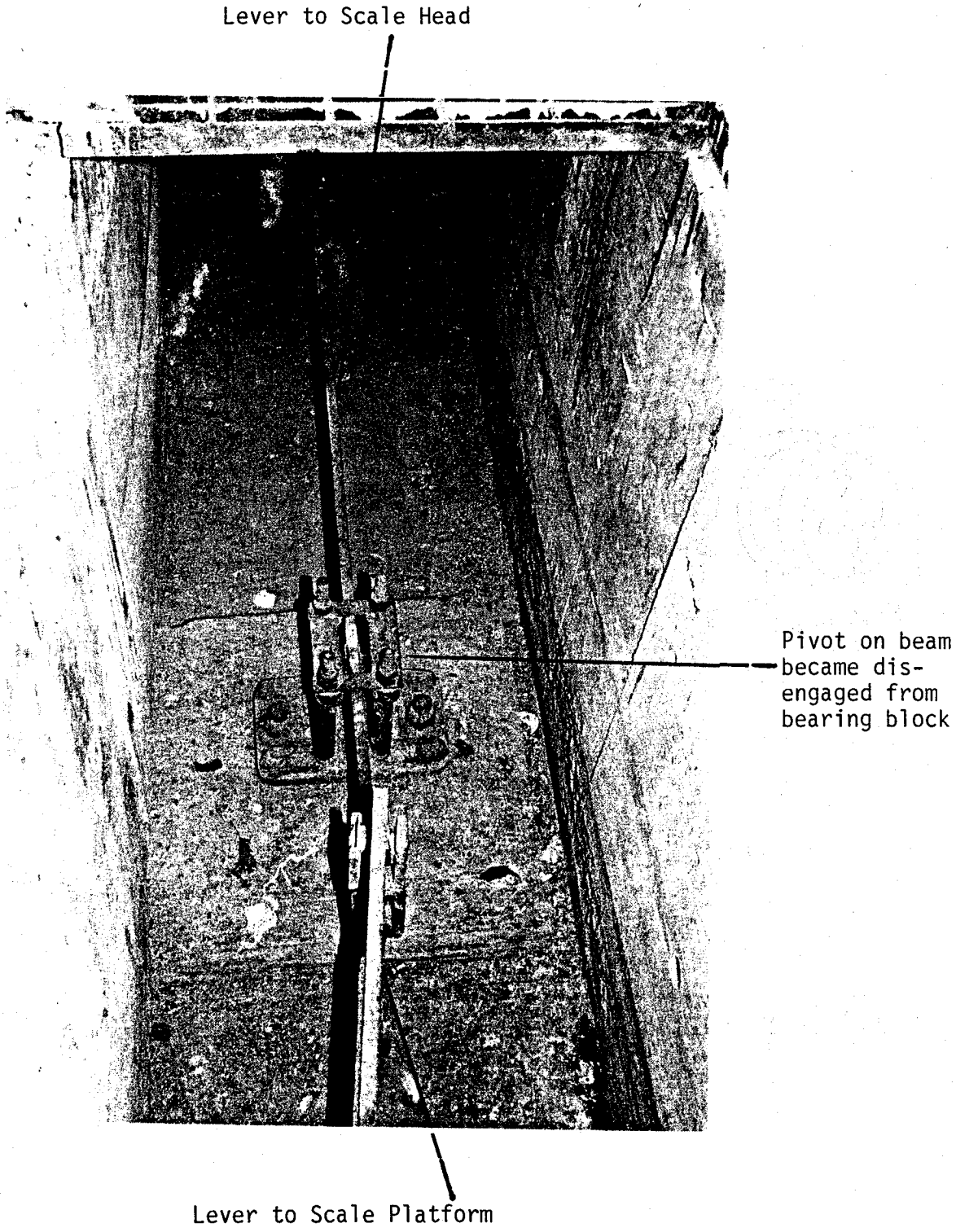

Figure 3.1 Beam and Pivot Assembly

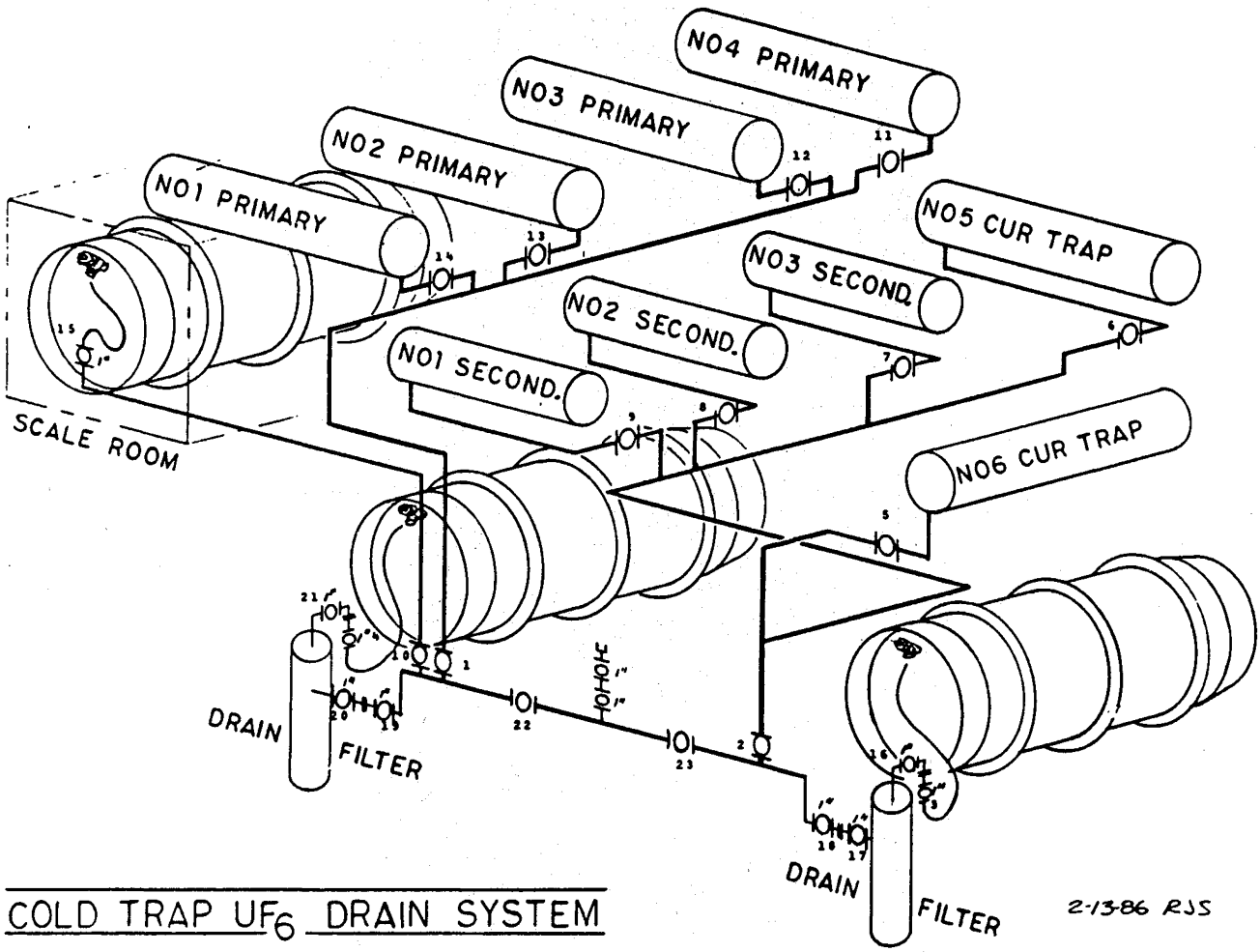

Figure 3.2 Cold Trap UF_6 Drain System

4 FINDINGS AND CONCLUSIONS

The Augmented Investigation Team has concluded that the overfilling of the cylinder had the following causes:

(1) The scale used for weighing the cylinder being filled was malfunctioning. It was determined that a beam linking the scale platform with the readout dial had become dislodged. With its pivot point displaced, the scale gave erroneously low indications of weight.

(2) The procedures for draindown did not include any provisions for ensuring proper scale functioning. Neither the one-time special procedure for conducting the draindown nor any of the regular procedures incorporated by reference required any use of check weights to determine the scales' accuracy and functioning. The procedure for filling UF_6 cylinders called only for cancelling out the tare weight by adjusting the uncalibrated tare poise.

(3) The supervision in charge of the operation did not recognize early indications of malfunction. When the chemical operator adjusted the tare poise to compensate for the empty cylinder weight, he reported to his supervisor that the poise was in an unusual position. The supervisor erroneously assumed that this resulted from the recent scale calibration activities, even though a detailed check of the north scale had not been performed. Later, a chemical operator observed that the flow rate, as indicated by the weight gain of the cylinder, was lower than anticipated. It was erroneously concluded that this was caused by contaminants clogging the newly replaced filters, even though this phenomenon was not observed on the south scale.

The Augmented Investigation Team further concluded that a serious accident was avoided by the following actions:

(1) The approved procedures prohibited the heating of any of the cylinders involved in the draindown operation. Even though the cylinder was overfilled, the special procedures precluded its heating. The workers appeared to have been adequately trained in these procedures. As long as the cylinder was not heated, it presented no danger.

(2) The overfilled cylinder was connected to a vent line and most of the overfill was removed to process equipment. In accordance with established procedures, the cylinder was vented to cold traps under vacuum. Nearly 4,800 pounds of UF_6 was removed from the cylinder before the temperature and applied vacuum equilibrated with the vapor pressure of the UF_6 and the vaporization ceased.

APPENDIX A

SPECIAL ONE-TIME INSTRUCTIONS FOR DRAINING COLD TRAPS

Subject: SPECIAL ONE-TIME INSTRUCTIONS FOR DRAINING COLD TRAPS

1.0 INTRODUCTION

1.1 Purpose:

To define the procedure to be followed for draining the process product, solidified uranium hexafluoride (UF_6), from all cold traps, preparatory for total shutdown.

1.2 Background:

An emergency shutdown of the plant was performed on January 4, 1986. Since that time all cold traps have been maintained on cold cycle. In this mode, all traps have been under a vacuum supplied by the off-gas blower which exhausts to the Hydrogen Fluoride Off-Gas Scrubber, or alternatively have been valved closed to prevent any venting.

The status of the cold traps at the time of shutdown is as follows:

COLD TRAP	CONTENTS	CAPACITY (TOTAL FILL OF LIQUID UF_6 AT 200°F)
No. 1 Primary	21,000 lbs.	44,000 lbs.
No. 2 Primary	6,000 lbs.	44,000 lbs.
No. 3 Primary	12,500 lbs.	44,000 lbs.
No. 4 Primary	EMPTY	44,000 lbs.
No. 5 Clean Up Reactor	3,000 lbs.	44,000 lbs.
No. 6 Clean Up Reactor	EMPTY	44,000 lbs.
No. 1 Secondary	EMPTY	12,900 lbs.
No. 2 Secondary	600 lbs.	12,900 lbs.
No. 3 Secondary	EMPTY	12,900 lbs.

Sufficient void space is available in all traps for safely heating and draining to 10-ton UF6 cylinders.

2.0 SAFETY PRECAUTIONS

```
* * * * * * * * * * * * * * * * * * * * *
*                  NOTE                 *
*                  ====                 *
*                                       *
* Paragraphs 2.1, 2.2, 2.6 and 2.7 must be *
* initialled by the two operators and shift *
* supervisor in the signature blocks to *
* verify that the required work has been *
* completed in accordance with the *
* indicated instructions.               *
* * * * * * * * * * * * * * * * * * * * *
```

2.1

```
* * * * * * * * * * * * * * * * * * * * *  * * * * * * *
*                  WARNING                *  *Oper. S.L.C. #1 DS
*                  =======                *  *              *
*                                         *  *Oper. R.S.C. #1 C.P.
* The UF6 dump tank pressure relief system *  *              *
* must be in service with a gauge reading of*  *S. S. C.B. #1 DMR
* 0.0 psig +/- 2 psig on the tap between the*  * * * * * * *
* rupture disc and relief valve.          *
* * * * * * * * * * * * * * * * * * * * *
```

2.2

```
* * * * * * * * * * * * * * * * * * * * *  * * * * * * *
*                  WARNING                *  *Oper.       *
*                  =======                *  *              *
* Review documents to assure that all     *  *Oper.       *
* system relief valves have been serviced *  *              *
* according to the established preventive *  *S. S.        *
* maintenance schedule. Correct any       *  * * * * * * *
* deficiencies before proceeding.         *
* * * * * * * * * * * * * * * * * * * * *
```

note #3 primary cold trap
The in line regulator valve (Fisher) is plugged. The 4" actuator is working proper.

3-12-86

2.3

```
* * * * * * * * * * * * * * * * * * * *
*                WARNING                *
*                =======                *
*                                       *
* Filled 10-ton cylinders from cold trap *
* draining activities are not to be placed *
* in the steam cabinets for reheating.  *
* * * * * * * * * * * * * * * * * * * *
```

2.4

```
* * * * * * * * * * * * * * * * * * * *
*                CAUTION                *
*                =======                *
*                                       *
* The pressure indicator on the cold trap *
* and cylinder fill systems are to be   *
* carefully monitored during the draining *
* and filling operation. Pressure must be *
* maintained within the ranges specified in *
* the referenced procedures.            *
* * * * * * * * * * * * * * * * * * * *
```

2.5

```
* * * * * * * * * * * * * * * * * * * *
*                CAUTION                *
*                =======                *
*                                       *
* Sampling of filled 10-ton cylinders from *
* cold trap draining activities will be *
* done only on those cylinders which    *
* required less than 4 hours to fill and do *
* not require re-heating in the steam   *
* cabinets.                             *
* * * * * * * * * * * * * * * * * * * *
```

2.6

```
* * * * * * * * * * * * * * * * * * * *  * * * * * * *
*                ==NOTE==               *  *Oper. S.L.C. *P.O.S.
*                                       *  *          *
* New pressure gauges are to be installed *  *Oper. R.J.C. *L.C.P.
* on the UFs drain header at the filter *  *          *
* inlet before draining begins.         *  *S. S. R.C.T.  *R
* * * * * * * * * * * * * * * * * * * *  * * * * * * *
```

3-12-86

2.7

```
* * * * * * * * * * * * * * * * * * * * *  * * * * * * *
*                ==NOTE==                 *  *Oper. ___ *P.D.S
*                                         *  *       ___ *
* Only ten-ton cylinders will be used for *  *Oper: ___ *L.C.
* this one-time draining. The maximum     *  *       ___ *
* cylinder fill weight is to be 20,000 lbs. *  *S. S. ___ *f.m.f.
* net weight rather than the weights      *  * * * * * * *
* specified in referenced procedure       *
* N-280-1, Rev. 6, page 7.                *
* * * * * * * * * * * * * * * * * * * * *
```

3-12-86

2.8

```
* * * * * * * * * * * * * * * * * * * *
*                ==NOTE==                *
*                                        *
* Ensure that the venting lines from the *
* cold traps are being properly heated by *
* the steam tracings.                    *
* * * * * * * * * * * * * * * * * * * *
```

2.9 All work is to be performed according to Operating Procedure G-001, Rev. 3, Health and Safety Precautions and Requirements.

3.0 REFERENCES

N-280-1, Rev. 6 Uranium Hexafluoride Product Handling and Shipping

E-008, Rev. 4 Emergency Procedure for UF6 Release

N-270-3, Rev. 2 Secondary Cold Trap Operation

N-270-4, Rev. 2 Primary Cold Trap Operation

N-270-5, Rev. 1 Emergency Dump Tank

N-270-9, Rev. 0 Freon Vapor Heating System

N-270-11, Rev. 0 Moving UF6 Scale Carts

QA-001, Rev. 0 Quality Assurance for UF6 Shipping Cylinders

QA-002, Rev. 0 Inspections - UF6 Cylinders

4.0 PROCEDURES

4.1 A Special Team consisting of one Shift Supervisor and two Chemical Operators who are experiences and trained in UF_6 handling shall be assigned the duty of draining all cold traps.

4.2 The Shift Supervisor shall review this procedure and the procedures referenced in section 3.0, above, with both Chemical Operators to ensure their complete understanding of these procedures before initiating the activity.

4.3 The cold trap draining is to be done during the dayshift. If draining of all traps heated in accordance with 4.4.c, cannot be completed in one shift and minimal overtime, the traps being drained will be completed and the remainder of the system shall be returned to the cold mode until the next day shift. Cold traps shall not be maintained in a heated state on evening and night shifts.

4.4 Draining of the cold traps will follow the procedure outlined in N-280-1, Rev. 6 Uranium Hexafluoride Product Handling and Shipping, dated 1/23/85 paragraphs II. A, B and C with the following exceptions:

a.
```
* * * * * * * * * * * * * * * * * * * *
*              ==NOTE==                 *
*                                       *
* Cylinders  shall  be filled only to   *
* the amount of   UF6   indicated in    *
* paragraphs 2.7 above.                 *
* * * * * * * * * * * * * * * * * * * *
```

b.
```
* * * * * * * * * * * * * * * * * * * *
*              ==NOTE==                 *
*                                       *
* The cold traps  are  to  be drained   *
* only  into ten-ton cylinders  that    *
* have  current   quality   assurance   *
* inspection documentation.             *
* * * * * * * * * * * * * * * * * * * *
```

c. Only three cold traps (one primary, one Clean Up Reactor and one secondary) shall be heated simultaneously. The remaining cold traps will remain on cold cycle.

d. There will be only one trap drained at a time; once started, draining must be completed before starting to drain another cold trap.

e. The secondary cold trap off-gas blower shall be in operation with normal purges on the fluorination towers. The secondary on line trap shall be on cold cycle.

f. The filled cylinders shall be check weighed and sampled in accordance with paragraph 2.5, above, on the Sample Room accountability weigh scale and then stored at the cooldown area east of the steam chests.

g. Filled 10-ton cylinders from cold trap draining activities are <u>not</u> to be placed in the steam cabinets for reheating.

h. The Shift Supervisor is responsible for properly completing the Cylinder Status Sheets. The Filled Cylinder Status Sheet shall be delivered to the Accountability Supervisor upon completion of the draining and weighing operation.

i. As items a. through h. are accomplished, the Shift Supervisor will indicate such on the cylinder status sheet log used for the activities. Cylinders status sheets for each shift shall be signed by supervisor and operators.

APPROVED BY:

Mgr., Sequoyah Facility William L. Elmore Date 3-5-86

APPENDIX B

INVESTIGATION OF A FAILED UF_6 SHIPPING CONTAINER

FINAL REPORT

on

INVESTIGATION OF A FAILED UF_6 SHIPPING CONTAINER

to

SEQUOYAH FUELS CORPORATION

April 23, 1986

by

T. P. Groeneveld, R. D. Buchheit,
T. A. Wall, and J. Ahmad

BATTELLE
Columbus Division
505 King Avenue
Columbus, Ohio 43201

TABLE OF CONTENTS

Table of Contents
(Continued)

LIST OF TABLES

List of Tables
(Continued)

APPENDIX A

LIST OF FIGURES

LIST OF FIGURES
(Continued)

LIST OF FIGURES
(Continued)

LIST OF FIGURES
(Continued)

LIST OF FIGURES
(Continued)

INVESTIGATION OF A FAILED UF_6 SHIPPING CONTAINER

SUMMARY

An investigation was conducted to determine, insofar as possible, the cause of the failure that occurred in a uranium hexaflouride (UF_6) shipping container. The container failed on January 4, 1986, while being heated in a steam chest at the Sequoyah Fuels Facility near Gore, Oklahoma. The vessel had been overfilled and it was being heated to liquify the UF_6 so that the excess material could be withdrawn to achieve the desired fill weight.

The investigation consisted of (1) an onsite inspection of the failed vessel, (2) laboratory evaluations of appropriate sections removed from the failed container to determine the mode(s) of fracture and the properties of the steels from the vessel shell and the stiffener rings, and (3) stress analyses to estimate the pressures required to cause failure.

Examination of the failed shipping container revealed the primary rupture through the vessel wall and the valve-end stiffener ring and that the middle- and drain-end stiffener rings were cracked through the butt welds. Cracks also were present in the fillet welds on either side of those two stiffener rings. The butt welds for all three stiffener rings were not full penetration welds which reportedly were specified for the vessel. The amounts of weld deposits that fused the ends of the stiffener rings together was determined to range from 10.5 to 23.5 percent of the stiffener ring-cross sections.

The markings on the fracture surfaces of the primary rupture indicated that the failure initiated in the region of the valve-end stiffener ring. It appeared that cracking of the butt weld in that stiffener ring occurred first. Cracking through the vessel shell appeared to start by extension of cracks through the fillet welds on either side of the stiffener into the vessel shell steel. Those cracks grew toward the inside surface of the vessel and axially in a ductile mode until the region of stable crack growth reached a critical size for the conditions of

temperature and pressure being experienced by the vessel. At that time, the vessel ruptured, with the crack propagating axially through the vessel wall in a shear mode in both directions from valve-end stiffener ring. Examinations of the fracture surfaces through the weld metal in the butt welds and the through the fillet welds on all sections revealed that cracks grew in all cases by a ductile rupture mode.

The various finite element elastic and elastic-plastic stress analyses conducted during this investigation and a fracture toughness analysis using the J_{Ic} value for the vessel shell steel indicated that, at the assumed failure temperature of 180 F, the crack in the vessel shell may have initiated at an internal pressure of 1250 psig and that final rupture occurred at an internal pressure of approximately 1800 psig. Those pressures are 3 and 4-1/2 times, respectively, the hydrostatic test pressure of 400 psig used to assess the integrity of the shipping container and 6 and 9 times, respectively, the standard service pressure of 200 psig.

Evaluation of the chemical composition of the vessel shell steel revealed that it was ASME SA516, Grade 70 steel, as specified. The tensile properties of the material determined at room temperature met those required for ASME SA516, Grade 70 steel. The fracture properties of the vessel shell steel determined by drop-weight-tear tests showed that at temperatures above 80 F, fractures would propagate from a critical flaw in a ductile shear mode. It was not reported to Battelle whether supplementary fracture toughness requirements were specified for the steel.

The steel specified for the stiffener rings was not reported to Battelle. The chemical composition of the steels from the three stiffener rings revealed that they were most likely fabricated from AISI/SAE 1020 steel. The average room temperature tensile properties of the steels from the stiffener rings were similar to those of the vessel shell steel. Also the tensile properties determined at 180 F of the steel from the vessel shell and the steel from the stiffener rings were similar. At 180 F the ultimate tensile strengths were 3 to 5 percent lower than those at room temperature.

The microstructures of the steels used to fabricate the vessel shell and the stiffener rings were judged to be acceptable for ASME SA516, Grade 70 steel and AISI/SAE 1020 steel. However, it was not reported to

Battelle if supplementary microstructural requirements were specified for the steels. Thus, there was no indication that the failure was related to material deficiencies.

INVESTIGATION OF A FAILED UF_6 SHIPPING CONTAINER

by

T. P. Groeneveld, R. D. Buchheit,
T. A. Wall, and J. Ahmad

INTRODUCTION

On January 4, 1986, a Model 48Y, uranium hexaflouride (UF_6) shipping container ruptured while being heated in a steam chest (under ambient atmosphere conditions) at the Sequoyah Fuels Facility near Gore, Oklahoma. It was reported to Battelle that the container was being heated to adjust the fill level of the UF_6. Battelle was requested to conduct an investigation of the failed shipping container.

The objective of this investigation was to establish, insofar as possible, the most probable cause of the failure. To accomplish that objective the following information was to be obtained from investigation of the rupture vessel, or calculated from the design configuration of the vessel and the properties of the materials used to fabricate the vessel:

(1) Mode of failure, fracture initiation site(s), sequence of failure events, and other factors that may have contributed to the failure.

(2) The estimated internal pressure required to cause failure based upon the design of the vessel using the design properties of the materials as specified, as well as the actual properties of the materials.

(3) Whether the materials of construction met the applicable specifications.

The Battelle study did not address the factors or events leading to the vessel failure except as they directly influenced the service conditions, or properties of the materials of construction, at the time of

failure. In addition, in accordance with the agreement between Battelle and Sequoyah Fuels, this study does not include recommendations for possible design changes to the vessel.

The study consited of (1) an onsite examination of the failed shipping container during which sections were selected for further examinations and analyses in the laboratory, (2) laboratory examinations and analyses of the steel from the vessel shell and stiffener rings, (3) fractographic analysis of the fracture surfaces from the vessel, and (4) stress analyses. The following sections of this report describe the procedures used to conduct the various analyses and the results obtained from them.

BACKGROUND INFORMATION

The following background information was obtained during meetings held at Sequoyah Fuels Facility near Gore, Oklahoma, on January 31, 1986, and February 14, 1986. At the meeting on January 31, representatives of Sequoyah Fuels, Kerr-McGee, Lawrence Livermore Laboratories, the Nuclear Regulatory Commission, and Battelle were present. Representatives of those same organizations plus Trinity Industries, Inc., were present at the meeting on February 14, 1986.

The information that Battelle received at those meetings indicated that the shipping container failed on January 4, 1986, while being heated in a steam chest under ambient pressure conditions for the purpose of liquifying the UF_6 inside the container. The vessel had been in the steam chest for about 2-1/2 hours prior to failure. The heating operation was being conducted because it was discovered by Sequoyah Fuels personnel that the container had been significantly overfilled (by weight) with UF_6. The details of how the overfilling was discovered or the exact amount of overfilling were not reported to the Battelle investigators. It was the intent of the Sequoyah Fuels personnel to withdraw sufficient UF_6, following liquification by heating in the steam chest, in order to achieve the desired weight of product in the vessel.

There were no eyewitnesses to the explosion, but several workers reportedly heard an explosion. As a result of the failure, the steam chest cover had been tipped up, the vessel had rotated about 90 degrees, and the UF_6 was draining out through the rupture. To minimize the escape of UF_6 after the failure was discovered, workers stuffed wet towels into the opening created by the failure. The vessel remained in that condition from the time of failure on Saturday, January 4, until the following Friday. At that time, the towels were removed and the escaping material (and the vessel) were sprayed with water. The vessel then was rotated so that the rupture opening was near the top; it was filled with water and a neutralizing chemical agent was added. It remained in that condition outdoors with the fracture unprotected until January 31, 1986. On January 31, the fracture surfaces were coated with grease to prevent further reaction with the environment. Prior to the onsite investigation that began on February 14, 1986, the vessel was drained, washed to reduce radioactive contamination, covered with plastic sheeting and moved indoors.

Information on the general configuration and requirements for Model 48Y shipping containers that was provided to Battelle are reproduced in Figures 1 and 2. That information was obtained from the U. S. ERDA publication ORO-651-REV.4, "Uranium Hexafluoride: Handling Procedures and Container Criteria", April, 1977. The failed shipping container was manufactured during 1977 by Trinity Industries, Inc. of Dallas, Texas. Battelle was informed that the vessel was fabricated from ASME SA516, Grade 70 steel and ASME Code UG-32D semi-ellipsoidal heads. However the purchase order specifications for the steel, and producer data for those materials were not reported. The grade of steel used to fabricate the stiffener rings also was not reported to the Battelle investigators. In addition, no information regarding the manufacturing procedures, including welding procedures and weld filler metals, were reported, and the engineering drawings for the vessel were not provided for Battelle's investigation.

Prior to being placed in service, the vessel was reportedly tested hydrostatically at 400 psig. As required by the NRC, it was successfully retested at 400 psig in 1982 (vessels are required to be hydrostatically tested every 5 years after being placed in service). Apparently, no problems were detected during those hydrostatic tests.

UF_6 CYLINDER MODEL 48Y

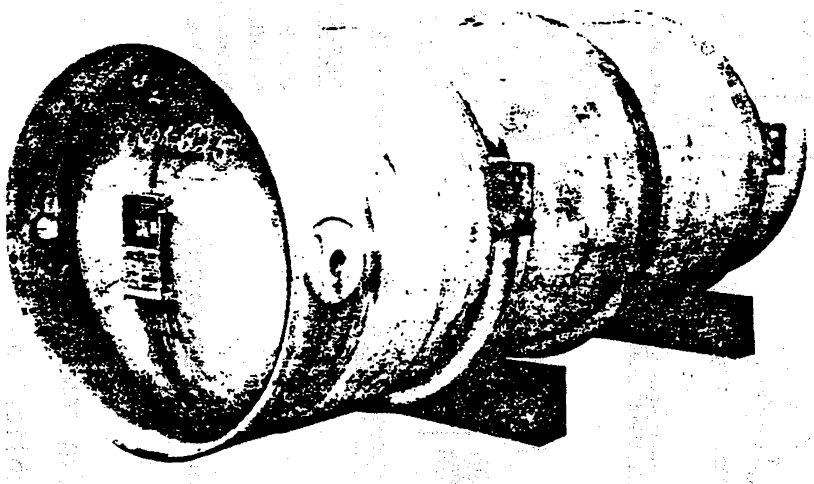

GENERAL DATA

Other Descriptive Terminology Used - 14-ton

ENGINEERING DRAWING REFERENCE	UNION CARBIDE CORPORATION, PGDP: E-S-12292-C
Nominal Diameter	48 in.
Nominal Length	150 in.
Wall Thickness	5/8 in.
Nominal Tare Weight	5,200 lb (2,359 kg)
Maximum Net Weight	27,560 lb (12,501 kg)
Nominal Gross Weight	32,760 lb (14,860 kg)
Minimum Volume	142.7 ft^3 (4.04 m^3)
Basic Material of Construction	Steel
Service Pressure	200 psig
Hydrostatic Test Pressure	400 psig
Isotopic Content Limit	4.5% U-235 max with moderation control

Valve Used - 1-in. Valve.

NOTE: Previously built 48F cylinders are similar in design, but do not have certified volumes; refer to table 3 for fill limits and other data applicable to this cylinder.

FIGURE 1. GENERAL INFORMATION ON MODEL 48Y SHIPPING CONTAINERS

This figure and information was reproduced from ERDA Publication ORO-651-REV. 4 (April, 1977).

(Best Copy Received by Battelle)

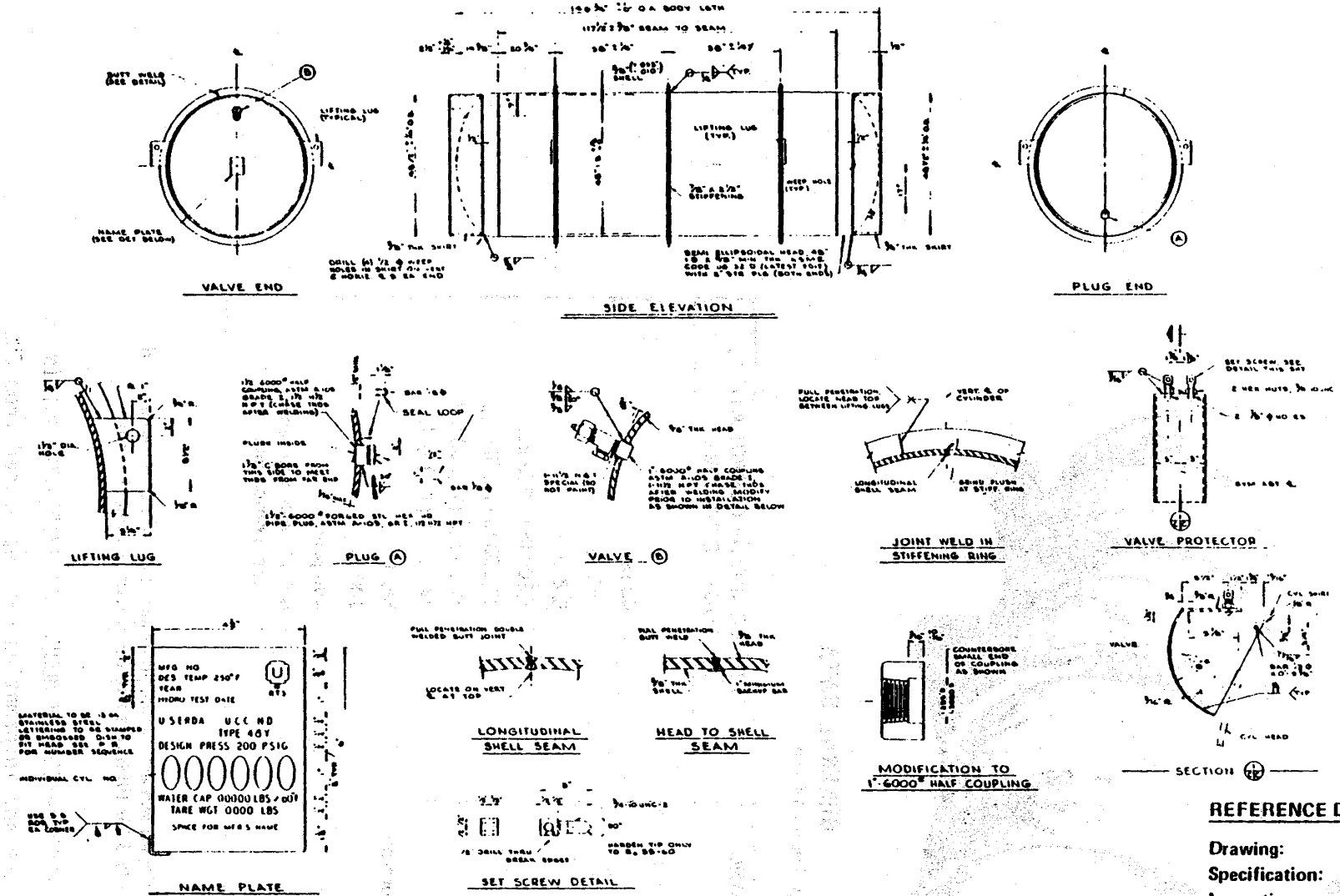

REFERENCE DOCUMENTS*

Drawing:	E-S-12292-C
Specification:	JSP-555
Inspection:	ME&I-11C
QA Plan:	QA-E-7

*UNION CARBIDE CORP., N.D. PADUCAH PLANT DOCUMENTS.

UF_6 CYLINDER MODEL 48Y

FIGURE 2. DRAWING FOR MODEY 48Y SHIPPING CONTAINER

Reproduced from U.S. ERDA publication ORO-651-REV 4 (April, 1977).

(Best Copy Received by Battelle)

The actual temperature of the vessel at the time of failure was not known with any certainty. Therefore, it was mutually agreed that a temperature of 180 F would be used in Battelle's experiments to estimate the properties of the materials at the time of failure. That temperature is about half way between the temperature at which UF_6 liquifies (147 F) and the temperature of the steam (212 F) used to heat the vessel.

ONSITE EXAMINATION OF FAILED SHIPPING CONTAINER

The initial work conducted by Battelle under this investigation consisted of a thorough examination of the failed shipping container at the Sequoyah Fuels Facility near Gore, Oklahoma. The objective of that examination was to obtain the dimensions of the vessel, document the appearance of the failure, identify the fracture initiation region(s), conduct nondestructive examinations of selected regions of the vessel, and to select sections of the vessel for further examinations and analyses in the laboratory.

Prior to the onsite examination, Sequoyah Fuels personnel had drained the liquid from the tank (the liquid was water and the neutralizing agent that had been placed in the tank following the rupture), cleaned the tank to reduce the level of radioactive contamination, coated the fracture surfaces with grease, covered the rupture region with plastic sheets, and moved the vessel to a location indoors where the onsite inspection was conducted.

The onsite inspection was conducted by three members of Battelle's staff and an inspector from Welding Consultants, Inc., Columbus, Ohio. The inspector from Welding Consultants was responsible for conducting ultrasonic thickness measurements, ultrasonic inspection of selected locations for indications of cracks or other defects, and magnetic-particle inspection of selected regions for the presence of surface cracks. The onsite inspection was conducted on February 14 and 15, 1986.

Figure 3 illustrates the failed vessel with the plastic sheets in place, as it appeared upon arrival of the inspection team. Figure 4 shows the vessel after removal of the plastic sheets. The rupture was

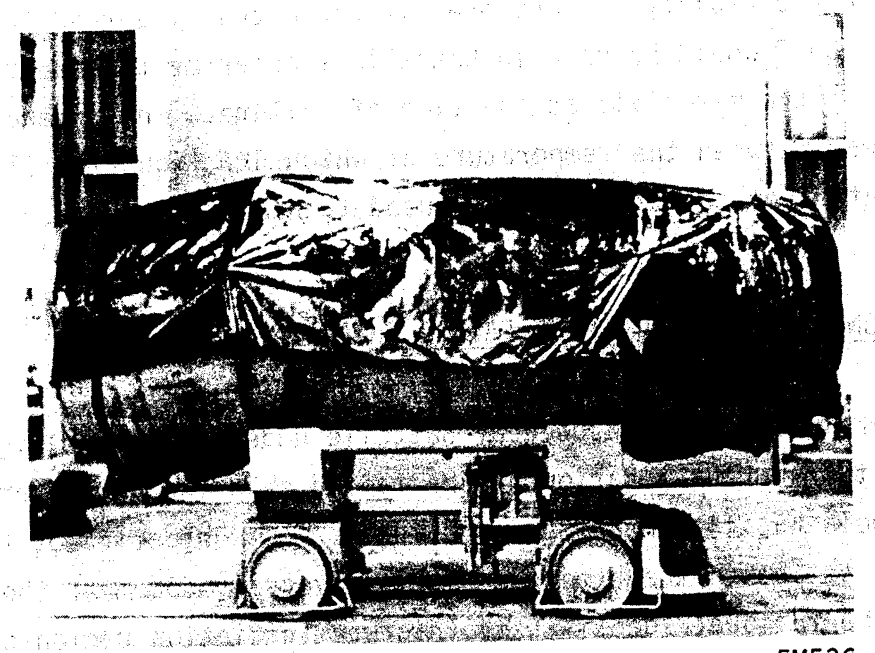

5M536

FIGURE 3. APPEARANCE OF THE VESSEL UPON ARRIVAL FOR THE ONSITE INSPECTION

Valve end

Drain end

5M540

FIGURE 4. THE FAILED VESSEL AFTER REMOVAL OF THE PLASTIC COVERING

located at the top of the vessel shown in Figure 4. The side of the vessel containing the rupture is shown in Figure 5, and the extent of the rupture is illustrated in Figure 6.

For purposes of this investigation, the following reference identifications were established: (1) the end of the vessel that contained the fill valve will be called the valve end; (2) the end of the vessel containing the drain valve will be called the drain end; (3) the longitudinal seam weld in the vessel is assumed to be at the 12 o'clock position. Also, when viewed from the valve end, the rupture will be to the left of the seam weld, the line of the rupture (approximately the 11:30 o'clock position) will be referred to as the 0-degree position; the stiffener ring located nearest the valve end of the vessel will be called the valve-end stiffener; the stiffener ring located at the mid-length of the vessel will be called the middle stiffener, and the stiffener ring located nearest the drain end of the vessel will be called the drain-end stiffener. The girth weld between the drain-end head and the vessel plate was established as the 0 reference point for length measurements.

The initial portion of the onsite examination involved conducting a visual examination of the vessel to determine if other cracks besides the primary rupture were present, and to document the locations of the primary rupture and other features on the vessel. That examination revealed that, besides the main rupture, the butt welds in the middle and drain-end stiffeners were cracked. No other cracks were apparent in the vessel shell or the heads.

To document the locations of the cracks and other features on the vessel, marks were made on its outer surface to facilitate making measurements. Those marks included the clock positions as described previously, and marks at 3-inch intervals along the length of the vessel, starting at the girth weld between the vessel shell and the drain-end head. Those marks at 3-inch intervals were made at the 3, 6, 9, and 12 o'clock positions to facilitate alignment of the measuring tapes during measurement of the circumference of the vessel.

In presenting the measurement results, the outer surface of the vessel shell is represented as a flat plate, as it was prior to forming the cylindrical vessel, with the ends of the plate that were joined by the

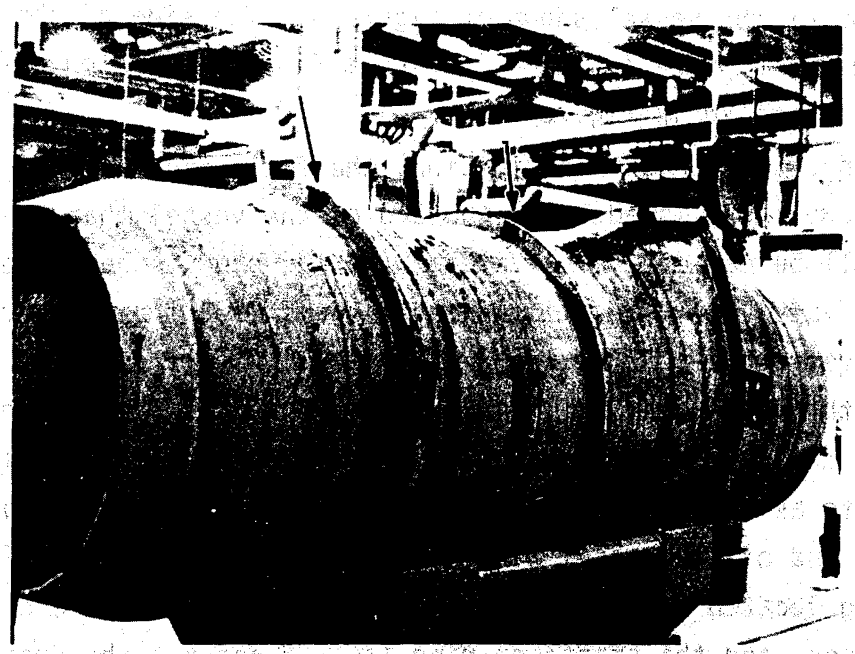

FIGURE VESSEL WITH RUPTURE LOCATED TOWARD THE DRAIN END

The arrows point to the cracks in the drain-end and middle stiffener rings.

FIGURE 6. APPEARANCE OF THE PRIMARY RUPTURE IN THE SHIPPING CONTAINER

longitudinal seam weld being at the 12 o'clock position and the other clock positions laid out as if the vessel was viewed from the valve end.

Figure 7 shows the representation of the vessel shell, indicating the locations of the stiffener rings, the lifting lugs, and the rupture. Also shown in that figure are the locations and dimensions of the sections of the vessel that were marked for removal from the body of the vessel and subsequent examination in the laboratory. Those sections will be described in a subsequent portion of this report.

As is shown in Figure 7, the length of the vessel shell was 117-1/2 inches; the centerlines of the valve-end and drain-end stiffener rings were located 20-1/2 inches from the respective girth welds; the spacing between those stiffener rings and the middle stiffener ring was 38 inches. The lifting lugs were attached to the shell on the valve-end side and the drain-end side surfaces of the valve end drain-end stiffener rings, respectively, and the bottoms of the lifting lugs were located at the 3 and 9 o'clock positions. Similarly, as is shown in Figure 8, the valve was located on the vertical centerline above the nameplate on the valve-end head. The drain-end plug was located on the vertical centerline near the bottom of the drain-end head. Also the longitudinal seam weld in the vessel was located at the top (12 o'clock position), and the butt welds in the stiffener rings were offset from the longitudinal seam weld about 7 inches in the circumferential direction toward the 11 o'clock position. All of those observations and measurements were in accordance with the dimensions indicated on the drawing (E-S-12292-C) for the UF_6 Cylinder Model 48Y shown previously in Figure 2.

The nameplate which appeared to be fabricated from stainless steel was located on the valve-end head of the vessel as was called out on Drawing E-S-12292-C. The location of nameplate is illustrated in Figure 8 and the information on the name is shown in Figure 9. Stenciled on the head immediately above the nameplate was "48F", as is shown in Figure 8. The reason for that stenciled "48F" and its significance were not reported to the Battelle investigators.

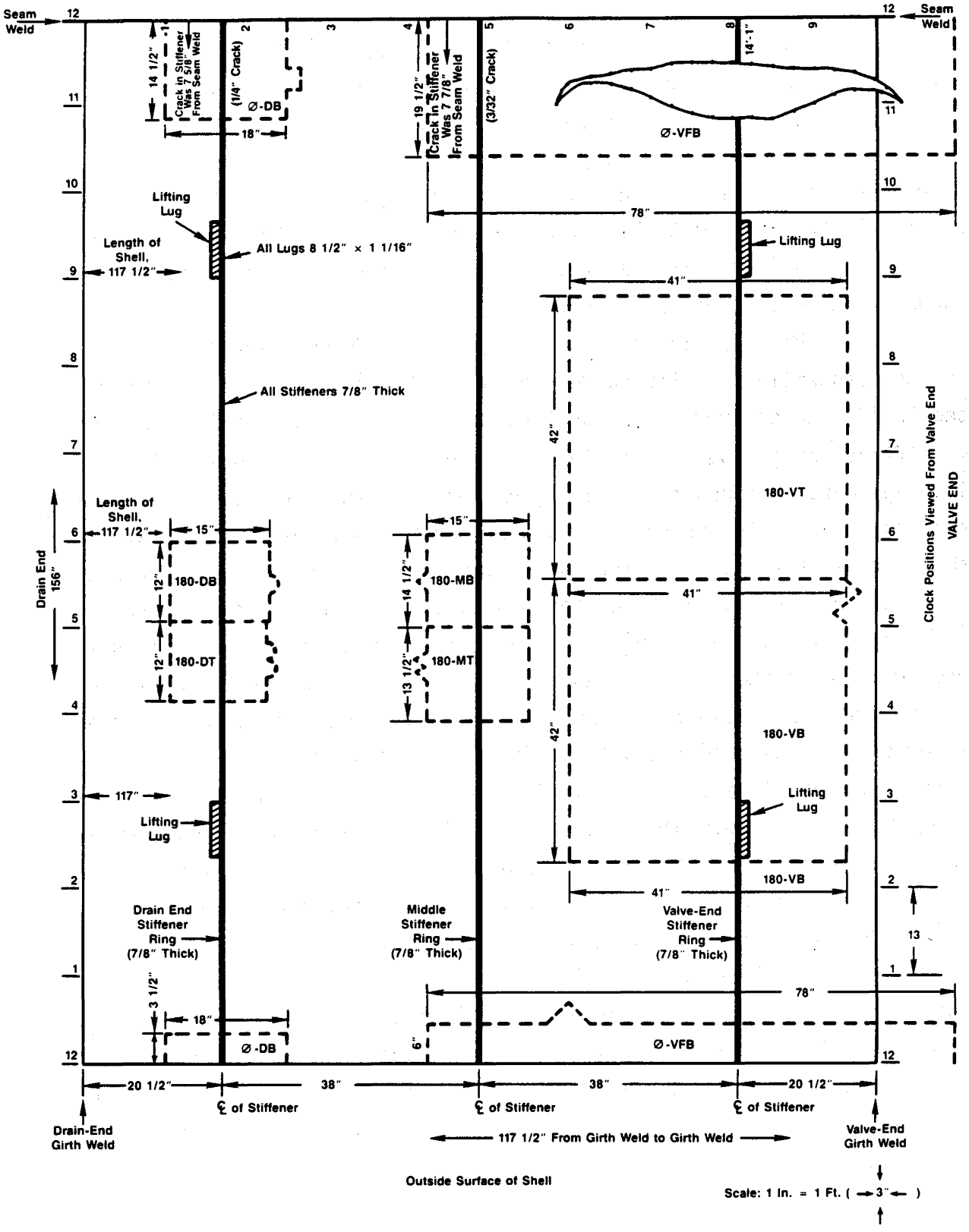

FIGURE 7. MAP OF VESSEL SHELL SHOWING THE APPROXIMATE LOCATION OF THE RUPTURE, THE STIFFENER RINGS, LIFTING LUGS, AND THE LOCATIONS OF SECTIONS REMOVED FROM THE VESSEL FOR EXAMINATION IN THE LABORATORY

The vessel outer surface is represented as a flat plate.

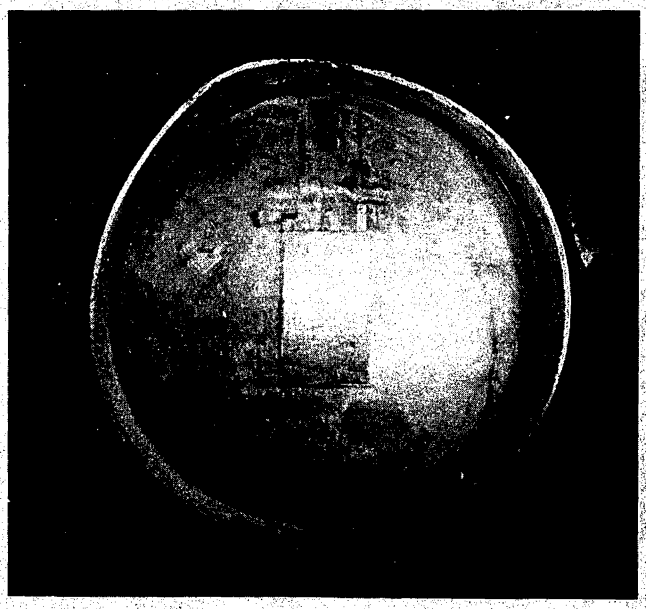

5M555

FIGURE 8. FILL VALVE AND NAMEPLATE ON THE VALVE-END HEAD

Note the "48 F" stenciled on the surface of the head above the nameplate and also the distortion of the skirt in the upper left portion of the photograph.

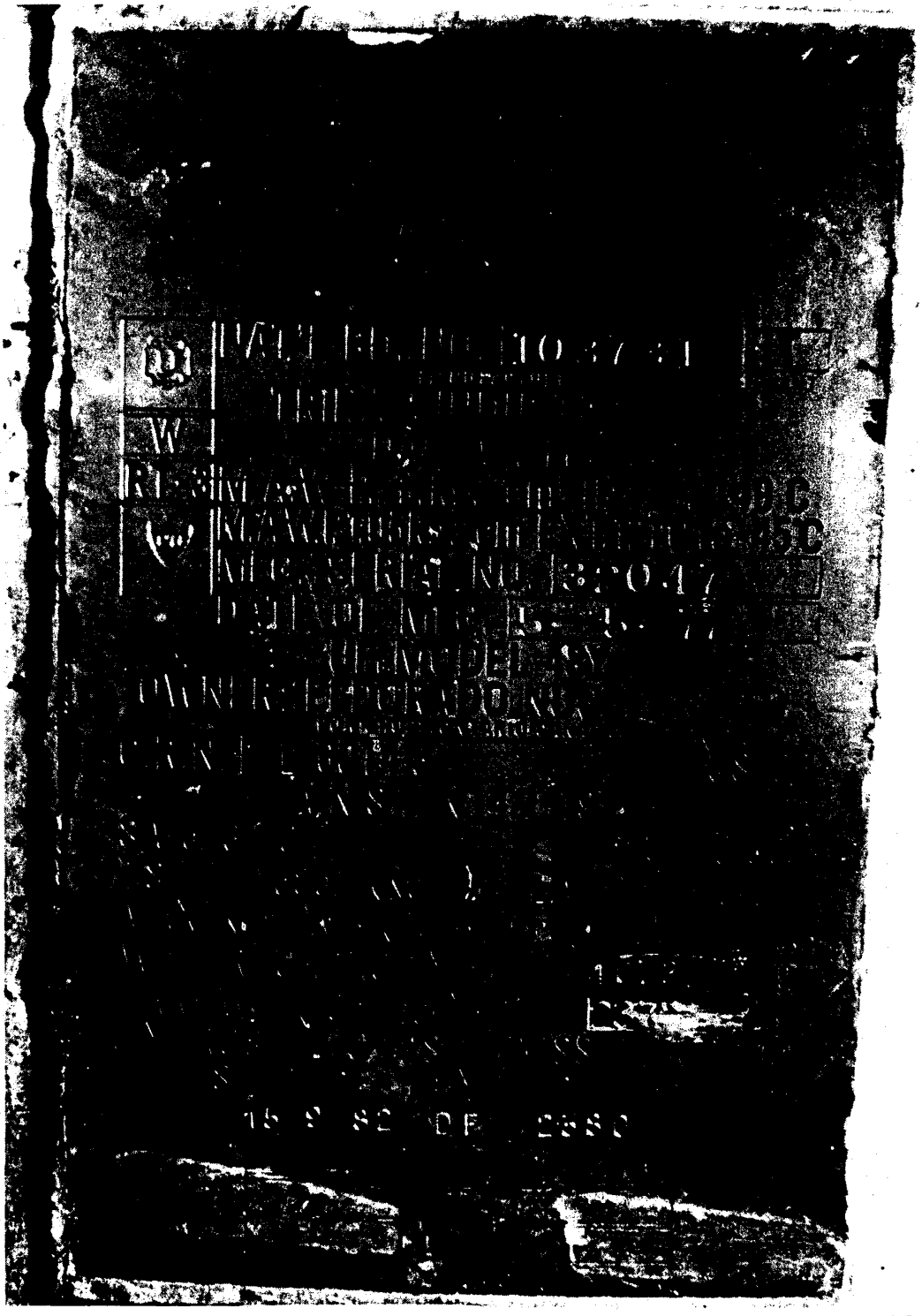

5M556

FIGURE 9. INFORMATION CONTAINED ON THE NAME PLATE WELDED TO THE VALVE-END HEAD

The number listed for Tare Wt. (10 mbar) is 2379 kg.

Description of the Fracture in the Vessel Shell and the Cracks in the Stiffener Rings

Initial visual examination of the failed shipping container revealed that the primary fracture occurred through the valve-end stiffener ring and vessel shell wall at about the 11:30 o'clock position, as was shown previously in Figures 5 and 6. The rupture extended axially slightly over two feet in both directions from the stiffener ring. Toward the valve end, the fracture propagated through the girth weld that joined the shell and the head and then turned and arrested in the head. The vessel shell surrounding the fracture was bulged substantially; the maximum separation (approximately 9 inches) between the fracture surfaces on the shell occurred in the region of the valve-end stiffener. In addition to the primary through-wall rupture, cracks through the cross section were present at the 11:30 o'clock position in the middle and valve-end stiffener rings. The fracture surfaces of the cracks in the stiffener rings and on the vessel shell were covered with corrosion products, which resulted from exposure to hydrofluoric acid, water, and the atmosphere subsequent to the failure, as was described previously.

To more precisely define the extent of the primary rupture, measurements of the distance of the fracture from the centerline of the longitudinal seam weld in the vessel shell (12 o'clock position) and the separation between the matching fracture surfaces were made at the 3-inch-interval marks described previously. Near the two ends of the crack, where the crack turned away from the seam weld, those measurements were at 1-inch intervals. Those measurements are shown in Figure 10.

Figure 10 shows that the rupture extended from the 5 ft-10-1/2-inch position to the 10 ft-2-inch position. Over most of that length, the fracture was aligned essentially axially, ranging between 6-7/8 inches and 9 inches from the longitudinal seam weld (about the 11:30 o'clock position). At about the 6-foot mark, the fracture turned away from the seam weld and extended about 4 inches nearly circumferentially prior to arresting. Toward the valve end of the vessel, the crack started turning at about the 9-ft-8-inch location, extended through the girth weld and propagated into the head

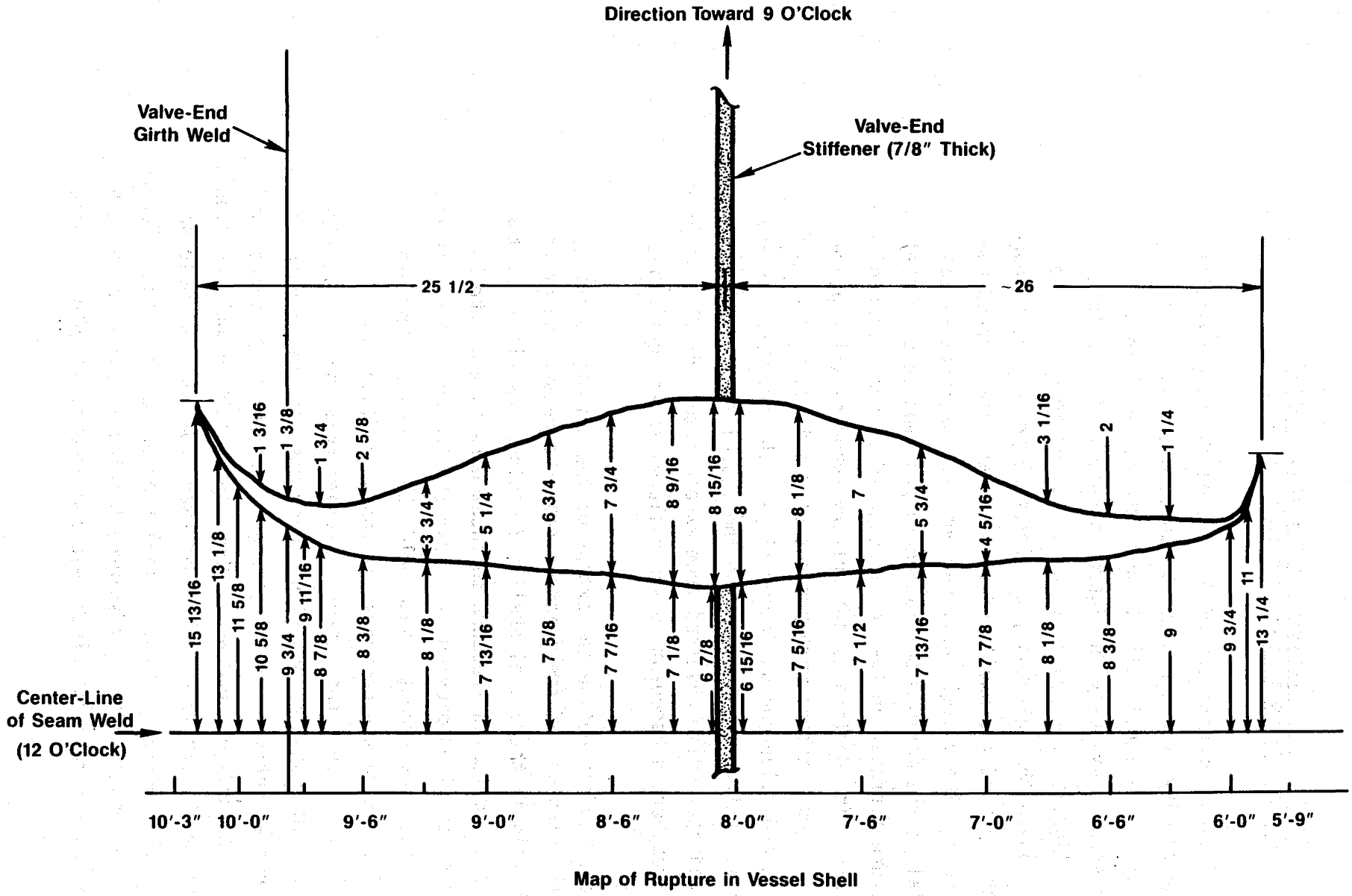

Map of Rupture in Vessel Shell

FIGURE 10. MAP OF RUPTURE IN VESSEL SHELL SHOWING THE LOCATION OF THE RUPTURE AND THE SEPARATION OF THE FRACTURE SURFACES WITH RESPECT TO THE LENGTH MEASUREMENTS, AND THE LONGITUDINAL SEAM WELD

The measurements are in inches.

for about 9 inches prior to arresting. The end of the crack in the valve-end head and the end toward the middle stiffener were located approximately 25-1/2 and 26 inches, respectively, in the axial direction from the center-line of the valve-end stiffener.

Examination of the surfaces of the primary fracture revealed that in the valve-end stiffener ring fracture occurred through the butt weld and into the vessel wall. That weld was not a full penetration weld as is called out on Drawing E-S-12292-C for Model 48Y shipping containers. On half of the stiffener-ring fracture surface nearer the seam weld, very little weld metal was present on the surface of the stiffener ring, and the pattern resulting from flame cutting the stiffener ring stock was clearly visible on that surface. It was estimated that about 10 percent of the cross-sectional area of that side of the butt weld contained weld metal. On the other half of the fracture surface (away from the vessel seam weld), the amount of weld metal covering the end of the stiffener was closer to 50 percent; the flame cut pattern was visible on the remainder of that surface. Those features are illustrated in Figure 11.

The fracture surfaces in the vessel wall directly below the butt weld in the valve-end stiffener ring contained a relatively flat region (essentially 90 degrees to the plate surfaces) except for the regions immediately adjacent to the fillet welds between the stiffener ring and the shell. The appearance of that flat region suggested that stable, slow-crack growth may have occurred in that region. Those features of the fracture appearance will be illustrated more clearly in a subsequent section of this report. The remainder of the surfaces of the fracture through the vessel shell exhibited features typical of crack propagation in a ductile (shear mode). In those regions, the fracture surfaces were at an angle of about 45 degrees to the plate surfaces.

The features observed on the surfaces of the rupture in the shipping container, suggest that the failure process began with failure of the valve-end stiffener ring through the butt weld. Cracks then extended through the fillet welds into the vessel shell below the fillet welds on either side of the stiffener ring. Those cracks joined forming a single crack front that extended both axially and through the vessel wall. When

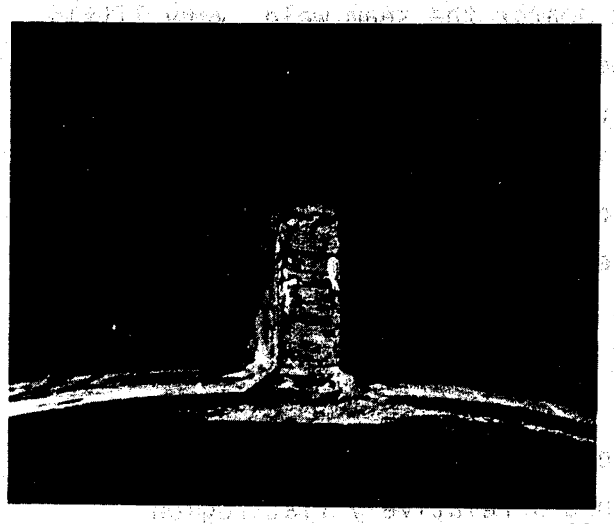

5M549

a. Fracture Surface on the Side Toward the Vessel Seam Weld

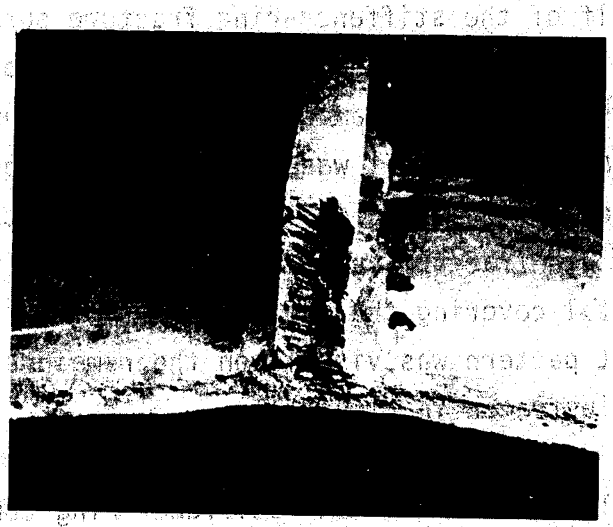

5M546

b. Matching Fracture Surface

FIGURE 11. FRACTURE SURFACES OF THE PRIMARY RUPTURE THROUGH THE VALVE END STIFFENER RING AND THE VESSEL SHELL

Note the flame cut surfaces on the ends of the stiffener rings, the flat region on the fracture through the vessel shell, and the shear fracture through the vessel shell, and the shear fracture through the vessel shell on both sides of the flat region.

that crack reached a critical size dictated by the conditions of temperature and pressure experienced by the vessel, rupture occurred by rapid crack propagation in a shear mode.

Visual examination of the outside surface of the shell surrounding the rupture did not reveal any other cracks. Also, no cracks were observed on the inside surfaces of the vessel shell that could be readily examined without entering the vessel.

In addition to the primary rupture, the onsite investigation revealed cracks in the middle and drain-end stiffener rings. Those cracks are shown in Figures 12 and 13, respectively. As is shown in Figure 12, the crack in the middle stiffener ring extended through the fillet weld between the ring and the shell on the valve-end side of the stiffener ring. That crack did not appear to extend axially in the vessel shell. No crack through the fillet weld or in the shell surface was observed on the opposite side of the middle stiffener ring. The maximum width of the crack at the top surface of the middle stiffener ring was 3/32 inch. The limited amount of the surface of that crack that could be observed showed that the crack occurred through the butt weld joining the ends of the ring and that the weld was not a full penetration weld.

The crack in the drain-end stiffener ring is illustrated in Figure 12. As is shown, the crack extended through the fillet weld between the ring and the shell on both sides of the stiffener. However, no evidence of crack extension into the vessel shell was observed. The maximum separation of the crack at the top surface of the drain-end stiffener was about 1/4 inch. The surfaces of the crack that could be seen revealed that it occurred through the butt weld and that the butt weld was not a full penetration weld. Evidence of significant grinding was present on the drain-end side of that stiffener ring.

Circumference Measurements

The circumference of the vessel was measured at 3-inch intervals along the length of the vessel shell between the girth welds used to join the vessel shell and the heads. Those measurements were made to assess whether significant deformation occurred during the failure.

Seam weld

5M543

a. Valve-End Side of Stiffener Rings

5M542

b. Drain-End Side of Stiffener Ring

Note the crack in the fillet weld.

FIGURE 12. CRACK THROUGH THE BUTT WELD IN THE MIDDLE STIFFENER RING

5M544

a. Valve-End Side of Stiffener Ring

5M545

b. Drain-End Side of Stiffener Ring

FIGURE 13. CRACK THROUGH THE BUTT WELD IN THE DRAIN-END STIFFENER RING

Note the cracks in the fillet welds on both sides of the stiffener ring.

In addition, a measurement of the circumference of each head was made; the drain-end head was measured approximately 2 inches from the girth weld and the valve-end head was measured approximately 1 inch from the girth weld. Those measurements were made with a flat steel tape graduated in 1/16-inch divisions and a Pi-tape. A Pi-tape is calibrated to read the diameter to the nearest 0.001 inch directly from a circumferential measurement of a cylindrical body. However, the Pi-tape cannot be used if the cylinder is no longer intact: Consequently, the Pi-tape was used only in those regions of the vessel where they were not cracked.

The results of the circumference measurements are listed in Table 1. To aid in visualizing the changes in circumference, the circumference measured for the vessel shell at the 1-inch location was assumed to be the nominal circumference of the vessel prior to failure. That value was subtracted from all the other measured values and the percent change in circumference from that value was calculated. Those results then were plotted as a function of length along the vessel as is shown in Figure 14.

The results of the circumference measurements and the Pi-tape measurements, where both measurements could be made, generally showed close agreement. The maximum differences between the measured circumference and the calculated circumference from the Pi-tape diameter was 0.188 inch or 0.12 percent (the 63-inch location). The circumference measurements show that, starting at the drain-end girth weld, the circumference increased with increasing length to the 9-inch location and then decreased toward the drain-end stiffener ring. Similarly, the circumference increased along the length of the vessel from the drain-end stiffener ring, reached a maximum at the 36 to 42-inch locations and then decreased toward the middle stiffener ring. Those patterns were repeated between the middle stiffener ring and the valve-end stiffener ring and between that stiffener ring and the valve-end girth weld; however, the symmetry of the change in the circumference was lost in the region of the valve-end stiffener ring where the rupture appeared to initiate. As is shown in Figure 14, the maximum change in circumference between the drain-end and middle stiffener rings was 1.4 percent; the maximum change in circumference between the middle stiffener ring and the

TABLE 1. RESULTS OF CIRCUMFERENCE MEASUREMENTS

Distance from Drain End Girth Weld, inches	Circumference,[a] inches	Pi-Tape Diameter, inches	Calculated Circumference,[b] inches
-2 (Drain-end head)	155-7/8	49.636	155.857
0 (Girth weld)	--	--	--
1	155-3/8	49.514	155.474
3	156	49.690	156.027
6	156-5/8	49.912	156.724
9	156-7/8	49.990	156.569
12	156-3/4	49.945	156.827
15	156-1/4	49.782	156.315
18	155-9/16	49.564	156.631
Drain End stiffener	171-1/8	--	--
21	155-3/8	49.495	155.414
24	156-1/8	49.688	156.020
27	156-11/16	49.900	156.686
30	157-1/8	50.041	157.129
33	157-3/8	50.125	157.393
36	157-9/16	50.149	157.468
39	157-9/16	50.208	157.653
42	157-9/16	50.207	157.650
45	157-1/2	50.185	157.581
48	157-1/4	50.120	157.377
51	156-7/8	49.984	156.950
54	156-3/16	49.772	156.284
57	155-1/2	45.540	155.556
Middle stiffener	171-3/16	--	--
60	155-5/8	49.580	155.681
63	156-1/4	49.821	156.438
66	157	50.025	157.079
69	157-1/2	50.200	157.628
72	158	--(c)	--
75	158-1/16	--	--
78	158-1/16	--	--
81	158-1/16	--	--
84	158-7/8	--	--
87	157-3/8	--	--
90	157	--	--
93	156-3/8	--	--
96	155-1/16	--	--
Valve End stiffener	169	--	--
99	157-1/4	--	--
102	157	--	--
105	157-9/16	--	--
108	157-13/16	--	--
111	157-7/16	--	--
114	156-9/16	--	--
116-1/2	155-7/8	--	--
117-1/2 (Girth weld)	--	--	--
118-1/2 (Valve-end head)	153-7/8	--	--

(a) Measured with flat steel measuring tape.
(b) Calculated using Pi = 3.14.
(c) Vessel rupture extended from about 70.5 to 122 inches; Pi tape could not be used.

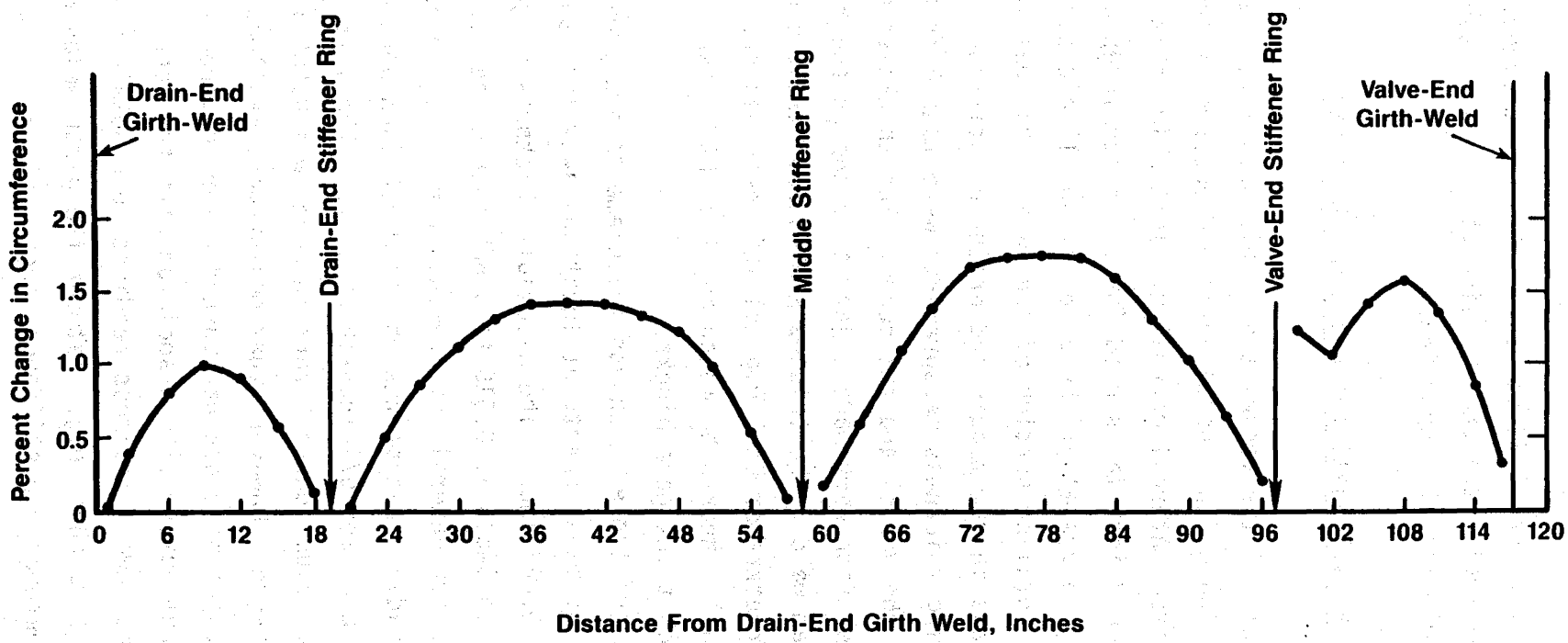

FIGURE 14. PERCENT CHANGE IN CIRCUMFERENCE ALONG THE LENGTH OF THE FAILED SHIPPING CONTAINER

The circumference measured at the 1-inch position was assumed to be the nominal circumference of the vessel prior to failure.

valve-end stiffener ring was 1.73 percent. The circumference measurements show that the vessel shell stretched considerably as the result of pressure buildup in the vessel prior to rupturing.

Vessel Shell Thickness Measurements

Measurements of the vessel shell thickness were made to determine if significant thinning of the vessel shell had occurred either during the failure process or from internal corrosion. Initially, those measurements were made at the same 3-inch marks used for the circumference measurements along the length of the vessel at the 3, 6, 9, and 12 o'clock locations and along a line in the unfailed portion of the vessel that was in line with the rupture and the cracks in the middle and drain-end stiffener rings. The starting and finishing thickness measurements were made 3 inches from the girth welds between the vessel and the heads. The thickness measurements at the 12 o'clock position were made adjacent to and on the rupture side of the longitudinal seam weld. The thickness measurements were made ultrasonically using a Krautkramer DM-2 Digital Thickness Tester. The thickness tester was periodically checked by measuring the thicknesses of standard 0.250- and 0.500-inch-thick gage blocks.

The results of those thickness measurements are presented in Table 2. The thickness measurements at locations away from the failure ranged from 0.630 to 0.666 inch. The allowable thickness range for 5/8-inch-thick plate produced to SA516 is 0.615 to 0.665 inch as set forth in ASME SA-20, "Specification for General Requirements for Steel Plates for Pressure Vessels"; thus all readings except the one at 0.666 inch were within the allowable thickness range for 5/8-inch-thick plate. The last thickness reading listed in the column under "Fracture Line" was 0.600 inch, below the allowable thickness range. However, that measurement was located in the region where the propagating crack had turned prior to arresting. Thus that low value resulted from deformation associated with the separation of the plate. Generally, the lower thickness readings were obtained in regions where the vessel had stretched, e.g., between the girth welds and the stiffener rings and between the stiffener rings. However, the change in thickness in those regions along the length of the vessel was not uniform as was the change in circumference.

TABLE 2. RESULTS OF ULTRASONIC THICKNESS MEASUREMENTS ALONG THE LENGTH OF THE FAILED UF_6 SHIPPING CONTAINER[a]

Distance from Drain End Girth Weld, inches	Thickness at Indicated Clock Position or Location, inch				
	3	6	9	12	Fracture Line[b]
3	0.656	0.654	0.658	0.648	0.644
6	0.654	0.642	0.650	0.648	0.646
9	0.657	0.645	0.646	0.645	0.641
12	0.656	0.646	0.650	0.650	0.643
15	0.657	0.649	0.653	0.650	0.643
18	0.662	0.654	0.657	0.656	0.636
21	fillet weld adjacent to the drain end stiffener, ring				
24	0.663	0.658	0.666	0.650	0.652
27	0.656	0.643	0.657	0.654	0.653
30	0.652	0.642	0.645	0.652	0.650
33	0.645	0.643	0.656	0.651	0.648
36	0.657	0.650	0.652	0.650	0.645
39	0.656	0.645	0.648	0.654	0.648
42	0.654	0.642	0.642	0.649	0.643
45	0.652	0.650	0.650	0.652	0.644
48	0.657	0.648	0.656	0.652	0.645
51	0.653	0.659	0.654	0.652	0.649
54	0.662	0.654	0.657	0.653	0.650
57[c]	0.659	0.651	0.660	0.652	0.642
60[c]	0.658	0.652	0.653	0.651	0.633
63	0.664	0.655	0.653	0.656	0.644
66	0.656	0.650	0.649	0.656	0.650
69	0.654	0.652	0.642	0.646	0.633
72	0.650	0.650	0.642	0.642	0.600[c]
75	0.655	0.643	0.646	0.641	--
78	0.653	0.646	0.651	0.642	--
81	0.651	0.644	0.636	0.640	--
84	0.652	0.649	0.643	0.641	--
87	0.657	0.641	0.648	0.640	--
90	0.661	0.651	0.657	0.639	--
93	0.665	0.648	0.649	0.640	--
96	fillet weld adjacent to the valve end stiffener ring				
99	0.660	0.644	0.646	0.639	--
102	0.653	0.642	0.644	0.636	--
105	0.646	0.632	0.640	0.630	--
108	0.643	0.636	0.636	0.630	--
111	0.644	0.652	0.639	0.639	--
114	0.649	0.649	0.643	0.639	--

(a) Measured with a Krautkramer Digital Ultrasonic Thickness Tester.
(b) In the unfailed portion of the vessel in line axially with the rupture and the cracks in the middle and drain-end stiffener rings.
(c) The middle stiffener ring was located between these inch marks.

Another series of thickness measurements was made on either side of the valve-end stiffener ring at each clock position around the circumference of the vessel. Those measurements are listed in Table 3. The thickness measured at those locations ranged from 0.637 to 0.655 inch. The minimum thicknesses were measured at the 11 o'clock position, which was approximately 6 inches circumferentially away from the region where the rupture initiated in the vessel plate.

To assess the extent of local deformation resulting from the failure process, a third series of thickness measurements was made between the 11 and 12 o'clock positions in the region where the vessel plate had ruptured (between the 5-ft-4-in and 9-ft-8-in-length marks). A 1-inch-square grid was drawn on the vessel surface and ultrasonic thickness measurements were made at the grid intersections. Figure 15 illustrates the grid network and the thickness measurements made are tabulated in Table 4.

Those thickness measurements show that the vessel shell had thinned significantly during the failure process, particularly in the regions where the crack propagated in a shear mode. For example, the measurements for Row A, about 1 inch from the fracture, and extending from the stiffener ring toward the valve-end head, decreased from 0.609 to 0.538 inch. Also the thickness was reduced over the region extending about 6 inches circumferentially on either side of the fracture. However, near the valve-end stiffener, as is indicated by the readings at the 7-ft-11-in- and 8 ft-3-in locations, the presence of the stiffener and the fillet welds between the stiffeners and the vessel plate restrained deformation.

After the section of the vessel was received at Battelle, thickness measurements were made as close to the fracture surface as was possible using a ball-end micrometer. Those measurements were made at 1-inch intervals along the length of the relatively straight portion of the fracture. Those readings were taken over a length of 20 inches from the valve-end stiffener ring in the direction of the girth weld between the shell and the valve-end head. In the other direction, measurements were made for a distance of 24 inches (where the crack turned between the valve-end stiffener and the middle stiffener. Those results are listed in Table 5.

TABLE 3. RESULTS OF THICKNESS MEASUREMENTS ADJACENT TO VALVE-END STIFFENER RING AROUND THE CIRCUMFERENCE OF THE VESSEL

Clock Position	Thickness, inch	
	Valve Side	Drain Side
1	0.641	0.646
2	0.648	0.646
3	0.655	0.654
4	0.650	0.653
5	0.650	0.653
6	0.645	0.648
7	0.649	0.651
8	0.643	0.645
9	0.643	0.648
10	0.645	0.651
11	0.637	0.639
12	0.643	0.644

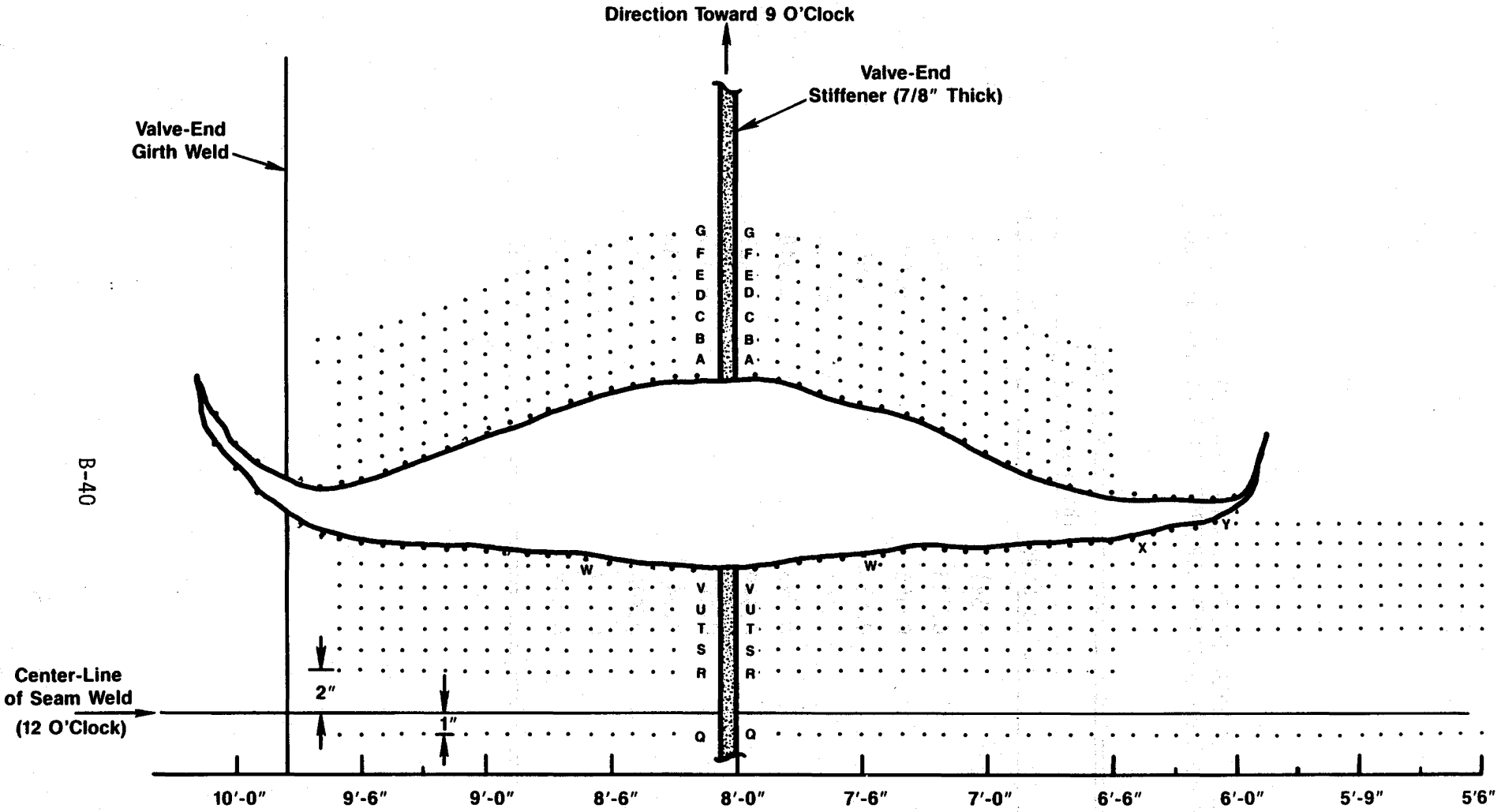

FIGURE 15. MAP SHOWING LOCATIONS OF VESSEL-SHELL WALL THICKNESS MEASUREMENTS ON EITHER SIDE OF THE RUPTURE

The measurements made in the laboratory with a micrometer were made at the locations of the dots adjacent to fracture surface.

TABLE 4. RESULTS OF ULTRASONIC VESSEL WALL THICKNESS MEASUREMENTS IN THE VICINITY OF THE RUPTURE AT THE LOCATIONS SHOWN IN FIGURE 15

A. Rows A through G

Distance From Drain End Girth Weld, feet and inches	Thickness, inches						
	A	B	C	D	E	F	G
6' - 6"	0.000	0.000	0.000	0.000	0.636	0.634	0.638
6' - 7"	0.581	0.599	0.614	0.625	0.627	0.632	0.636
6' - 8"	0.587	0.608	0.618	0.625	0.630	0.637	0.640
6' - 9"	0.587	0.608	0.611	0.629	0.633	0.636	0.635
6' - 10"	0.586	0.000	0.622	0.629	0.641	0.640	0.638
6' - 11"	0.596	0.613	0.620	0.632	0.638	0.642	0.643
7' - 0"	0.594	0.613	0.619	0.627	0.633	0.638	0.637
7' - 1"	0.603	0.627	0.625	0.628	0.633	0.636	0.636
7' - 2"	0.602	0.628	0.624	0.639	0.636	0.634	0.637
7' - 3"	0.596	0.626	0.624	0.631	0.637	0.638	0.638
7' - 4"	0.610	0.624	0.626	0.627	0.636	0.639	0.640
7' - 5"	0.607	0.627	0.626	0.630	0.639	0.637	0.640
7' - 6"	0.597	0.615	0.627	0.630	0.638	0.637	0.640
7' - 7"	0.596	0.617	0.626	0.630	0.636	0.639	0.637
7' - 8"	0.601	0.621	0.629	0.635	0.640	0.642	0.638
7' - 9"	0.608	0.629	0.636	0.645	0.644	0.642	0.640
7' - 10"	0.616	0.632	0.637	0.644	0.641	0.644	0.640
7' - 11"	0.635	0.637	0.638	0.636	0.639	0.639	0.636
(The drain-end side of the stiffener is in approximate alignment with 8' - 0".)							
8' - 3"	0.609	0.627	0.632	0.633	0.637	0.635	0.634
8' - 4"	0.598	0.617	0.628	0.630	0.636	0.639	0.638
8' - 5"	0.592	0.613	0.622	0.629	0.637	0.635	0.636
8' - 6"	0.586	0.610	0.619	0.627	0.640	0.635	0.636
8' - 7"	0.588	0.608	0.615	0.624	0.632	0.633	0.635
8' - 8"	0.588	0.608	0.619	0.625	0.630	0.635	0.635
8' - 9"	0.585	0.606	0.619	0.622	0.625	0.634	0.634
8' - 10"	0.584	0.608	0.616	0.621	0.628	0.628	0.633
8' - 11"	0.582	0.605	0.615	0.626	0.626	0.639	0.629
9' - 0"	0.577	0.604	0.615	0.626	0.626	0.630	0.636
9' - 1"	0.572	0.604	0.612	0.620	0.626	0.630	0.628
9' - 2"	0.574	0.604	0.610	0.621	0.628	0.630	0.629
9' - 3"	0.558	0.600	0.613	0.622	0.625	0.634	0.630
9' - 4"	0.556	0.610	0.615	0.623	0.626	0.630	0.635
9' - 5"	0.561	0.604	0.612	0.618	0.625	0.627	0.631
9' - 6"	0.555	0.602	0.607	0.623	0.623	0.628	0.630
9' - 7"	0.538(a)	0.589(b)	--(c)	--(c)	--(c)	0.627	0.633
9' - 8"	--	--	--	--	--	0.627	0.632

(a) Edge of fracture, 1/4" from girth weld
(b) Edge of girth weld
(c) Over girth weld

TABLE 4. RESULTS OF ULTRASONIC VESSEL WALL THICKNESS MEASUREMENTS IN THE VICINITY OF THE RUPTURE AT THE LOCATIONS SHOWN IN FIGURE 15

B. Rows Q through Y

Distance From Drain End Girth Weld, feet and inches	Thickness, inches								
	Q	R	S	T	U	V	W	X	Y
5' - 4"				0.640	0.650	0.647	0.649	0.647	0.646
5' - 5"				0.637	0.650	0.649	0.642	0.635	0.633
5' - 6"				0.637	0.637	0.637	0.635	0.636	0.636
5' - 7"				0.637	0.643	0.635	0.634	0.631	0.628
5' - 8"				0.634	0.635	0.634	0.633	0.622	0.620
5' - 9"				0.636	0.626	0.626	0.618	0.611	0.607
5' - 10"				0.630	0.623	0.623	0.607	0.598	0.589
5' - 11"				0.629	0.621	0.614	0.602	0.587	0.566
6' - 0"				0.624	0.622	0.616	0.597	0.580	0.545
6' - 1"				0.625	0.619	0.615	0.591	0.568	
6' - 2"				0.621	0.610	0.601	0.590	0.555	
6' - 3"				0.617	0.608	0.600	0.586	0.551	
6' - 4"				0.616	0.608	0.600	0.579	0.529	
6' - 5"				0.615	0.613	0.597	0.582		
6' - 6"	0.643	0.632	0.622	0.612	0.605	0.586	0.575		
6' - 7"	0.643	0.632	0.623	0.620	0.607	0.591	0.574		
6' - 8"	0.642	0.633	0.623	0.619	0.605	0.594	0.572		
6' - 9"	0.638	0.632	0.624	0.619	0.606	0.592	0.573		
6' - 10"	0.639	0.638	0.625	0.614	0.606	0.588	0.570		
6' - 11"	0.640	0.630	0.622	0.610	0.612	0.591	0.575		
7' - 0"	0.647	0.639	0.625	0.613	0.612	0.585	0.563		
7' - 1"	0.646	0.646	0.638	0.611	0.609	0.588	0.553		
7' - 2"	0.643	0.629	0.623	0.613	0.601	0.587	0.551		
7' - 3"	0.642	0.626	0.620	0.617	0.604	0.589	0.546		
7' - 4"	0.643	0.625	0.620	0.618	0.606	0.588	0.580		
7' - 5"	0.644	0.624	0.621	0.620	0.605	0.584	0.569		
7' - 6"	0.648	0.629	0.620	0.621	0.606	0.593	!		
7' - 7"	0.649	0.628	0.622	0.620	0.610	0.587	Too		
7' - 8"	0.644	0.631	0.624	0.623	0.618	0.590	Close		
7' - 9"	0.653	0.634	0.628	0.626	0.617	0.590	to		
7' - 10"	0.647	0.635	0.634	0.629	0.628	0.607	Crack		
7' - 11"	0.644	0.640	0.631	0.635	0.636	0.618	!		
(The drain-end side of the stiffener is in approximate alignment with 8'-0".)									
8' - 3"	0.643	0.636	0.633	0.637	0.629	0.607	!		
8' - 4"	0.645	0.631	0.628	0.627	0.618	0.594	Too		
8' - 5"	0.644	0.629	0.624	0.624	0.613	0.594	Close		
8' - 6"	0.640	0.629	0.621	0.623	0.607	0.585	to Crack		
8' - 7"	0.644	0.627	0.620	0.621	0.607	0.582	!		
8' - 8"	0.641	0.623	0.619	0.623	0.604	0.583	0.561		
8' - 9"	0.642	0.622	0.616	0.617	0.605	0.584	0.571		
8' - 10"	0.641	0.631	0.617	0.616	0.605	0.585	0.569		
8' - 11"	0.649	0.623	0.619	0.627	0.605	0.587	0.540		
9' - 0"	0.639	0.623	0.618	0.620	0.602	0.585	0.546		
9' - 1"	0.638	0.626	0.620	0.613	0.601	0.595	0.560		
9' - 2"	0.639	0.628	0.620	0.616	0.613	0.590	0.566		
9' - 3"	0.641	0.629	0.625	0.614	0.607	0.601	0.564		
9' - 4"	0.649	0.631	0.624	0.620	0.600	0.596	0.569		
9' - 5"	0.643	0.631	0.624	0.618	0.605	0.592	0.562		
9' - 6"	0.645	0.632	0.626	0.623	0.610	0.593	0.572		
9' - 7"	0.643	0.638	0.627	0.622	0.611	0.596	0.583		

TABLE 5. VESSEL WALL THICKNESS MEASUREMENTS MADE ADJACENT TO THE FRACTURE SURFACE WITH A MICROMETER

A. Thickness adjacent to the fracture surface toward the vessel seam weld.

Distance toward Valve End from Valve End Stiffener, inches	Thickness at the Fracture Surface Edge, inches (a)	Distance toward Drain End from Valve End Stiffener, inches	Thickness at the Fracture Surface Edge, inches (a)
1	0.544	1	0.526
2	0.531	2	0.529
3	0.531	3	0.522
4	0.512	4	0.505
5	0.501	5	0.500
6	0.496	6	0.496
7	0.485	7	0.482
8	0.483	8	0.485
9	0.484	9	0.487
10	0.482	10	0.491
11	0.479	11	0.478
12	0.477	12	0.480
13	0.476	13	0.475
14	0.479	14	0.485
15	0.477	15	0.475
16	0.477	16	0.477
17	0.479	17	0.475
18	0.479	18	0.475
19	0.476	19	0.477
19 1/2	0.486	20	0.475
20	Edge of the girth weld	21	0.476
		22	0.481
		23	0.487
		24	0.500

(a) Thickness measurements made with 1-inch ball-end micrometer at Battelle.

TABLE 5. VESSEL WALL THICKNESS MEASUREMENTS MADE ADJACENT TO THE FRACTURE SURFACE WITH A MICROMETER

B. Thickness adjacent to the surface on the fracture half away from the seam weld.

Distance toward Valve End from Valve End Stiffener, inches	Thickness at the Fracture Surface Edge, inches (a)	Distance toward Drain End from Valve End Stiffener, inches	Thickness at the Fracture Surface Edge, inches (a)
1	0.526	1	0.530
2	0.522	2	0.528
3	0.507	3	0.512
4	0.500	4	0.505
5	0.497	5	0.499
6	0.490	6	0.492
7	0.485	7	0.492
8	0.486	8	0.485
9	0.478	9	0.490
10	0.487	10	0.490
11	0.481	11	0.486
12	0.487	12	0.490
13	0.478	13	0.492
14	0.479	14	0.491
15	0.475	15	0.490
16	0.475	16	0.492
17	0.474	17	0.492
18	0.484	18	0.493
19	0.495	19	0.490
19-1/2	0.494	20	0.494
19-7/8	(Edge of Girth Weld)	21	0.492
		22	0.491
		23	0.492
		24	0.494

(a) Thickness measurements made with 1-inch ball-end micrometer at Battelle.

The thickness measurements adjacent to the fracture surface between the valve-end stiffener and the girth weld ranged from 0.544 to 0.474 inch. Near the stiffener ring and near the girth weld, the thickness was not reduced as much as in the region between 10 inches to 19 inches from the stiffener. Over that 9-inch length the thickness was nearly constant. A similar pattern of thickness variation was observed over the 24-inch length of fracture extending from the valve-end stiffener toward the middle stiffener.

Various thickness measurements made during the onsite investigation and after the sections containing the rupture surfaces were received at Battelle show that the vessel shell did measurably thin over a distance extending approximately 6 inches circumferentially on either side of the rupture. The greatest amount of thinning occurred adjacent to the fracture surfaces which would be expected for a ductile failure. The minimum thickness measured, 0.474 inch, represented a 24-percent reduction from the nominal wall thickness of 0.625 inch.

As was stated previously, for most of its length, the fracture in the vessel shell propagated in a ductile shear mode. It was requested that the angle of the fracture surface relative to the plate surfaces be determined. To assess that angle, the length of the slanted or angled face on the fracture surface was measured at each location that a micrometer thickness measurement was made. The angle then was calculated by dividing the wall thickness by that length. That ratio defined the sine of the angle of fracture. Those calculations showed that the fracture angle in the regions of shear propagation ranged from about 44.5 to 54.3 degrees. In the regions where the thickness was essentially constant, the fracture angle was 51 degrees. Near the stiffener that angle increased; for example, one inch from the stiffener the fracture angle ranged from 61 to 70 degrees and immediately below the stiffener, that angle appeared to be essentially 90 degrees to the vessel inner and outer surfaces.

Examination of Inside Surface of the Vessel

After the external features of the vessel were examined and the various measurements described in the previous sections were made, the drain-end head was removed by plasma-arc cutting to permit access to the inside of the vessel. The inner surfaces of the vessel then were cleaned to provide an acceptable level of radioactivity prior to entering the vessel. The plasma arc cutting and the cleaning were performed by Sequoyah Fuels personnel.

Examination of the inside surface of the vessel revealed no evidence of cracking of the shell material and no evidence of significant general corrosion or localized pitting of the surfaces. Cracks were detected in the butt welds of the internal backup rings used for the girth welds between the valve-end and drain-end heads and the vessel shell. Those cracks were located about 1 inch and 3-1/2 inches below the 9 o'clock position in the two backup rings, respectively, and about 9 and 4 inches, respectively, below the 3 o'clock position. Thus, those cracks were not aligned with the vessel rupture and did not contribute to the failure.

The regions of the vessel shell immediately below the cracks in the middle and drain-end stiffener rings also were inspected from the inside surface by the investigator from Welding Consultants, Inc., using a Parker DA200 AC/DC Magnetic Particle Unit. No evidence of cracks were obtained using the magnetic particle inspection unit. Subsequently, those regions were inspected using a Nortec No. 131 Ultrasonic Ultrascope with a 0.5-inch-diameter, 2.25 MHz, 70-degree probe; cellulose gel was used as the couplant. That inspection revealed one indication of a flaw below the fillet weld on the drain-end side of the drain-end stiffener. The depth of that indication was estimated to be 3/16 inch maximum. No other indications of flaws were obtained during that inspection.

The extent of bulging on the inside surface was measured between the stiffeners by laying a straightedge across the internal locations corresponding to stiffeners and measuring the maximum gap between the straightedge and the inner surface of the vessel shell. The maximum gap occurred approximately midway between the stiffeners. The results of those measurements are listed in the following tabulation:

Clock Position	Maximum Bulge at Inner Surface, inch	
	Between Valve End and Middle Stiffeners	Between Drain End and Middle Stiffeners
1	-(a)	14/32
2	15/32	14/32
3	15/32	14/32
4	14/32	13/32
5	13/32	13/32
6	11/32	12/32
7	10/32	13/32
8	15/32	13/32
9	15/32	13/32
10	(a)	13/32
11	(a)	11/32
12	(a)	10/32

(a) No measurements could be made at these locations because of deformation of vessel shell during failure.

Where direct comparisons can be made (the 3 and 9 and the 2 and 8 clock positions), those measurements indicate that the amount of bulge or increase in diameter was somewhat greater between the valve-end stiffener and the middle stiffener than it was between the drain-end stiffener and the middle stiffener. That same result was obtained from the circumference measurements described previously.

Selection of Sections for Laboratory Examination

Following the inspection of the failed vessel, sections of it were selected for further examination and analyses at Battelle. Those sections included the rupture region, the crack in the middle stiffener, and the crack in the drain-end stiffener and sections located approximately 180 degrees from the rupture and the cracks in the stiffeners. In addition, the Battelle team was asked to select sections approximately 180 degrees from the rutpure and the stiffener cracks for evaluation by the vessel manufacturer, Trinity Industries, Inc. The sizes and locations of the various sections selected for evaluation at Battelle are shown in Figure 7. The locations and sizes of those sections, designated by the letter T, also are shownin in Figure 7.

Outlines of the sections to be removed were drawn on the outer surface of the vessel as is shown in Figure 16. Sequoyah Fuels personnel removed those sections by plasma arc cutting. Spot check temperature measurements made using Tempil Sticks and a Kiethly Temperature Indicator with a surface probe thermocouple at various times during the thermal cutting process revealed that the temperature of the steel at distances greater than 2 inches from the plasma-arc cut did not exceed 200 F. After cutting, the sections for Battelle were scrubbed by Sequoyah Fuels personnel and the alpha radiation level was determined by a Sequoyah Fuels health-physics representative. The values for the alpha radiation ranged from less than 500 to 6,000 counts, radiation dosage ranged from less than 0.2 to 3.0 mR/hr, and the smearable radiation was less than 200. Those sections then were crated and shipped by truck to Battelle on February 15, 1986.

METALLURGICAL INVESTIGATION AT BATTELLE

Decontamination and Initial Sectioning of the Vessel Samples

When the crate containing the sections from the failed shipping container was opened at Battelle, radiation measurements on the various sections were conducted. Those surveys revealed that the total counts of all forms of radiation (alpha, beta, and gamma) being emitted to be greater than 250,000 counts on some of those sections. The counts for only alpha radiation and the smearable radiation were similar to those obtained by the Sequoyah health-physics personnel. The high level of total counts precluded handling of the sections in Battelle's normal "cold" laboratory facilities because of the risk of contaminating those facilities. This situation resulted in material handling difficulties and added significant effort early in the study to decontaminate the sections to acceptable radiation levels for general laboratory work. The decontamination treatments consisted of removing the paint from the outer surfaces of the sections and washing all surfaces, except the fracture surfaces from the rupture and the stiffener cracks, with detergents. Various solvents, such as acetone, methylene chloride, chlorothane and a commercial paint remover, were used to remove the paint; the

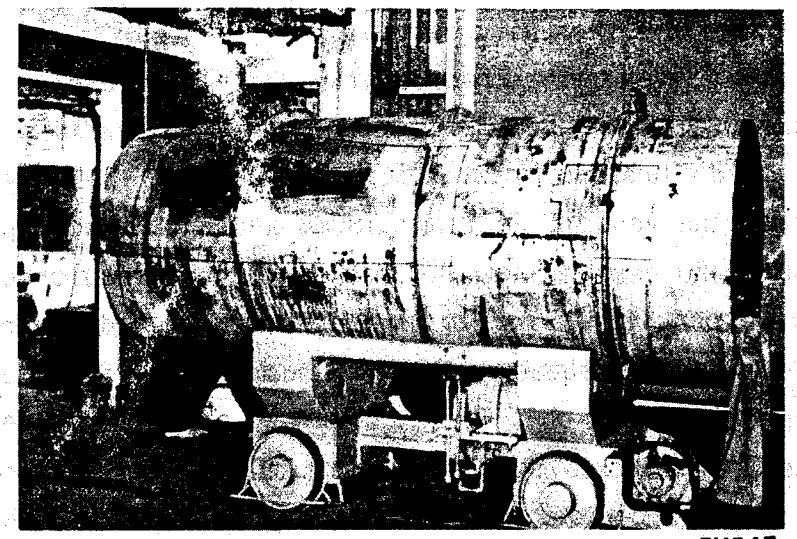

5M547

a. Locations of Sections 0VFB and 0DB

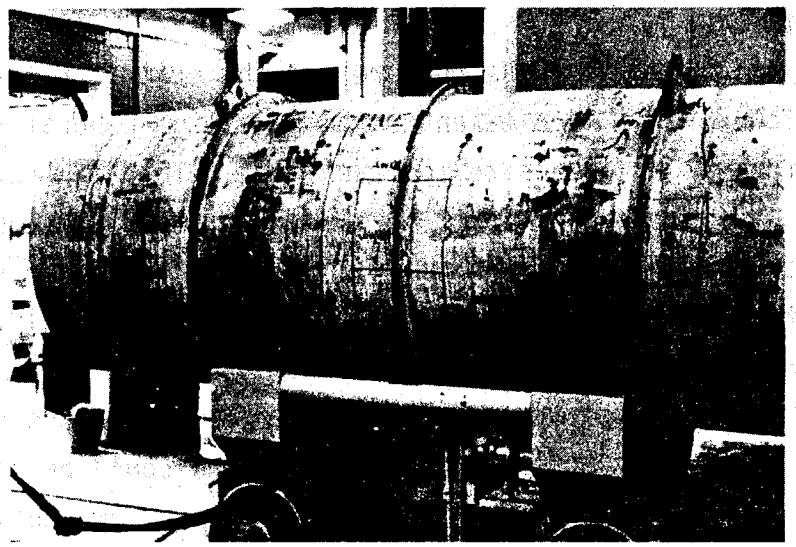

5M548

b. Locations of Sections 180VFB, 180MB, 180MT, 180DB, and 180DT

FIGURE 16. LOCATIONS OF SECTIONS TO BE REMOVED FROM THE FAILED VESSEL

commercial paint remover, which contained methylene chloride and alcohol, was the most effective for the paint removal.

Although those procedures reduced the radiation levels, the remaining radiation levels were still too high to permit handling and sectioning in the "cold" laboratory facilities. Subsequently, the two smaller sections from the vessel, Sections 180MB and 180DB, were pickled in a hot (120 to 140 F) 50 percent aqueous solution of hydrochloric acid. Pickling under those conditions for about 30 minutes reduced the radiation levels to below background on these smaller pieces. Thereafter, Section 180VB which was approximately 3-1/2 feet square was shipped to the Hot Laboratory at Battelle's West Jefferson, Ohio, site to be sectioned into six smaller pieces which could be treated in the pickling tank. After sectioning, these pieces were returned to Battelle's King Avenue site and pickled. That treatment reduced the levels of radiation on those six pieces to acceptable levels for further handling in the laboratory. Figure 17 shows the six pieces from Section 180VB, identified as 180VB-A through 180VB-F, after sectioning.

The sections containing the rupture and the cracks in the middle and drain-end stiffener rings were taken to the Beryllium Laboratory, which is in the shop at the King Avenue site for machining. That laboratory is equipped to handle radioactive and toxic metals. Initially Section OVFB, which contained the rupture and the crack in the middle stiffener ring, was saw cut to remove the portion that contained the crack in the stiffener ring. That section then was identified as OMB. Saw cuts then were made axially from the ends of the remaining portion of OVFB to the ends of the rupture in valve-end-head and the vessel plate so that the rupture could be separated into two halves to facilitate examination of the fracture surfaces.

In addition, axial saw cuts were made in the vessel shell in Sections OMB and ODB to the edges of the fillet welds between the stiffener rings and the vessel shell. Those sections were immersed in liquid nitrogen and the remaining portion of the steel in the vessel shell was fractured in a hydraulic press to separate the surfaces of the cracks in the stiffener rings. That procedure was conducted in such a manner so as not to damage the surfaces of the cracks. The surfaces of the press and the surrounding floor

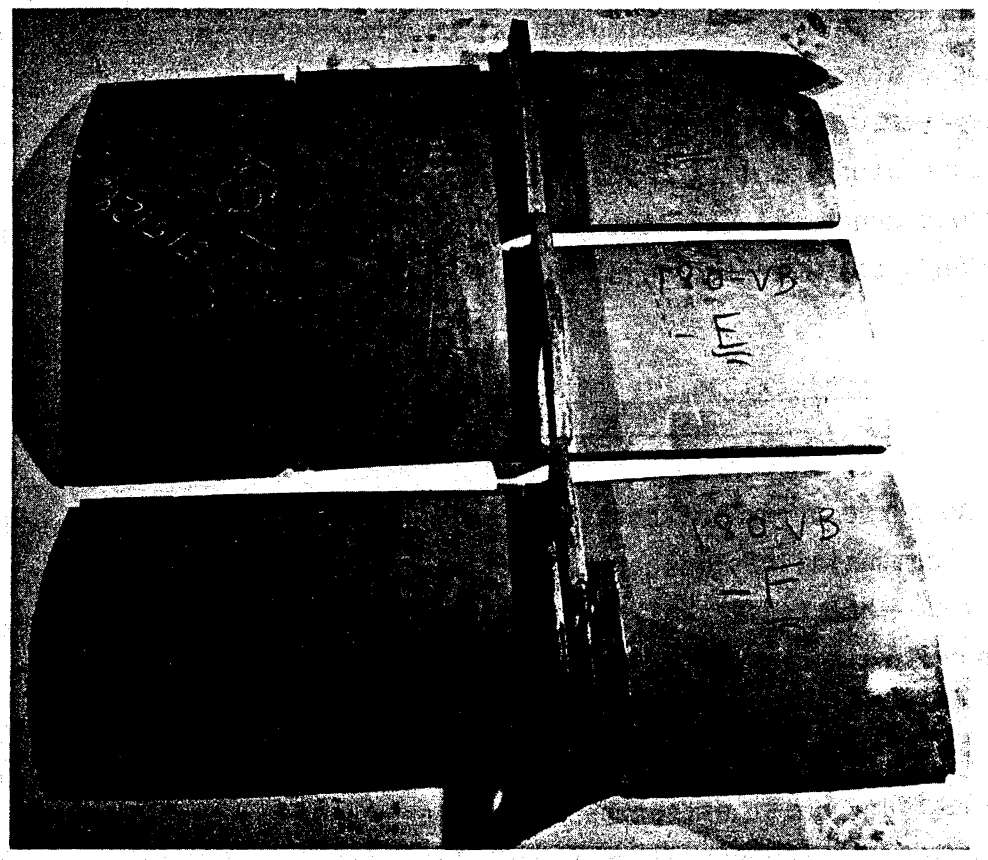

7766-12

FIGURE 17. SECTION 180 VB AFTER SAWING INTO SIX SMALLER PIECES TO FACILITATE DECONTAMINATION BY ACID PICKLING

were covered with heavy paper to prevent radioactive contamination. Also, radiation surveys were conducted in the area of the press before and after the fracturing procedure to assure that contamination did not occur. The procedure of separating the surfaces on the stiffener-ring cracks was witnessed by representatives of Kerr-McGee, Lawrence Livermore Laboratories, and Dr. Robert Block from the University of Oklahoma. Subsequently, the sections containing the matching fracture surfaces through the valve-end, middle, and drain-end stiffener rings, including the vessel shell material below these fractures were removed from the various larger sections in the Beryllium Laboratory so that they could be examined more readily. This sectioning was done with the concurrence of the previously mentioned representatives and was witnessed by them.

Evaluations of the Steels From the Vessel Shell and the Three Stiffener Rings

The purpose of this portion of the investigation was to evaluate the chemical compositions, mechanical properties, and microstructures of the steels from the vessel shell and the three stiffener rings to determine whether the materials met the applicable specifications, to determine whether microstructural features were present that may have contributed to the failure, and to provide data for use in the stress analysis portion of the investigation. Most of the specimens for these evaluations were taken from the sections of the vessel that were located approximately 180 degrees from the failure location. The specific locations of the various samples and the procedures used in the various evaluations will be described in the subsequent sections.

As was described previously, the vessel shell was specified to be fabricated from steel conforming to the requirements of ASME SA516, Grade 70. The specification for the steel used to fabricate the stiffeners was not reported to Battelle. However, for other shipping containers, ASME SA36 steel reportedly has been used for the stiffener rings.

Chemical Analyses

Chemical analyses of the shell and each of the three stiffener rings were obtained using emission spectrographic analytical techniques by the Worthington Steel Company, Worthington, Ohio. The samples of the shell and of the three stiffener rings that were analyzed were obtained from regions of the failed shipping cylinder that were located approximately 180 degrees from the ruptured side of the cylinder. The identifications of the samples and a description of the location from which they were obtained are given below:

Sample Identification	Sample Source
180VB-A	The sample of the shell was removed from Part A of Piece 180VB at a location adjacent to the CT specimens
180VB-E	The sample of the valve-end stiffener ring was removed from Part E of Piece 180VB at a location adjacent to the tensile specimens of the stiffener ring
180MB	The sample of the middle stiffener ring was removed from Piece 180MB at a location adjacent to the tensile specimens of that stiffener ring
180DB	The sample of the drain-end stiffener ring was removed from Piece 180DB at a location adjacent to the tensile specimens of that stiffener ring

The chemical analyses were made in accordance with ASTM Specification E415-71. All samples were flattened under a press to increase the cross-sectional area available for multiple analyses. A total of twenty determinations of the chemical composition of each sample were made and the average content, standard deviation, and coefficient of variance of each element analyzed was calculated. Ten determinations were made on one surface of each sample, after which that surface of each sample was ground below the burn and ten more determinations were made on the freshly ground surface.

In addition, the compositions of two NBS standard steel samples for chemical analyses were determined to verify the accuracy of the analytical procedures. Seven determinations were made on one of the standards, NBS1261A, and 14 determinations were made on the second standard, NBS1262. After the first 7 determinations were made, the NBS1262 standard sample was ground and 7 additional determinations were made. The average of the elemental contents of the NBS standard samples and the standard deviations and coefficients of variance of the results were calculated for each element. The results fo the chemical analyses of the shell are presented in Table 6. Table 7 presents the results of the chemical analyses of the three stiffener rings along with the product analysis ranges for SA-36 steel bars and AISI 1020 steel. For information purposes to show the accuracy of the chemical analyses, the results of the emission spectrographic analyses of the NBS1261A and NBS1262 standard samples are presented in Tables 8 and 9, respectively.

The chemical composition determined for the cylinder shell satisfied the chemical requirements of SA516, Grade 70 steel. The contents of the residual elements in the shell were considered to be normal. The results of the analyses of the stiffener rings indicated that the chemical compositions of the three stiffener rings were very similar. The carbon, phosphorus, and sulfur contents of each stiffener ring satisfied the chemical requirements of those elements for SA36 steels, but the managanese content of each stiffener was less than that specified for a product analysis of SA36 steel. Thus, the chemical compositions indicate that the stiffener rings were not fabricated from SA36 steel. However, the chemical compositions determined for the steels from the stiffener rings did meet the check analyses range for AISI/SAE 1020 steel. Those analyses also would satisfy the check analyses requirements for AISI/SAE 1015, 1017, and 1023 steels. Thus, it is likely that the stiffener rings were produced from one of those grades of steels, probably AISI/SAE 1020.

Tensile Properties

The tensile properties of the steel from the vessel shell and the three stiffener rings were determined at both room temperature and 180 F. The specimens used for those measurements were standard round

TABLE 6. RESULTS OF THE EMISSION SPECTROGRAPHIC ANALYSES OF THE RUPTURED SHELL OF THE CYLINDER

Elements	Content, weight percent: SA516 Grade 70 Chemical Requirements[a]	Content, weight percent: Cylinder Shell, Sample 180VB-A, average[b]	Standard Deviation	Coefficient of Variance
Carbon	0.28 max	0.199	0.006	2.9
Manganese	0.79-1.30	0.925	0.012	1.3
Phosphorus	0.035 max	0.007	0.000	4.1
Sulfur	0.04 max	0.022	0.002	8.6
Silicon	0.13-0.45	0.171	0.003	1.8
Copper		0.091	0.001	1.5
Tin		0.005	0.000	8.5
Nickel		0.120	0.002	1.3
Chromium		0.127	0.002	1.5
Molybdenum		0.042	0.001	2.6
Aluminum		0.013	0.002	12.0
Vanadium		0.002	0.000	15.0
Niobium		0.001	0.001	70.0
Zirconium		0.000		
Titanium		0.000		
Boron		0.000		
Tungsten		0.000		
Cobalt		0.007		
Lead		0.000		

(a) Product analysis for sections over 1/2 inch in thickness.

(b) Average of 20 individual analyses.

TABLE 7. RESULTS OF THE EMISSION SPECTROGRAPHIC ANALYSES OF THE THREE STIFFENER RINGS

Element	SA36 (Bars) Chemical Requirements[a]	AISI/SAE 1020 Steel, Check Analysis Range	Valve-End Stiffener, Sample 180VB-E, Average, (S.D.)[b] (C.V.)[c]	Middle Stiffener, Sample 180MB, Average, (S.D.)[b] (C.V.)[c]	Drain-End Stiffener, Sample 180DB, Average, (S.D.)[b] (C.V.)[c]
	Content, weight percent				
Carbon	0.31 max	0.16-0.25	0.205 (0.010) (4.8)	0.203 (0.007) (3.6)	0.195 (0.006) (3.1)
Manganese	0.54-0.98	0.22-0.63	0.461 (0.007) (1.6)	0.462 (0.011) (2.5)	0.455 (0.010) (2.1)
Phosphorus	0.05 max	0.045 max	0.019 (0.001) (3.8)	0.018 (0.001) (5.0)	0.017 (0.001) (4.3)
Sulfur	0.06 max	0.055 max	0.038 (0.003) (6.7)	0.035 (0.002) (6.7)	0.031 (0.002) (6.2)
Silicon	--	0.32 max	0.053 (0.002) (3.6)	0.053 (0.003) (5.8)	0.053 (0.003) (4.8)
Copper			0.145 (0.004) (3.0)	0.152 (0.006) (3.8)	0.149 (0.005) (3.5)
Tin			0.011 (0.001) (6.6)	0.011 (0.001) (8.2)	0.010 (0.001) (7.1)
Nickel			0.105 (0.002) (1.8)	0.109 (0.003) (2.5)	0.108 (0.002) (2.3)
Chromium			0.108 (0.002) (1.8)	0.111 (0.003) (2.7)	0.110 (0.003) (2.5)
Molybdenum			0.021 (0.001) (4.7)	0.022 (0.002) (7.6)	0.021 (0.001) (7.0)
Aluminum			0.001 (0.001) (71)	0.001 (0.001) (73)	0.001 (0.001) (88)
Vanadium			0.000	0.000	0.000
Niobium			0.000	0.000	0.000
Zirconium			0.000	0.000	0.000
Titanium			0.000	0.000	0.000
Boron			0.0002	0.0002	0.0001
Tungsten			0.000	0.000	0.000
Cobalt			0.006	0.006	0.006
Lead			0.000	0.000	0.000

(a) Includes product analysis tolerances per ASME SA-6 Specification, Table B.
(b) S.D. - Standard Deviation.
(c) C.V. - Coefficient of Variance.
(d) Silicon content can be specified as 0.10 max, 0.10/0.22, or 0.15 to 0.30.

TABLE 8. RESULTS OF THE EMISSION SPECTROGRAPHIC ANALYSIS OF NBS 1261A STANDARD STEEL SAMPLE FOR CHEMICAL ANALYSES

Element	Content, Weight Percent: NBS 1261A, Certified Composition	Content, Weight Percent: Check Analysis, Average	Standard Deviation	Coefficient of Variance	NBS 1261A vs. Check Analysis, Difference, weight percent
Carbon	0.391	0.401	0.006	1.6	0.010
Manganese	0.670	0.679	0.010	1.5	0.009
Phosphorus	0.016	0.016	0.000	3.1	0.000
Sulfur	0.015	0.015	0.001	5.9	0.000
Silicon	0.228	0.223	0.005	2.3	-0.005
Copper	0.042	0.045	0.002	3.5	0.003
Tin	0.010	0.011	0.001	6.3	0.001
Nickel	2.000	2.047	0.026	1.3	0.047
Chromium	0.693	0.679	0.011	1.6	-0.014
Molybdenum	0.190	0.200	0.004	2.0	0.010
Alminum	0.021	0.021	0.001	3.3	0.000
Vanadium	0.011	0.013	0.000	3.5	0.002
Niobium	0.022	0.028	0.002	6.4	0.006
Zirconium	0.009	0.010	0.000	3.9	0.001
Titanium	0.021	0.022	0.000	1.9	0.001
Boron	0.0005	0.0005	0.0000	9.5	0.0000
Tungston	0.017	0.018	0.002	12.0	0.001
Cobalt	0.032	0.032	0.001	2.8	0.000
Lead	0.000	0.003	0.000	14.0	0.003

TABLE 9. RESULTS OF THE EMISSION SPECTROGRAPHIC ANALYSIS OF NBS 1262 STANDARD STEEL SAMPLE FOR CHEMICAL ANALYSES

Element	Content, weight percent: NBS 1262, certified composition	Content, weight percent: Check Analysis, average	Standard Deviation	Coefficient of Variance	NBS 1262 vs. Check Analysis, Difference, weight percent
Carbon	0.160	0.149	0.010	6.6	-0.011
Manganese	1.040	1.071	0.053	5.0	0.031
Phosphorus	0.042	0.038	0.004	11.0	-0.004
Sulfur	0.038	0.032	0.004	12.0	-0.006
Silicon	0.390	0.388	0.021	5.5	-0.002
Copper	0.500	0.541	0.024	4.5	0.041
Tin	0.016	0.019	0.002	13.0	0.003
Nickel	0.590	0.610	0.027	4.5	0.020
Chromium	0.300	0.295	0.015	5.0	-0.005
Molybdenum	0.068	0.069	0.006	9.0	0.001
Aluminum	0.092	0.076	0.003	4.0	-0.016
Vanadium	0.041	0.041	0.003	6.2	0.000
Niobium	0.290	0.287	0.021	7.4	-0.003
Zirconium	0.190	0.204	0.018	8.6	0.014
Titanium	0.084	0.100	0.006	6.2	0.016
Boron	0.0025	0.0022	0.0003	14.0	-0.0003
Tungsten	0.210	0.227	0.011	5.0	0.017
Cobalt	0.300	0.307	0.013	4.3	0.007
Lead	0.000	0.004	0.001	28.0	0.004

tensile specimens with a reduced-section diameter of 0.5 inch. The specimens from the vessel shell were removed from Piece 180VB-A, which was located approximately 180 degrees from the rupture. The locations of the tensile specimen blanks prior to sectioning are shown in Figure 18. Those specimens were oriented parallel to the primary rolling direction of the plate which was determined by metallographic examination of specimens oriented normal to and parallel to the axis of the cylinder removed from the steel. Examination of those metallographic specimens revealed that the primary rolling direction (longitudinal) was the circumferential direction in the shell. The piece from which the tensile specimens were removed was not flattened.

The tensile specimens from the valve-end, middle, and drain-end stiffener rings were removed from Pieces 180VB, 180MB, and 180DB, respectively. Figure 19 illustrates the locations of the tensile specimen blanks in Pieces 180VE, 180MB, and 180DB prior to sectioning. Because one of the specimens from the middle stiffener ring was damaged during loading into the testing machine, two additional tensile specimens were prepared from Piece 0MB; the locations of those specimens blanks also are shown in Figure 19.

The tensile tests conducted at room temperature were performed in accordance with the procedures set forth in ASTM Designation, "Standard Methods and Definitions for Mechanical Testing of Steel Products". The tensile tests conducted at 180 F were performed in accordance with the procedures set forth in ASTM Designation E21, "Standard Recommended Practice for Elevated Temperature Tension Tests of Metallic Materials". Electric resistance heated tapes were used to heat the specimens to 180 F. Two Chromel-Alumel (Type K) thermocouples attached to the shoulders of the specimens at each end of the reduced section were used to monitor the temperature of the specimens. The specimens were heated to 180 F $\pm$ 5 F and heated for 20 minutes after the temperature had equalized and there was less than 5 F difference in the readings of the two thermocouples.

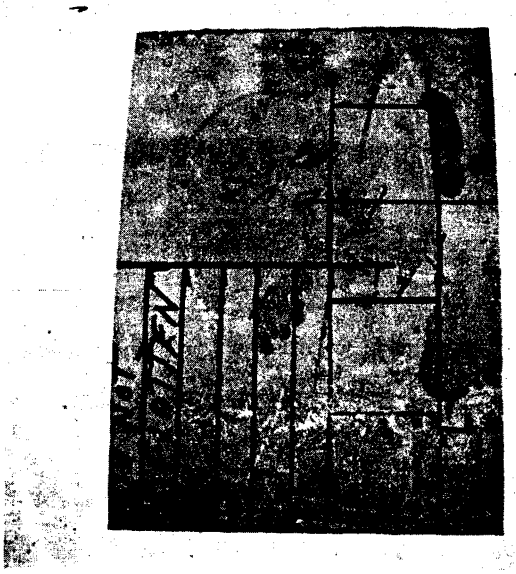

5M551

FIGURE 18. LOCATION OF TENSILE SPECIMEN BLANKS 1 THROUGH 6, COMPACT TENSION SPECIMEN BLANKS CHEMICAL ANALYSIS SPECIMEN AND METALLOGRAPHIC SPECIMENS IN PIECE 180 VB-A FROM THE VESSEL SHELL

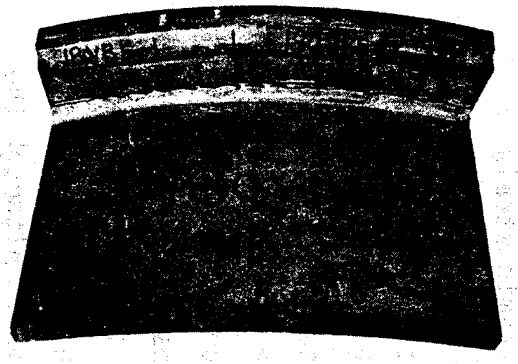

5M554

a. Valve-End Stiffener Ring, Piece 180VBE

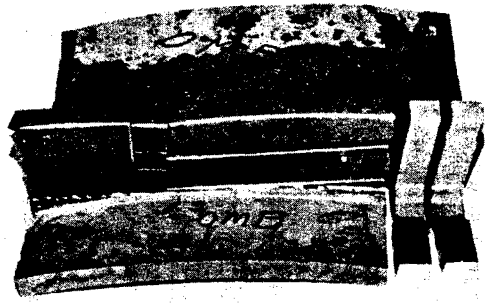

5M552

b. Middle Stiffener Ring, Piece 0MB

5M553

c. Middle Stiffener Ring Piece 180MB

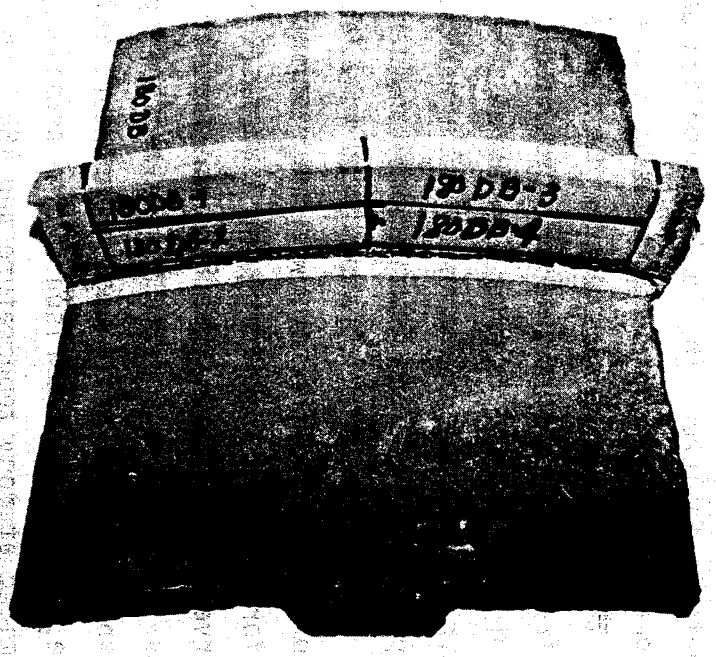

SM550

d. Drain-End Stiffener Ring, Piece 180DB

FIGURE 19. LOCATIONS OF THE TENSILE SPECIMEN BLANKS FROM THE STIFFENER RINGS

The tests at room temperature were conducted at a strain rate of 0.005/minute through maximum load and then the strain rate was increased to 0.05/minute to failure. The load/deformation data for the specimens were plotted on an x-y recorder and also on a disc in a computer. The engineering tensile properties and the true stress-true strain curves were calculated from the data obtained from each test. The engineering tensile properties of the steels from the vessel shell and the three stiffener rings at both room temperature and 180 F are listed in Table 10. For comparison purposes, the room temperature tensile property requirements for ASME SA516, Grade 70 steel also are listed in Table 10. Since the material specified for the stiffener rings was not reported to us, no specified properties for the stiffener rings are listed. The true stress-true strain data and curves for the specimens are presented in Appendix A.

As is shown in Table 10, the tensile properties of the steel from the vessel shell determined at room temperature met the requirements for SA516, Grade 70 steel. Comparison of the tensile properties of the vessel steel determined at room temperature and 180 F shows that at 180 F the ultimate tensile strength was reduced by 5 percent, the yield strength was increased by 7.5 percent, the percent elongation was reduced by 7.6 percent, and the reduction in area was increased by 1.8 percent. The increase in yield strength with test temperature was attributed to strain aging of the specimen during heating to the test temperature or to dynamic strain aging during testing.

The tensile specimens from the stiffener rings tested at both room temperature and 180 F exhibited tensile properties that were dependent upon the location the specimens were within the rings. Those specimens that were located near the outer surface of the rings (see Figure 19) exhibited higher yield strengths and reduction in areas, but lower elongation than did the specimens that were located nearer the inner surfaces of the rings. The differences in the yield strengths exhibited by the specimens from the stiffener rings is believed to be the result of the Bauschinger effect, which was caused by the strain introduced when the rings were formed. Although the forming procedures were not reported to Battelle, it appeared that the rings

TABLE 10. TENSILE PROPERTIES OF THE STEELS FROM THE VESSEL SHELL AND THE STIFFENERS AT ROOM TEMPERATURE AND AT 180 F[a]

Sample Number	Component	Test Temperature,[b] F	Ultimate Tensile Strength, ksi	Yield Tensile Strength, (0.2% Offset) ksi	Elongation, percent in 2 inches	Reduction in Area, percent
180 VBA-1	Vessel Shell	RT	73.5	47.4	29.0	66.9
180 VBA-2	Vessel Shell	RT	72.9	48.1	30.0	66.7
SA-516, Grade 70 Steel Specified Properties		RT	70/ 90	38.0 min	21.0 min	--
180 VBA-4	Vessel Shell	180	69.5	50.7	27.5	70.0
180 VBA-5	Vessel Shell	180	69.5	52.0	27.0	66.0
180 VB E-1	Valve-End	RT	72.5	57.8	23.5	57.4
180 VB E-2	Stiffener	RT	73.2	48.9	24.0	51.1
180 VB E-3	Valve-End	180	70.2	54.4	18.5	54.1
180 VB E-4	Stiffener	180	71.6	44.8	21.5	48.3
180 MB-2	Middle	RT	72.1	58.0	23.0	56.0
180 MB-2	Stiffener	RT	70.0	45.9	26.0	51.7
0 MB-1	Middle	180	69.1	52.0	20.0	54.6
180 MB-4	Stiffener	180	69.0	42.4	23.0	51.2
180 DB-1	Drain-End	RT	70.9	55.7	24.5	58.6
180 DB-2	Stiffener	RT	70.6	43.6	27.0	55.3
180 DB-3	Drain-End	180	69.4	53.6	21.0	56.0
180 DB-4	Stiffener	180	68.6	40.4	22.0	54.1

(a) Properties determined with standard round tensile specimens with a 0.500-inch-diameter reduced section. The specimens were oriented parallel to the primary rolling direction of the plate or bar.

(b) RT = Room Temperature.

were formed by rolling nominally 7/8-inch-thick by 2-1/2-inch-wide bar stock into the ring configuration. As a result of that forming, the material nearer the outer surface was strained in tension and the material nearer the inner surface was strained in compression. Thus when the specimens from nearer the inner surface were strained in tension during the tensile tests, they exhibited a lower yield strength. The yield strengths of the specimens from nearer the outer surface probably were higher than those that would be measured from undeformed stiffener ring steel because of work hardening that occurred during forming. Thus, the differences in the yield strengths of the specimens from the stiffener rings were not surprising.

Comparison of the properties of the specimens from the stiffener rings tested at 180 F with those tested at room temperature shows that the tensile properties were reduced slightly at the higher test temperature as would be expected. The ultimate tensile strengths were reduced by about 3 percent and the yield strengths were reduced by between 4 and 10 percent.

Comparison of the tensile properties of the vessel shell and the stiffener rings shows that on the average they were similar at both room temperature and at 180 F.

Drop-Weight-Tear Tests (DWTT) of Vessel-Shell Steel

To assess the toughness of the vessel-shell steel, the fracture propagation transition temperature was determined by conducting drop-weight-tear tests in accordance with the procedures set forth in ASTM Designation E-436, "Standard Method for Drop-Weight-Tear Tests of Ferritic Steels". Specimens parallel to the primary rolling direction of the vessel steel plate were prepared from Pieces 180VB B and C. Thus, the crack in the specimens would propagate in the same direction as the fracture in the vessel. The specimens were 3 inches wide, by 12 inches long, by the actual wall thickness (nominally 0.625 inch). After the specimen blanks were cut from Pieces 180VB and 180VBC, they were flattened by reverse rolling. The 12-inch-long sides were machined parallel and the notch was pressed into one of the sides at the midlength of the specimens.

The specimens were tested over the temperature range from 0 to 130 F to define the brittle-to-ductile fracture appearance transition temperature. The results of the drop-weight-tear tests are presented in Table 11 and plotted in Figure 20. The fracture appearances of the specimens as a function of test temperature are illustrated in Figure 21. In rating the fracture appearance, the regions on the fracture surfaces equivalent to one thickness of the specimen below the notch and also adjacent to the opposite edge (the region where the hammer strikes) is disregarded.

As is shown from the data presented in Table 11 and Figure 20, fractures in the steel from the vessel shell will propagate from a critical size flaw in a completely ductile (shear) mode at temperatures of 80 F and above. The temperature of the vessel at the time that rupture occurred was estimated to be about 180 F, and the crack propagated in a completely ductile (shear) mode as would be expected based upon the DWTT results.

J-Resistance Curves

The stress-analysis portion of the failure investigation required data regarding the fracture initiation and propagation behavior of the steel at the estimated failure temperature. That information was obtained by determining the J-resistance (J-R) curves for the vessel steel. J is a measure of fracture toughness of ductile materials and a J-R curve shows how J varies with crack extension in the material.

The J-R curves were determined with specimens removed from Piece 180VBA (see Figure 18). The specimens were machined to the configuration shown in Figure 22 (1T compact-tension specimen), except that the specimen thickness was 0.594 inch. The specimens were precracked in accordance with the procedures set forth in ASTM Designation 813, "Standard Test Method for J_{Ic}, A Measure of Fracture Toughness". Electrical leads were welded to the specimens to permit the electric-potential (E-P) technique to be

TABLE 11. RESULTS OF DROP-WEIGHT TEAR TESTS OF THE STEEL FROM THE VESSEL SHELL

Specimen Number	Test Temperature, F	Energy Absorbed, ft-lbs	Shear Area, percent
2C	0	345	4
3C	30	345	5
10B	30	345	8
4C	50	1104	45
12B	50	553	27
5C	60	1396	42
9B	60	5035	100
1C	70	4889	100
7B	70	2521	86
6C	80	4527	100
8B	80	4889	100
11B	130	4817	100

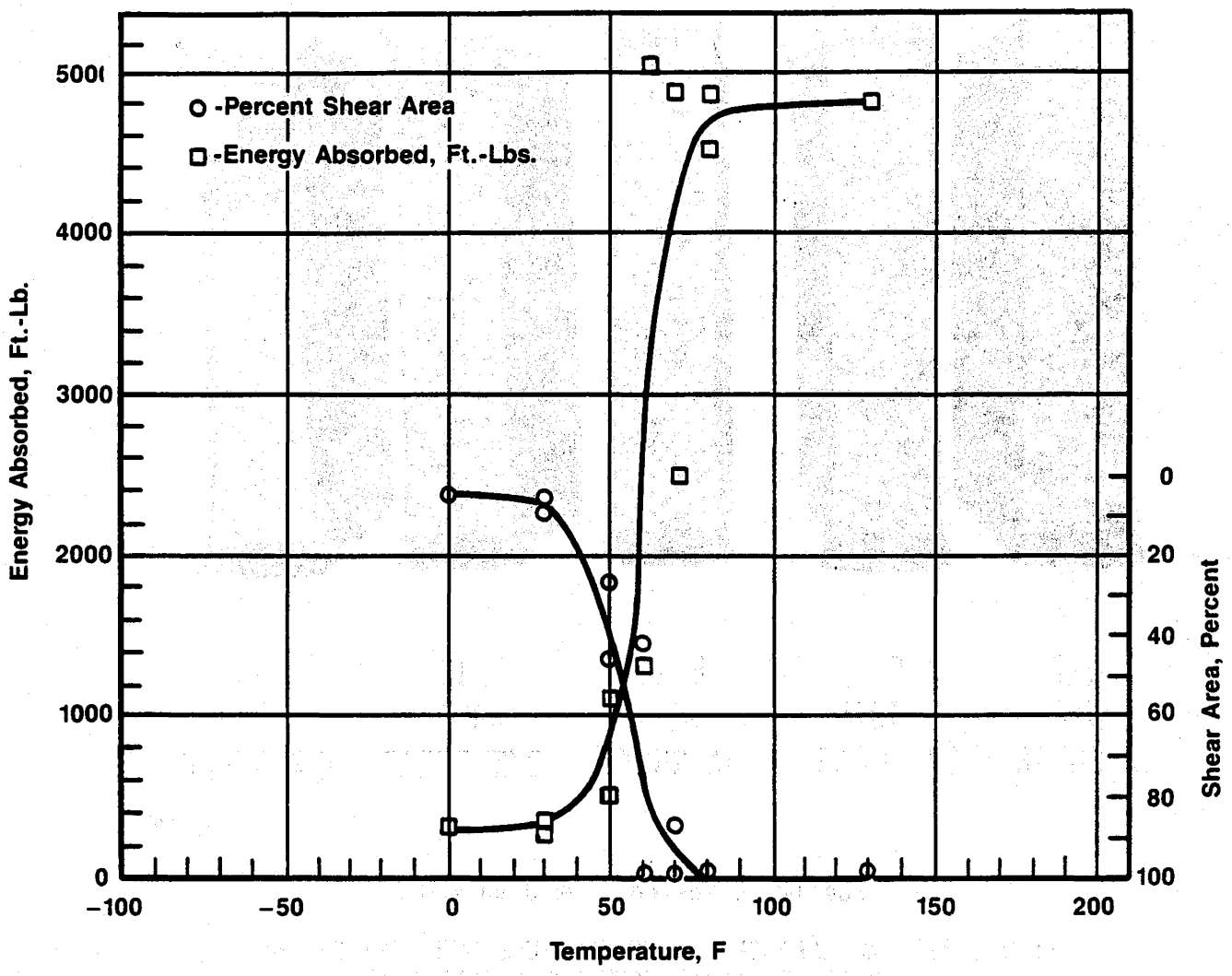

FIGURE 20. RESULT OF DROP-WEIGHT-TEAR TESTS OF SPECIMENS FROM THE VESSEL SHELL

Longitudinal specimens.

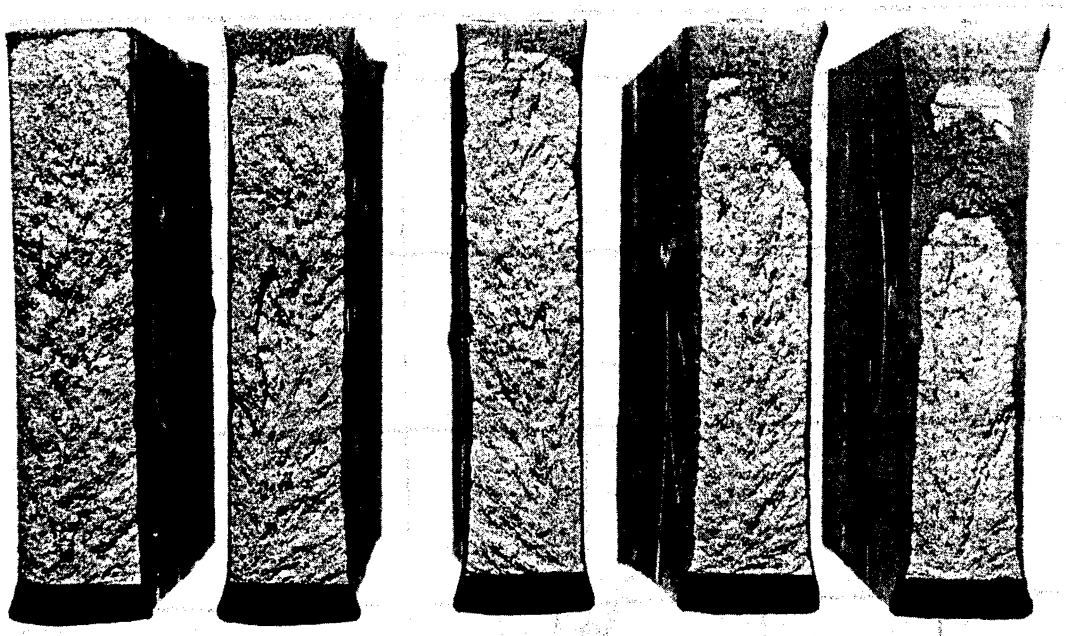

C-2	C-3	B-10	B-12	C-4
0°F	30°F	30°F	50°F	50°F
4% SHEAR	5% SHEAR	8% SHEAR	27% SHEAR	45% SHEAR

4M883

1X

a. Specimens Tested from 0 to +50 F

FIGURE 21. APPEARANCE OF THE FRACTURE SURFACES OF THE DWTT SPECIMENS FROM THE VESSEL PLATE

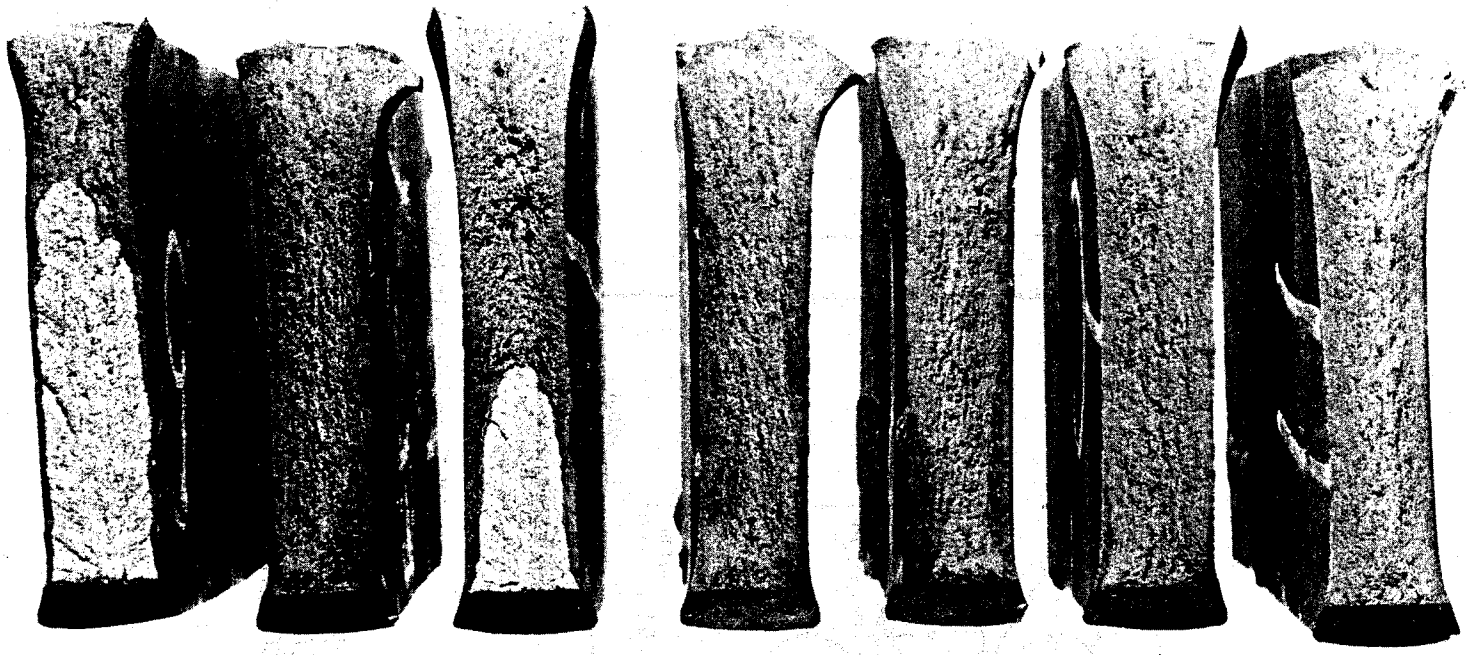

C-5	B-9	B-7	C-1	B-8	C-6	B-11
60°F	60°F	70°F	70°F	80°F	80°F	130°F
42% SHEAR	100% SHEAR	86% SHEAR	100% SHEAR	100% SHEAR	100% SHEAR	100% SHEAR

1X 4M884

b. Specimens Tested from +60 to +130 F

FIGURE 21. (Continued)

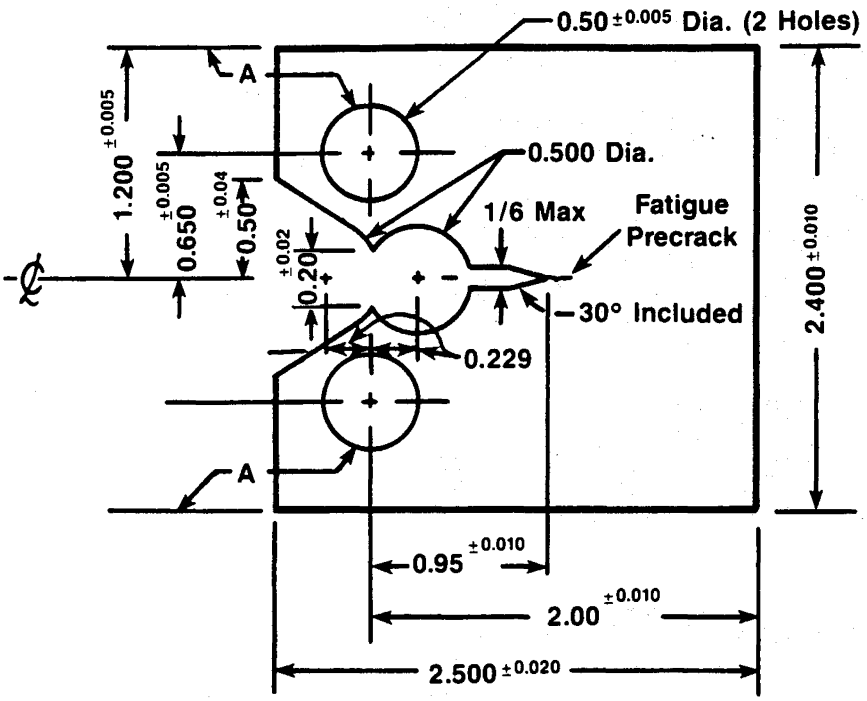

FIGURE 22. PLAN-VIEW DIMENSIONS OF THE COMPACT TENSION SPECIMENS USED TO DETERMINE THE J-RESISTANCE CURVES; THE SPECIMEN THICKNESS WAS 0.594 INCH

used to indicate crack initiation and crack propagation. Duplicate tests were conducted at 180 F. The temperature was monitored with a Type J thermocouple spot welded to the specimen at a location approximately 1/2 inch from the crack tip. Heating was accomplished by electric resistance heated tapes wrapped around the specimens. The specimen and heating tape were surrounded by 1-inch-thick ceramic fiber insulation to minimize heat loss.

Deformation $J(J_D)$ and modified $J(J_M)$ were calculated from the data obtained from each specimen. J_D was calculated in the manner specified in ASTM E813-81 following a method developed by Ernst and Paris that takes into account crack growth:*

$$J_{D(i+1)} = \left[J_{D(i)} + \left(\frac{\eta}{b}\right)_i \left(\frac{A_{i,i+1}}{B_N}\right)\right] \left[1 - \left(\frac{\gamma}{b}\right)_i \left(a_{i+1} - a_i\right)\right] .$$

The subscripts i and i+1 relate to test record increments, and the parameters η, γ, and b (defined below) are updated between each step.

$$\eta = 2 + 0.522\ b/W$$
$$\gamma = 1 + 0.76\ b/W$$
$$b = [W - (a_o + \Delta a)]$$

J_M was calculated in the manner developed by Ernst, Paris, and Landes using the following expression:**

$$J_{M(i+1)} = J_{D(i+1)} + \int_{a_o}^{a_{i+1}} J_p \left(\frac{\gamma}{b}\right) da .$$

In calculating both J_D and J_M, no account was taken of the thinning of the specimen ahead of the crack or of the thickening at the at the back edge.

---

* Ernst, H. A., and Paris, P. C., "Techniques of Analysis of Load-Displacement Records by J-Integral Method", U.S. Nuclear Regulatory Commission Report NUREG (CR-122), January 1980.

** Ernst, H. A., Paris, P. C., and Landes, J. D., "Estimation of the J-Integral and Tearing Modulus T from Single Specimen Test Records", Fracture Mechanics-13th Conference, ASTM STP 743, R. Roberts, Ed., American Society for Testing and Materials, 1981, pp 476-502.

Plots of J_D and J_M versus crack extension are shown in Figures 23 and 24 for the two specimens. Tabulated data for the compact specimens are presented in Table 12.

Comparison of the data from the two specimens showed that the results were extremely reproducible. Thus, the data for the initial portion of the J-R curve were used to determine J at initiation of the crack extension in accordance with the procedures in ASTM E813-81. Evaluation of that value of J with regard to the validity criteria in the ASTM procedure revealed that a valid J_{Ic} resulted from the tests. The values of J_{Ic} for the vessel steel at 180 F was 600 in-lb/in^2. The information obtained from the J-R measurements was provided to the investigators conducting the stress analysis portion of this study.

Microstructural Evaluations of Sections From the Vessel Shell and the Stiffener Rings

The microstructures of sections of the steel from the vessel shell and the three stiffener rings were evaluated to assess if features present in those microstructures may have contributed to the failure. Initially, two sections of the vessel shell were removed from Piece 180-MB to determine the primary rolling direction of the steel plate. The surface examined on one of those sections was parallel to the axis of the vessel and the surface examined on the other section was parallel to the circumferential direction of the vessel. Based upon the lengths of the inclusions observed in those sections, it was concluded that the primary rolling direction of the plate was the circumferential direction in the vessel.

Sections parallel to and transverse to the primary rolling direction were removed from Piece 180VBA and prepared for metallographic examination. Sections parallel to and transverse to the length of each stiffener ring also were prepared for metallographic examination. Those sections were removed from the portions of the stiffener rings on Pieces 180VB, 0-MB and 0DB. The sections from the middle and drain-end stiffeners were removed from those portions of the stiffeners on Pieces 0MB and 0DB because insufficient nonheat-affected (from the plasma arc cutting) material remained on Pieces 180MB and 180DB after the tensile specimens and chemical analysis

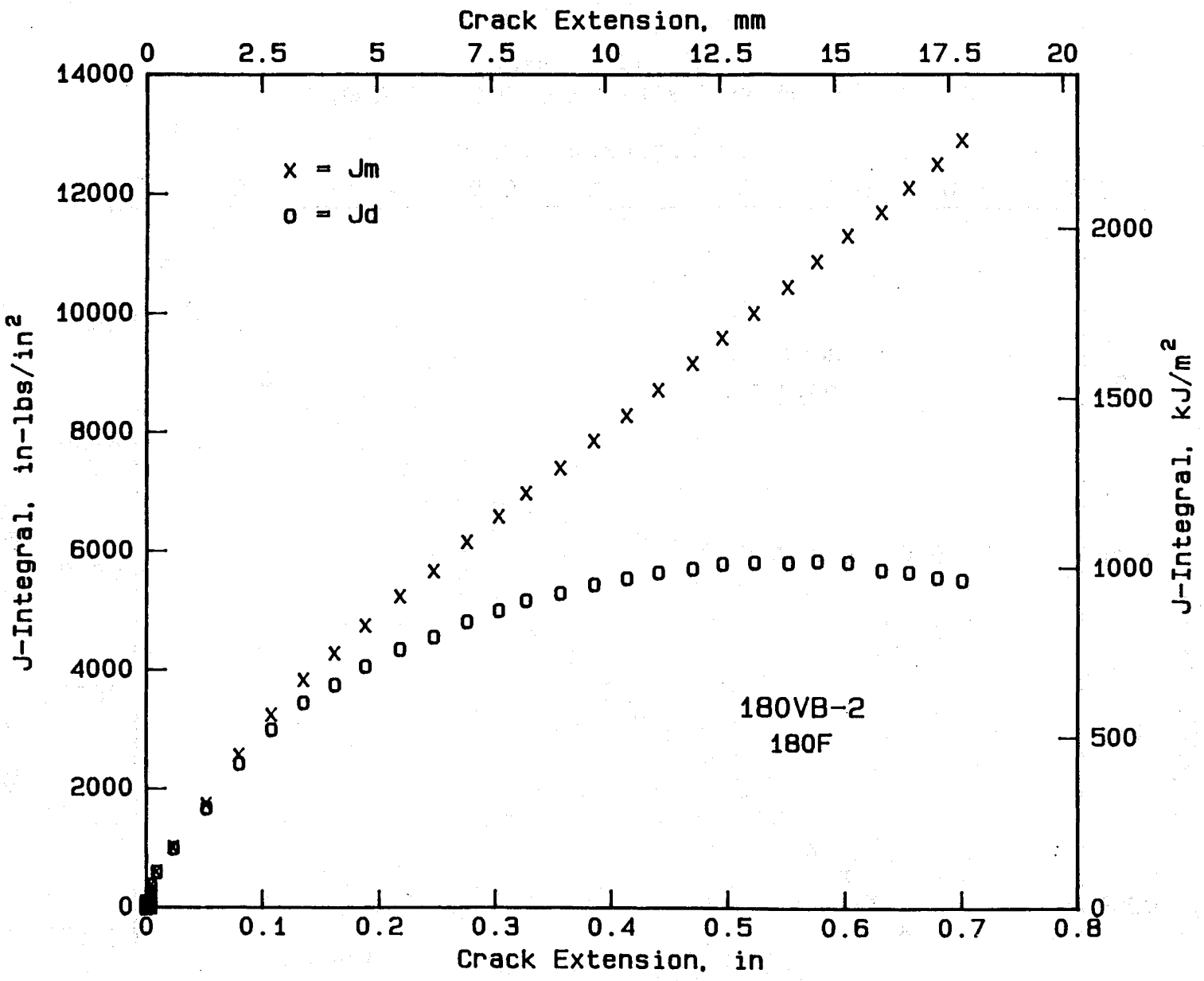

FIGURE 23. J-RESISTANCE CURVE FOR SPECIMEN 180VB-2 TESTED AT 180 F

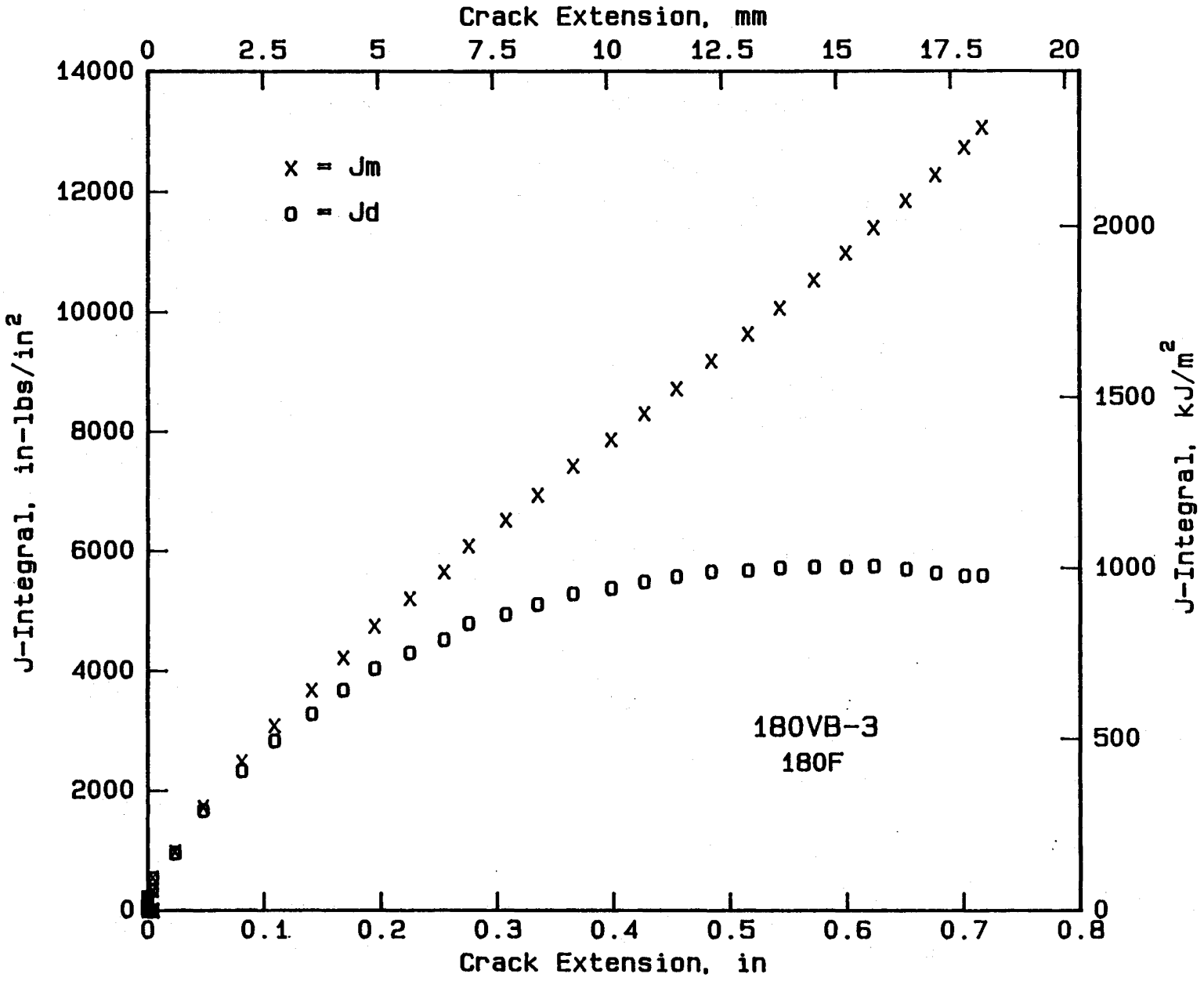

FIGURE 24. J-RESISTANCE CURVE FOR SPECIMEN 180VB-3 TESTED AT 180 F

TABLE 12. RESULTS OF J-RESISTANCE CURVE TESTS

A. Specimen 180VB-2

180vb-2	2.000	0.594 W	1.0247 B	1.05 A0	500.5 2y	1.6986 U0	180F Af
Load, lbs	Disp, in	EP, uV	Crack Length, in	Jd, lbs/in	Delta-a, in	Jmod, lbs/in	
0	0	500.5	1.0247	0.0	0.0000	0.0	
348.31	0.0008	500.5	1.0247	0.5	0.0000	0.5	
766.81	0.002	502.9	1.0293	3.1	0.0046	3.1	
1165.6	0.0029	500.5	1.0247	6.6	0.0000	6.6	
1541.6	0.0038	500.5	1.0247	11.3	0.0000	11.3	
1941.6	0.0047	500.5	1.0247	17.4	0.0000	17.4	
2454.6	0.0059	500.5	1.0247	27.7	0.0000	27.7	
2864.6	0.007	498	1.0247	39.1	0.0000	39.1	
3279.6	0.0084	498	1.0247	55.8	0.0000	55.8	
3675.6	0.0099	500.5	1.0247	76.1	0.0000	76.1	
4061.6	0.0115	500.5	1.0247	100.2	0.0000	100.2	
4515.6	0.0139	502.9	1.0293	139.3	0.0046	139.6	
4920.6	0.0168	502.9	1.0293	192.8	0.0046	193.1	
5257.6	0.0201	502.9	1.0293	258.4	0.0046	258.7	
5638.6	0.0259	502.9	1.0293	381.9	0.0046	382.2	
5984.6	0.0356	505.4	1.0342	598.1	0.0095	600.7	
6253.6	0.0532	512.7	1.0484	1000.3	0.0237	1015.8	
6385.6	0.083	527.3	1.0766	1678.8	0.0519	1742.0	
6297.6	0.1157	542	1.1049	2421.5	0.0802	2563.7	
6116.6	0.1426	556.6	1.1326	2993.4	0.1079	3242.8	
5862.6	0.1659	571.3	1.1600	3445.4	0.1353	3825.6	
5589.6	0.1841	585.9	1.1865	3746.3	0.1618	4272.4	
5330.6	0.2036	600.6	1.2128	4054.5	0.1881	4742.5	
5047.6	0.2245	617.7	1.2427	4340.7	0.2180	5233.5	
4769.6	0.2429	634.8	1.2717	4546.2	0.2470	5656.3	
4490.6	0.2649	651.9	1.3002	4808.9	0.2755	6151.7	
4222.6	0.2844	668.9	1.3277	4993.6	0.3030	6579.6	
3924.6	0.3028	683.6	1.3511	5165.9	0.3264	6973.0	
3641.6	0.3235	703.1	1.3808	5286.7	0.3561	7394.4	
3392.6	0.3467	722.7	1.4100	5430.4	0.3853	7853.2	
3162.6	0.3687	742.2	1.4380	5532.3	0.4133	8276.9	
2918.6	0.3919	761.7	1.4652	5634.3	0.4405	8710.7	
2723.6	0.4163	783.7	1.4946	5694.6	0.4699	9152.0	
2503.6	0.4407	803.2	1.5200	5779.2	0.4953	9584.4	
2298.6	0.4651	825.2	1.5471	5800.9	0.5224	9999.5	
2098.6	0.492	849.6	1.5759	5799.5	0.5512	10440.2	
1932.6	0.5188	871.6	1.6010	5822.5	0.5763	10869.2	
1732.6	0.5469	896	1.6273	5803.0	0.6026	11300.5	
1546.6	0.5738	925.3	1.6563	5668.2	0.6316	11690.7	
1399.6	0.603	949.7	1.6799	5634.3	0.6552	12103.3	
1258.6	0.6323	976.6	1.7041	5547.0	0.6794	12500.1	
1111.6	0.6629	1001	1.7253	5499.4	0.7006	12899.1	

TABLE 12. (Continued)

B. Specimen 180VB-3

180vb-3	2.000	0.5935 W	1.0092 B	1.065 A0	498 2y	1.6924 U0	180F Af
Load lbs	Disp in	EP uV	Crack Length in	Jd lbs/in	Delta-a in	Jmod lbs/in	
0	0	500.5	1.0140	0.0	0.0048	0.0	
357.79	0.00134	500.5	1.0140	0.9	0.0048	0.9	
731.29	0.00213	500.5	1.0140	2.6	0.0048	2.6	
1207.89	0.00334	500.5	1.0140	7.1	0.0048	7.1	
1476.89	0.00402	498	1.0092	10.7	0.0000	10.7	
1964.89	0.00523	498	1.0092	18.7	0.0000	18.7	
2365.89	0.0063	498	1.0092	27.6	0.0000	27.6	
2780.89	0.00749	498	1.0092	39.4	0.0000	39.4	
3190.89	0.00884	498	1.0092	54.8	0.0000	54.8	
3600.89	0.01013	498	1.0092	71.7	0.0000	71.7	
4000.89	0.01168	498	1.0092	94.3	0.0000	94.3	
4469.89	0.01394	498	1.0092	131.1	0.0000	131.1	
4816.89	0.01606	498	1.0092	168.9	0.0000	168.9	
5197.89	0.01935	498	1.0092	232.1	0.0000	232.1	
5602.89	0.02461	500.5	1.0141	338.9	0.0049	340.1	
5929.89	0.03392	500.5	1.0141	546.0	0.0049	547.2	
6203.89	0.05296	510.3	1.0333	965.1	0.0241	982.6	
6334.89	0.08421	522.5	1.0572	1675.6	0.0480	1732.7	
6207.89	0.11502	539.6	1.0904	2334.0	0.0812	2481.2	
5968.89	0.13962	554.2	1.1183	2832.8	0.1091	3082.2	
5753.89	0.16442	571.3	1.1504	3284.5	0.1412	3678.7	
5480.89	0.18692	585.9	1.1774	3679.9	0.1682	4217.4	
5221.89	0.20932	600.6	1.2042	4043.0	0.1950	4743.3	
4923.89	0.22952	617.7	1.2343	4299.2	0.2251	5203.7	
4640.89	0.24942	634.8	1.2638	4523.2	0.2546	5646.4	
4328.89	0.26942	647	1.2849	4790.8	0.2757	6083.6	
4059.89	0.29012	666.5	1.3168	4941.0	0.3076	6512.2	
3815.89	0.31092	683.6	1.3442	5109.2	0.3350	6935.8	
3576.89	0.33532	703.1	1.3748	5285.1	0.3656	7418.4	
3292.89	0.35852	725.1	1.4076	5376.4	0.3984	7861.9	
3053.89	0.38172	744.6	1.4359	5486.5	0.4267	8294.3	
2809.89	0.40492	764.2	1.4635	5570.9	0.4543	8712.3	
2584.89	0.43172	786.1	1.4933	5651.7	0.4841	9176.5	
2379.89	0.45862	810.5	1.5247	5672.5	0.5155	9626.8	
2179.89	0.48542	832.5	1.5521	5715.2	0.5429	10065.2	
2003.89	0.51472	856.9	1.5812	5731.7	0.5720	10528.3	
1828.89	0.54402	881.3	1.6088	5733.9	0.5996	10979.3	
1666.89	0.57212	903.3	1.6328	5743.2	0.6236	11400.6	
1510.89	0.60382	930.2	1.6603	5696.1	0.6511	11855.8	
1388.89	0.63442	957	1.6859	5632.0	0.6767	12285.4	
1251.89	0.66732	983.9	1.7105	5580.9	0.7013	12736.4	
1159.89	0.69172	1001	1.7257	5590.3	0.7165	13069.4	

specimens were obtained. Following metallographic preparation, the various sections were examined to identify the microconstituents present, to assess the grain size and to assess the cleanliness of the steels. The grain size was determined using the procedures set forth in the Comparison Method in ASTM Designation E-112, "Standard Methods for Estimating the Average Grain Size of Metals". The inclusion contents of the steels were assessed using the procedures for Microscopic Method A, in ASTM Designation E45-76, "Standard Recommended Practice for Determining the Inclusion Content of Steel".

Typical Microstructures

Figures 25a and b illustrate the typical microstructure of the SA516, Grade 70 steel from the vessel shell. The microstructure was banded and consisted of a mixture of ferrite and pearlite. Those features are typical of hot-rolled carbon steel plate material such as SA516 Grade 70. The average ferrite grain size of the steel was ASTM 9-1/2. That grain size is considered to be relatively fine for a normally produced hot-rolled plate and would be expected to have beneficial effects on the yield strength and toughness of the steel.

Examination of the sections from the stiffener rings revealed a segregation pattern present in the bar stock from which they were produced. That pattern in the transverse section from the three stiffener rings is illustrated in Figure 26. The pattern in the sections of the drain-end and valve-end stiffeners were similar, but that pattern was less pronounced in the section from the middle stiffener. Such segregation patterns frequently are observed in hot-rolled, carbon steel bar stock. The typical microstructures of the steel outside of that central segregation region is shown in Figure 27, and the typical microstructure within the region of segregation is shown in Figure 28. Those figures show that the microstructure consisted of a mixture of ferrite and pearlite with the microstructure in the segregation zone containing more pearlite. The presence of more pearlite in the segregation zone indicates somewhat higher carbon and manganese contents in that region. However, the ferrite grain sizes were virtually the same in both regions and the average grain sizes of the steel from each stiffener was ASTM 8 to 8-1/2.

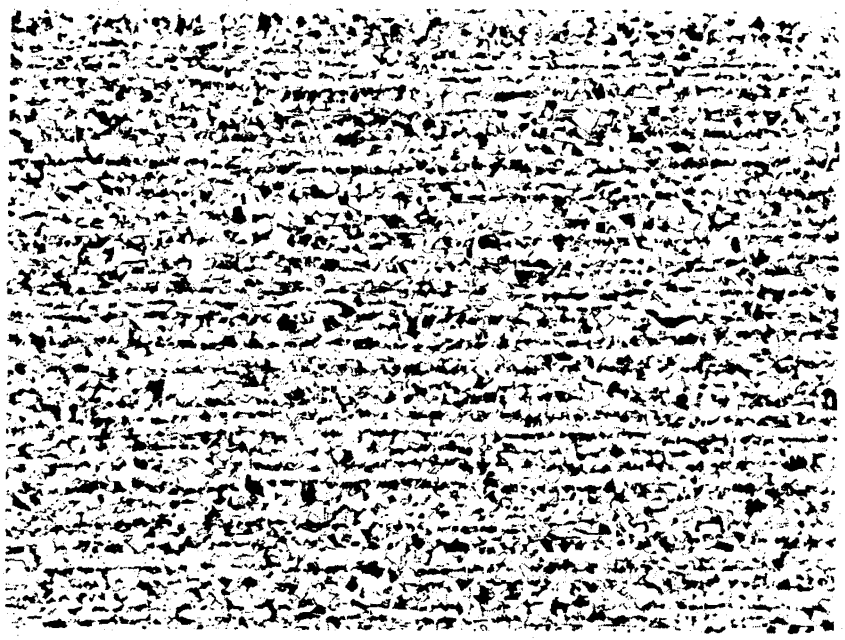

100X Nital Etch 4M879

a.

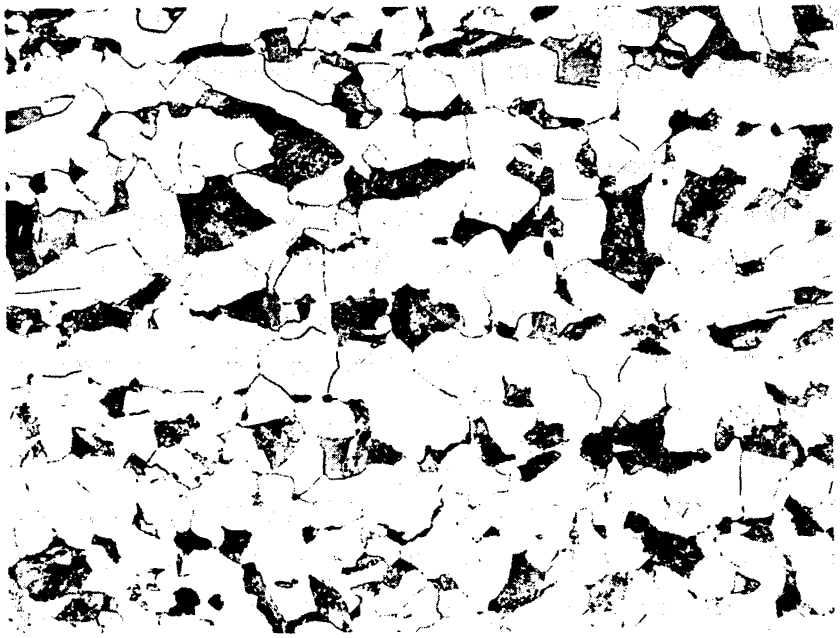

100X Nital Etch 4M880

b.

FIGURE 25. TYPICAL MICROSTRUCTURE OF THE STEEL FROM THE VESSEL SHELL AT TWO MAGNIFICATIONS

The microstructure is banded and consists of a mixture of ferrite and pearlite.

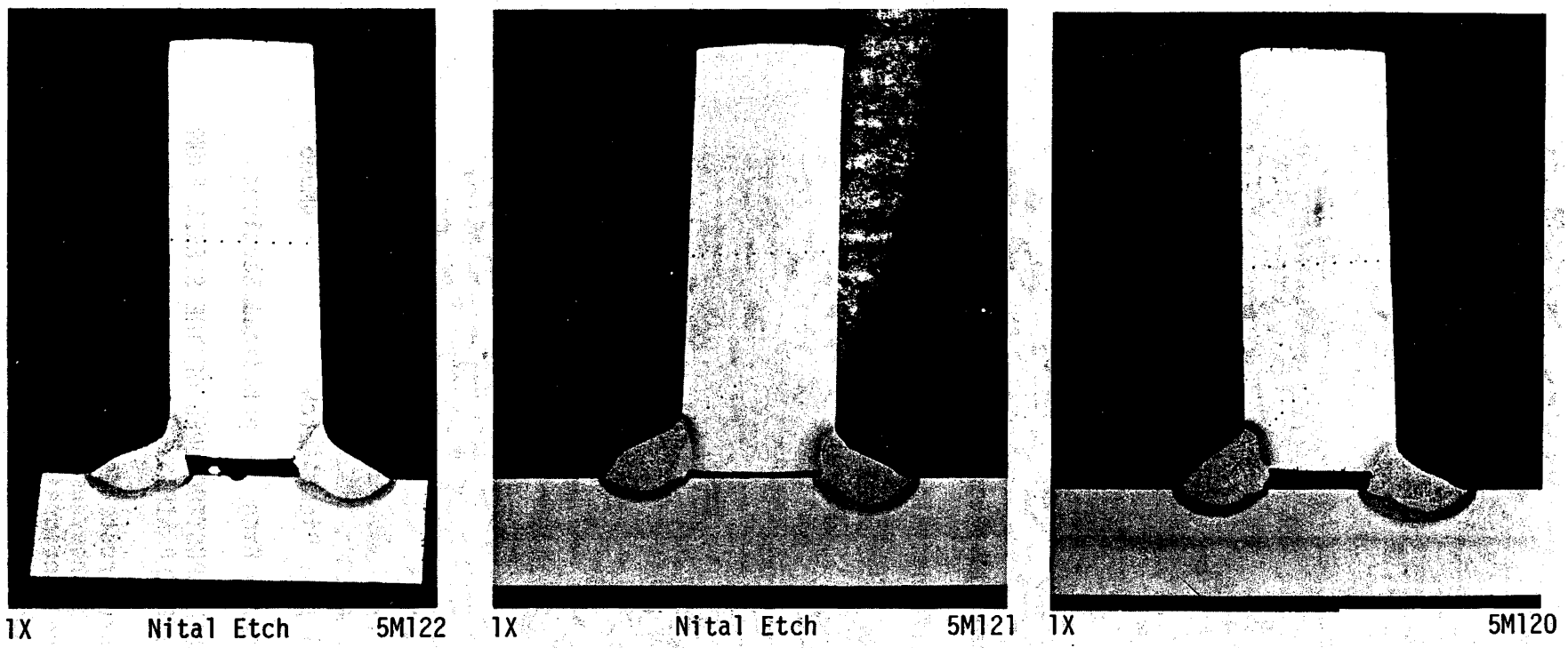

a. Valve-End Stiffener Ring, Specimen OVFB-2

b. Middle Stiffener Ring, Specimen OMBW1

c. Drain-End Stiffener Ring, ODBW1

FIGURE 26. PHOTOMACROGRAPHS OF SECTIONS THROUGH THE STIFFENER RINGS, FILLET WELDS AND VESSEL PLATE SHOWING SEGREGATION PATTERN IN THE CENTRAL REGIONS OF THE STIFFENER RINGS AND THE LOCATIONS OF HARDNESS TRAVERSES

These specimens were located between 1 and 2 inches from the fracture surfaces.

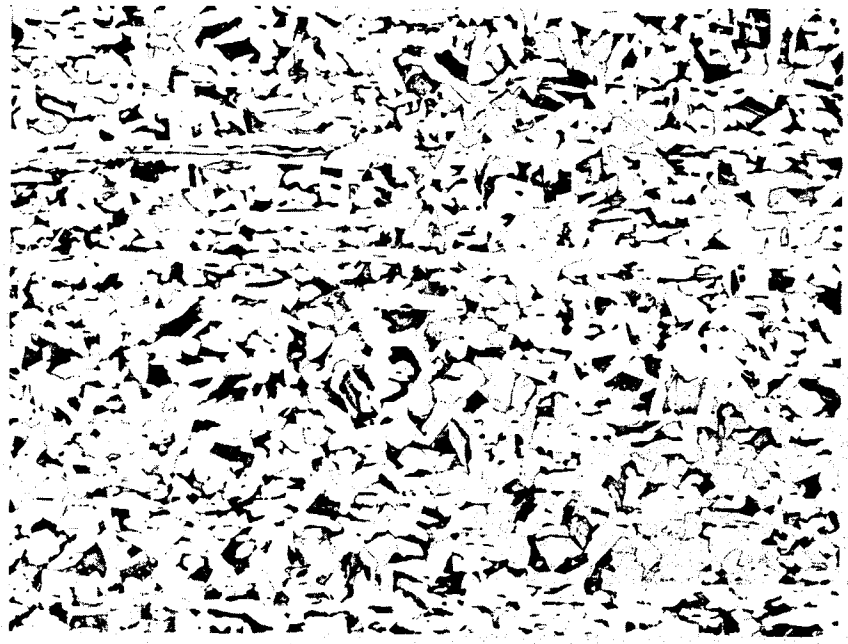

100X Nital plus Picral Etch 4M992

a. Valve-End Stiffener Ring, Longitudinal Section

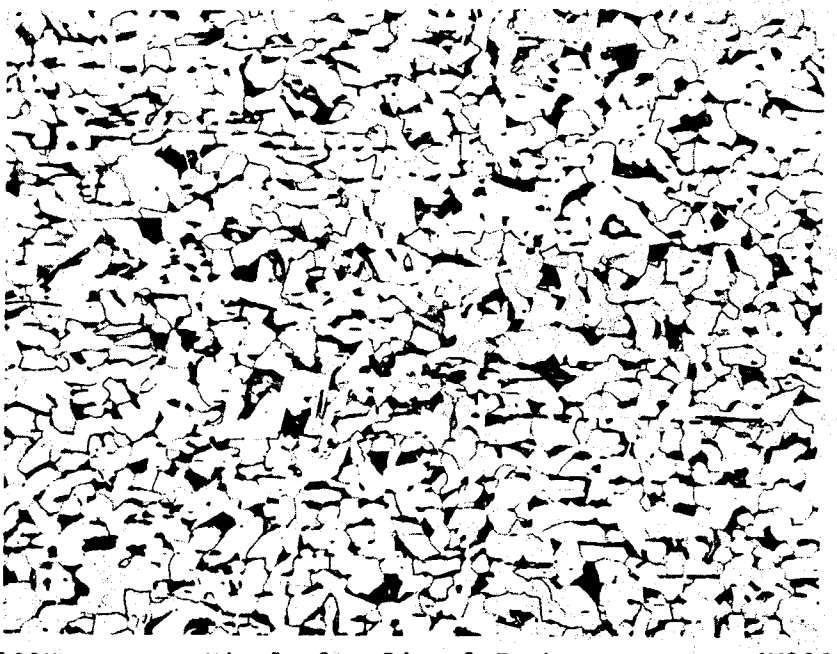

100X Nital plus Picral Etch 4M986

b. Middle Stiffener Ring, Longitudinal Section

FIGURE 27. TYPICAL MICROSTRUCTURES OF THE STEELS FROM THE STIFFENER RINGS

The microstructures consist of ferrite and pearlite; they are less banded but exhibit a coarser grain size than the steel from the vessel shell.

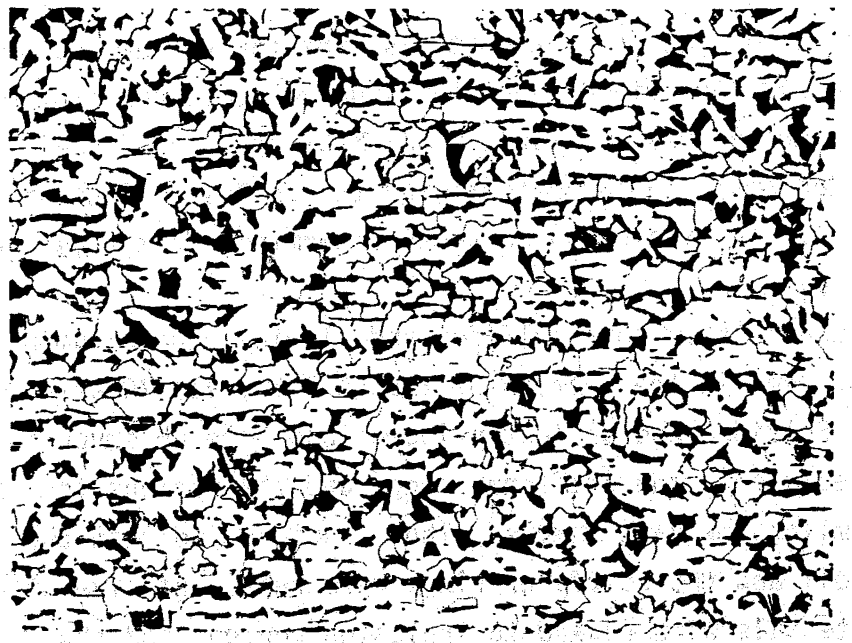

100X Nital + Picral Etch 4M979

c. Drain-End Stiffener Ring, Longitudinal Section

FIGURE 27. (Continued)

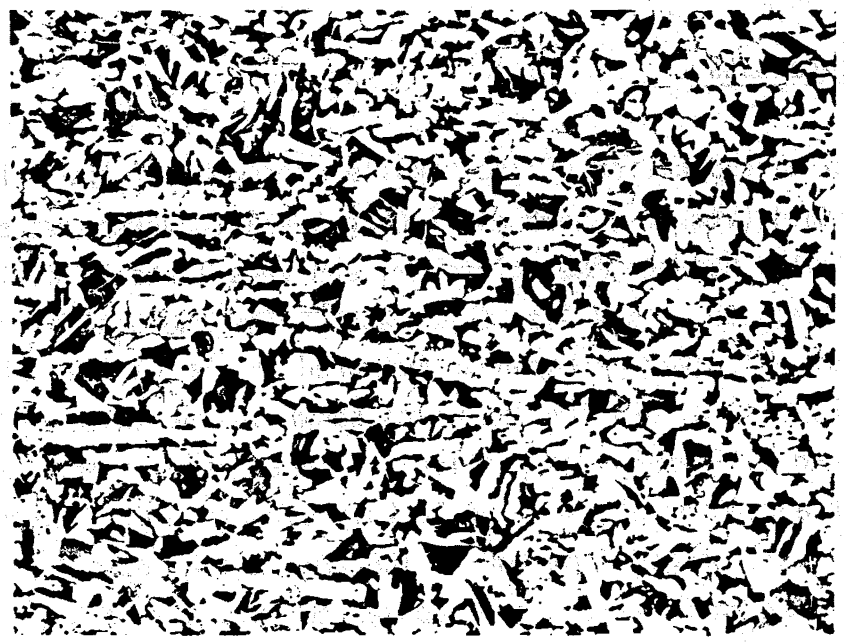

100X Nital + Picral Etch 4M985

FIGURE 28. TYPICAL MICROSTRUCTURE IN THE SEGREGATION ZONE IN THE STIFFENER RINGS

The microstructure contains more pearlite than the regions outside the zone. Specimen OMBW1, transverse section.

Inclusion Content

The inclusion content of the steels from the vessel shell and each stiffener ring was determined on the longitudinal sections from each component using the procedures set forth in ASTM Designation E-45-76, "Standard Recommended Practice for Determining the Inclusion Content of Steel", Microscopic Method A. The inclusion contents determined from those sections are summarized in Table 13.

Those results show that sulfides and alumina type (aluminate) inclusions were observed in the section of the SA-516 Grade 70 steel from the vessel plate. Sulfides and silicates inclusions were observed in the sections of the steels from the stiffener rings and the ratings for those inclusions were similar for each sample. Those ratings indicate the steels from the vessel shell and the stiffener rings were representative of commercially produced materials with regard to inclusion content and thus, it is unlikely that the inclusion content was responsible for the failure. It was not reported to the Battelle investigators whether an inclusion content was specified for these steels.

Microhardness Measurements

To obtain an indication of the tensile strengths of the fillet welds, Diamond Pyramid (Vickers) hardness (10 kg load) traverses were made across the fillet welds between the stiffeners and vessel shell, as is shown in Figure 25. Hardness traverses also were made across the central regions of the stiffener rings. The average hardness measured in the various fillet welds were 203, 197, and 200 DPH for the welds shown in the valve-end, middle, and drain-end stiffeners, respectively. Those hardenesses convert to ultimate tensile strengths of 97, 94, and 96 ksi respectively. The hardnesses measured in vessel shell ranged from 180 to 188 DPH, which convert to ultimate tensile strengths of 87 to 90 ksi. Those converted values were higher than the tensile strengths of about 72 ksi measured from the vessel shell. The hardnesses at the central region in the stiffener rings ranged from 126 to 137 DPH, with the higher readings generally being in the segregation zone. Those values convert to tensile strengths of less than 72 ksi. However, at other locations near the top and bottom surfaces stiffener rings were ranged from 150 to 170 DPH, which convert to tensile strengths ranging from 72 to 83 ksi.

TABLE 13. INCLUSION CONTENTS OF THE STEELS FROM THE VESSEL SHELL AND THE THREE STIFFENER RINGS[a]

Specimen Identification	Inclusion Content			
	Type A (Sulfides)	Type B (Alumina)	Type C (Silicates)	Type D (Globular Oxides)
180VBA Vessel Shell	2T	3T	NR[b]	NR
180VBE Valve-End Stiffener	3T	NR	3T	NR
OMB Middle Stiffener	3T	NR	3T	NR
ODB Drain-End Stiffener	3T	NR	2T	NR

(a) ASTM Designation E45-76, "Standard Recommended Procedure for Determining the Inclusion Contenst of Steels", Microscopic Method A.

(b) Not rated; less than a 1T when examined at 100X.

EXAMINATION OF SECTIONS CONTAINING FRACTURE SURFACES

The work conducted under this portion of the study involved visual and low-power-microscopic examinations of sections containing the surfaces of the primary rupture and the cracks in the stiffener rings, fractographic examinations of the surfaces of the fractures in those sections with the scanning electron microscope (SEM), and finally, metallographic examination of selected samples removed from those sections. The purposes these examinations were to:

(1) Verify and augment the observations made during the onsite inspections
(2) Determine the modes of fracture present to aid in establishing the most probable cause of failure
(3) Determine if other features present on the surfaces of those sections may have contributed to the failure
(4) Evaluate the extent of fusion or bonding in the stiffener ring butt welds
(5) Identify microstructural features associated with fracture regions
(6) Conduct microhardness measurements on the butt-weld metal to obtain an indication of its tensile strength.

Visual and Low-Power-Microscopic Examination

The initial work involved visual and low-power-microscopic examinations of the surfaces and adjacent areas from the vessel shell and the stiffener rings. As was described previously, the grease on the fracture surfaces and the paint and loosely adhering corrosion products on the surfaces of the sections from the failed vessel were removed by cleaning with solvents, paint remover, and detergents. That level of cleaning permitted observations of the various features on the surfaces of the vessel shell and the stiffener rings. However, the fracture surfaces on the various sections were covered with considerable amounts of corrosion products, which prevented examination of the details of the fracture surface even during the

initial visual and low-power-microscope examinations. Therefore, those corrosion products were removed prior to further examinations. Initially, the fracture surfaces on Section OVFB were cleaned using a nonreactive stripping technique. Cellulose acetate strips were moistened with acetone and pressed onto the fracture surfaces. After the strips dried, they were pulled from the surfaces, mechanically removing corrosion products that adhered to the strips. That process was repeated until no further evidence of removal of corrosion products was observed on the strippings. However, continued examination revealed that considerable corrosion products remained on the fracture surfaces. Therefore, it was mutually decided among representatives of Battelle and Kerr-McGee and Dr. Robert Block to use an electrolytic cleaning procedure developed by Yuzawich and Hughes* in an attempt to remove the remaining corrosion products on those surfaces and the surfaces of the cracks from the other two stiffener rings.

That cleaning technique involves the use of an electrolytic cell consisting of a graphite anode, the specimen as the cathode, and an aqueous solution of Endox 214, a water-soluble, powdered alkaline cleaner, as the electrolyte. A current density of 250 mA/cm^2 was used. During the cleaning, the electrolyte was agitated ultrasonically and the specimen was rotated. The specimen was subjected to the electrochemical cleaning for 1 minute, after which it was rinsed in an ultrasonically agitated waterbath containing detergent and a wetting agent, rinsed in clean water, rinsed in alcohol, and dried with an air blast, followed by examination to assess the amount of corrosion products removed. That process was repeated until the fracture surfaces were cleaned of virtually all corrosion products. The fracture surfaces required between 9 and 16 cleaning treatments to remove the bulk of the corrosion products.

After that cleaning treatment was completed the specimens were examined visually and with a low power microscope. Then they were examined in the scanning electron microscope (SEM). Those examinations are described in the following sections of this report.

---

* Yuzawich, P. M., and Hughes, C. W., "An Improved Technique of Removal of Oxide Scale from Fractured Surfaces of Ferrous Materials", Practical Metallography, 15, 184-194 (1978).

Specimens OVFB and OVFB-W, Sections from the Origin Region of the Primary Rupture

Figure 29 shows Specimens OVFB AND OVFB-W that contained the surfaces of the origin region of the primary rupture through the butt weld in the valve-end stiffener ring and the vessel shell after they had been removed from the large section identified as OVFB and cleaned in the laboratory. As is shown in Figure 29; the deformation in this region of the vessel prevented the matching fracture surfaces on these sections from fitting together closely. Figure 29 shows grinding marks on the top surface and the valve-end surface of the stiffener ring on either side of the crack through the butt weld. That grinding presumably was done to smooth the surfaces after the butt weld was deposited. In addition, numerous small pits were present on both sides of the valve-end stiffener ring. Those pits most likely occurred after the vessel rupture. Figures 29b and c also show short cracks extending circumferentially in the fillet welds adjacent to the stiffener surfaces in Specimen OVFB-W. Figure 30 shows short axial cracks in the vessel shell surface adjacent to the fracture surface beneath the stiffener ring and near the fillet welds, particularly on the right-hand side of the figure. Those cracks formed as a result of the plastic deformation in those areas during the failure process.

Figure 31 illustrates the matching fracture surfaces on Specimens OVFB and OVFB-W. The lack of full weld penetration and the pattern from the flame cutting of the stiffener surfaces during fabrication are clearly evident. There was a gap between the bottom of the stiffener ring and the outer surface of the vessel shell. That gap was about 1/8 inch on Specimen OVFB-W and 1/16 inch on Specimen OVFB. Also the region of flat fracture (essentially 90 degrees to the shell inner and outer surfaces) can be seen clearly on the fracture through the vessel wall. The appearance of that flat fracture region indicates stable slow-crack growth prior to the final rupture which occurred by rapid crack propagation by a shear fracture mode. The beginnings of the shear propagation are visible on the fracture surfaces on the vessel shell at each end of the sections where the fracture surface is not perpendicular to the inner and outer surfaces of the vessel shell.

1X Cleaned 4M888

a. Top Surface of Valve-End Stiffener Ring

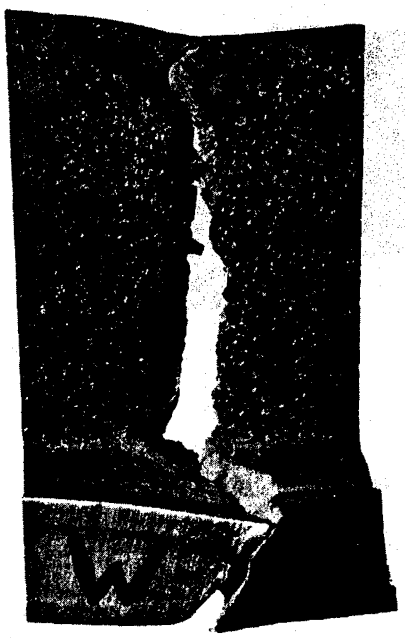

1X Cleaned 4M890

b. Drain-End Side

1X Cleaned 4M889

c. Valve-End Side

FIGURE 29. SURFACES OF SPECIMENS OVFB AND OVFB-W CONTAINING THE SURFACES OF THE FRACTURE THROUGH THE BUTT WELD IN THE VALVE-END STIFFENER RING AND THE VESSEL SHELL AFTER REMOVAL FROM SECTION OVFB AND CLEANING IN THE LABORATORY

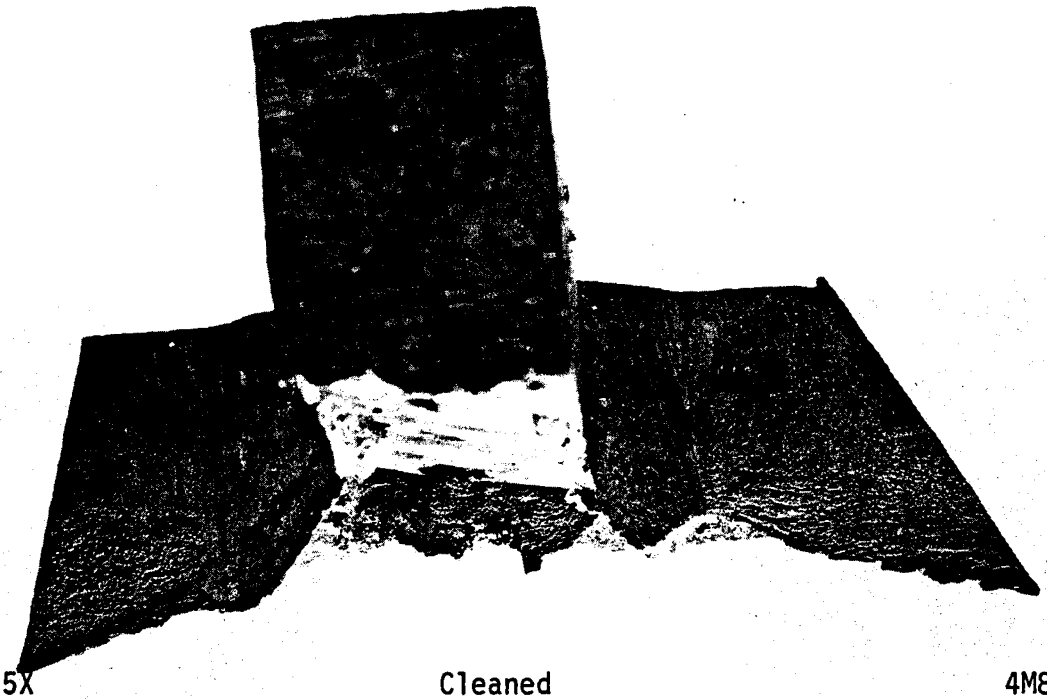

1.5X Cleaned 4M893

FIGURE 30. CRACK IN THE VESSEL SHELL SURFACE ON SPECIMEN OVFB-W

Half of butt weld of valve-end stiffener ring viewed from top.

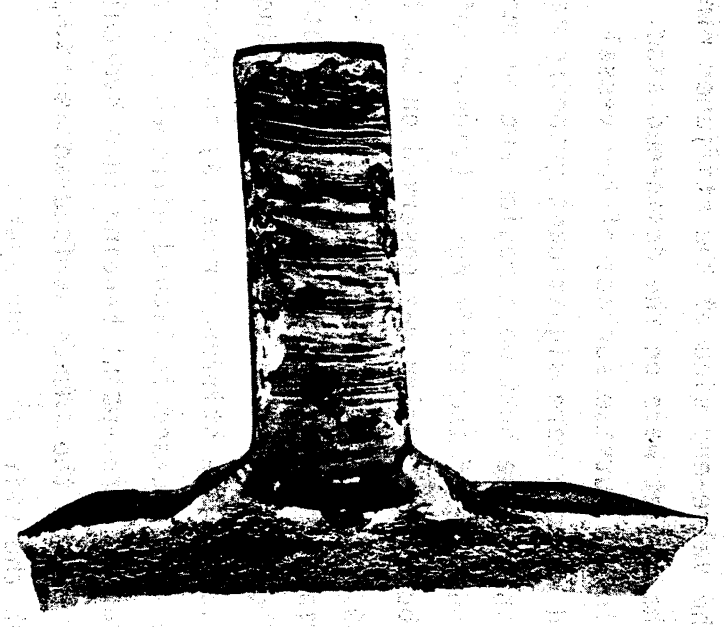

1X Cleaned 4M887

a. Specimen OVFB-W

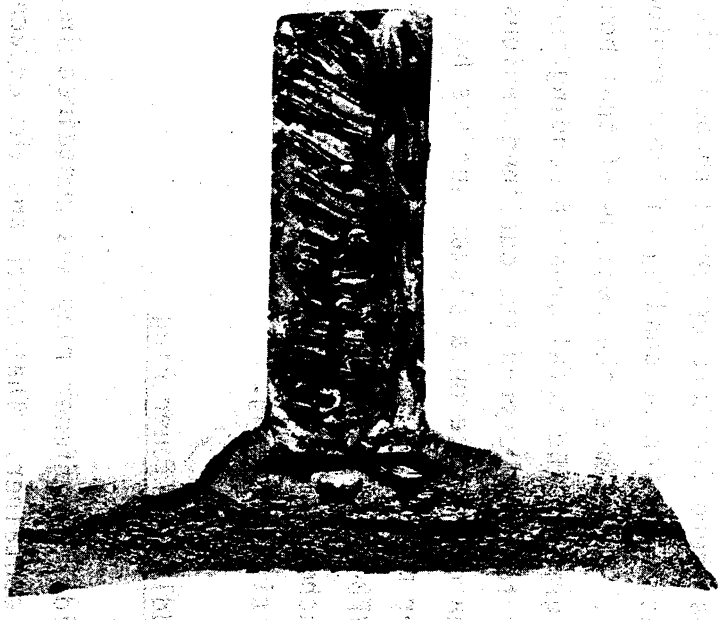

1X Cleaned 4M891

b. Specimen OVFB

FIGURE 31. MATCHING FRACTURE SURFACES ON SPECIMENS OVFB AND OVFB-W CONTAINING THE SURFACES OF THE CRACK THROUGH THE VALVE-END STIFFENER RING AND THE ORIGIN REGION OF RUPTURE THROUGH THE VESSEL SHELL

During the examination of surfaces of the fractures at magnifications up to 30X, the regions where fracture occurred through the weld metal of the butt weld indicating fusion or bonding in those regions, could be estimated quite well. Therefore, the regions of that bonding were outlined on a photomacrograph. The total area of bonding then was determined using a planimeter to trace around the outlined regions. A planimeter determines the area of a shape on a planar surface based upon its perimeter. The planimeter measurements made on the photomacrograph of the surface of Specimen OVFB-W indicated that area of fractured butt weld metal was 0.22 square inches, or only about 10.5 percent of the cross-sectional area of the stiffener ring.

Section OMB, Crack in the Middle Stiffener Ring

The crack in the middle stiffener ring was contained in Section OMB from the failed shipping container. That crack and the adjacent material from the stiffener ring and vessel shell are shown in Figures 32a, b, and c. The separation of the crack surfaces at the top of the middle stiffener ring was 3/32 inch. The crack in the butt weld extended nearly through the fillet weld on the valve-end side of the stiffener ring, but only a short distance into the fillet weld on the drain-end side. There was no evidence of cracking in the outside surface of the vessel shell. As is shown in Figure 32b and c there were significant grinding marks on the sides of the stiffener ring in the butt weld region and on the vessel shell surface on the drain-end side of the stiffener. Evidence of extensive grinding to smooth the butt weld region was observed on the top surface of the stiffener ring, but it does not show celarly in Figure 32a.

To examine the surfaces of the fracture through the butt weld, saw cuts were made axially from the surfaces of Section OMB ending near the fillet welds on either side of the stiffener ring, as is shown in Figure 32. The section then -as immersed in liquid nitrogen and the remaining material was fractured in three-point bending in a hydraulic press. The technique used was to push from the inside surface so as to spread surfaces of the crack through the stiffener ring apart.

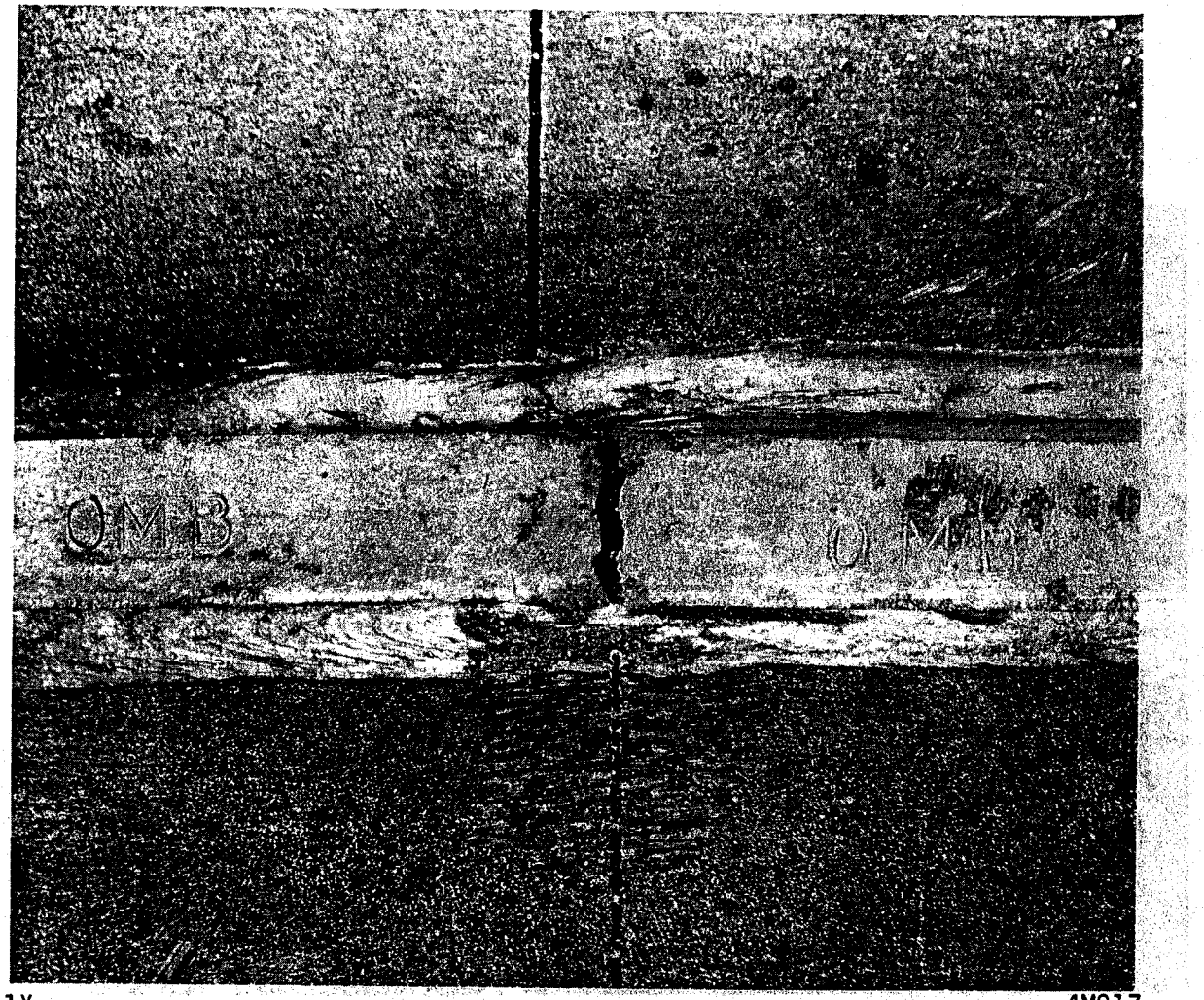

Specimen OMB-W Specimen OMB

a. View of the Crack Across the Top Surface of the Middle Stiffener Ring

FIGURE 32. PHOTOMACROGRAPHS OF THE CRACK THROUGH THE BUTT WELD IN THE MIDDLE STIFFENER RING

Straight saw-cuts are evident in a, b, and c, that were made to facilitate opening the crack in the laboratory.

1X 4M915

Specimen OMB Specimen OMB-W

b. View of the Crack in the Valve-End Side of the Middle Stiffener Ring

FIGURE 32. (Continued)

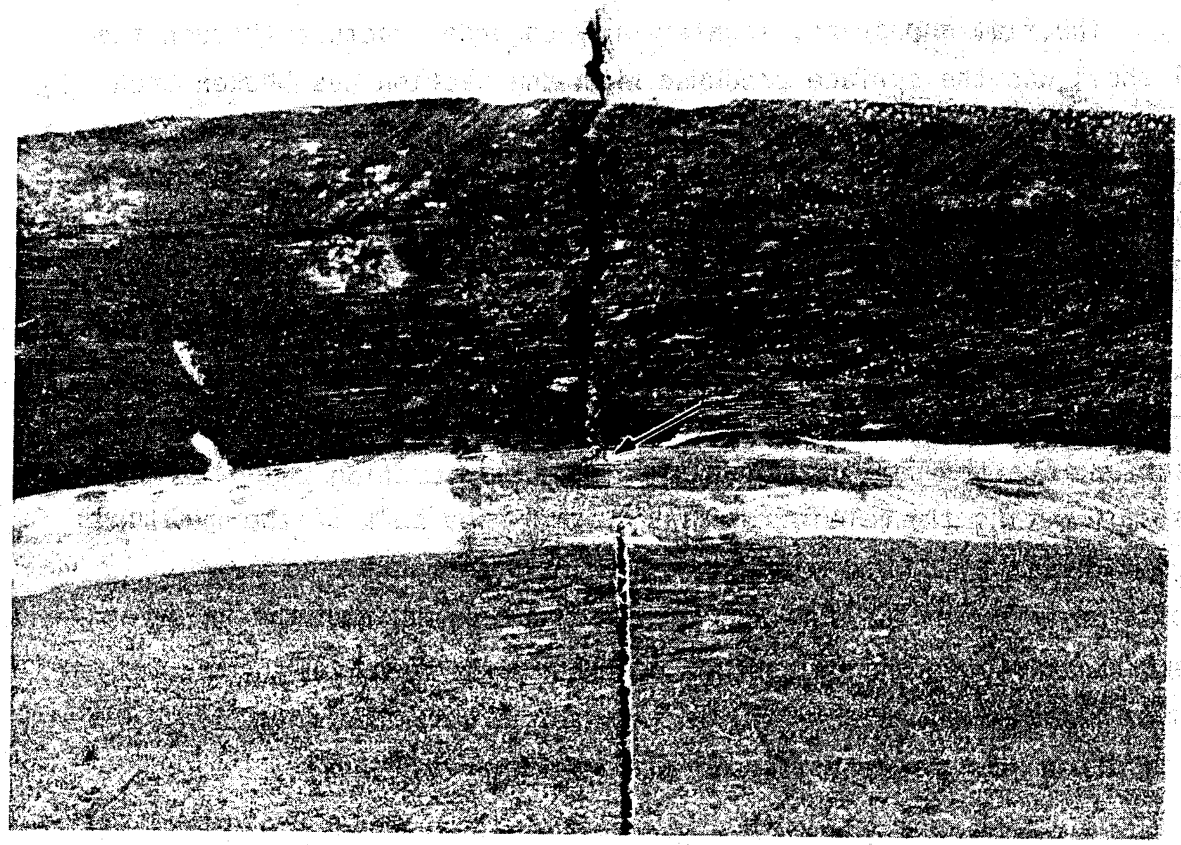

1X 4M918

Specimen OMB-W Specimen OMB

c. View of the Crack in the Drain-End Side of the Middle Stiffener Ring.

FIGURE 32. (Continued)

Note the slight crack extension into the fillet weld shown by the arrow.

Sections containing the fracture surfaces then were cut from Section OMB. Examination of those surfaces revealed that they were corroded. Thus, prior to further examinations, those surfaces were cleaned electrolytically using the procedures described previously. The surfaces of the crack through the middle stiffener ring after that cleaning are shown in Figure 33.

The flat-appearing, lighter-gray-colored fracture through the vessel shell was the surface produced when the section was broken open with the hydraulic press. The darker appearing region on the fracture through the vessel shell, adjacent to the root of the fillet weld on the left-hand side of Figure 33a, resulted from ductile crack growth into the vessel shell, pressumably during the failure of the vessel.

The surface of fracture through the butt weld in the stiffener ring shows that, as with the valve-end stiffener, the weld was not a full penetration weld. The horizontal lines or bands on the central portion of that surface are the pattern resulting from flame cutting the stiffener ring steel, during the manufacturing process. The bulk of the fracture through the butt-weld metal shown in Figure 33 appeared similar to that observed on the surfaces of the fracture through the valve-end stiffener ring. The percentage of fused weld metal on the surface of Specimen OMB was measured to be 14.8 percent of the cross section using the planimeter measuring technique described previously.

Section ODB, Crack Through Drain-End Stiffener

The crack through the butt weld in the drain-end stiffener ring was contained in Section ODB which was removed from the failed shipping container. The crack and the adjacent material from the stiffener ring and the vessel shell are shown in Figure 34a, b, and c. As is shown in the 1X photograph in Fiugre 34, the maximum separation between the crack surfaces at the top of the stiffener ring was 0.25 inch. It can be seen clearly in Figure 34 that the crack extended into the fillet welds on both sides of the stiffener ring. However, there was no evidence of crack

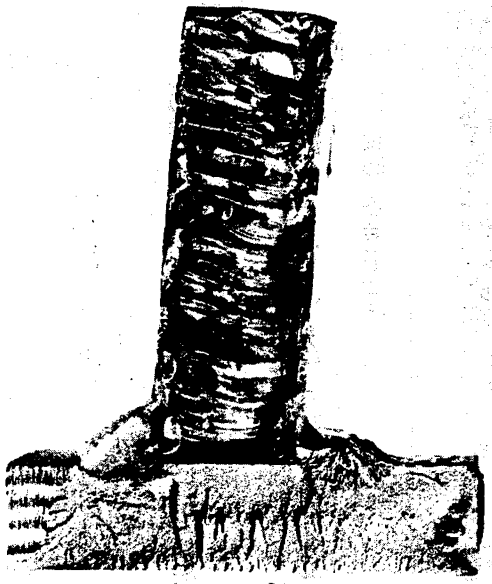

1X Cleaned 4M906

a. Specimen OMB

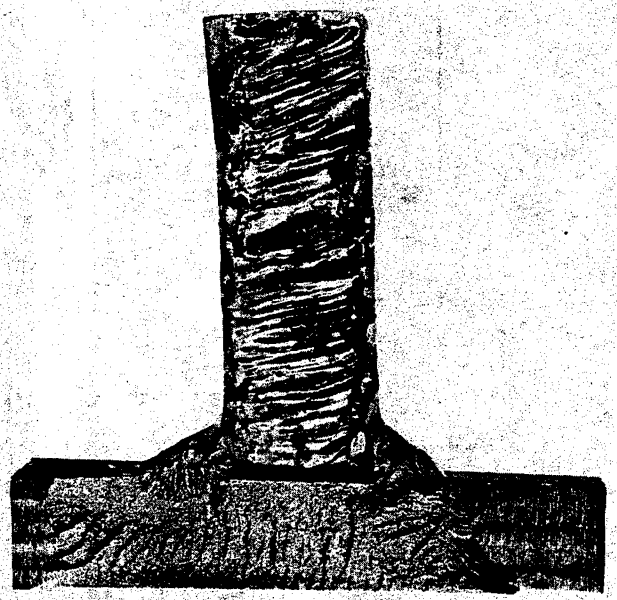

1X Cleaned 4M907

b. Specimen OMB-W

FIGURE 33. MATCHING FRACTURE SURFACES ON SPECIMENS OMB AND OMB-W FROM THE CRACK THROUGH BUTT WELD OF THE MIDDLE STIFFENER RING

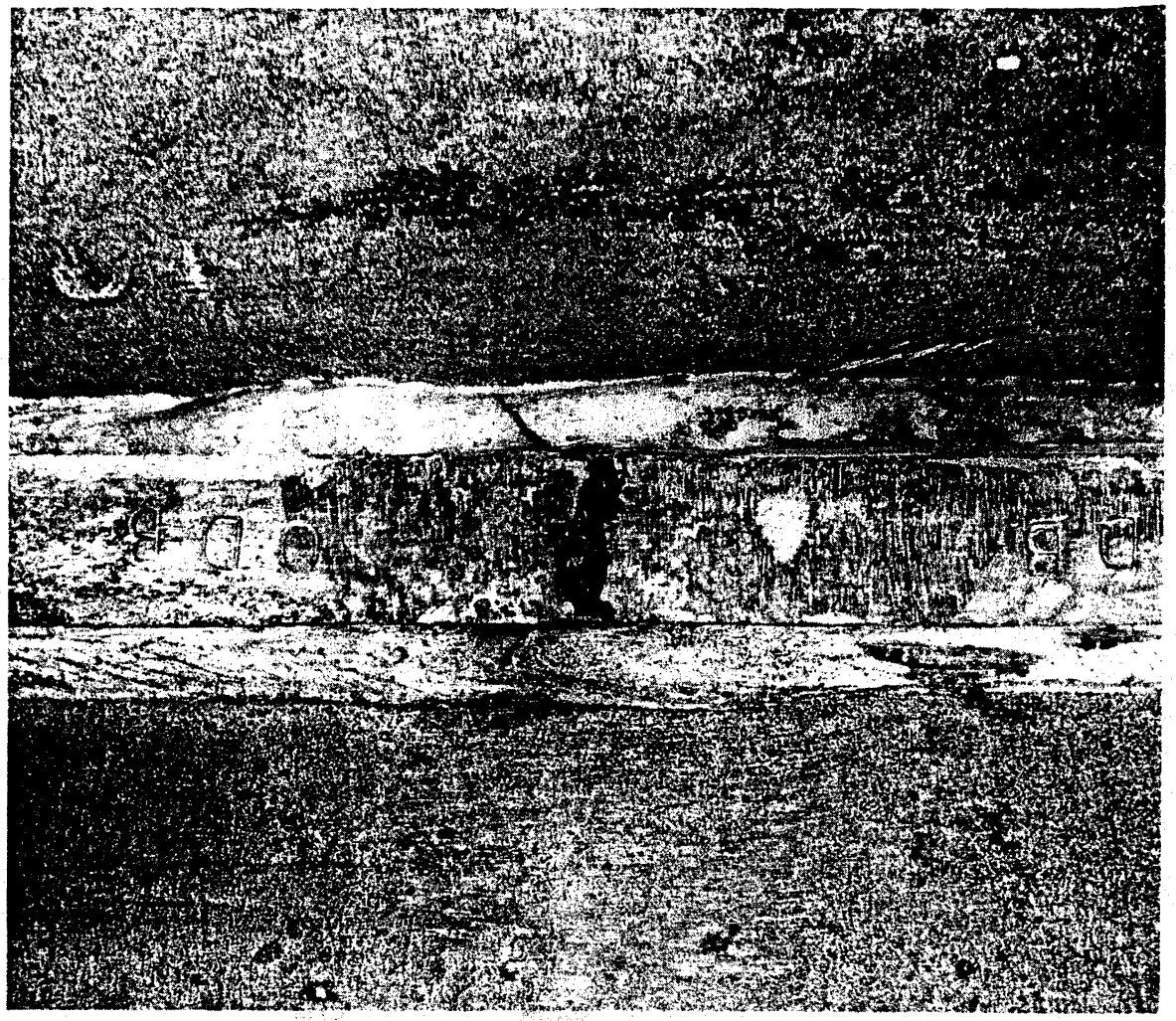

1X 4M934

Specimen ODB-W Specimen ODB

a. View of the Crack Across the Top Surface of the Drain-End Stiffener Ring

FIGURE 34. PHOTOMACROGRAPHS OF THE CRACK AT THE BUTT WELD IN THE STIFFENER RING AT THE DRAIN-END OF THE CYLINDER

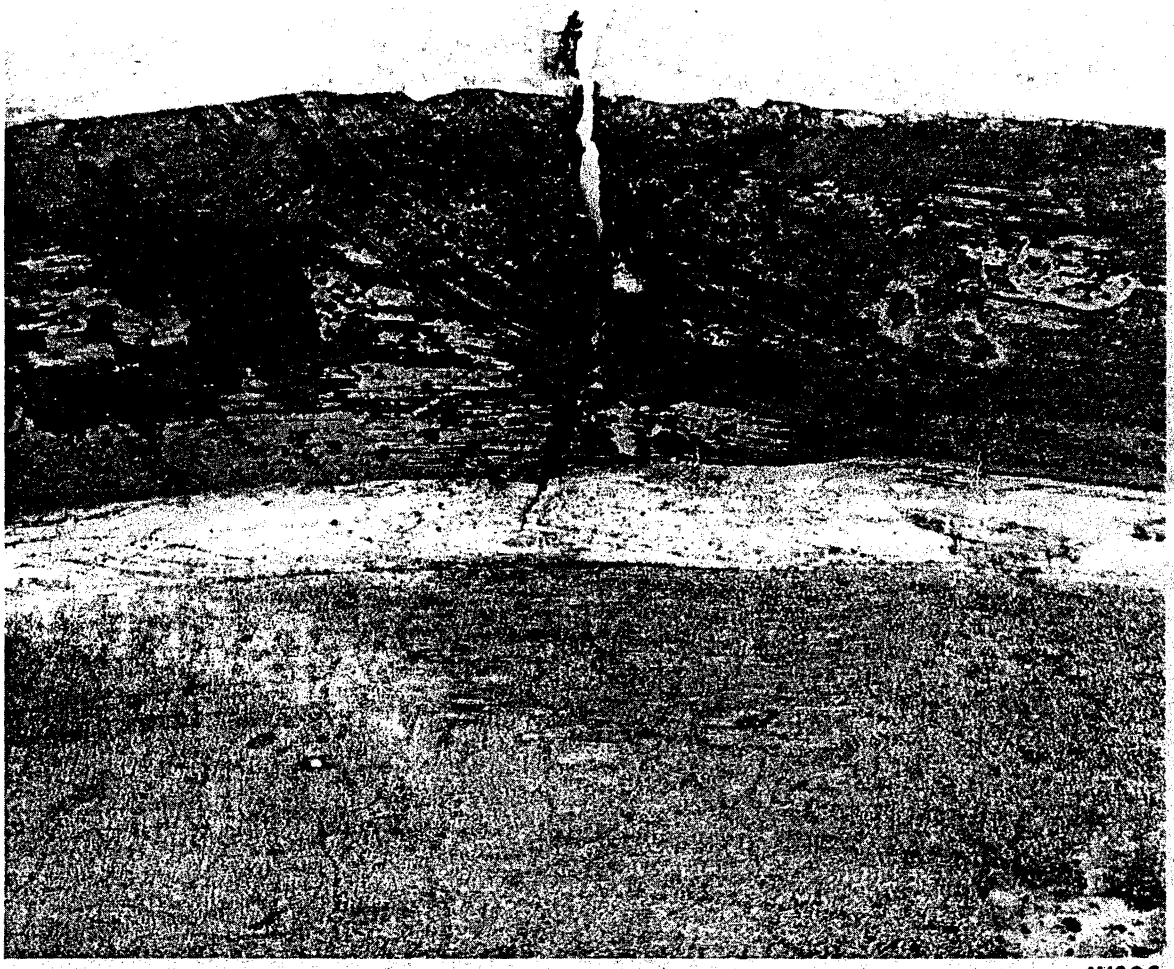

1X 4M936

Specimen ODB-W Specimen ODB

b. View of the Crack in the Drain-End Side of the Drain-End Stiffener Ring

FIGURE 34. (Continued)

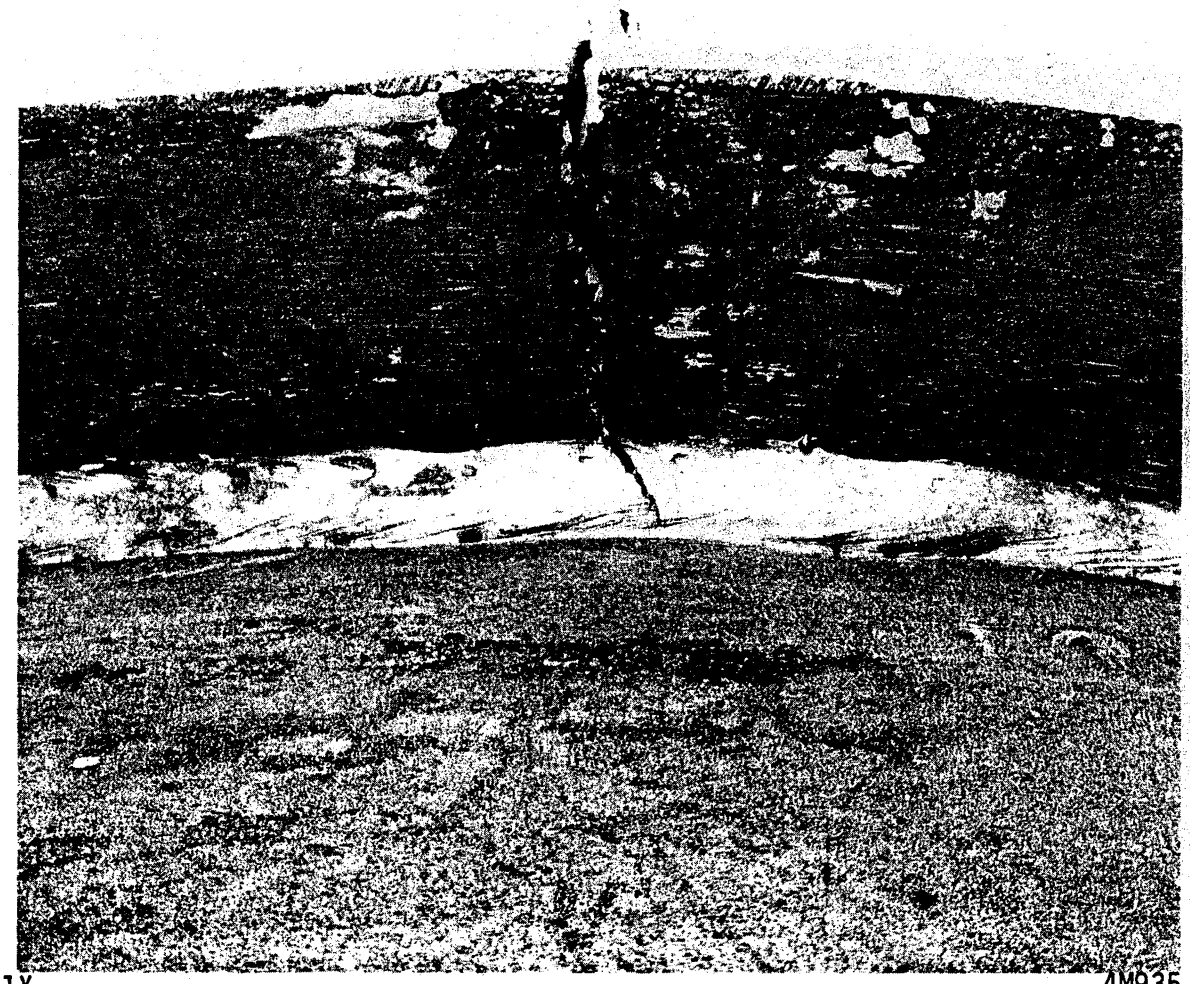

Specimen ODB Specimen ODB-W

c. View of the Crack in the Valve-End Side of the Drain-End Stiffener Ring

FIGURE 34. (Continued)

extension on the outer surfaces of the vessel shell. Again, grinding marks from smoothing of the butt-weld region were visible on the top and sides of the stiffener ring. Those marks were particularly severe on the drain-end side, as is shown in Figure 34b.

The crack in Section ODB was opened, using the procedures described previously, to allow examination of the fracture surfaces. The surfaces of the crack after removal of Specimens ODB and ODB-W from Section ODB and after electrolytically cleaning are shown in Figure 35. Those surfaces shown the typical pattern from the flame cutting operation during the fabrication of the ring over a substantial portion of the ends of the ring. However, there appeared to be significantly more fractured weld metal on those surfaces than was present on the surfaces of the middle and valve-end stiffener rings. It appeared that the gap between the ends of the drain-end stiffener ring was probably wider than those in the other stiffener rings; that wider gap could have allowed more weld metal to be deposited during the butt welding operation.

The surfaces of the fracture through the weld metal of the butt weld, shown in Figure 35, contained several oval-shaped, flat regions. Such regions were not as apparent on the fracture surfaces through the butt weld metal in the other two stiffener rings. For Specimen ODBW, the percentage of fused weld metal was 23.6 percent of the area of the stiffener cross section as measured by the planimeter tracings.

The examination of these fracture surfaces also revealed evidence of crack growth in the vessel shell steel, particularly below the roots of the fillet welds. The details of those fracture surfaces will be described in the section which presents the results of the fractographic examinations.

Fractographic Examination

A specimen containing one of the cleaned fracture surfaces from each Section (OVFB, OMB, and OMD) was examined in the scanning electron microscope to determine the fracture modes present on the fracture surfaces. Each specimen was examined thoroughly and during those examinations 150 fractographs were taken to document the fracture features observed. All of

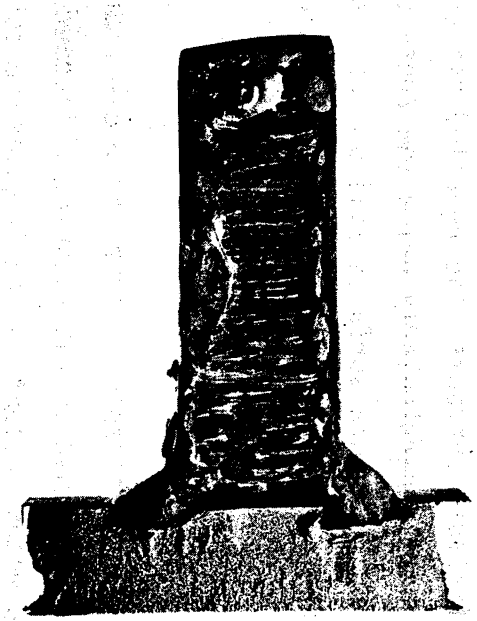

1X Cleaned 4M921

a. Specimen ODB-W

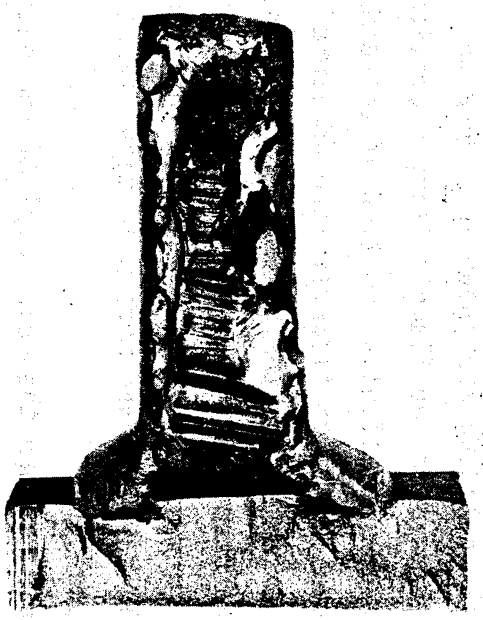

1X Cleaned 4M922

b. Specimen ODB

FIGURE 35. MATCHING SURFACES ON SPECIMENS ODB-W AND ODB FROM THE CRACK IN THE DRAIN-END STIFFENER RING

those fractographs will not be presented in this report but will be retained in numbered laboratory books at Battelle. Since many regions exhibited similar appearances, only fractographs illustrating the significant features and fracture modes on each section will be presented.

Specimen OVFB-W

Specimen OVFB-W contained the fracture surfaces through the butt weld in the valve-end stiffener and the vessel shell. Those surfaces after cleaning are illustrated in Figure 36. The SEM examination of those surfaces concentrated on the flat-appearing region of the fracture through the vessel shell, the regions of fracture in the vessel shell immediately below the fillet welds, the fractures surfaces on the fillet welds, and the fractures surfaces through the weld metal.

The numbers on Figure 36 indicate regions where fractographs of the butt weld were taken during the examination. As is shown in Figure 36, the amount of weld metal from the butt weld comprised a relatively small fraction of the surface on the end of the stiffener ring and the pattern resulting from flame cutting the stiffener ring steel was clearly visible.

The SEM examination of the fracture surface of the rupture through the vessel shell contained in Sample OVFB-W, revealed that the fracture mode was ductile rupture in all areas. The typical appearance of the fracture surfaces in Area 2 is shown in Figure 37.

Examination of the surfaces of the fracture through the fillet welds between the valve-end stiffener ring and the vessel shell contained on Specimen OVFB-W revealed only evidence of ductile rupture. The typical appearance of these fracture surfaces are illustrated in Figure 38.

SEM examination of the fracture surfaces through the weld metal from butt weld between the ends of the valve-end stiffener ring again revealed that fracture mode in all regions was ductile rupture. That examination also revealed that in some regions where weld metal was present, there appeared to be no bond (fusion) between it and the base metal.

SEM fractographs illustrating ductile rupture on the butt-weld fracture surfaces are shown in Figure 39. Similar features were observed in Areas 5, 6, 13, 15, 16, 17, 22-30.

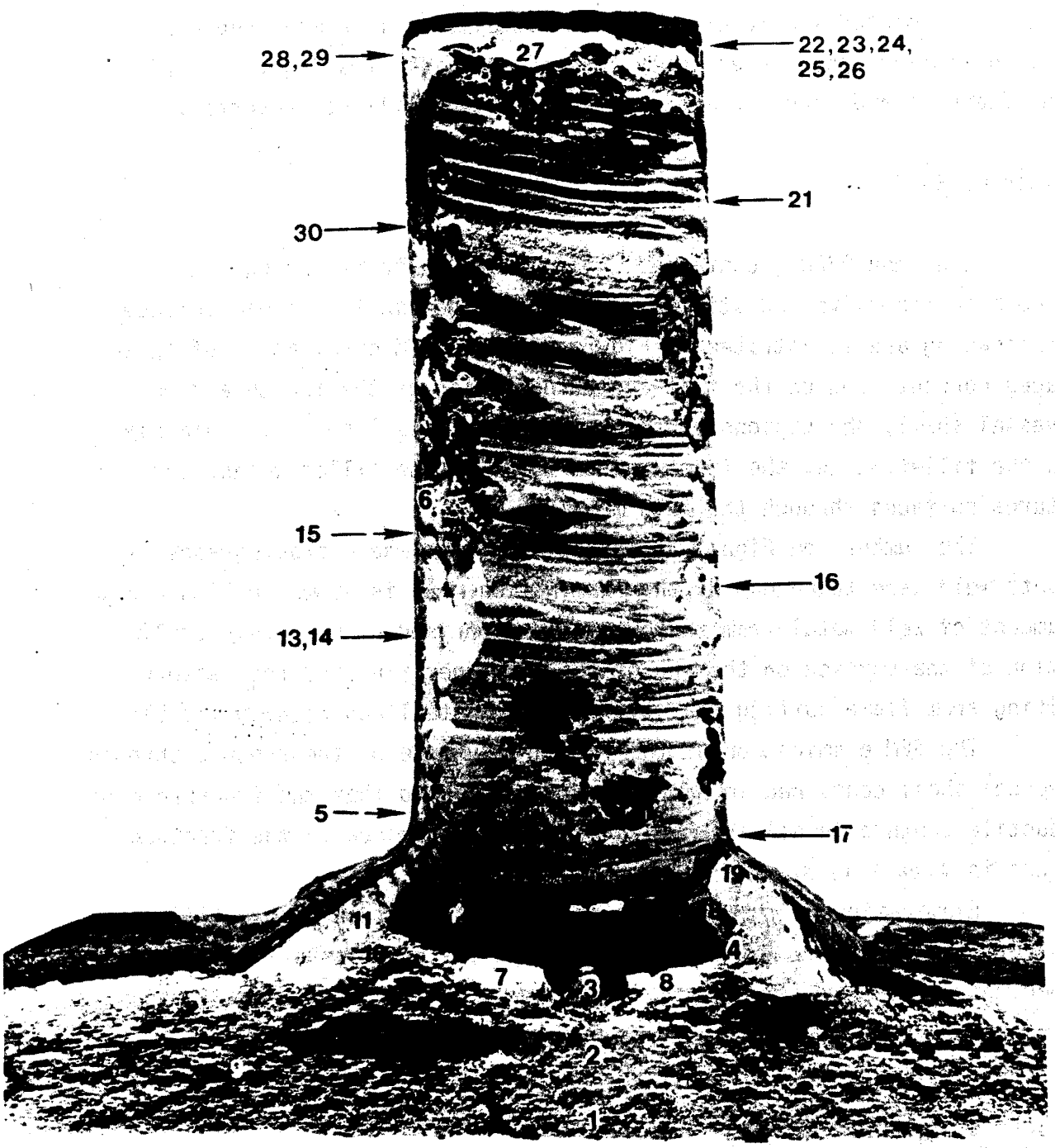

2.4X Cleaned 4M887E

FIGURE 36. FRACTURE SURFACE ON SPECIMEN OVFP-W (VALVE-END STIFFENER AND ADJACENT VESSEL SHELL) EXAMINED IN THE SEM

The numbers and arrows indicate areas where SEM fractographs were taken.

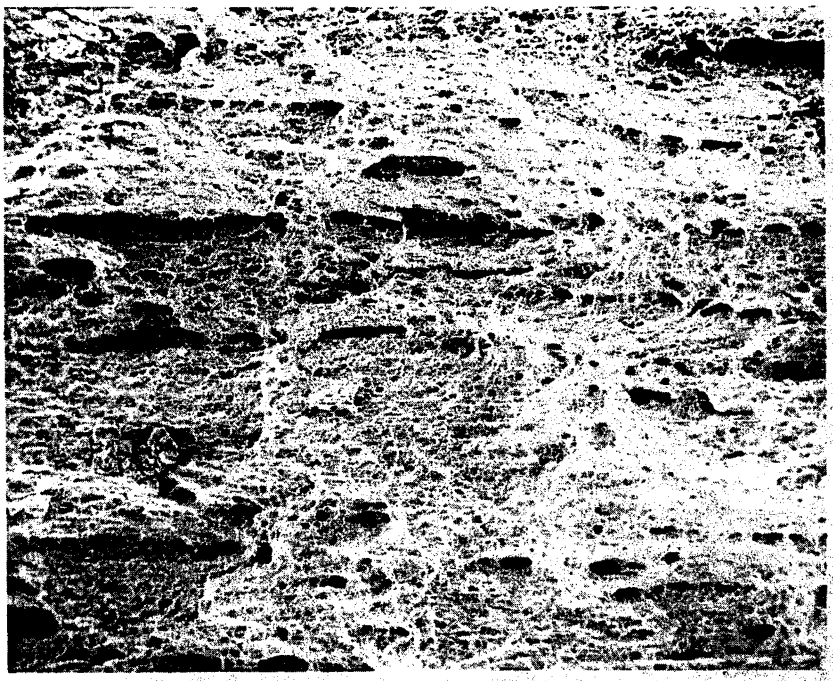

100X 56710

a. Low Magnification Fractograph of Area 2

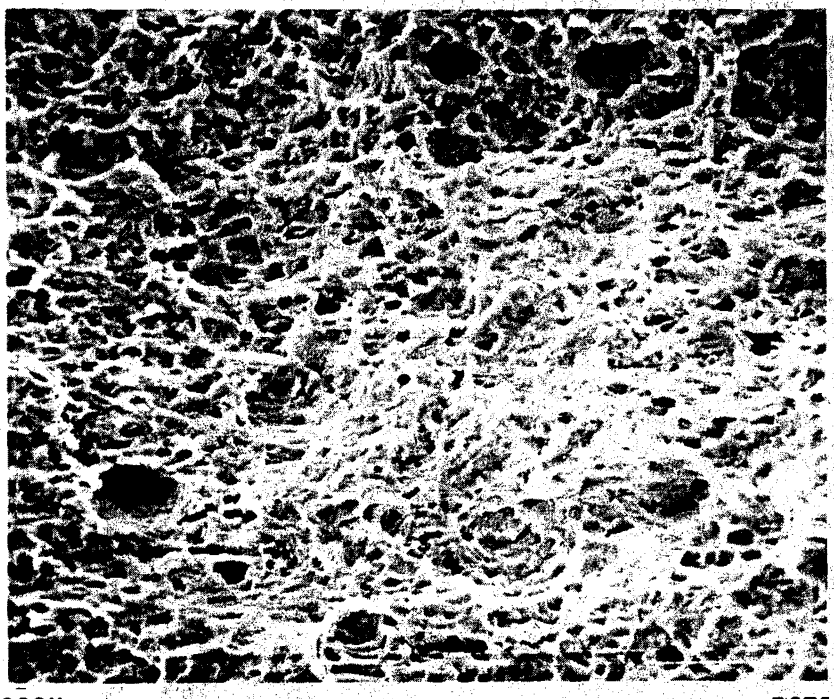

1000X 56711

b. Higher Magnification Fractograph Showing Ductile Dimples

FIGURE 37. TYPICAL DUCTILE FRACTURE APPEARANCE IN AREA 2 ON FIGURE 36 OF THE FRACTURE SURFACE OF THE VESSEL SHELL

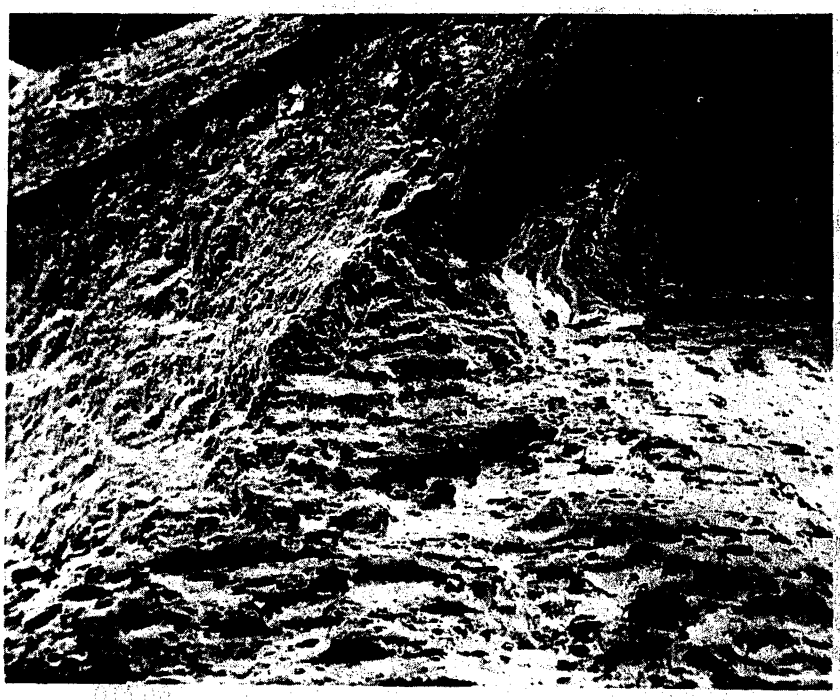

7X 56779

a. Fracture Surface Through Fillet Weld and Vessel Shell in Area 11

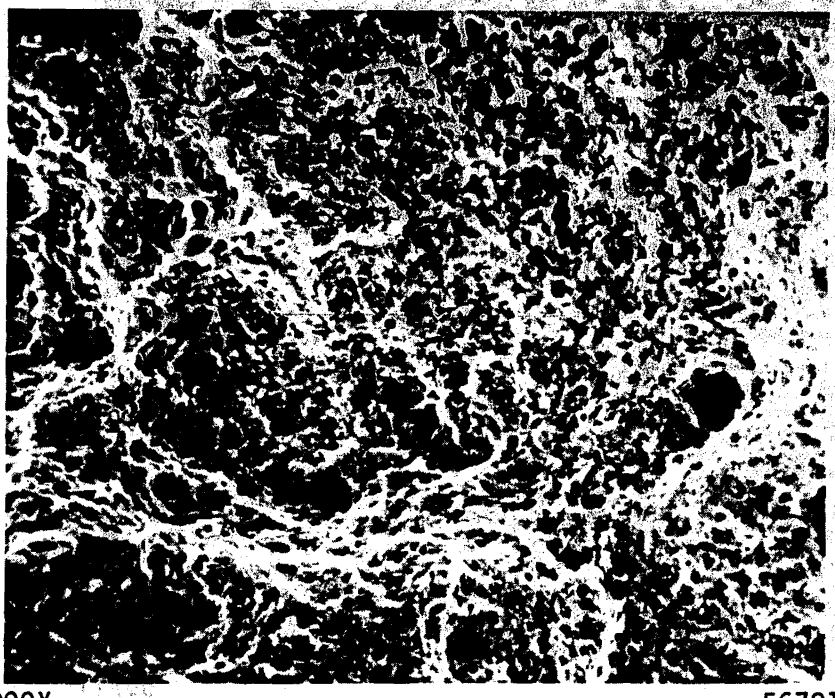

1000X 56781

b. Ductile Rupture in Fillet Welds from Area 11

FIGURE 38. TYPICAL APPEARANCE OF FRACTURE SURFACE THROUGH FILLET WELDS BETWEEN THE VALVE-END STIFFENER AND THE VESSEL SHELL ON SPECIMEN OFVB-W

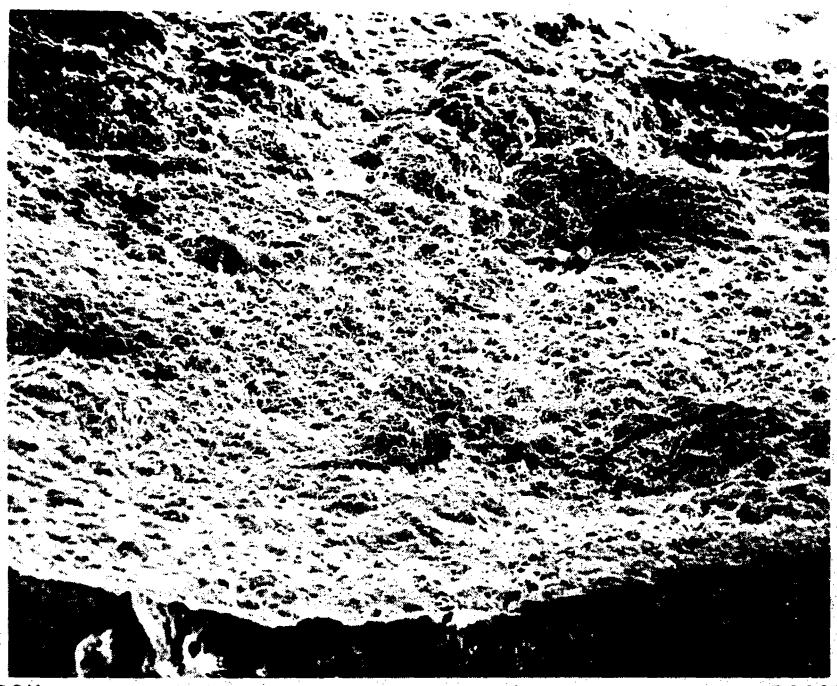

100X 56809

a. Appearance of Area 27

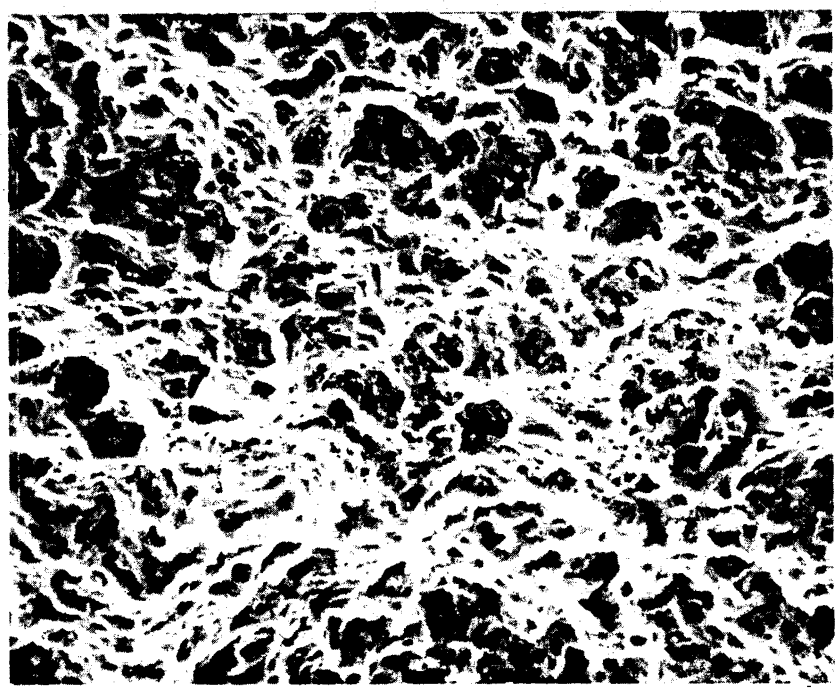

1000X 56810

b. Ductile Rupture in Area 27

FIGURE 39. TYPICAL DUCTILE RUPTURE OBSERVED ON THE SURFACES OF FRACTURE THROUGH THE BUTT WELD METAL ON THE VALVE-END STIFFENER

These fractographs were taken in Area 27 at the top of the stiffener ring.

Figure 40a, b, and c illustrates the appearance of the fracture through the butt-weld metal (Area 13) and the appearances of the surface of a weld nugget (no bonding) through which fracture did not occur (Area 14). The fractograph shown in Figure 41c was on the side of the weld nugget adjacent to the ductile rupture observed in Area 13. The features shown in Figure 40 were typical of much of the butt-weld metal deposited on the ends of the stiffener rings in that a significant portion of the surface of weld metal visible was not bonded to the stiffener ring steel or an adjacent weld deposit. Thus, basing the amount of weld penetration on the total area of weld metal visible on those surfaces would result in a considerably greater amount than was obtained based upon the fracture area on the weld deposits as was done when the planimeter measurements were made.

Figure 41 shows the flame cut surface on the end of the stiffener ring in Area 21. There appeared to be no weld metal from the butt weld over the bulk of this region.

a. Fracture Through Area 13 and the Unbonded Surface of the Weld Nugget in Area 14 Shown on Figure 36.

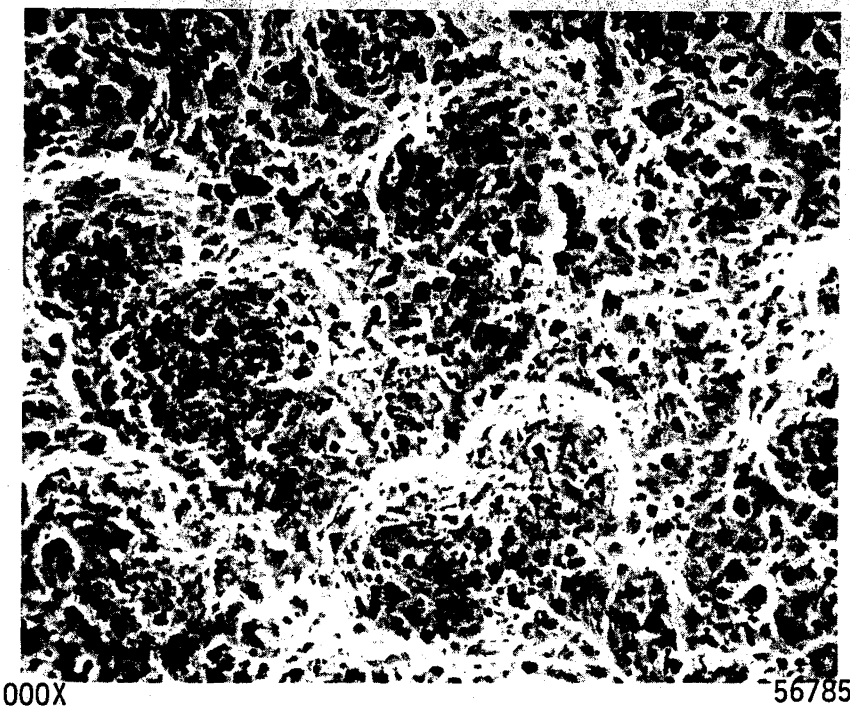

b. Ductile Rupture in Area 13

FIGURE 40. FRACTURE APPEARANCE IN AREA 13 AND THE SURFACE OF A WELD NUGGET (AREA 14)

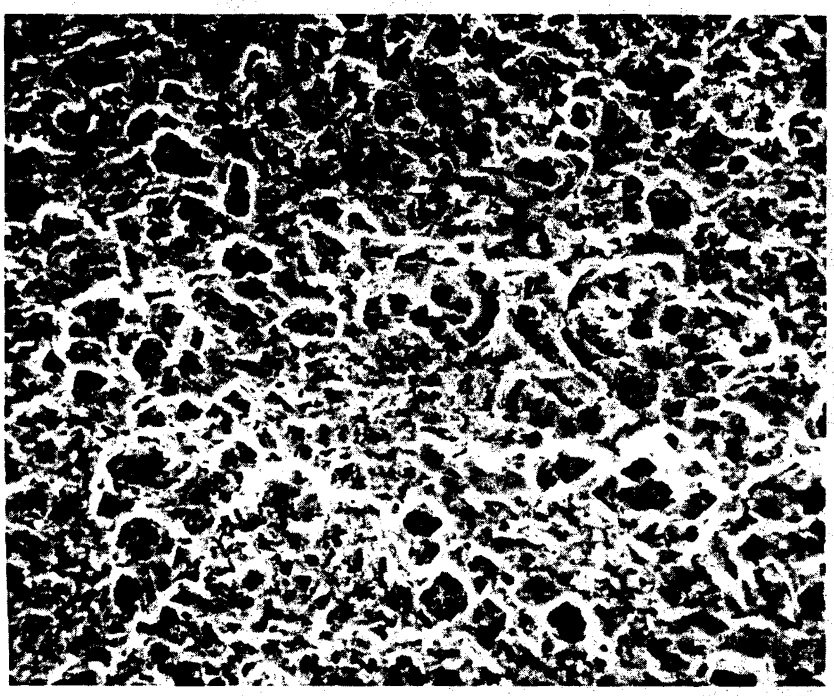

1000X 56788

c. Surface of Unbonded Weld Nugget in Area 14 Adjacent to Ductile Fracture Through Area 13

FIGURE 40. (Continued)

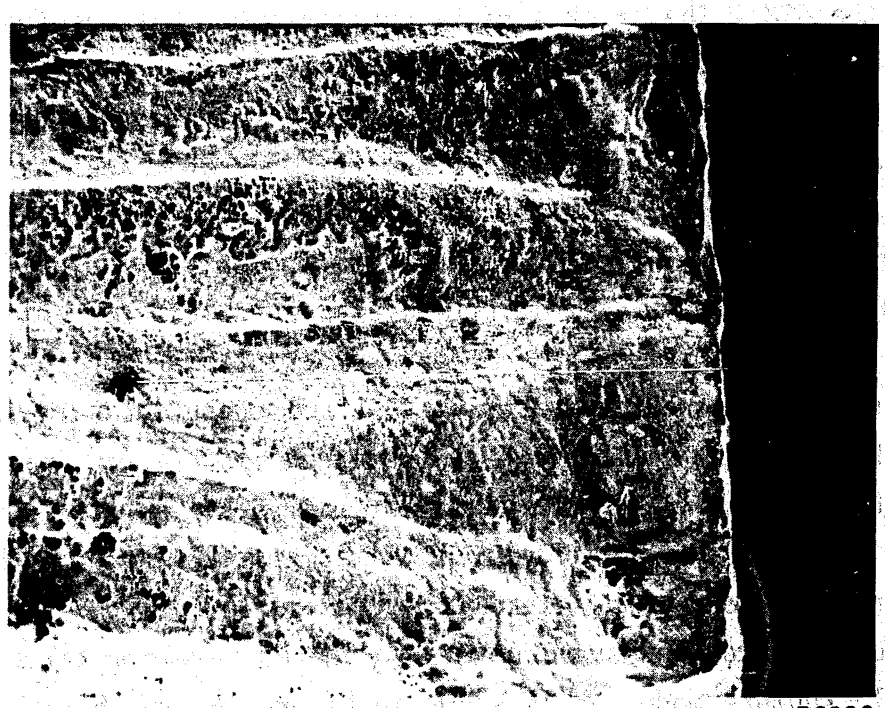

FIGURE 41. APPEARANCE OF AREA 21 INDICATING LACK WELD METAL OVER A PORTION OF THE END OF THE VALVE-END STIFFENER RING

Specimen OMB, Crack Through the Butt Weld in the Middle Stiffener Ring

To determine the fracture modes present on the surfaces of the crack in the middle stiffener ring, Specimen OMB, was selected for examination in the SEM. The crack surface contained on that specimen is shown in Figure 42; the numbers and arrows on that figure refer to regions where SEM fractographs were taken to document the fracture appearance.

As is shown in Figure 42, there was evidence of crack extension for about 1/8 inch into the vessel shell immediately below the fillet weld on the valve-end side of the stiffener ring. That region was identified as Area 13 on Figure 42. The ductile nature of that crack extension into the vessel shell is shown in the SEM fractographs in Figure 43. The fresh fracture surface through the vessel shell produced in the laboratory after cooling the section in liquid nitrogen exhibited cleavage fracture as is shown in Figure 44, which was taken in Area 5. The fracture surfaces through the fillet welds on both sides of the stiffener ring also exhibited a ductile rupture mode as is shown in Figure 45.

Most of the fracture surface through the butt-weld metal exhibited a ductile rupture mode, as is shown in Figure 46, which was taken in Area 19. Areas 2, 6, 7, 17, and 18 exhibited virtually the same fracture appearance.

Areas 3 and 4 on Figure 42 exhibited a flat region on the fracture through the butt-weld metal and somewhat different fracture appearances than the ductile rupture exhibited in nearly all other regions of fracture through the butt-weld metal. However, at higher magnifications those regions exhibited features indicative of ductile rupture as is shown in Figures 47 and 48. In Area 3, there appeared to be some small, featureless facets on the fracture surface. Those may have resulted from fracture through or along oxide films or merely may have been regions where corrosion products still remained on the surface after cleaning. In Area 4, the

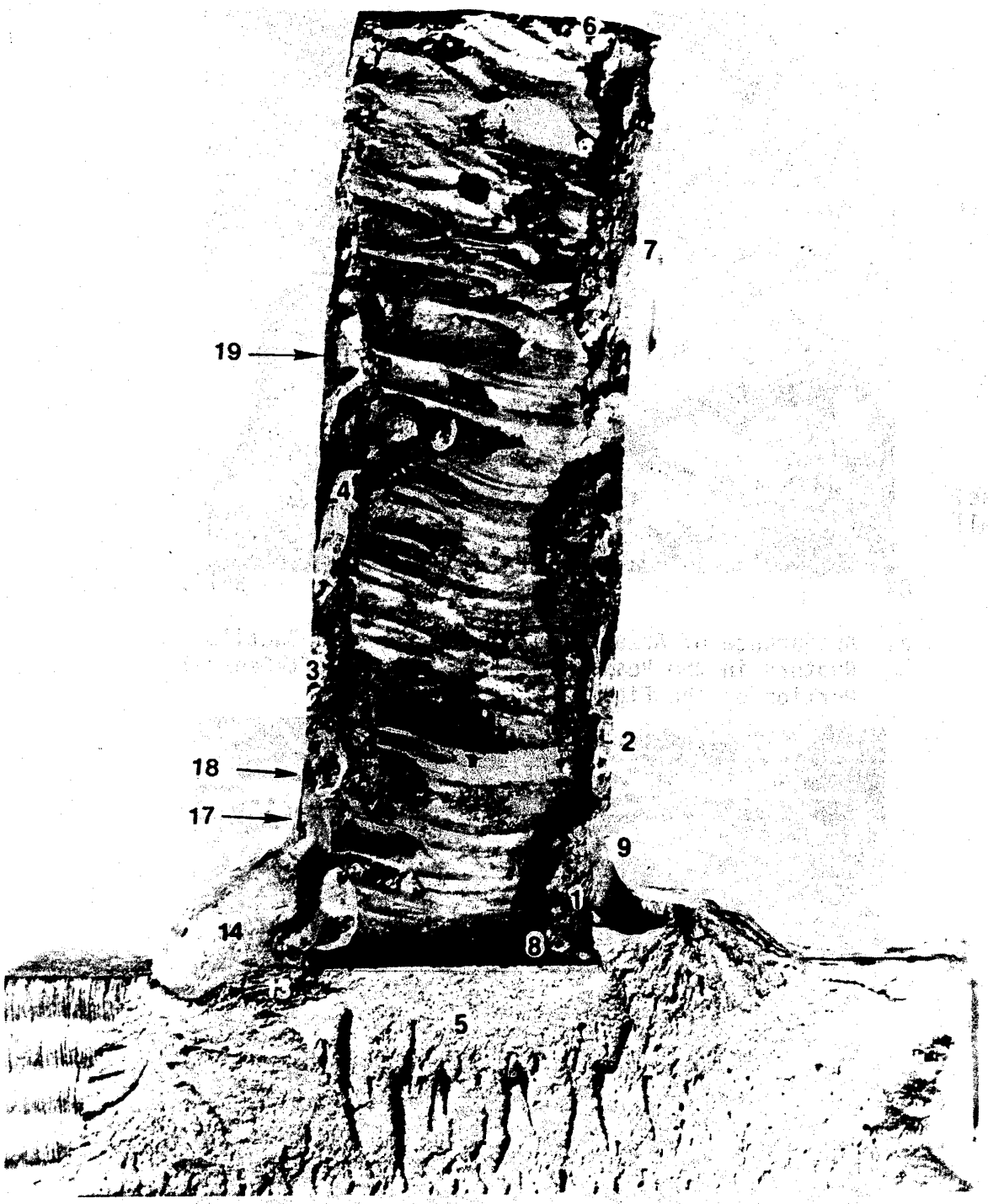

2.4X 4M906E

FIGURE 42. SURFACE OF CRACK THROUGH THE MIDDLE STIFFENER RING THAT WAS EXAMINED IN THE SEM, SPECIMEN OMB

The numbers and arrows refer to the locations where SEM fractographs were taken.

8X 56761

a. Appearance of Area 13 on Figure 42. The Ductile Rupture in the Vessel Shell is in the Left-Central Portion of the Figure

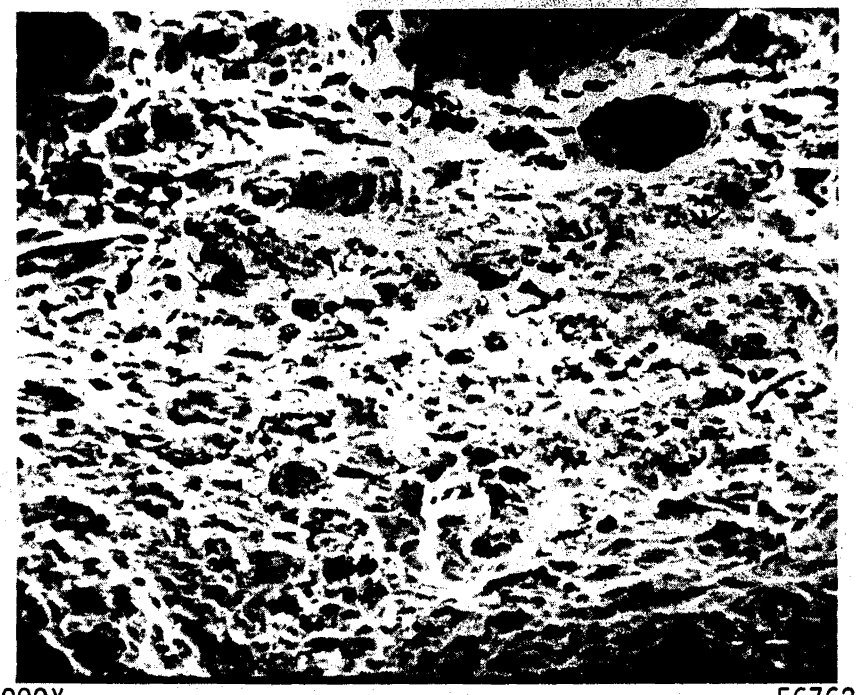

1000X 56762

b. Ductile Rupture in Area 13

FIGURE 43. DUCTILE CRACK GROWTH IN THE VESSEL SHELL BELOW THE FILLET WELD ON THE VALVE-END SIDE OF THE MIDDLE STIFFENER RING

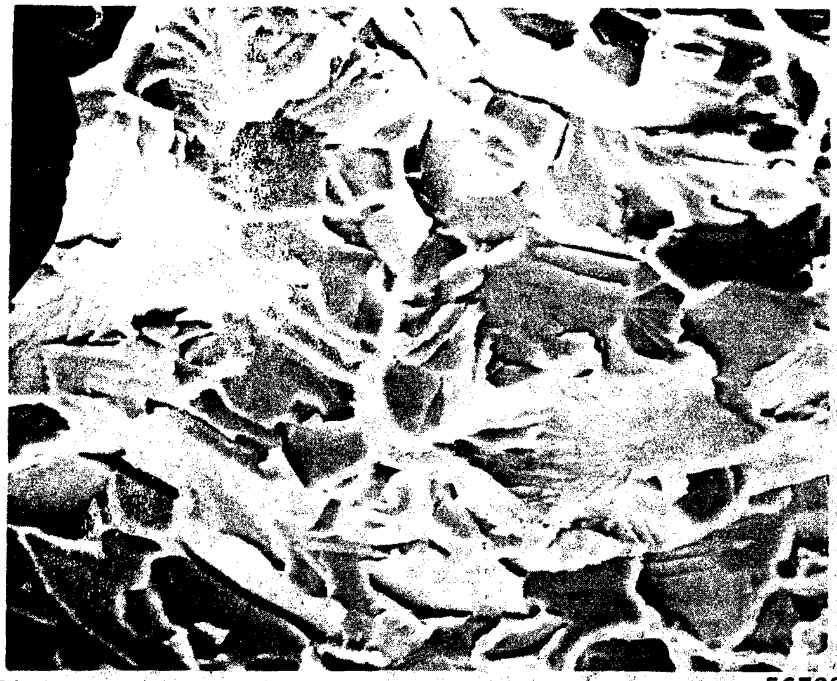

1000X 56729

FIGURE 44. TYPICAL CLEAVAGE FRACTURE OBSERVED ON THE FRACTURE SURFACE THROUGH THE VESSEL SHELL PRODUCED IN THE LABORATORY (AREA 5 ON FIGURE 42)

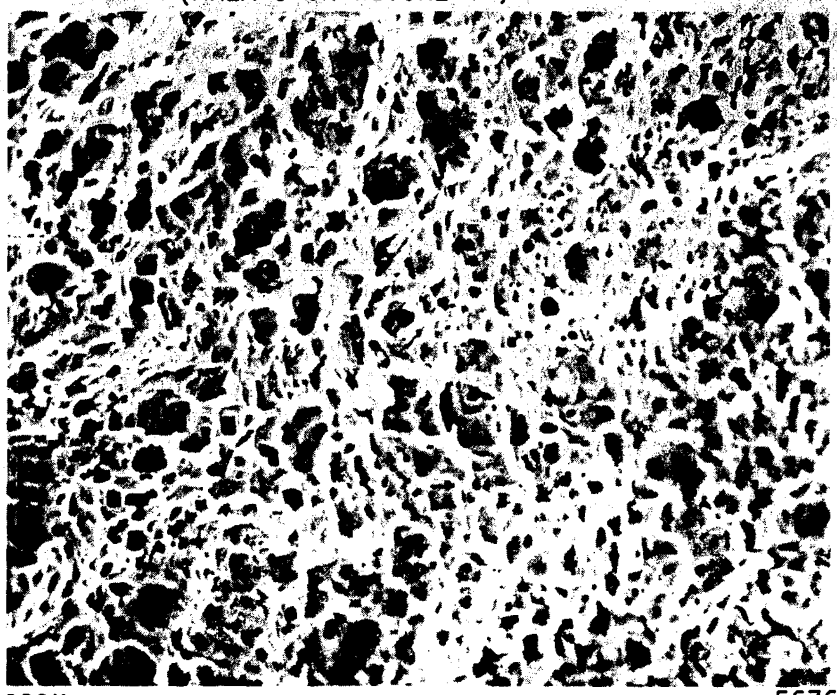

1000X 56764

FIGURE 45. TYPICAL DUCTILE RUPTURE THROUGH THE FILLET WELD ON THE VALVE-END SIDE OF THE MIDDLE STIFFENER RING (AREA 14 ON FIGURE 42)

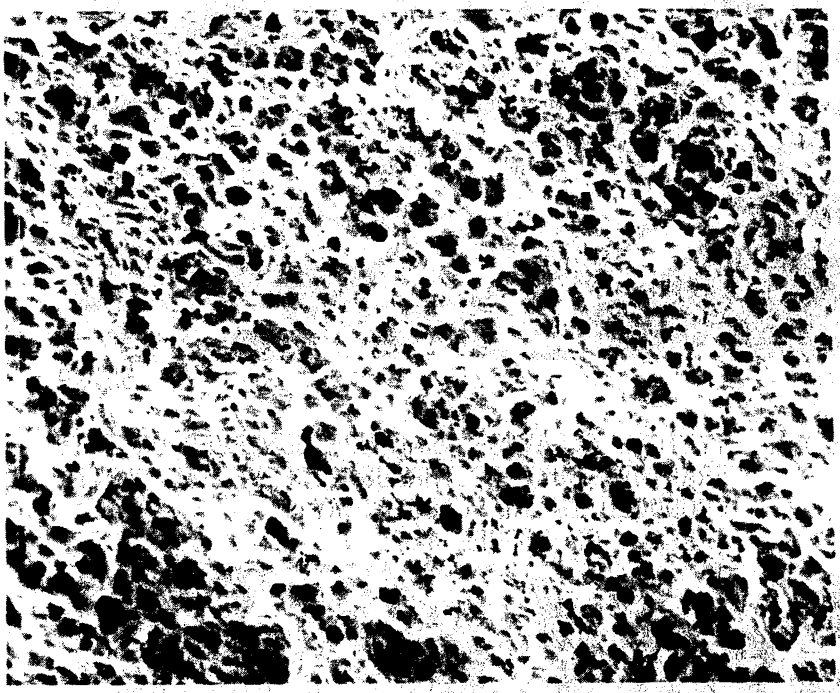

1000X 56771

FIGURE 46. DUCTILE RUPTURE TYPICAL OF THE FRACTURE SURFACES THROUGH THE WELD METAL ON THE BUTT WELD IN MIDDLE STIFFENER RING

This fractograph was taken in Area 19 on Figure 42. Areas 2, 3, 6, 7 and 18 exhibited virtually the same fracture appearance.

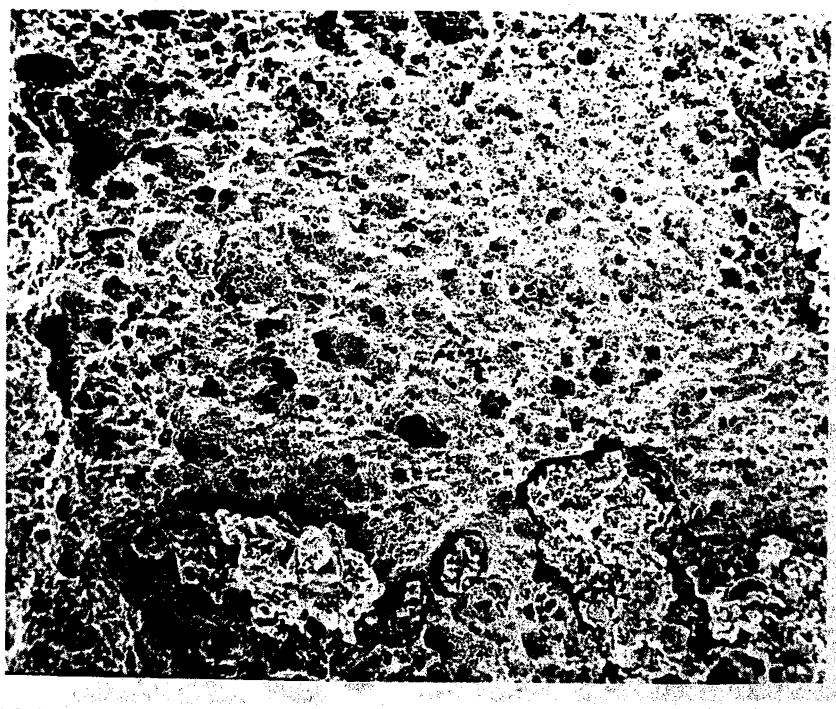

100X 56725

a. Typical Appearance of the Flat Fracture Region in Area 3 on Figure 42

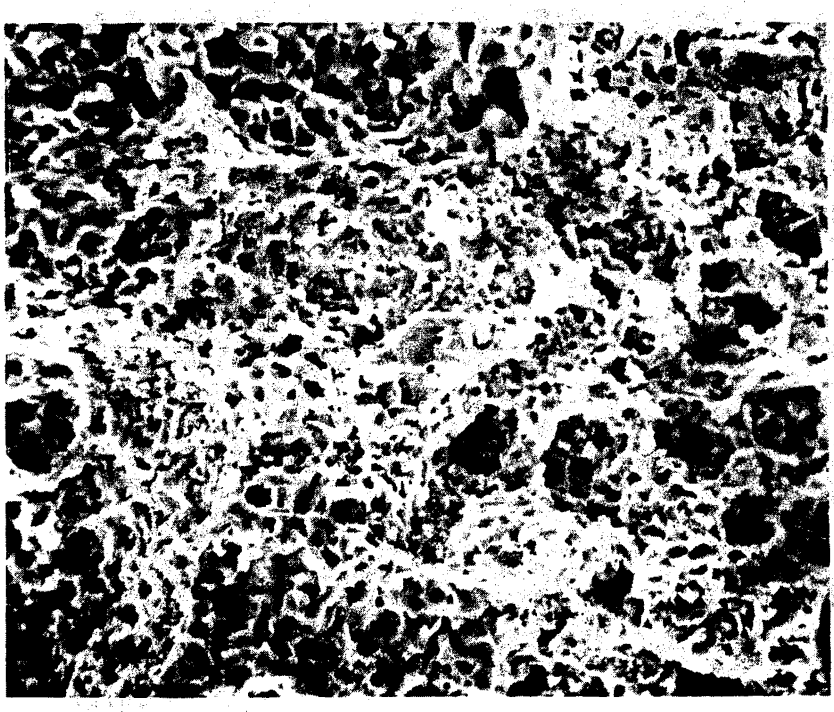

1000X 56726

b. Mixture of Ductile and Faceted Rupture in Area 3

FIGURE 47. APPEARANCE OF THE FRACTURE SURFACE IN AREA 3 ON THE FRACTURE THROUGH THE MIDDLE STIFFENER RING

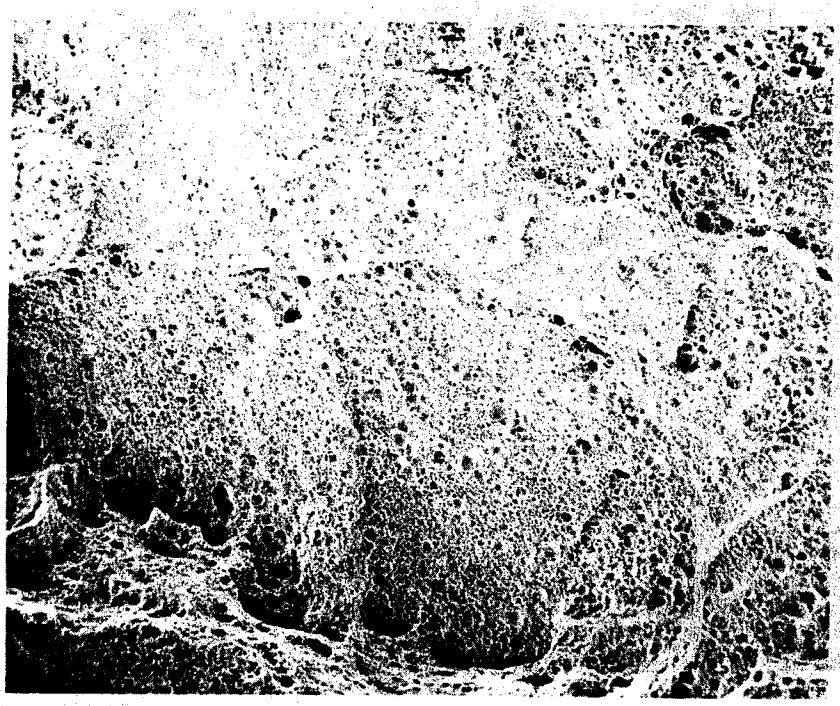

100X 56728

a. Flat Fracture Feature in Area 4 on Figure 42

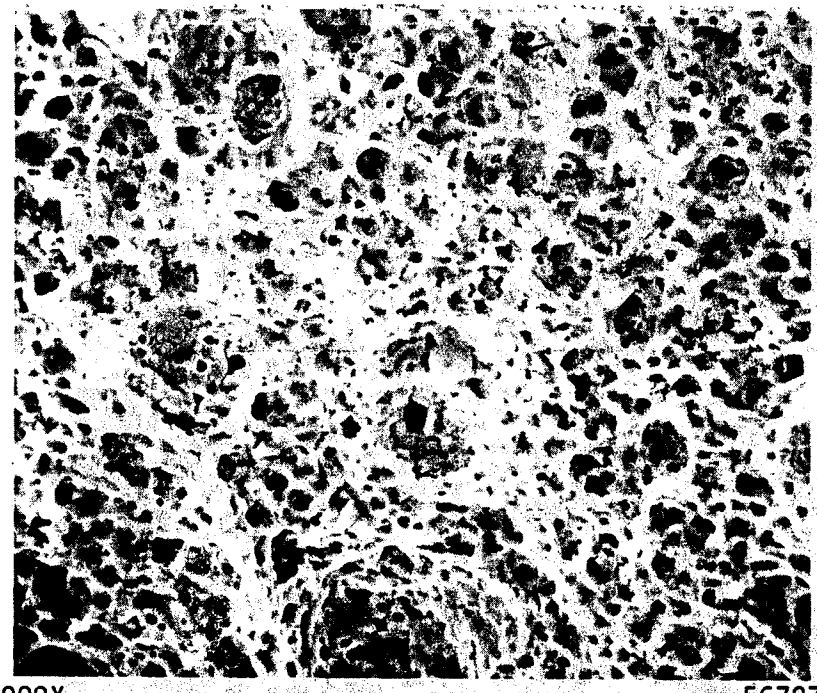

1000X 56727

b. Coarser Ductile Dimples and Corrosion Damage in Area 4

FIGURE 48. APPEARANCE OF AREA 4 ON THE FRACTURE THROUGH THE BUTT WELD IN THE MIDDLE STIFFENER RING

fracture surface appeared to be ductile but the dimple size was larger than that observed in most of the other areas. In addition, there appeared to be more corrosion damage in the fracture surface in that area.

Specimen OMD, Crack Through Butt Weld in the Drain-End Stiffener Ring

The fracture surfaces contained on Specimen ODB-W were examined in the SEM to determine the mode of fracture present in the various regions. That fracture surface is shown in Figure 49. The SEM examination revealed that the fracture surface produced in the laboratory when Section ODB was broken to expose the fracture crack surfaces was cleavage as would be expected since after immersion in liquid nitrogen the temperature of the steel was well below its ductile-to-brittle fracture transition temperature. The appearance of that fracture mode was shown previously in Figure 44.

Examination of the fracture surfaces on the vessel shell adjacent to the fillet welds, Areas 4 and 25 in Figure 49, revealed that some crack growth into the vessel shell had occurred prior to the rupture of the vessel. That crack extension occurred by ductile rupture, as is illustrated in Figure 50, and it occurred below the fillet welds on either side of the stiffener ring, even though the ultrasonic inspection indicated crack below the fillet weld only on the drain-end side. It appeared that the depth crack growth into the vessel shell below the fillet welds ranged from 1/16 to 1/8 inch.

The fracture through the fillet welds on either side of the drain-end stiffener ring occurred by ductile rupture as was the case for the fracture through the fillet welds in the valve-end stiffener. A region of ductile rupture, Area 6 on Figure 49, typical of those fracture surfaces is illustrated in Figure 51. A crack extending circumferentially in the fillet on the drain-end side of the drain-end stiffener was observed; that crack is illustrated in Figure 52.

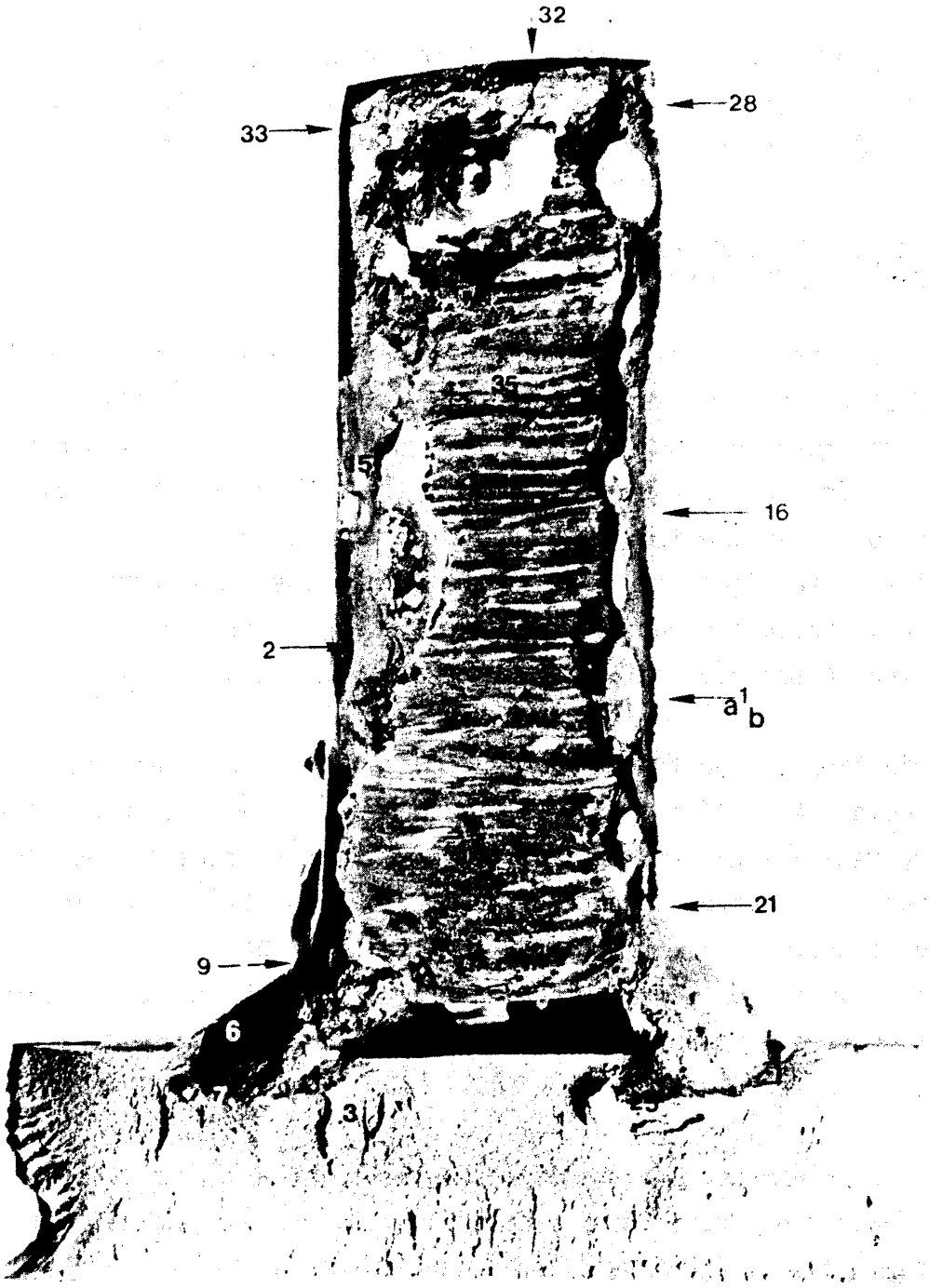

2.4X Cleaned 4M921E

FIGURE 49. SURFACE OF SPECIMEN ODB-W, FROM THE DRAIN-END STIFFENER RING THAT WAS EXAMINED IN THE SEM

The number and arrows indicate the locations where fractographs were taken to document the fracture appearance

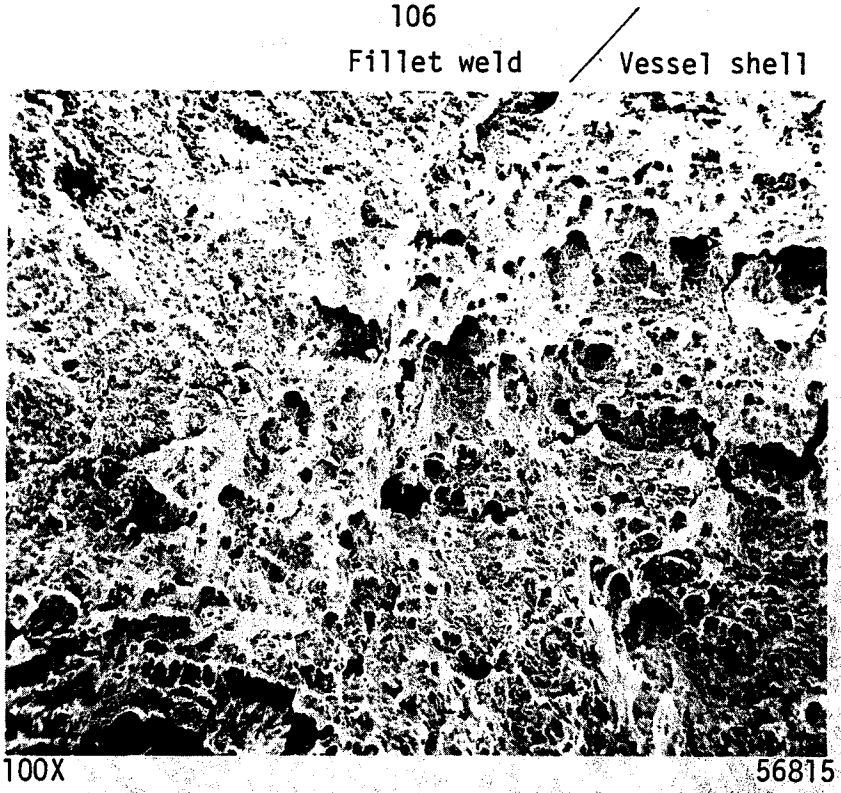

a. Appearance of Area 4

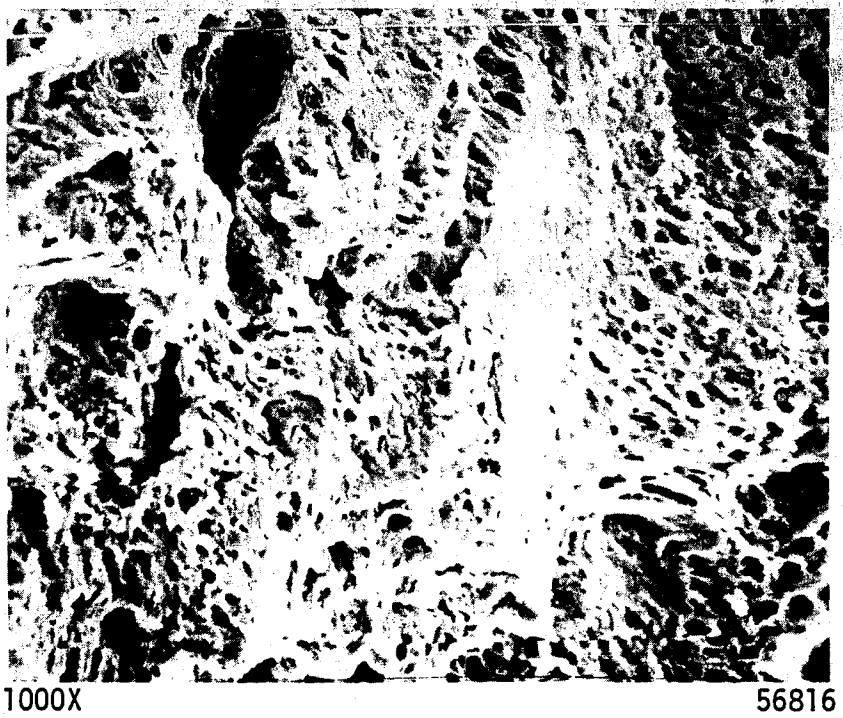

b. Ductile Rupture in the Vessel Shell in Area 4

FIGURE 50. DUCTILE CRACK EXTENSION INTO THE VESSEL SHELL ADJACENT TO THE FILLET WELD ON THE DRAIN-END STIFFENER

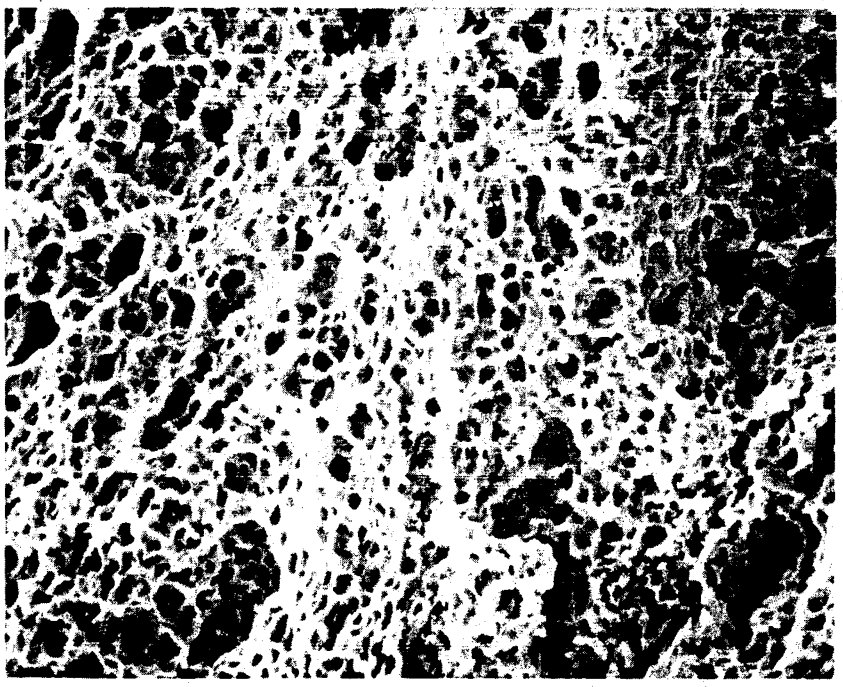

1000X 56818

FIGURE 51. TYPICAL DUCTILE RUPTURE OBSERVED ON THE FILLET WELDS IN SPECIMEN ODBW FROM THE DRAIN-END STIFFENER RING

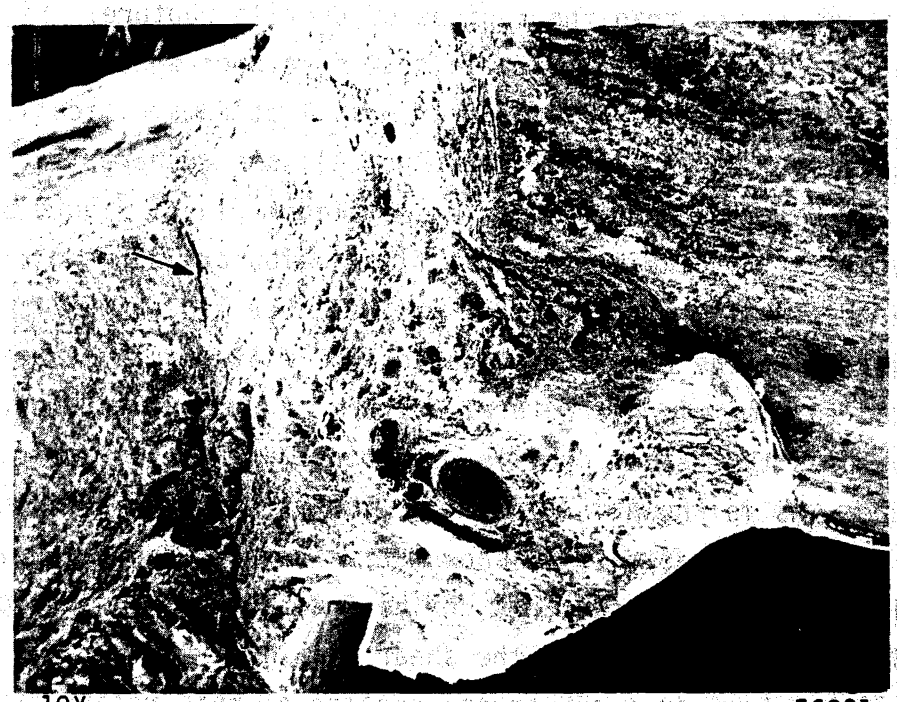

FIGURE 52. CRACK EXTENDING CIRCUMFERENTIALLY IN THE FILLET WELD ON THE DRAIN-END SIDE OF THE DRAIN-END STIFFENER RING

The arrow points to the crack.

Examination of the surfaces of the fracture through the butt-weld metal in the drain-end stiffener revealed features that were not observed on the surfaces through the fracture in the valve-end stiffener ring. Those features were the flat oval shaped regions shown in Figure 49. Examination of those regions in the SEM revealed that they exhibited a significantly different appearance than the regions of ductile rupture. Figure illustrates the fracture appearance of the flat fracture region, shown in Area 1 on Figure 49. Figure 53a illustrates Area 1 at a magnification of 8X. It shows the oval shaped flat region (Area A), and a shear lip (Area B) extending from Area A to the surface of the stiffener ring. Figure 53b illustrates the unusual appearance of that flat region at 100X and Figure 53c illustrates the flat region and the start of the shear lip at 350X. Figures 53b and c suggest that the coarse features on the flat fracture area may have been related to some microstructural feature of the weld deposit. They did not show features typical of ductile rupture, cleavage, or truly intergranular fracture. As is shown in Figure 53c and at higher magnification in Figure 53d, that region appears to show more corrosion damage as indicated by the small circular pit-like features on the fracture surface. Figure 53e shows the ductile rupture typical of the shear lip (Area B).

As will be shown in a subsequent section of this report, the flat fracture regions, such as Area A just described, were related to microstructural features in the weld metal deposit. Some of those regions appear to have cracked when a subsequent layer of weld metal was deposited during the butt-welding operation during vessel fabrication.

All other regions examined on the fracture surfaces through the butt weld in the drain-end stiffener showed ductile rupture. Figure 54 illustrates the ductile rupture features in Areas 2 and 33 on Figure 49. As is shown in Figure 55, some regions of the fracture through the butt-weld metal in the drain-end stiffener ring also contained significant porosity.

The fractographic examination of the specimens from the origin region of the rupture and the cracks in the other two stiffener rings has shown that flat fracture region in the vessel shell was below the valve

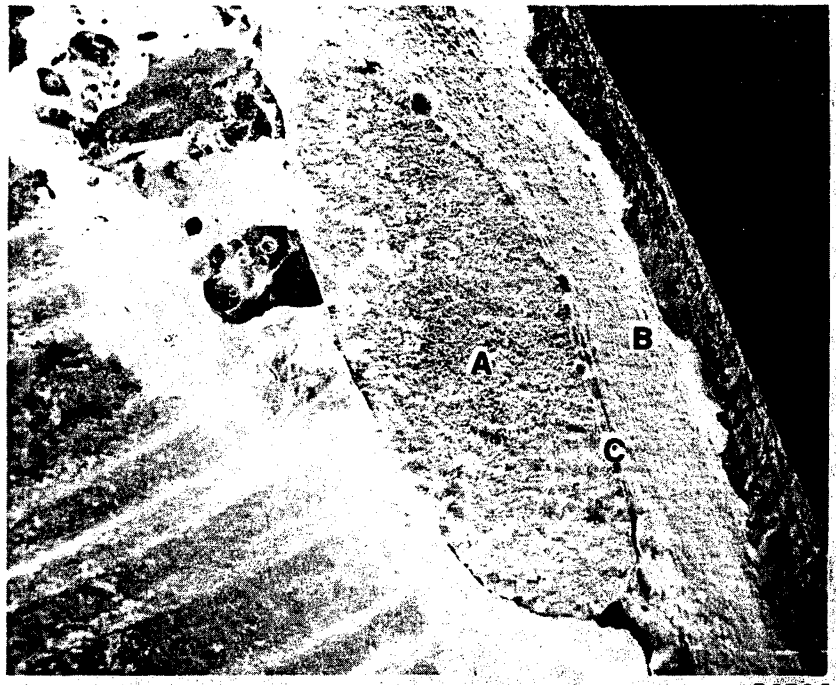

8X 56736

a. Appearance of the Fracture Surface in Area 1 on Figure 49

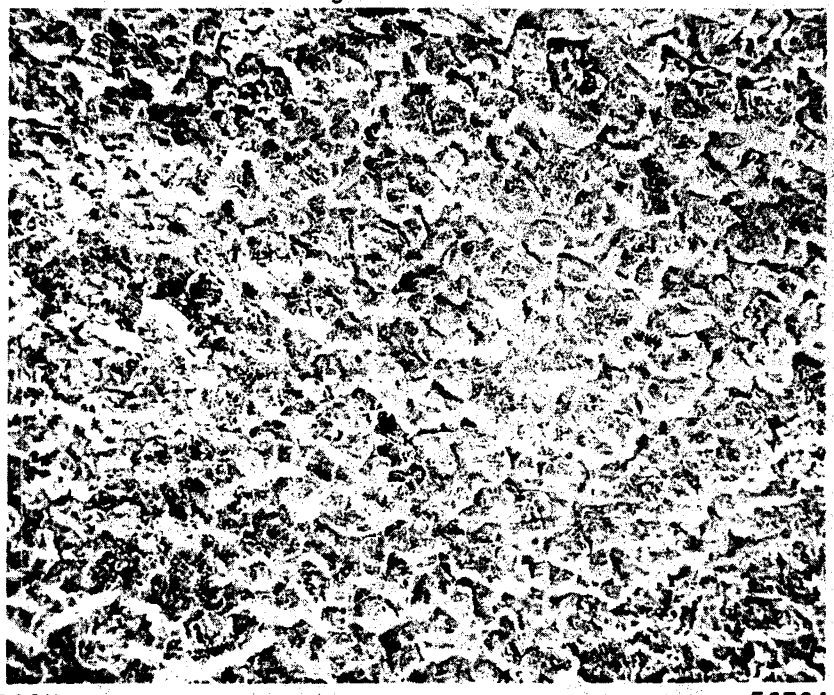

100X 56734

b. Typical Appearance of the Flat Fracture Region in Area A of Figure 53a

FIGURE 53. TYPICAL FEATURES OBSERVED ON THE REGIONS OF FLAT FRACTURE THROUGH THE BUTT WELD IN THE DRAIN-END STIFFENER RINGS

350X 56739

c. Transition from Flat Fracture to the Shear Lip in Area 1 shown in Figure 53a.

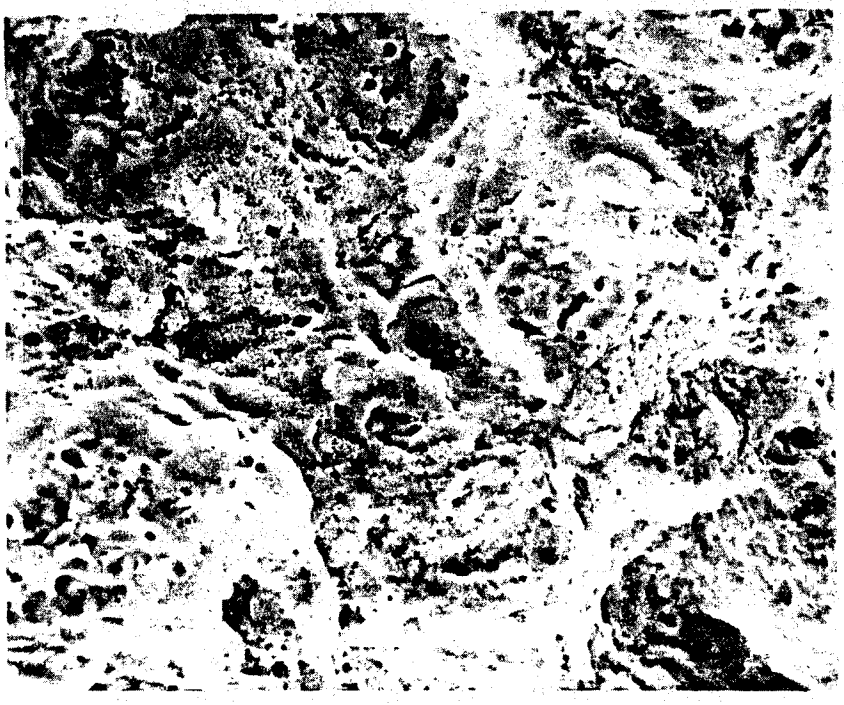

1000X 56735

d. Appearance of Flat Fracture, Area A Showing Corrosion Damage and Perhaps Some Ductile Rupture

FIGURE 53. (Continued)

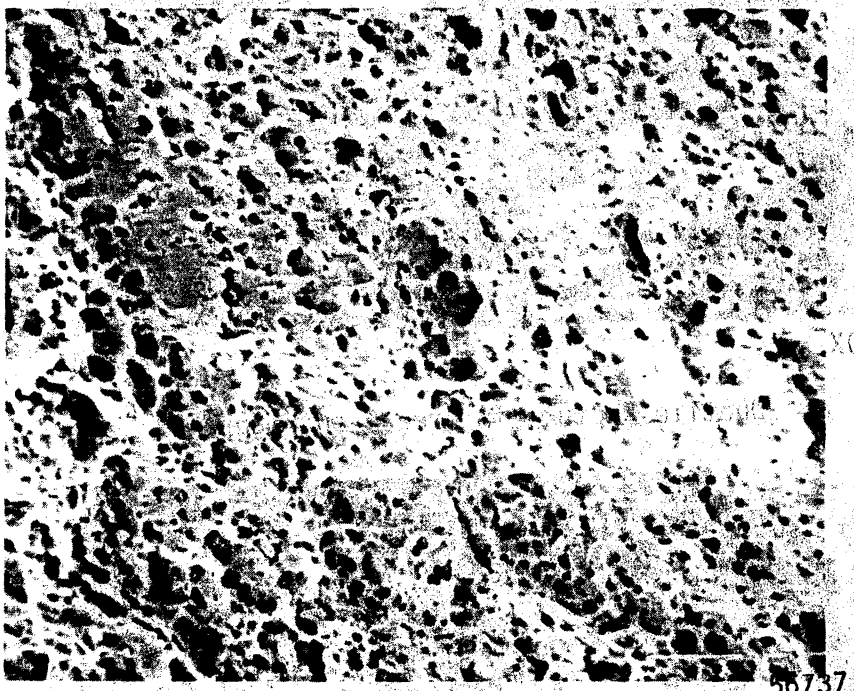

1000X

e. Typical Ductile Shear Fracture in Area B of Figure 53a

FIGURE 53. (Continued)

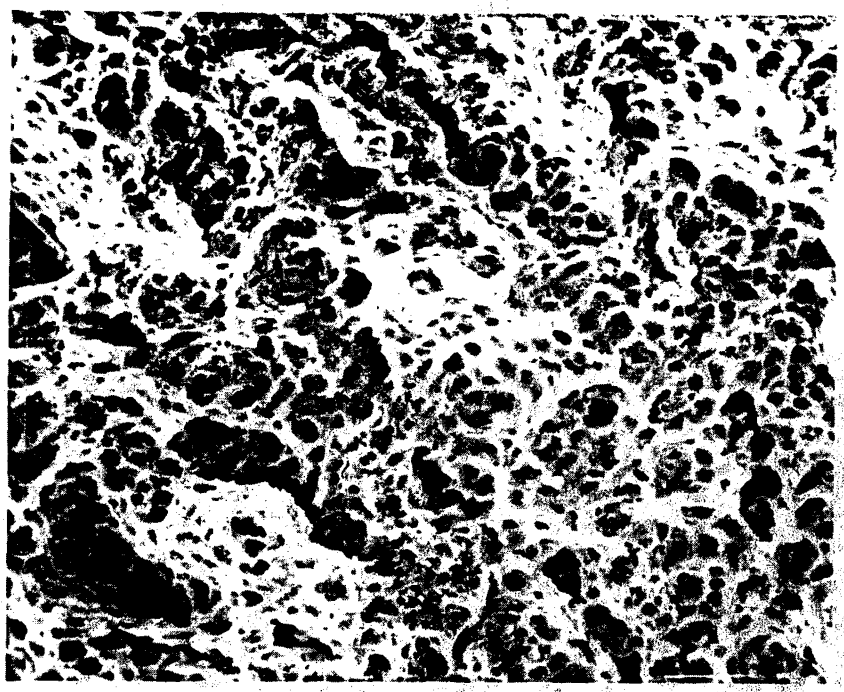

1000X 56744

a. Ductile Rupture in Area 2 on Figure 49

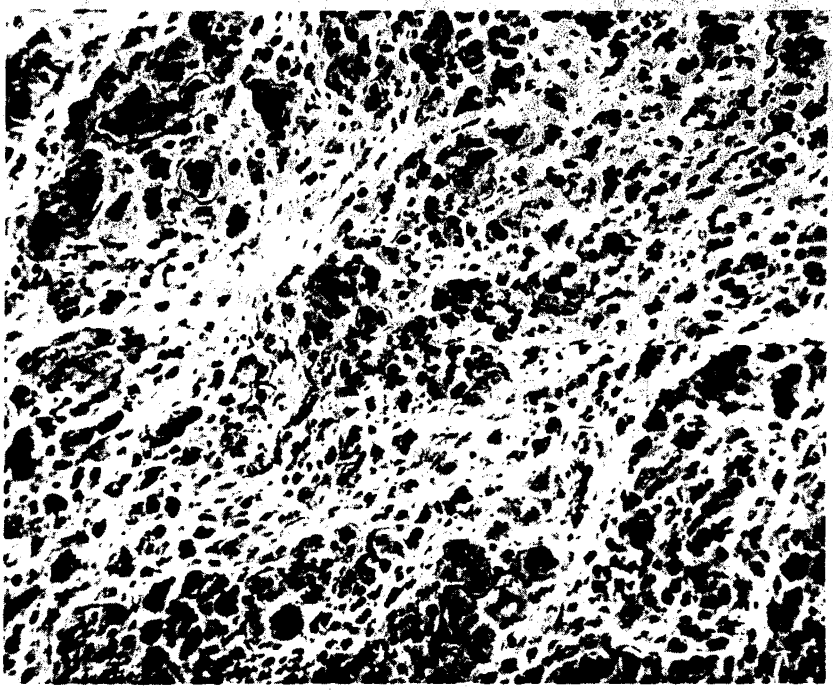

1000X 56846

b. Ductile Rupture in Area 33 on Figure 49

FIGURE 54. EXAMPLES OF DUCTILE RUPTURE ON THE SURFACE OF THE FRACTURE THROUGH BUTT WELD CONTAINED ON SPECIMEN ODBW FROM THE DRAIN-END STIFFENER RING

Top surface of stiffener ring

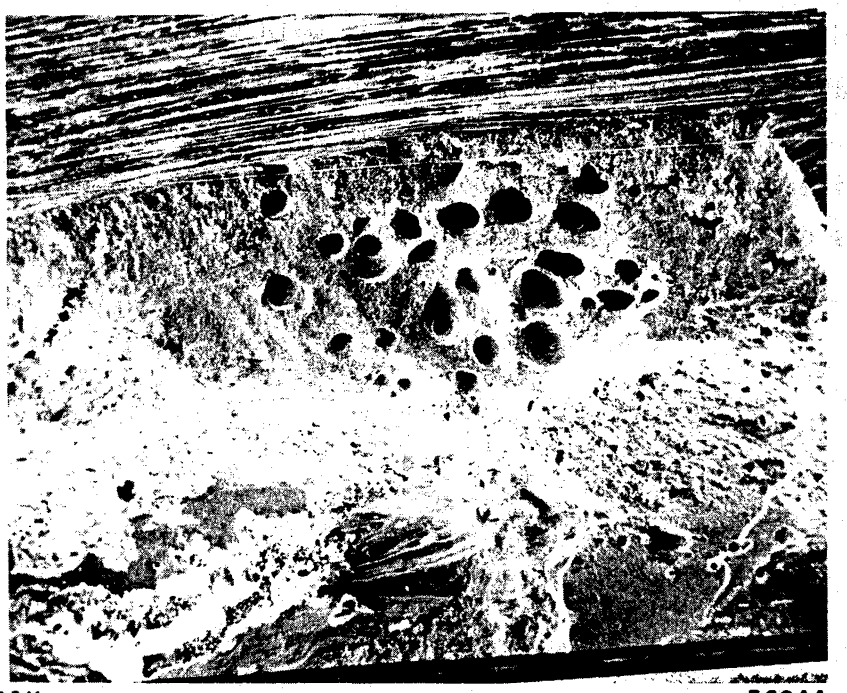

11X 56844

FIGURE 55. POROSITY IN THE BUTT WELD METAL IN AREA 32 ON FIGURE 49

end stiffener was a region of ductile crack growth. Also, cracks extended a short distance into the base metal in a ductile mode below the fillet welds between the vessel shell and the middle and the drain-end stiffener rings. The fractures through all of fillet welds also were ductile. Finally, although a few unusual appearing regions were observed on the fracture surfaces of the butt-weld metal deposits, the bulk of those butt weld metal fracture surfaces exhibited ductile ruptures. Even the unusual appearing fracture region in the butt-weld fractures were not indicative cleavage, intergranular, or fatigue failure. Thus, this portion of the investigation has demonstrated that the rupture in the shipping container and the cracks through the butt welds in the stiffener rings occurred by ductile rupture.

Stress Analysis of UF_6 Cylinder

The objective of this task was to determine the internal pressure required to cause failure of the UF_6 vessel for both the design properties and the actual properties. This was accomplished by means of a series of finite element stress analyses of the vessel. These analyses are categorized according to the following analysis types:

(1) Linear elastic stress analysis
(2) Elastic-plastic stress analysis
(3) Fracture mechanics analysis.

The linear elastic and elastic-plastic stress analyses were peformed using the SAVFEM computer code. For the fracture mechanics analysis, BCLFEM was used. BCLFEM is a specialized version of SAVFEM which contains the fracture mechanics principles necessary for the J-integral computations.

Both the linear elastic and elastic-plastic stress analyses used an axisymmetric finite element model. An axisymmetric analysis contains certain inherent assumptions. These assumptions, as well as other assumptions necessary for the analyses, are given below:

(1) A detailed drawing of the actual vessel was not available. Therefore, the generic drawing received from Kerr-McGee (UF_6 Cylinder Model 48Y) is assumed to be an accurate representation of the vessel geometry.
(2) The cylinder is axisymmetric; thus, the following items are assumed to be constant at every cross-section.
    (a) Shell thickness
    (b) Stiffener thickness and height (lifting lugs are not included in the analysis)
    (c) Fillet weld geometry (i.e., weld bead shape, penetration depth, gap between shell and stiffener).
(3) Longitudinal welds do not exist. Both types of longitudinal welds (shell seam weld and stiffener butt weld) call for full penetration, and as such, are assumed to deform the same as the surrounding base metal.

(4) The stiffener is assumed to be perpendicular to the shell and remains perpendicular during deformation. Thus, the centerline of the stiffener is modeled as a symmetry plane.

(5) The points located on the cross-section midway between two stiffeners or a stiffener and an elliptical head are assumed to remain in a plane that is perpendicular to the longitudinal axis of the cylinder. Thus, the longitudinal displacement at the midway point is constant through the shell wall.

(6) Each material is assumed to be homogeneous and exists, initially, in its virgin state. Thus, residual stresses and strains due to forming and/or welding are not included in the analysis.

(7) Since stress-strain data for the welds could not be obtained, the fillet-weld and butt-weld materials were assumed to have the same properties as the vessel material.

(8) The only loads acting on the cylinder are due to the internal pressure. The weight of the cylinder and its contents are not included in the analysis.

Linear Elastic Stress Analysis

The linear elastic stress analysis calculations were peformed to assess the structural integrity of the UF_6 vessel from a design engineer's viewpoint. Based on the available data, the UF_6 vessel was designed to behave elastically. Therefore, from a design engineer's viewpoint, failure occurs when the vessel begins to yield and only a linear elastic stress analysis is required.

The elastic analysis consisted of four separate cases:

(1) No penetration along the stiffener/vessel interface at the fillet weld.

(2) Full penetration at the fillet weld.

(3) 1/16-inch gap between the stiffener and vessel, with 1/8-inch penetration at the fillet weld.

(4) 1/16-inch gap; with no penetration at the fillet weld.

The finite element models for each of these cases are shown in Figures 56 through 59. Each of these models contains approximately 350 nodal points and 280 elements. The model for Case No. 1 also contains four lift-off spring elements to model the stiffener/vessel interface. In each of these cases, only the portion of the cylinder between an end stiffener and a point halfway between the stiffener and the elliptical head was modeled (see Assumptions 4 and 5 above). The symmetry condition at the stiffener centerline was applied by fixing in the axial direction the nodal points along the centerline. The symmetry condition at the midway point between the stiffener and the elliptical head was applied by tying together the nodal points at this location through the use of rigid spring elements. These spring elements act only in the axial direction; therefore, the axial displacement at the midway point is constant through the shell thickness and the radial displacements are not affected by the spring elements.

An internal pressure of 1000 psi was applied to each of these models. In order to account for the axial force produced by the pressure acting on the elliptical head, a total axial force of 288000 lbs/radian was applied to the nodal points corresponding to the midway point between the stiffener and the head (Figure 60).

The materials are assumed to be linear elastic steel. Thus, an elastic modulus of 30×10^6 psi and Poisson's ratio of 0.3 were used for all materials present.

The results from this analysis show that the maximum stress in the vessel occurs on the inner surface of the vessel at the point midway between the stiffener and the head. The maximum stress in the stiffener occurs at the top of the fillet weld, as shown in Figure 61. Stress contours for the effective stress (von Mises) for each case at P = 1000 psi are shown in Figures 62 through 65. The stress levels corresponding to the contour numbers are presented in Table 14. The maximum effective stresses in the vessel and the stiffener at 1000 psi pressure are given in Table 15.

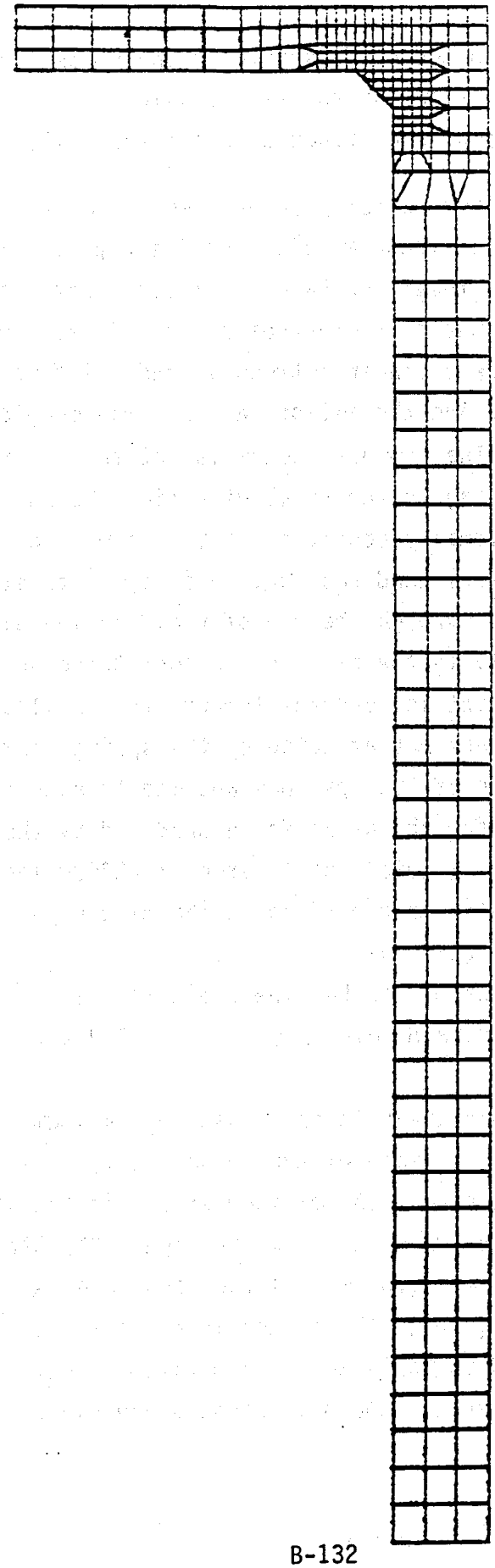

FIGURE 56. FINITE ELEMENT MODEL FOR ELASTIC ANALYSIS - CASE 1

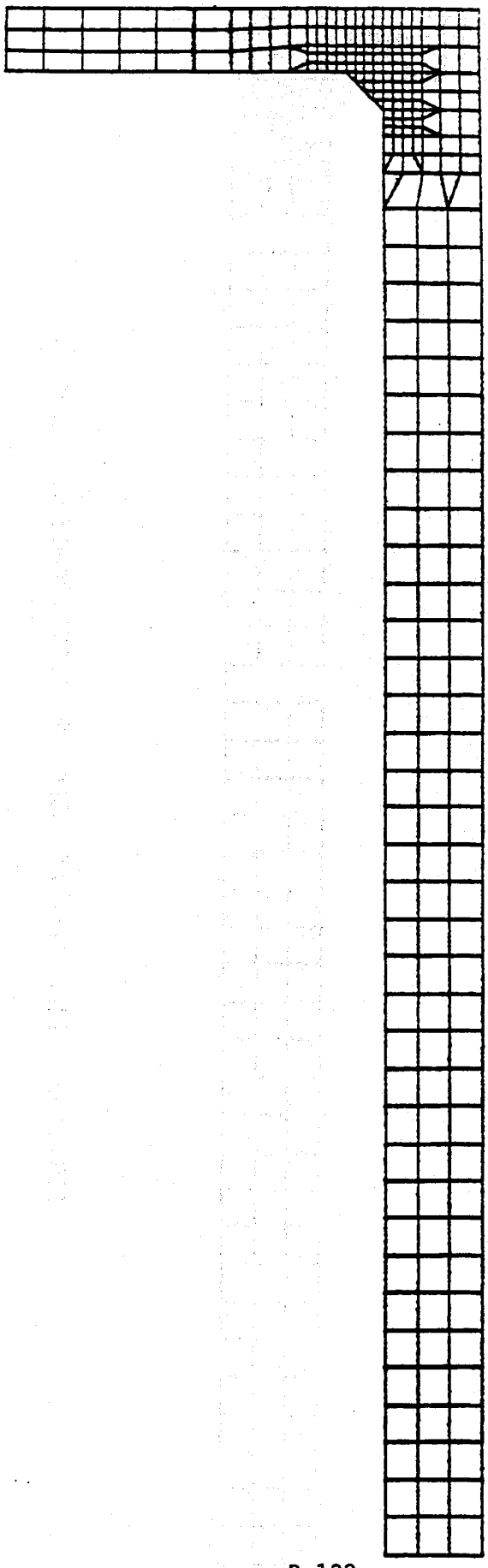

FIGURE 57. FINITE ELEMENT MODEL FOR ELASTIC ANALYSIS - CASE 2

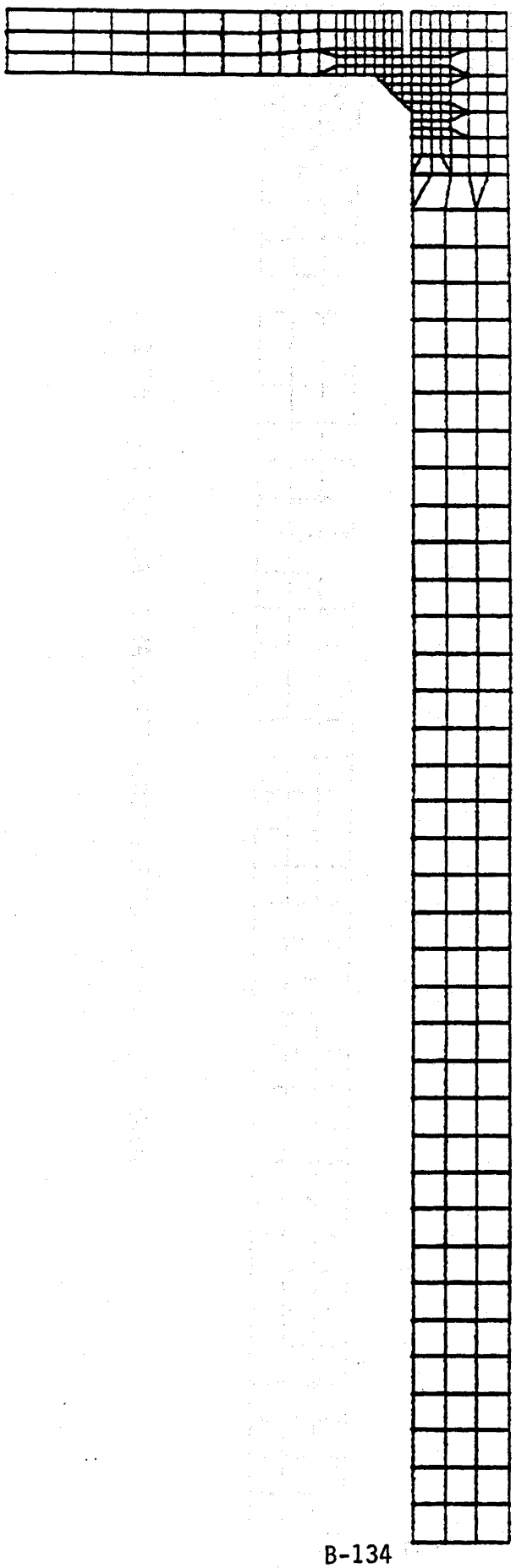

FIGURE 58. FINITE ELEMENT MODEL FOR ELASTIC ANALYSIS - CASE 3

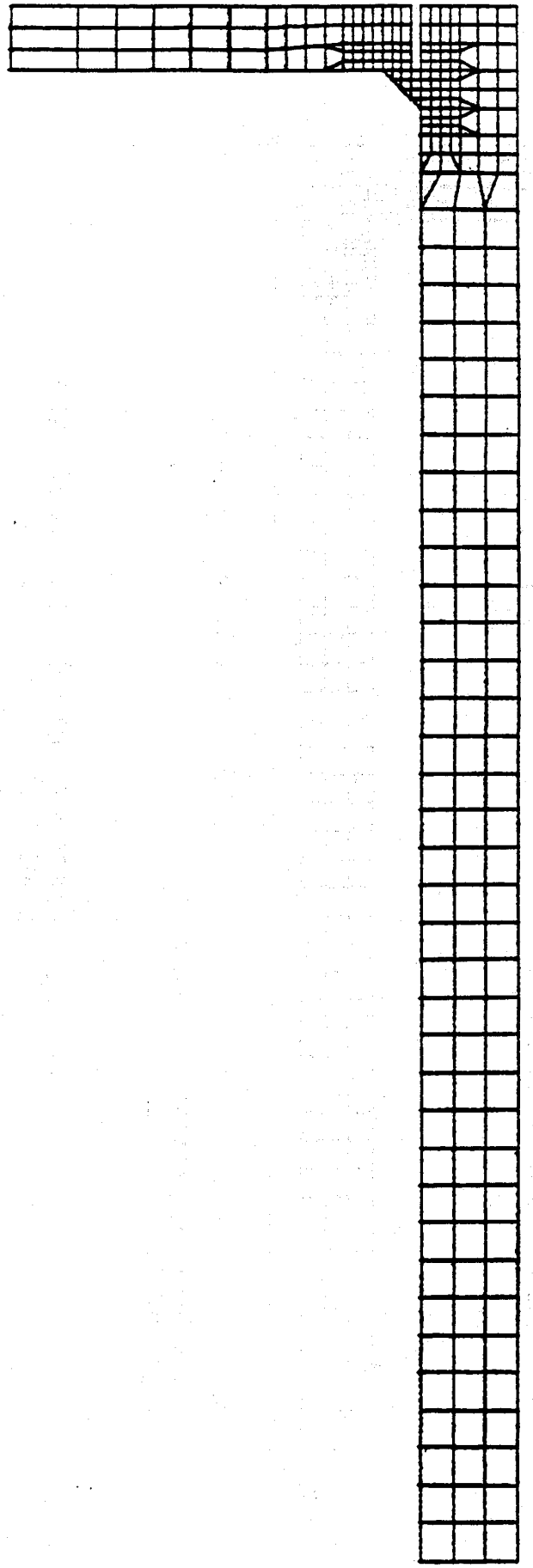

FIGURE 59. FINITE ELEMENT MODEL FOR ELASTIC ANALYSIS - CASE 4

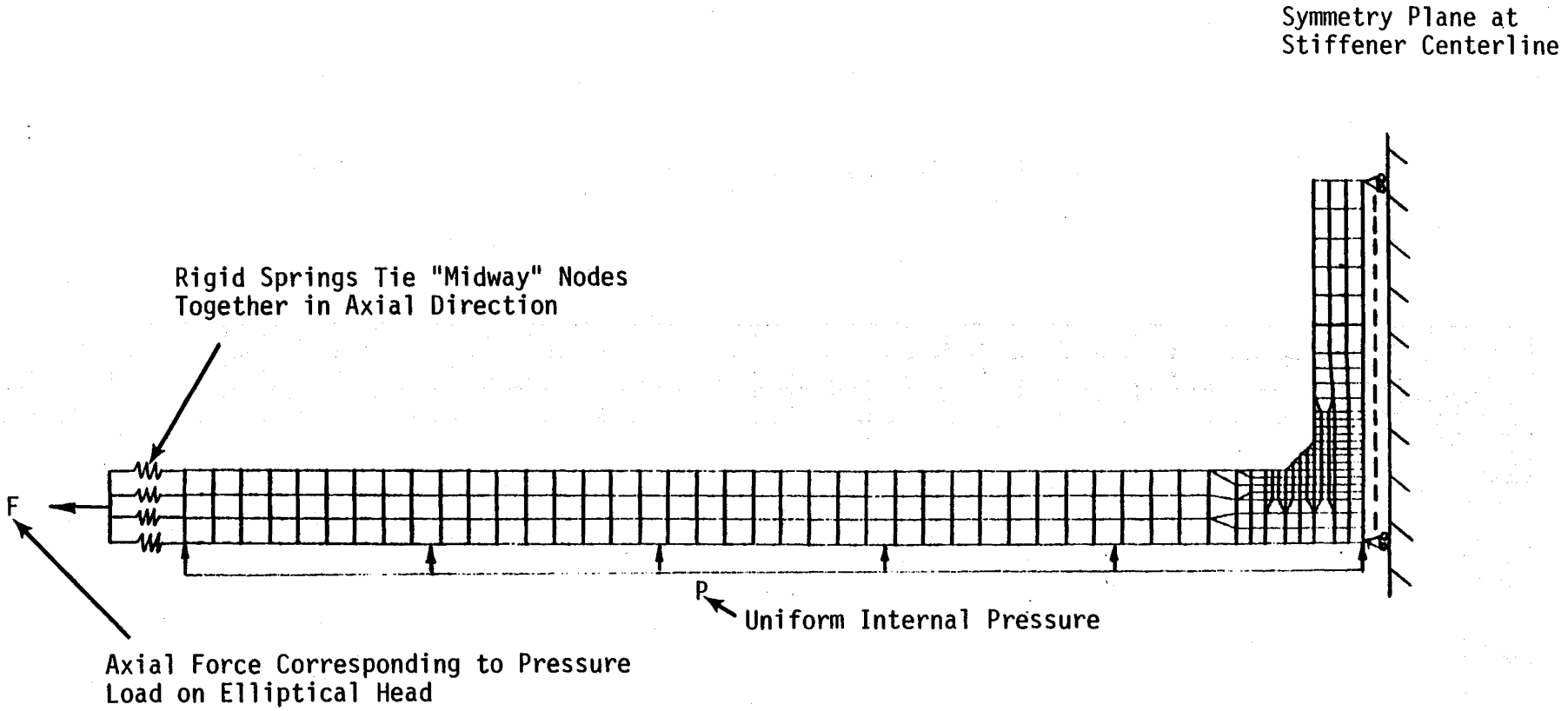

FIGURE 60. BOUNDARY CONDITIONS AND LOADS ON FINITE ELEMENT MODEL

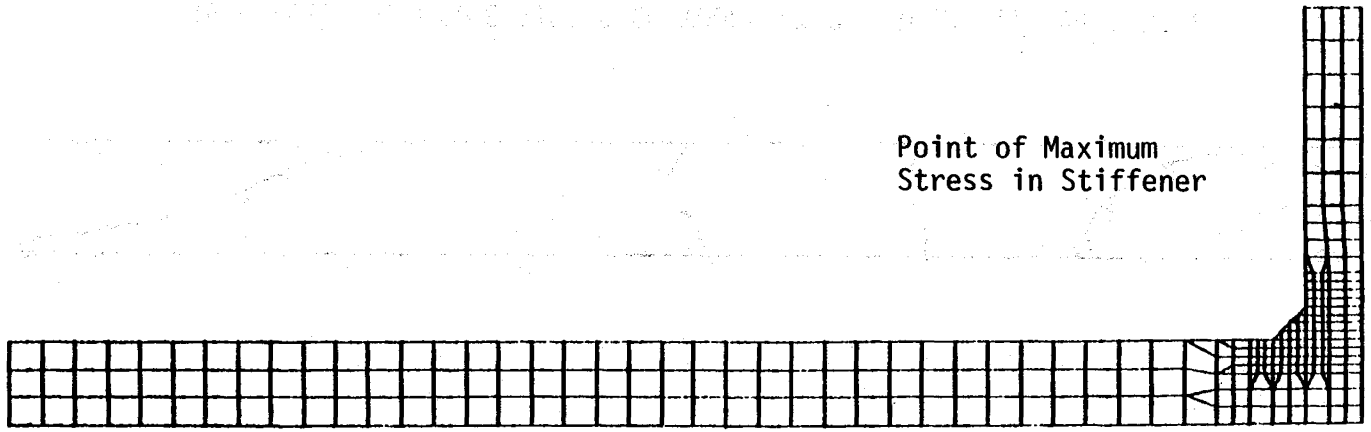

FIGURE 61. MAXIMUM STRESS LOCATIONS IN VESSEL AND STIFFENER

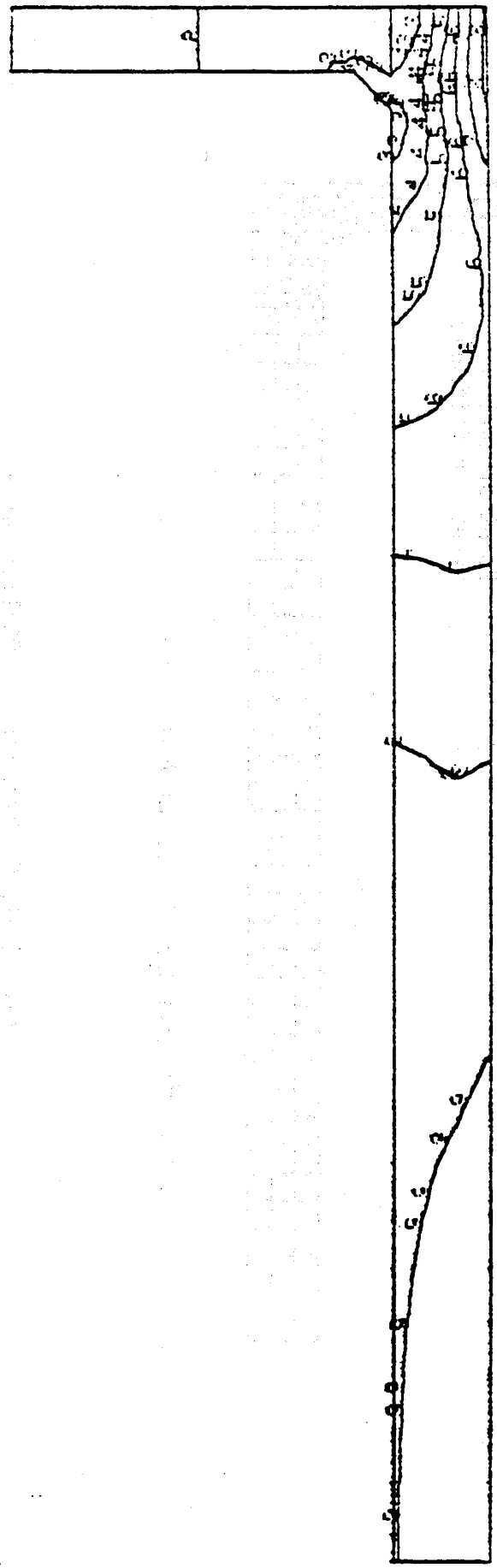

FIGURE 62. EFFECTIVE STRESS CONTOURS AT P = 1000 psi FOR CASE 1

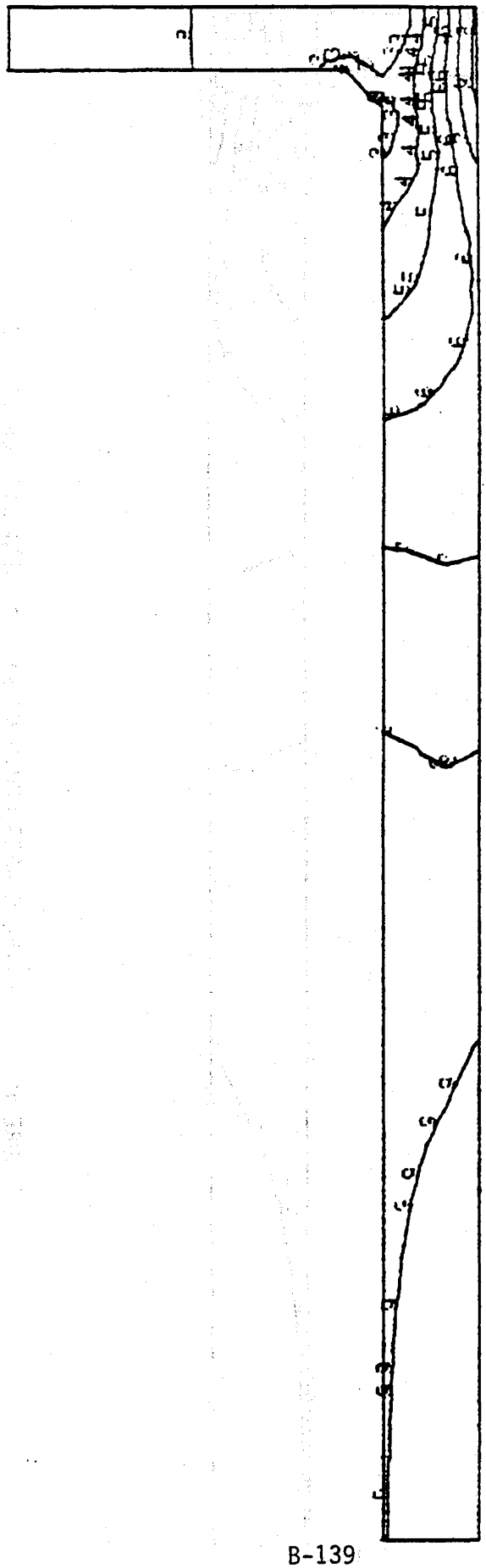

FIGURE 63. EFFECTIVE STRESS CONTOURS AT P = 1000 psi FOR CASE 2

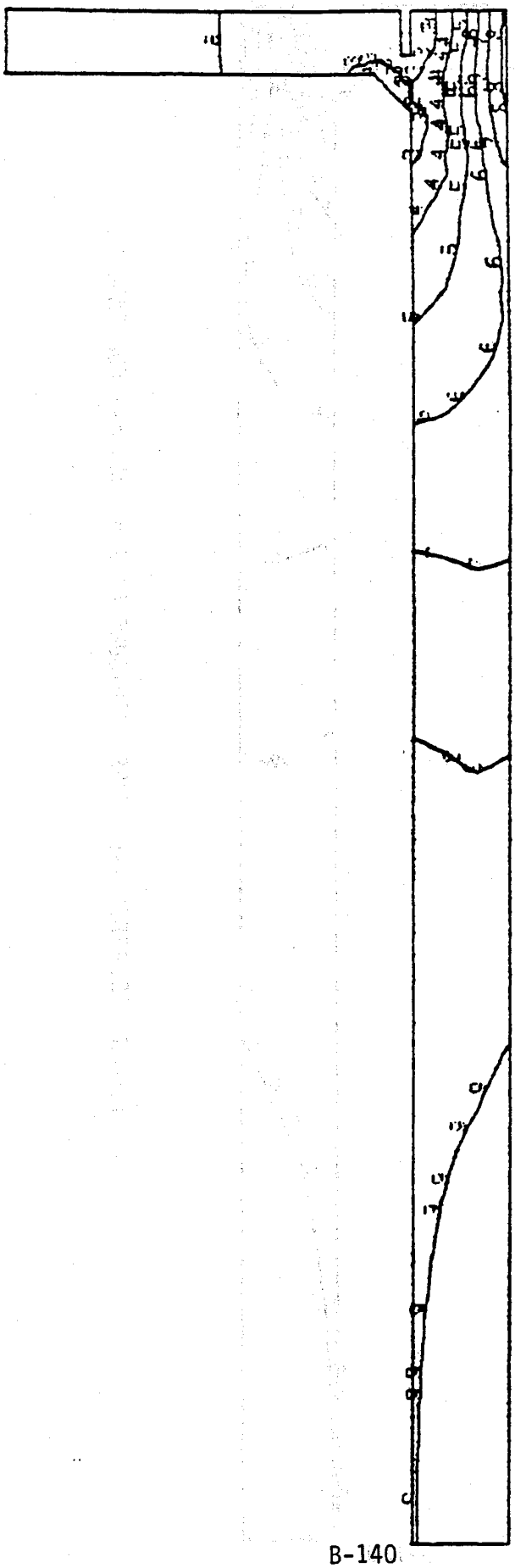

FIGURE 64. EFFECTIVE STRESS CONTOURS AT P = 1000 psi FOR CASE 3

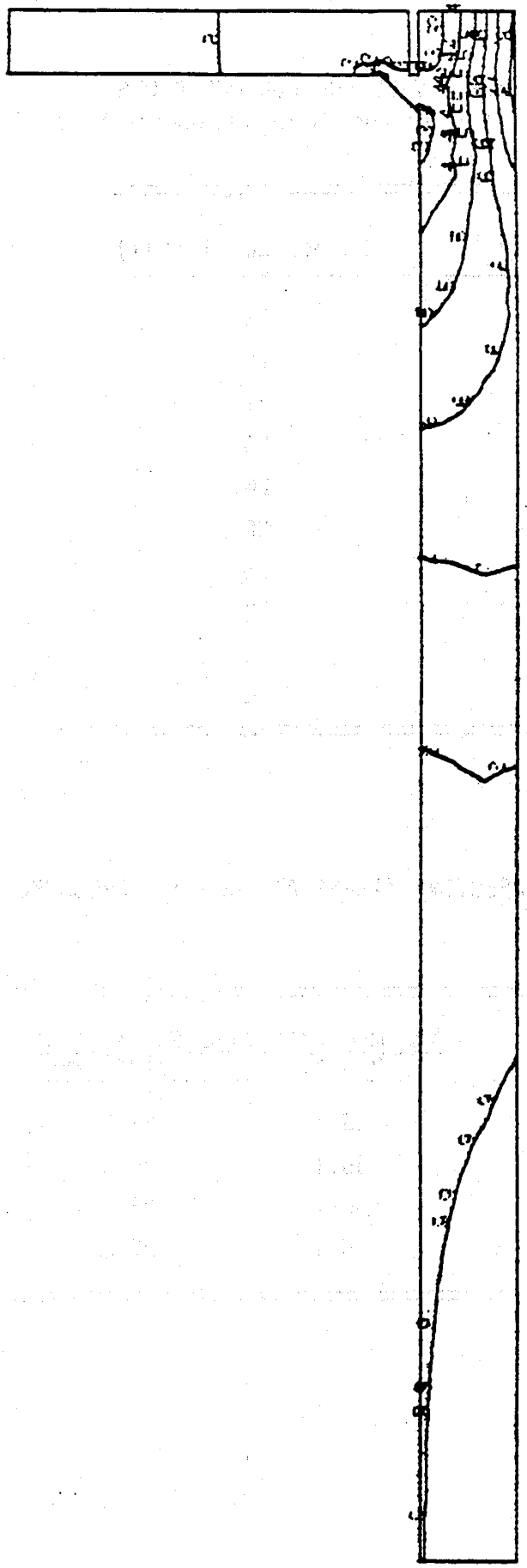

FIGURE 65. EFFECTIVE STRESS CONTOURS AT P = 1000 psi FOR CASE 4

TABLE 14. STRESS LEVELS FOR CONTOUR PLOTS
(Stress Level given in Von Mises Effective Stress))

Contour Number	Stress Level (ksi)
1	18
2	20
3	22
4	24
5	26
6	28
7	30
8	32
9	34
10	36

TABLE 15. MAXIMUM EFFECTIVE STRESS AT 1000 psi PRESSURE

Case No.	Maximum Effective Stress (ksi) Vessel	Stiffener
1	35.1	26.8
2	35.1	26.8
3	35.1	26.7
4	35.1	27.8

Since the elastic analysis is small strain, small displacement, and linear elastic, the internal pressure required to initiate yielding of the vessel can be calculated by scaling the effective stress at 1000 psi to the yield stress.

$$\frac{\sigma_Y}{\sigma_e} = \frac{P_Y}{1000} \qquad (1)$$

The internal pressure at the onset of yield is shown in Table . Based on information from Kerr-McGee, the design properties are assumed to be those of A516 steel Grade 70 for the vessel and A36 steel for the stiffener. Therefore, the design yield strengths are 70 ksi and 36 ksi for the vessel and stiffener, respectively. Material tests conducted at Battelle have shown that the actual minimum yield strengths (at proportional limit) are 49.0 ksi and 38.3 ksi at 180 F for the vessel and stiffener materials, respectively.

TABLE 16. INTERNAL PRESSURE AT ONSET OF YIELD

	Internal Pressure (psi)			
	Design Yield Strength		Actual Yield Strength	
Case	Vessel	Stiffener	Vessel	Stiffener
1	1994	1343	1396	1429
2	1994	1343	1396	1429
3	1994	1348	1396	1434
4	1994	1295	1396	1378

The results given in Table 16 indicate that a perfectly constructed cylinder (Case No. 2) of this type using A36 steel stiffeners should be able to withstand an internal pressure of 1343 psi before yielding occurs. This, of course, assumes that no weld defects are present.

Elastic-Plastic Stress Analysis

The elastic-plastic stress analysis was peformed to determine the internal pressure in the cylinder at the time of rupture. Circumferential measurements of the vessel made at the onsite investigation revealed that the entire cylindrical portion of the vessel had deformed plastically. The objective of this analysis was to calculate the internal pressure required to induce the same plastic deformations as those measured. It is believed that the maximum pressure occurred just prior to the rupture of the vessel, since once the vessel ruptured, the internal pressure was relieved.

The measured plastic deformations between the middle stiffener and the drain-end stiffener were essentially symmetric about the midway point and, as such, were not affected by the excessive deformations at the rupture site. Therefore, a finite element model of this section was used for the elastic-plastic analysis. This finite element model is the same as that for Case 2 (full penetration fillet weld) of the elastic analysis, with an additional 136 nodal points and 102 elements that were required to extend the "Midway point" from 10-3/8 inches to 19 inches. As described in the previous section, on the elastic analysis, the symmetry conditions at the stiffener centerline and midway point were applied by fixing the axial displacement at one end and tying the axial displacements together at the other end.

An internal pressure of 1400 psi and the corresponding axial force were initially applied to the vessel. The pressure was increased by increments of 50 psi to a maximum pressure of 1800 psi. The axial force was also increased an appropriate amount. However, since the elastic-plastic analysis utilizes the large displacement option of SAVFEM, the axial force increase is not constant for a constant pressure increase. The axial force increase was calculated by the following formula and required several interations to obtain the correct axial force once yielding occurred.

$$F = \frac{\pi(r_o + \Delta r)^2}{2\pi} \qquad (2)$$

where F = total axial force (lbs/radian)
P = internal pressure (psi)
r_o = initial internal radius at midway point
Δr = radial displacement at midway point (internal surface).

When the pressure reached 1800 psi, the vessel was unloaded ($P = 0$ and $F = 0$) elastically to recover the elastic strain and reveal the permanent deformation in the vessel. A similar analysis was performed using 1750 psi as the maximum pressure.

The material properties used in these analyses were taken as the minimum values (in terms of strength) determined experimentally at Battelle for the stiffener and vessel materials. The fillet weld material was assumed to be identical to the vessel material.

The displacement results from this analysis are shown, with the measured values, in Figures 66 and 67. In Figure 66, the measured radial displacement was calculated from the measured circumferences, using an initial (undeformed) outer radius of the vessel as 24.625 inches (24 inches I.D. plus 5/8-inch plate thickness). In Figure 67, the apparent tangential strain was calculated by assuming a value of tangential strain of zero at the edge of the stiffener, as shown below.

$$\varepsilon_{ta} = \frac{\Delta r - \Delta r_s}{r_s} \qquad (3)$$

where ε_{ta} = apparent tangential strain
Δr = radial displacement
Δrs = radial displacement at edge of stiffener
rs = deformed radius at edge of stiffener.

The elastic-plastic analysis shows that the internal pressure at rupture was greater than 1750 psi. The results of this analysis indicate that the maximum pressure was approximately 1775 psi. However, the analysis was performed using the minimum material properties. Thus, the actual pressure at rupture may have been greater than 1775 psi.

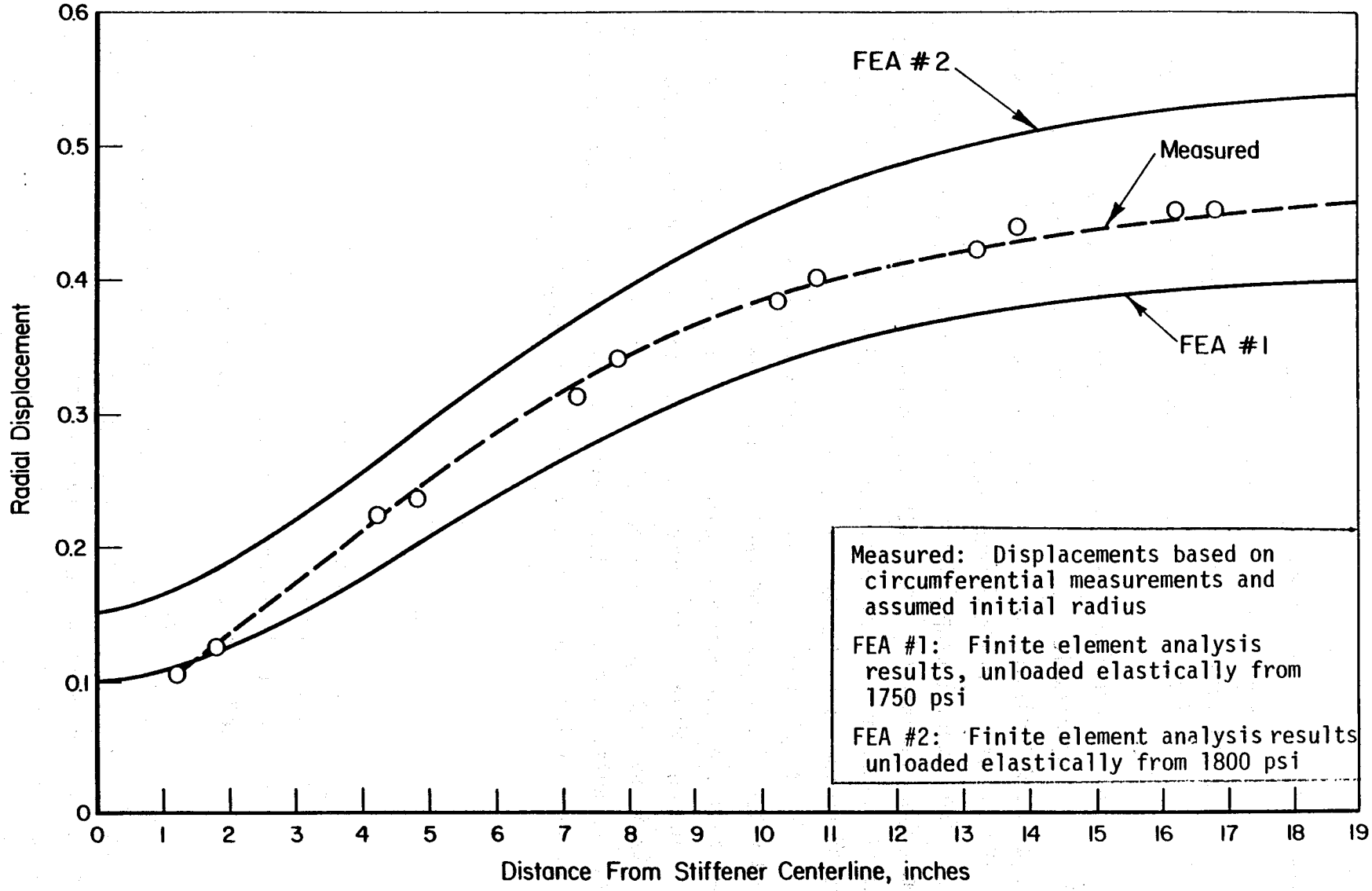

FIGURE 66. RADIAL DISPLACEMENT BETWEEN TWO STIFFENERS

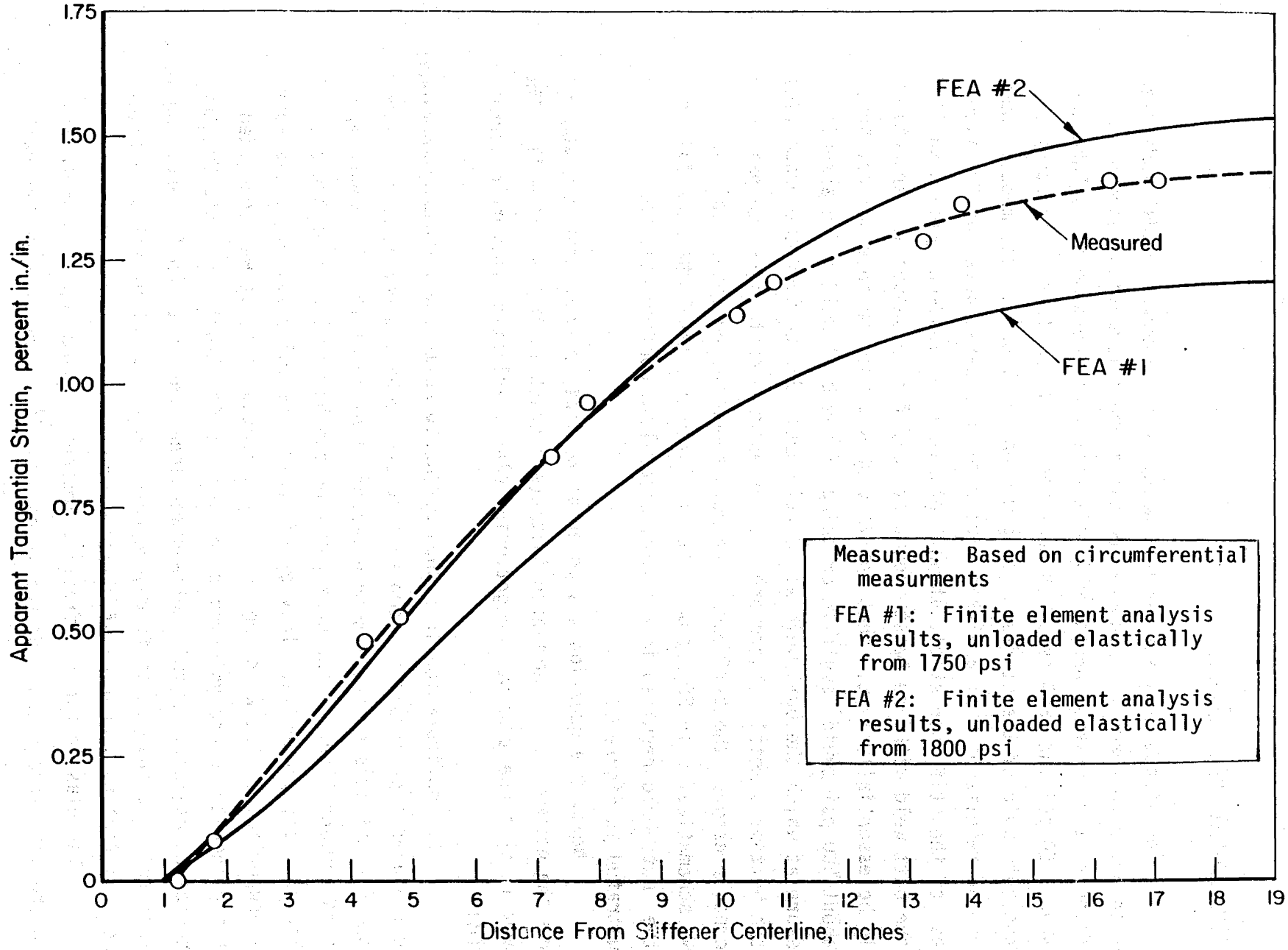

FIGURE 67. APPARENT TANGENTIAL STRAIN BETWEEN TWO STIFFENERS

Fracture Mechanics Analysis

The stress analysis results using an axisymmetric model indicated that in order to reach the measured post-failure deformation between stiffeners, the internal pressure in the vessel at the time of failure was between 1750 psi and 1800 psi. In that analysis, the lack of penetration in the butt weld of the stiffener ring was not included in the model. However, the results of that analysis were used to assess, based on the flow stress of the stiffener steel, at what pressure the load-carrying capacity of the butt weld with the least amount of weld fusion (about 10 percent) could be essentially lost. That analysis showed that an internal pressure of about 500 psi could result in cracking of the butt weld. The actual pressure at which the butt weld would fail would depend upon the properties of the butt-weld metal. Therefore, it was assumed that above 500 psi internal pressure, the stiffener butt weld supported no load. This is shown schematically in Figure 68. It was further assumed that the failure of the butt weld resulted in a sharp, crack-like configuration as illustrated in Figure 68.

Next, the question was posed as to what internal pressure would cause the geometry in Figure 68 to initiate a crack in the vessel wall. The answer to this question was sought using elastic-plastic fracture mechanics (EPFM).

The configuration in Figure 68 clearly calls for a three-dimensional stress analysis procedure to compute fracture mechanics parameters. However, if one concentrates on the midcircumferential plane of the stiffener, and ignores surface effects, the configuration can be modeled using a plane-strain analysis procedure. In view of other uncertainties, e.g., the material properties of the weld and the heat-affected zone, it was concluded that a plane-strain analysis would provide a sufficiently accurate fracture mechanics assessment. A full three-dimensional analysis, while resulting in a several-fold increase in staff and computer cost, is not expected to significantly affect the accuracy of the assessment.

The elastic-plastic fracture mechanics assessment was performed using the path independent contour integral $J^{(1)}$ as the measure of crack

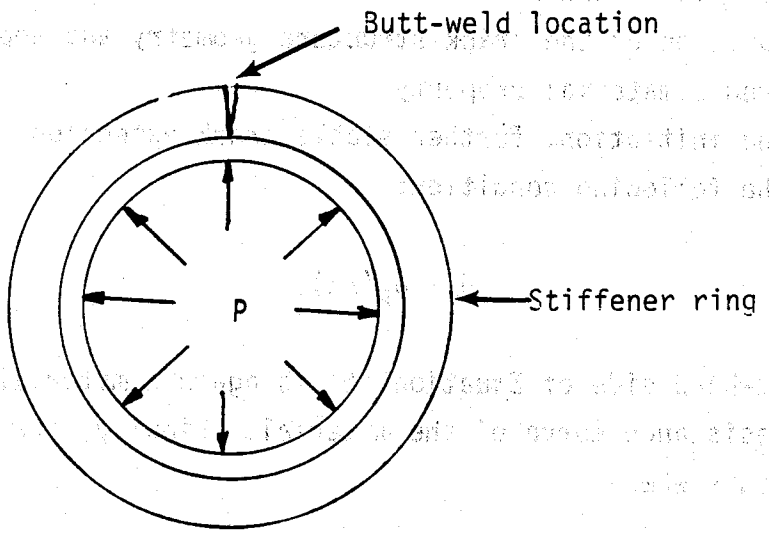

FIGURE 68. POSTULATED CONDITION OF CONTAINER WITH CRACK THROUGH THE STIFFENER RING BUTT WELD AT INTERNAL PRESSURES GREATER THAN 500 psi

"driving-force". Briefly, the use of J in predicting crack initiation amounts to satisfying the following Equation[2]:

$$J = J_{Ic} \tag{4}$$

where J signifies the applied value representing the propensity of the crack to grow, and J_{Ic} is the critical value of J, representing the materials resistance to crack initiation under plane-strain conditions. While J is a function of the crack-structure geometry and applied loads, J_{Ic} is considered a material property.

Beyond initiation, further stable crack extension occurs according to the following condition:

$$J = J_R(\Delta a) \tag{5}$$

where the right-hand side of Equation (5) is again a material property, called the J-resistance curve of the material. Finally, crack-growth instability occurs when

$$\frac{dJ}{da} > \frac{dJ_R}{da} \tag{6}$$

i.e., the slope of the applied J-versus-a curve exceeds the slope of the J-resistance curve.

Under elastic-plastic conditions, stable crack extension prior to instability is possible. That is, as opposed to purely elastic conditions, the structure can carry increasing load beyond crack initiation until the instability condition (Equation 6) is met. For a given material, this additional load-carrying capacity depends upon the elastic energy stored in the structure, and on whether the structure is under load control or displacement control. Under load control, the load at which Conditions (4) and (5) are met are typically not much different from each other. Therefore, in the present investigation, which involves a load control situation,

the analysis was restricted to finding the load (internal pressure) at which the Condition (4) for crack initiation would be met. It was assumed that crack growth instability and crack penetration through the vessel wall would occur only with a small further increase in pressure. The critical value of J was taken to be that of the vessel material, i.e, 600 in-lb/in^2 as found in the experimental part of this investigation. Note that since the experiments to establish J_{Ic} were performed using specimens in which the crack was oriented in the vessels axial direction, the assumption was made that the J_{Ic} in the axial and radial directions was the same.

The computations were performed using Battelle's BCLFEM non-linear finite element analysis code on the CYBER mainframe computer. BCLFEM is primarily a fracture mechanics analysis code with elastic-plastic crack growth modeling capability. It can be used for both generation phase computations (in which an experimental P or δ versus Δa record is provided as part of the input, and a resistance curve is computed), and application phase computations (in which crack advance occurs according to a prescribed resistance curve). During the analysis, the J-integral values are computed using the path-independent contour integral definition[1]* for plane stress and plane strain problems, and the virtual crack extension (VCE) method for three-dimensional problems. The code contains several different constitutive models for elastic-plastic analysis. The nonlinear solution procedures include the Tangent Modulus method and the Modified and Full Newton Raphson iteration techniques. The code contains a large-deformation and finite strain analysis capability. The element library in BCLFEM includes linear and quadratic one-, two-, and three-dimensional isoparametric elements, doubly curved shell isoparametric elements, and a general elastic stiffness element. Crack propagation is modeled by gradually releasing the initial coupled set of nodes along the projected crack propagation path.

For the present analysis, the finite element model (Figure 69) included 599 eight-noded isoparametric elements and 1962 nodal points. A 3 x 3 Gaussian quadrature was used for stiffness generation. The Newton Raphson iteration method was selected for equilibrium compensation. The hardening was assumed isotropic and the J_2 flow theory was used in the constitutive model. The material's behavior was modeled by a multilinear

---

* References listed on page 143.

representation of the stress-strain curve. The J-integral was computed using three different contours as indicated in Figure 69.

Analysis was first performed assuming the materials stress-strain curve to be linearly elastic. For 1000 psi internal pressure, the three contours in Figure 70 yielded values: 336, 339, and 336 in-lb/in^2 for J. This provided the indication of path-independence of J, and therefore, of the adequacy of finite element model refinement.

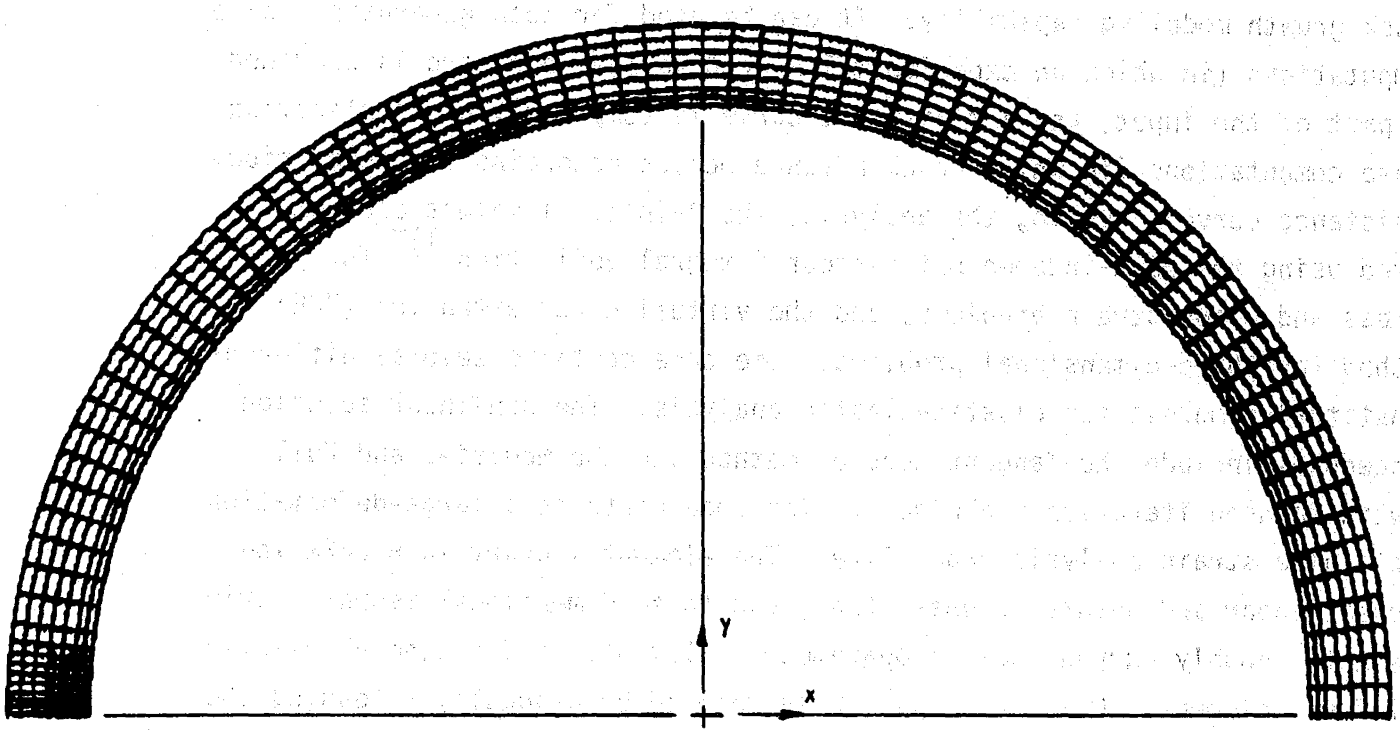

FIGURE 69. FINITE ELEMENT MODEL FOR FRACTURE MECHANICS ANALYSIS

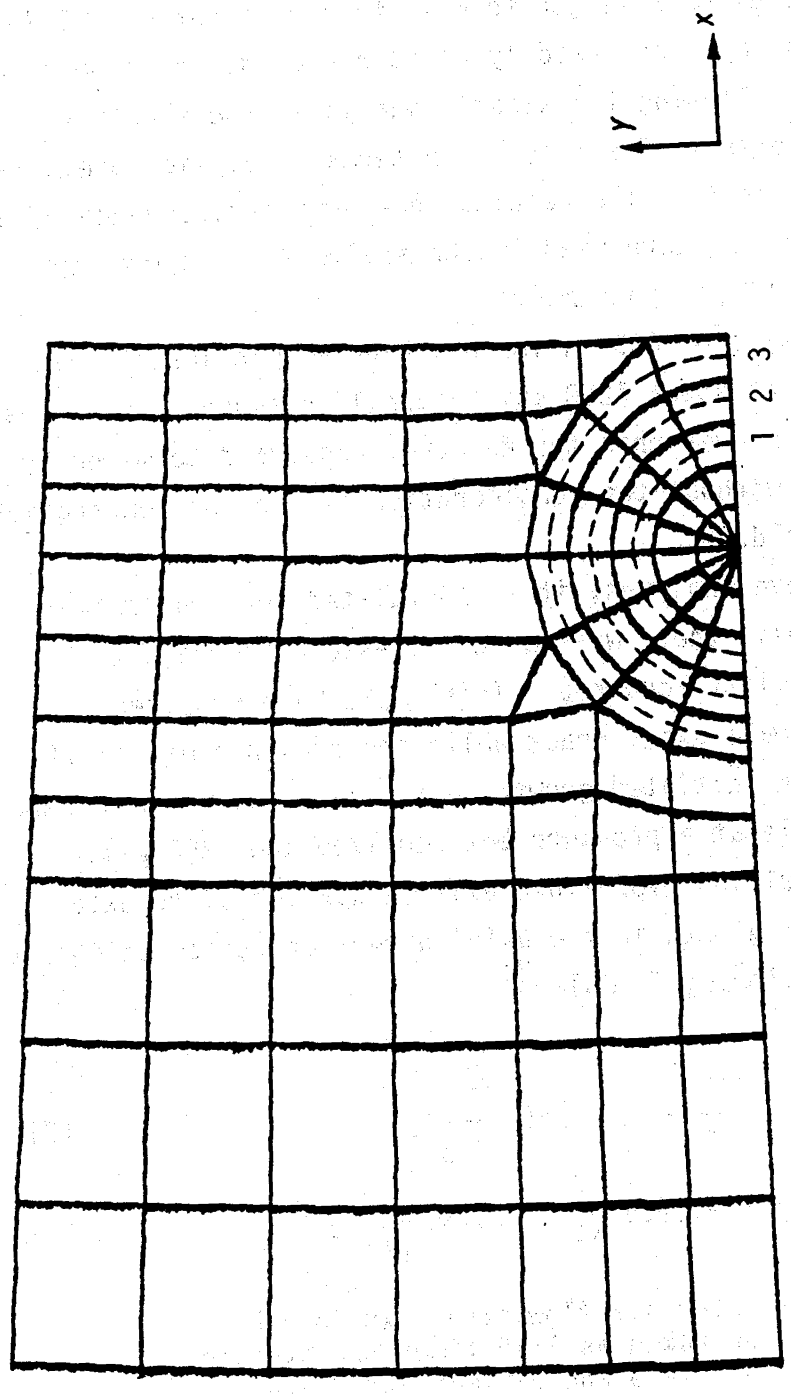

FIGURE 70. DETAILS OF NEAR-CRACK-TIP FINITE ELEMENT MESH SHOWING THE THREE J-CONTOURS

Using these values of J, the average stress intensity factor (K) is 100·55 ksi $\sqrt{in}$. For the crack length to wall thickness ratio of 0.794, a handbook solution for K could not readily be found for direct comparison of the present results. Following the elastic analysis, the elastic-plastic analysis was performed. The results in terms of applied pressure versus J are shown in Figure 71. The results show path independence of J all the way to the maximum pressure used in the analysis. The pressure was applied incrementally in 100 psi increments.

Using the J_{Ic} value of 600 in-lb/in^2, Figure 71 indicates that crack initiation occurred at about 1250 psi internal pressure. This pressure is roughly 29 percent lower than the failure pressure determined by the stress analysis performed without the consideration of lack of penetration in the stiffener's butt weld.

Based on the above analyses, it is postulated that following initiation at about 1250 psi, there was further pressure increase till radial crack-growth instability occurred. This could have resulted in a relatively tight, through-wall axial crack while the pressure was still rising. Finally, the crack initiated growth in the axial direction, grew stably, then became unstable at a pressure between 1750 and 1800 psi.

The J of the resulting 0.875-inch axial crack (equal to axial dimension of stiffener) for growth in the axial direction can be calculated approximately using the following formula[2].

$$J = \frac{8a\sigma_o^2}{\pi E} \ln \left[\sec\left(\frac{\pi}{2}\frac{M\sigma_n}{\sigma_o}\right)\right] \qquad (7)$$

where

$$M = \left[1+1\cdot255\,\frac{a^2}{Rt} - 0.0135\,\frac{a^4}{R^2t^2}\right]^{1/2} \qquad (8)$$

σ_o = materials flow stress which can be taken as 1·15 times the average of yield and ultimate strengths

E = Young's modulus

σ_n = Hoop stress in the vessel

a = half the axial crack length.

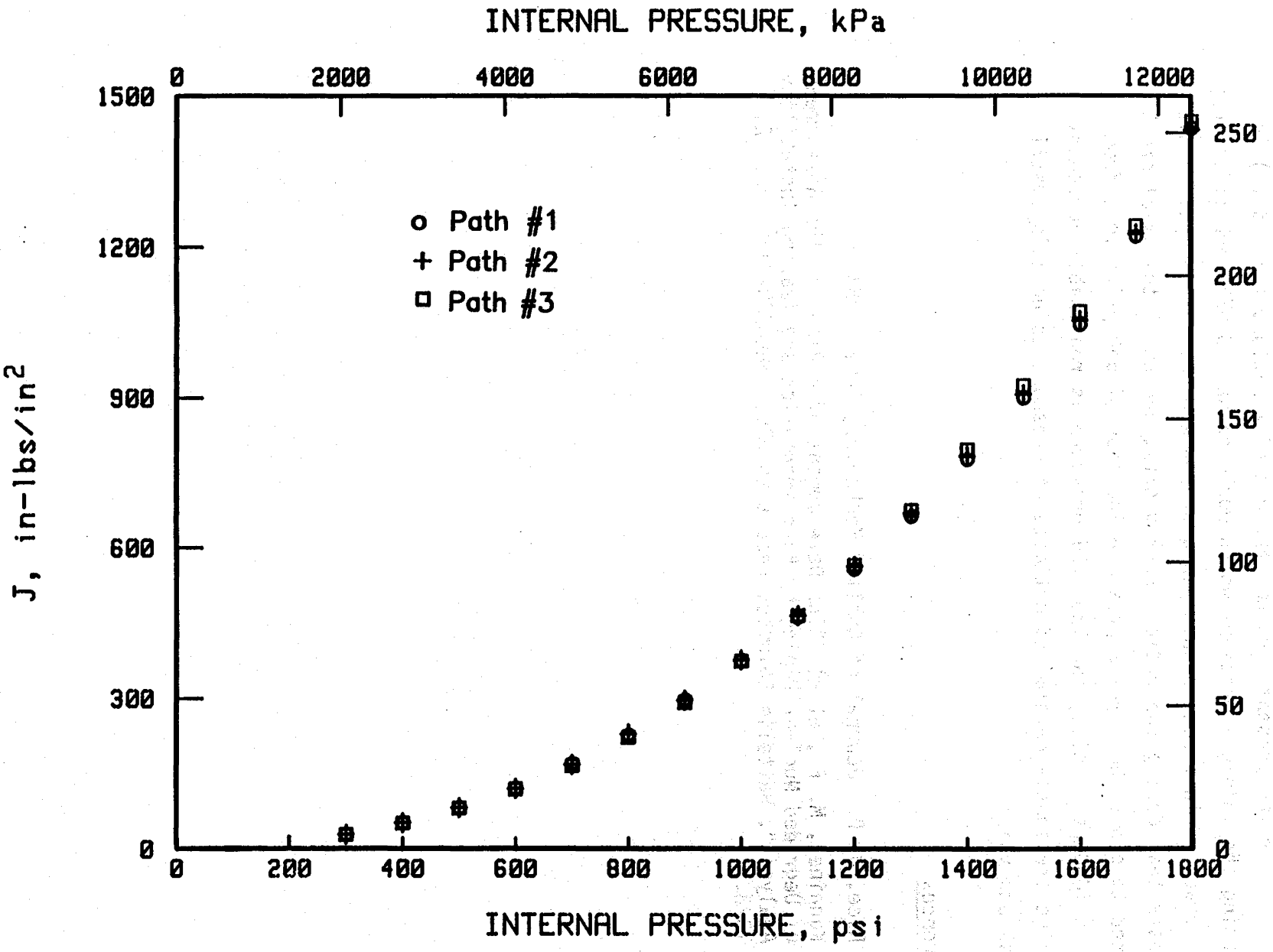

FIGURE 71. RESULTS OF THE ELASTIC-PLASTIC FINITE ELEMENT ANALYSIS

For the present problem, the use of Equations (7) and (8) in determing the internal pressure which would cause a 0.875 inch (=2a) long axial crack to initiate, results in a pressure of about 1800 psi. This suggests that during the radial crack growth, and until the axial crack started to grow, there was a pressure increase of 550 psi, i.e., from 1250 to 1800 psi. Also, the 1800 psi pressure is reasonable agreement with the previously determined estimate of pressure using axisymmetric stress analysis.

References

(1) Rice, J. R., Journal of Applied Mechanics, June, 1968.

(2) Kanninen, M. F., et al, "The Development of a Plan for the Assessment of Degraded Nuclear Piping by Experimentation and Tearing Instability Analysis", Battelle-Columbus report to NRC, NUREG/CR-3142, Vol. 2, 1983.

APPENDIX A

TRUE STRESS-TRUE STRAIN CURVES AND TABULATIONS FROM THE TENSILE TESTS OF THE STEEL FROM THE VESSEL SHELL AND THE STIFFENER RINGS AT ROOM TEMPERATURE AND 180 F (SEE TABLE 10 FOR SPECIMEN IDENTIFICATION)

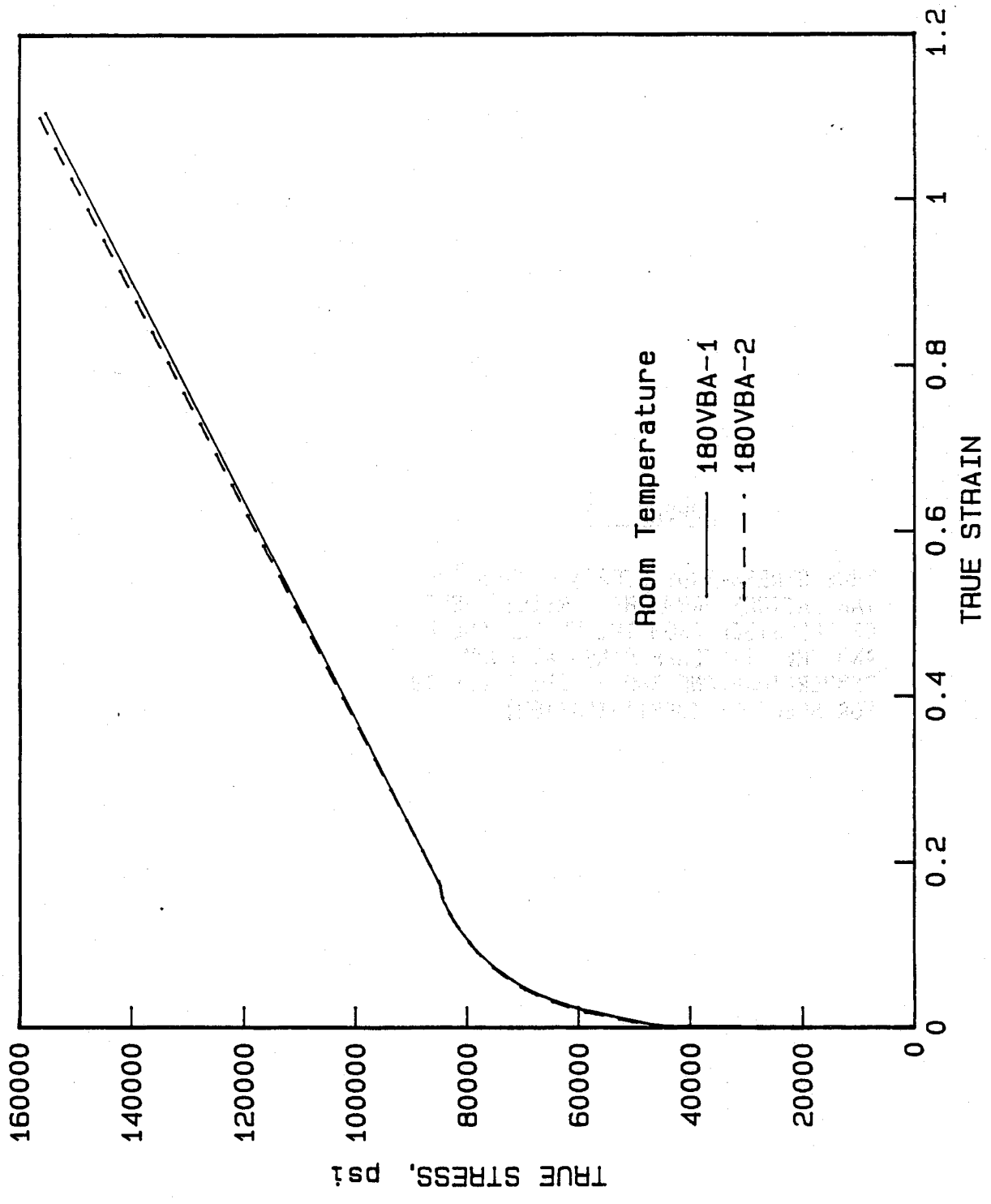
TRUE STRESS, psi
160000
140000
120000
100000
80000
60000
40000
20000
0
0.2
0.4
0.6
0.8
1
1.2
TRUE STRAIN
Room Temperature
180VBA-1
180VBA-2

Specimen No. 180vb-a2

True Stress, psi	Strain
0	0
2175.24	4.9999e-05
4866.98	0.00015999
7477.59	0.00022997
9917.68	0.00031995
12661.9	0.00040992
15374.9	0.00050987
18173.5	0.00060981
20903.7	0.00071974
23703.4	0.00081966
26375.7	0.00090959
29432.5	0.0010095
32041.9	0.0010994
35169.7	0.0012193
37903.7	0.0013391
40447.4	0.0014789
43129.7	0.0017285
45823.6	0.0023173
48146.2	0.0045496
50385.6	0.0075018
52713.2	0.010643
54729.5	0.013558
56977.3	0.017024
59247	0.019685
62123.4	0.025794
64746.2	0.031722
67252.1	0.038769
69524.3	0.045996
71522.7	0.054488
73510.5	0.06321
75182.2	0.071902
76801.1	0.081856
78074.1	0.0908
79239.9	0.099664
80403.4	0.1098
81321.7	0.11894
82303.8	0.128
82959.2	0.13593
83614.5	0.14527
84219.9	0.15469
84595.5	0.16284
84785.9	0.17252
156400	1.10087

Specimen No. 180vb-a1

True Stress, psi	Strain
0	0
2479.86	3e-05
4907.46	7.9997e-05
7703.54	0.00015999
10445.2	0.00023997
13029.9	0.00031995
15644.4	0.00041991
18562.9	0.00051987
21131.8	0.00061981
23841.4	0.00072973
26692	0.00083965
29472.8	0.00094955
32324.9	0.0010694
35254.4	0.0012193
37969.9	0.001399
40613.2	0.0016486
43200.1	0.0020379
44863.4	0.0025168
47385.1	0.0045496
49544	0.0076904
51928.4	0.010841
54198.8	0.014248
56427	0.017889
59358.8	0.021791
61739.4	0.026671
64903.1	0.033928
67184.4	0.040076
69777.8	0.048571
71535	0.056049
73487.6	0.065038
75271.8	0.073901
76865.3	0.084065
78276	0.093217
79376.6	0.10229
80404.7	0.11109
81485.4	0.1204
82376.6	0.12967
83136.4	0.13885
83846.7	0.14816
84469	0.15636
84676.5	0.16611
84959.3	0.17433
155200	1.10455

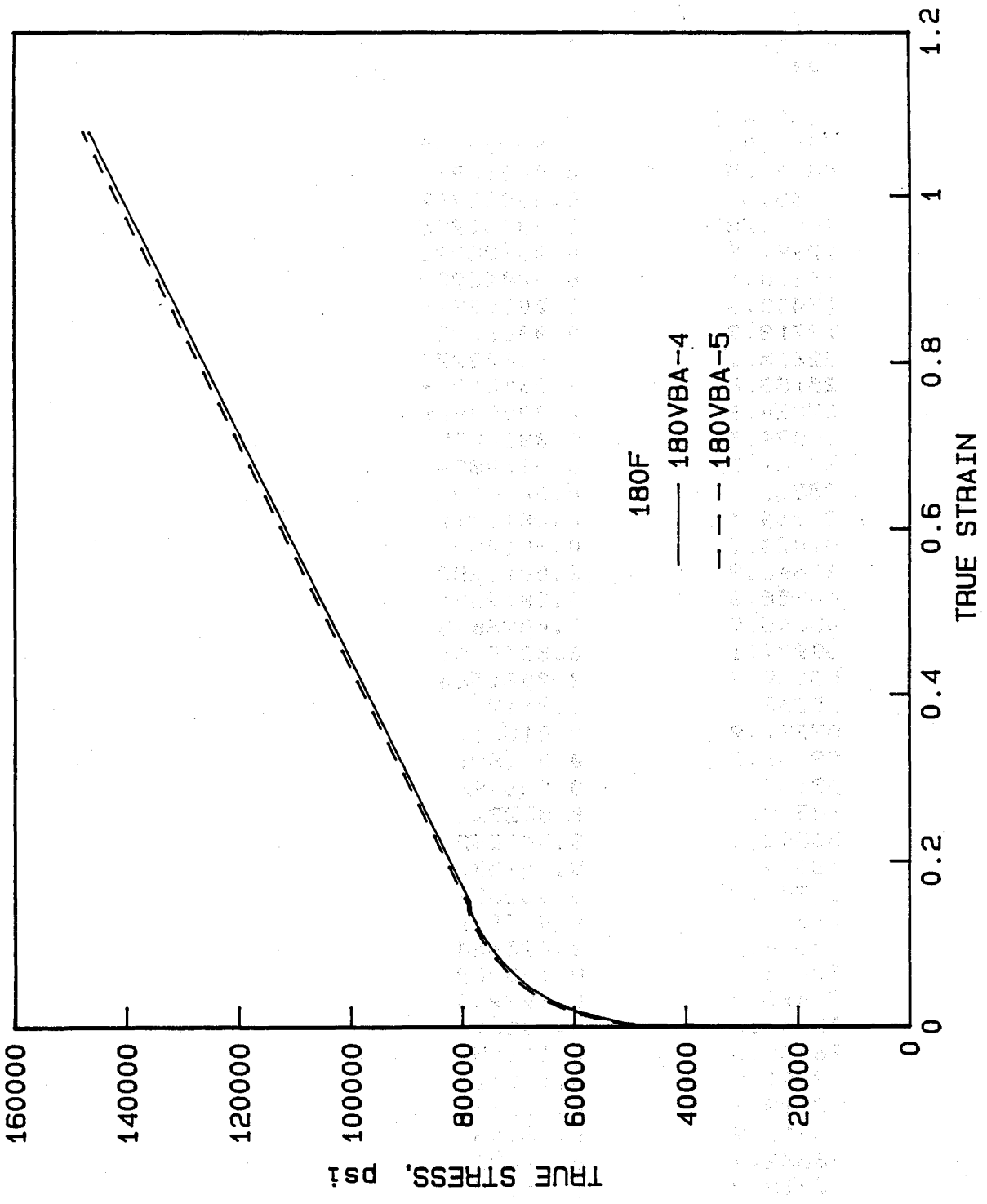
TRUE STRESS, psi
160000
140000
120000
100000
80000
60000
40000
20000
0
0.2
0.4
0.6
0.8
1
1.2
TRUE STRAIN
180F
180VBA-4
180VBA-5

Specimen No. 180vb-a4

True Stress, psi	Strain
0.631448	0
2245.03	9.9995e-05
4609.25	0.00015999
7163.34	0.00022997
9495.78	0.00031995
12091.8	0.00038992
14830.1	0.00045989
17400.4	0.00052986
19718.9	0.0006298
22675.1	0.00072973
25183.8	0.00081966
27824.9	0.00090959
30524.5	0.0010095
32781.7	0.0010894
35551	0.0011993
38384.4	0.0013091
41024.2	0.001439
43603.9	0.0016287
46258.8	0.0019381
48605.9	0.0026066
50979.1	0.0048681
53159.6	0.0081864
55267	0.01177
57291.9	0.015519
59361.7	0.018881
62138.6	0.026496
64279.5	0.032922
66502.4	0.041862
68174	0.049504
69742.2	0.058552
71244.7	0.067939
72364.8	0.075664
73413	0.083789
74492.3	0.092944
75404.2	0.10201
76255.4	0.11015
77091.2	0.11951
77723.9	0.12769
78316.9	0.13606
78662.4	0.14432
78713.2	0.15272
146400	1.07761

Specimen No. 180vb-a5

True Stress, psi	Strain
0	0.00019998
2229.93	0.00032995
4753.41	0.0004499
7090.98	0.00054985
9586.04	0.00065978
12025.4	0.00073973
14749.9	0.00082966
17291.9	0.00091958
20083.3	0.0010095
22569.9	0.0010794
25052.1	0.0011593
27723	0.0012492
30827	0.0013591
33560.1	0.0014489
35861.3	0.0015488
38596.3	0.0016586
41332.3	0.0017884
44010	0.0019681
46442.9	0.0022175
49138.1	0.0027063
51531.3	0.004002
53684	0.0070749
55932	0.010712
58163.9	0.014682
60160.8	0.018773
62452.5	0.024
64579.8	0.030393
66663.8	0.038134
68658.4	0.047256
70064.3	0.055198
71317.6	0.063022
72642.1	0.072367
73731.9	0.080519
74745.4	0.089704
75626.6	0.097716
76629.4	0.10719
77248.9	0.11525
78004	0.1235
78646.4	0.13317
79007.9	0.14146
79145.8	0.14988
147600	1.07899

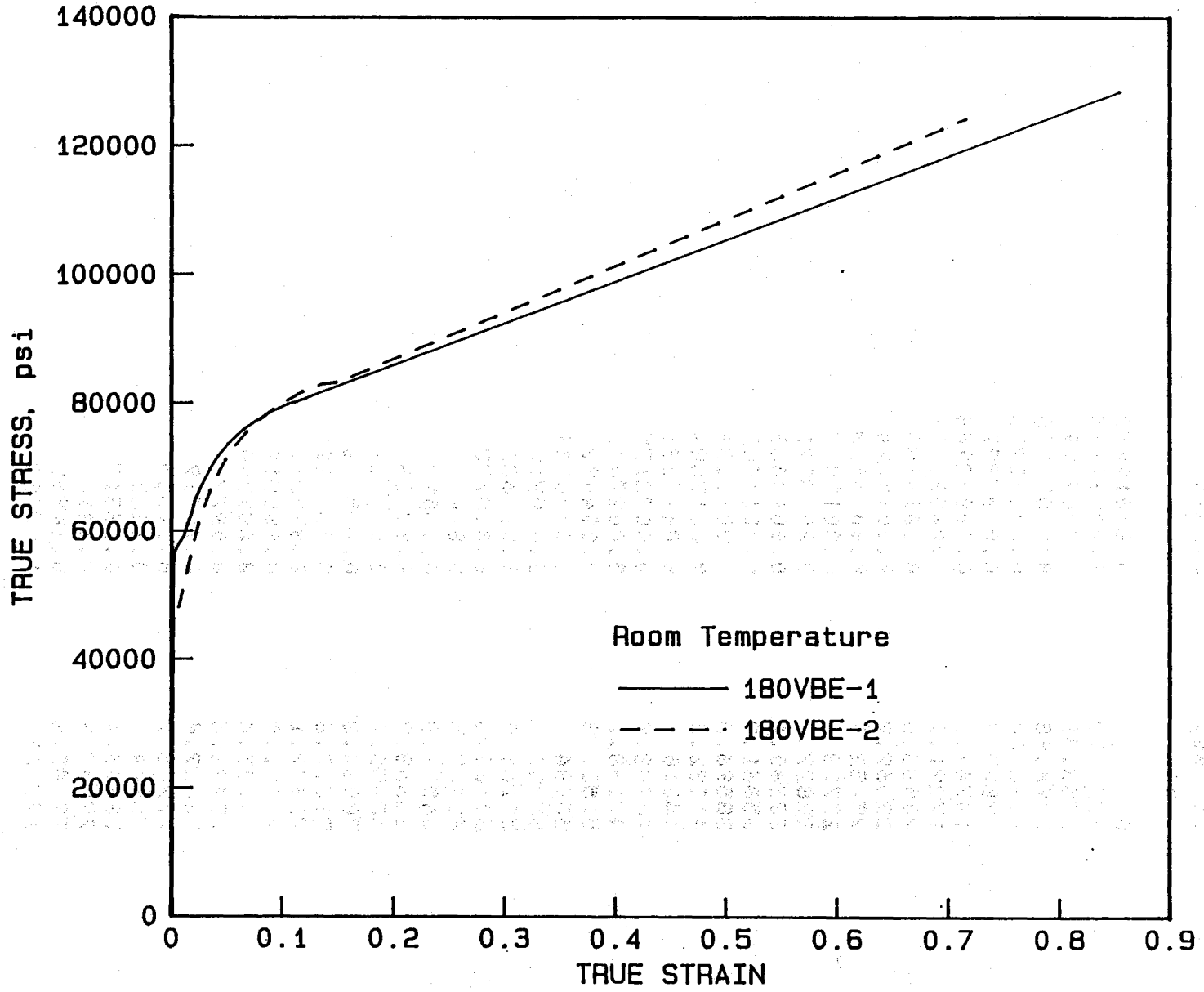
140000
120000
100000
80000
60000
40000
20000
0
TRUE STRESS, psi
0
0.1
0.2
0.3
0.4
0.5
0.6
0.7
0.8
0.9
TRUE STRAIN
Room Temperature
180VBE-1
180VBE-2

Specimen No. 180vb-e1

True Stress, psi	Strain
0	0
2389.31	1e-05
4841.17	0.00015999
7592.93	0.00028996
9947.45	0.00039992
12530.6	0.00048988
15586.2	0.00059982
18373.4	0.00068976
21039.4	0.00078969
23517.8	0.00086962
26433.7	0.00097952
29040.2	0.0010694
31641.9	0.0011593
34808.4	0.0012692
37477.4	0.0013691
40208	0.0014689
43061	0.0015588
45482.2	0.0016486
48280.7	0.0017485
51206.8	0.0018583
54006.9	0.0019681
56691.9	0.0027263
57981.5	0.0065684
59107.6	0.01094
61135.7	0.01478
62901.2	0.018311
64800.5	0.021321
67305.8	0.02778
69809.8	0.0353
71524.7	0.04167
73566.8	0.050788
74633	0.057231
75885.1	0.065273
76820.3	0.07325
77723.6	0.081396
78541.5	0.088331
79154.3	0.096809
79696.8	0.10364
80194.9	0.11199
80722.2	0.12067
128500	0.8538

Specimen No. 180vb-e2

True Stress, psi	Strain
0	0
2377.3	1e-05
5025.86	9.9995e-05
7683.4	0.00016999
10051.7	0.00019998
12944.3	0.00027996
15547.7	0.00035994
18217.6	0.0004499
21015.1	0.00052986
23929.9	0.00061981
26479.1	0.00069975
29522.3	0.00078969
32133.6	0.00087961
34806.7	0.00097952
38035.2	0.0010894
40770.1	0.0011693
43636.7	0.0013491
46074	0.0016886
48346.5	0.003743
47991.7	0.0066677
49849.2	0.0089498
52138.9	0.011968
54415.9	0.015076
56774.3	0.018459
59350.7	0.021761
61835	0.025843
64900.4	0.032119
67195.7	0.037402
69496.3	0.043969
71548.6	0.050408
73282.8	0.057325
74994.3	0.065835
76361.9	0.073111
77484	0.080566
78521.3	0.088194
79397.6	0.095765
80296.1	0.1035
81103.7	0.11141
81856.6	0.11925
82413.3	0.12743
82913.4	0.13558
83027.5	0.14258
83256.7	0.151
124300	0.71564

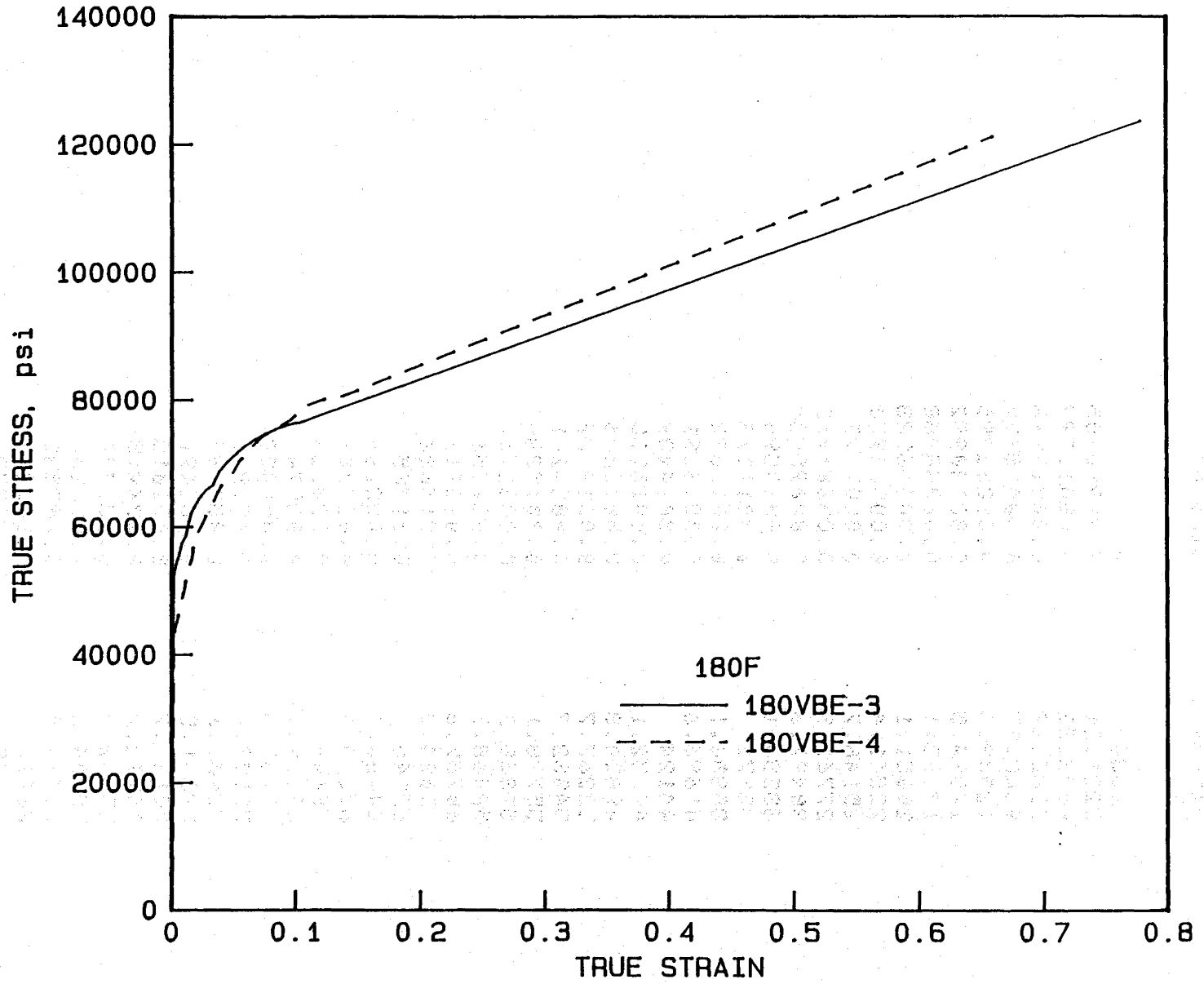
140000
120000
100000
80000
60000
40000
20000
0
TRUE STRESS, psi
0
0.1
0.2
0.3
0.4
0.5
0.6
0.7
0.8
TRUE STRAIN
180F
180VBE-3
180VBE-4

Specimen No. 180vb-e3

True Stress, psi	Strain
1.83055	0
2221.21	6.9998e-05
4692.32	0.00011999
7282.88	0.00019998
9648.37	0.00025997
12309.4	0.00032995
14894.5	0.00040992
17195.1	0.00048988
20051.1	0.00058983
22541.4	0.00068976
25148.7	0.0007797
27761.9	0.00086962
30497.6	0.00095954
33234.1	0.0010594
35971	0.0011593
38836.1	0.0012692
41696.6	0.0013691
44124	0.0014489
47052.1	0.0015588
49854.3	0.0016886
52267.7	0.0018682
54032.7	0.0034241
55788.1	0.0065386
57368.2	0.0082161
58468.9	0.011256
60789.6	0.013913
62034.2	0.015686
62945	0.01785
64464.5	0.022163
65868.4	0.027703
66649	0.033154
68819.1	0.03874
70168.5	0.044428
71557.4	0.051976
72462.6	0.057089
73361.5	0.063491
74188.7	0.071018
74792.2	0.076915
75342.4	0.082777
75904.2	0.090206
76294.4	0.097535
76452	0.10328
123600	0.77873

Specimen No. 180vb-e4

True Stress, psi	Strain
0	1e-05
2217.36	5.9998e-05
4624.71	0.00014999
7094.5	0.00024997
9814.42	0.00034994
12189.4	0.00045989
14889.6	0.00053985
17499.2	0.00063979
20104	0.00072973
22902.8	0.00082966
25697	0.00092957
28181.6	0.0010295
31164.7	0.0011194
33716.5	0.0012193
36329.8	0.0013291
39191.8	0.0015288
41880	0.0019281
44297.5	0.0031749
45843.7	0.0056639
47713.9	0.0069557
49528.8	0.0096235
50607.5	0.011167
52883.1	0.012423
54784.5	0.016149
56253	0.017476
58095.9	0.018046
59971.3	0.023453
61993.5	0.028393
63370	0.031973
65441.2	0.03719
67259.1	0.042283
68251.9	0.048304
70332.2	0.054393
71807.7	0.061518
73409.2	0.06864
74463.8	0.074783
75223.4	0.081995
76097.2	0.089155
76975.8	0.096264
78183	0.10314
79186.9	0.11015
79740.1	0.11712
80196.1	0.12425
80534.5	0.13134
80639.7	0.13841
121100	0.65946

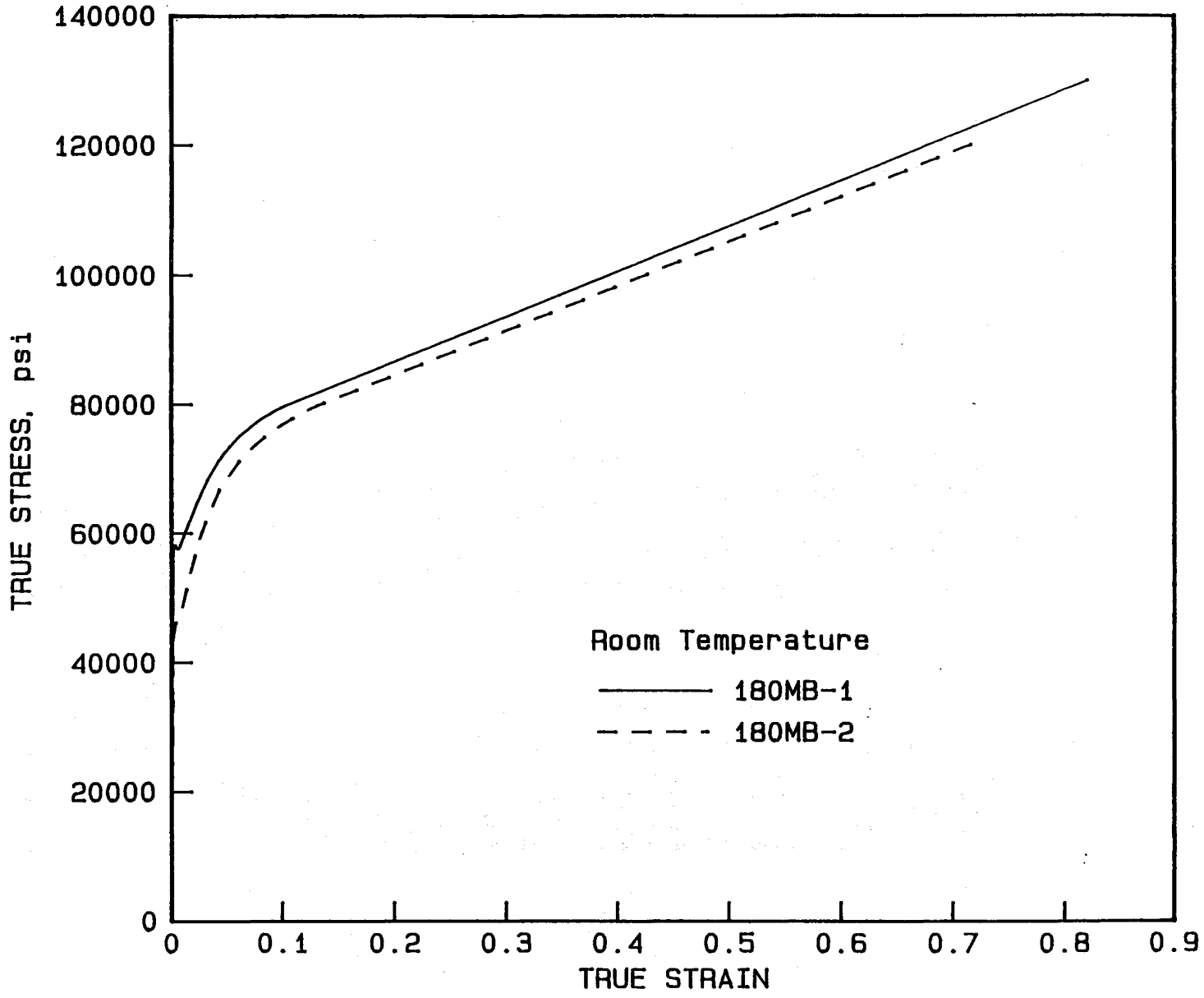
140000
120000
100000
80000
60000
40000
20000
0
TRUE STRESS, psi
0
0.1
0.2
0.3
0.4
0.5
0.6
0.7
0.8
0.9
TRUE STRAIN
Room Temperature
180MB-1
180MB-2

Specimen No. 180mb-1

True Stress, psi	Strain,
0	0
4142.88	9.9995e-05
10295.7	0.00029996
15891.6	0.00049987
22252.8	0.00069975
27980.5	0.00089959
34041.3	0.0010994
40079	0.0012992
45813.7	0.0014989
51881.6	0.0016986
55380.3	0.0018982
56664.7	0.0020978
57312.9	0.0022974
57630.1	0.0024969
58100.2	0.0026964
58239.3	0.0028958
58146.6	0.0034939
58175.6	0.003992
58153.5	0.0044899
57927	0.0049875
57623.7	0.0054849
57524.5	0.0059821
57553.1	0.006479
57632.8	0.0069756
57815.1	0.007472
57946.3	0.0079682
58180.1	0.0084641
60400.2	0.01341
64637.8	0.023228
68289.9	0.032951
71204.8	0.04258
73359.6	0.052118
75137.1	0.061565
76389.3	0.070924
77651.5	0.080197
78646.2	0.089384
79505.5	0.098487
129950	0.82087

Specimen No. 180mb-2

True Stress, psi	Strain
0	5.9998e-05
2059.51	0
4108.9	1e-05
6447.73	5.9998e-05
8492.8	0.00013999
10660.1	0.00022997
12954.8	0.00032995
15123	0.00042991
17479.5	0.00052986
19648.3	0.00061981
21883.9	0.00071974
24175.6	0.00080967
26350.7	0.00089959
28551.4	0.00097952
30782.9	0.0010594
33111.8	0.0011493
35410.5	0.0012392
37582.5	0.0013291
39943.6	0.001439
42275.9	0.0015688
44286	0.0022175
46056.3	0.004231
46842.3	0.0070948
47814.2	0.0091579
49485.4	0.011375
50830.3	0.013212
52338	0.015401
53839.9	0.017467
55257.3	0.019763
56511.6	0.02182
57872.8	0.022945
60091.2	0.027917
62377.1	0.032796
64373.7	0.037768
66789	0.043979
68934.8	0.05207
71009.2	0.060625
72528	0.068593
73760.8	0.076127
74879.7	0.083789
76020.9	0.091576
76754.1	0.099348
77665.4	0.10751
78386.7	0.11493
79070	0.12253
79726	0.13006
120900	0.72877

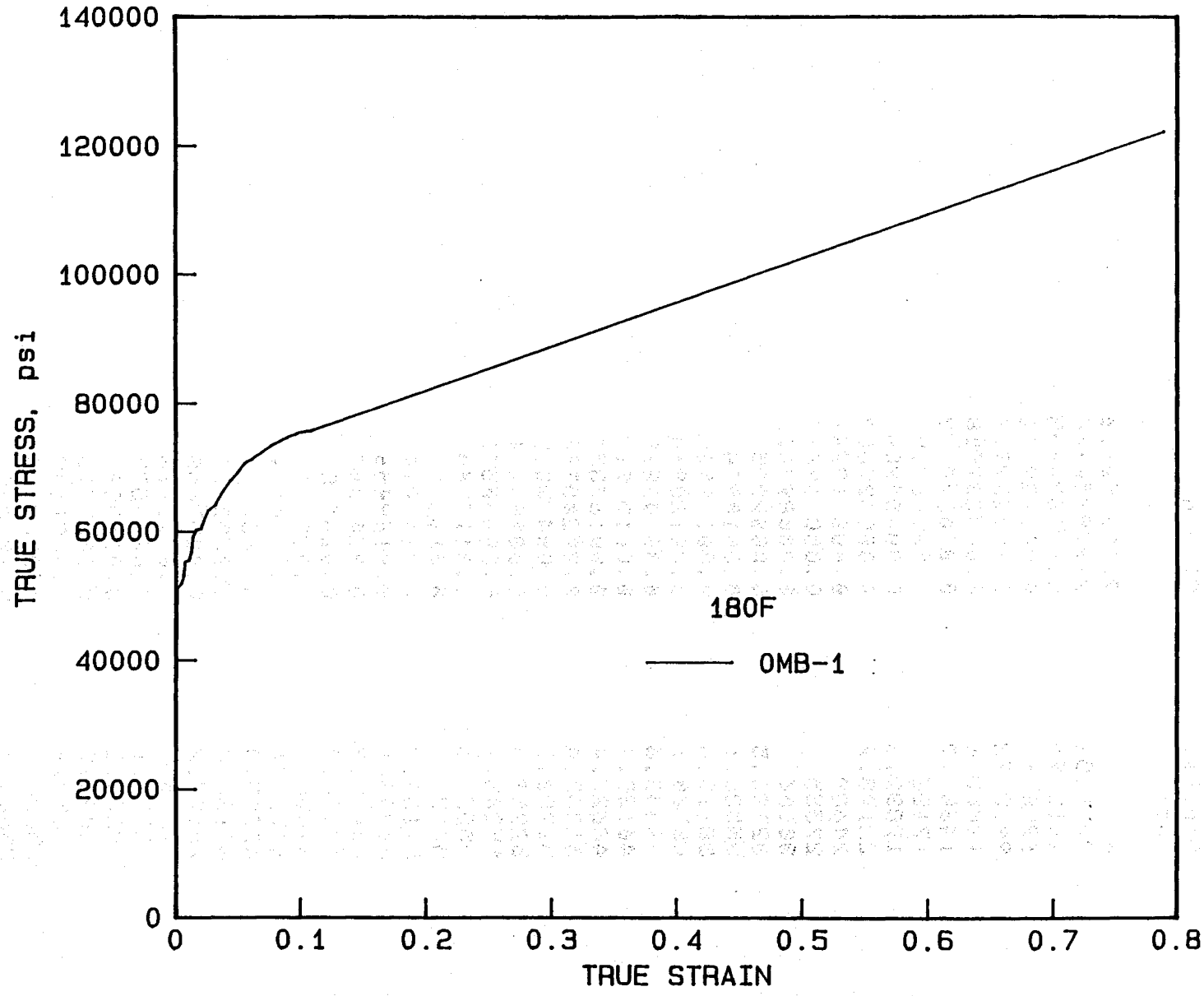
140000
120000
100000
80000
60000
40000
20000
0
TRUE STRESS, psi
0
0.1
0.2
0.3
0.4
0.5
0.6
0.7
0.8
TRUE STRAIN
180F
OMB-1

Specimen No. 0mb-1

True Stress, psi	Strain
0	9.99995e-06
2219.54	9.99995e-06
4612.95	5.99982e-05
6998.67	0.000129992
9413.72	0.000209978
12063.6	0.000289958
14601.9	0.000379928
17156	0.00046989
19832.6	0.000549849
22198.9	0.000629802
24688	0.000719741
27555	0.000819664
30106	0.000899595
32724.5	0.0009995
35338.1	0.0010994
38018.6	0.00119928
40700.1	0.00130914
43443.6	0.00141899
46125.9	0.00152883
48627.4	0.00167859
51085.4	0.00205788
51788.3	0.00478852
52983.8	0.00707491
55205.9	0.00830541
55523.6	0.0112564
56773	0.013311
59183.9	0.0147999
60243.1	0.0169456
60418.2	0.0207042
63170.3	0.026418
64060.1	0.032167
65794.4	0.0369489
67795.3	0.0438829
69136.2	0.0502177
70597.9	0.0557658
71276	0.0615183
72252.1	0.0690595
73276.2	0.076359
74044.2	0.0837895
74609.6	0.0891549
75198	0.0962643
75564.7	0.103369
75727	0.109258
122200	0.7891

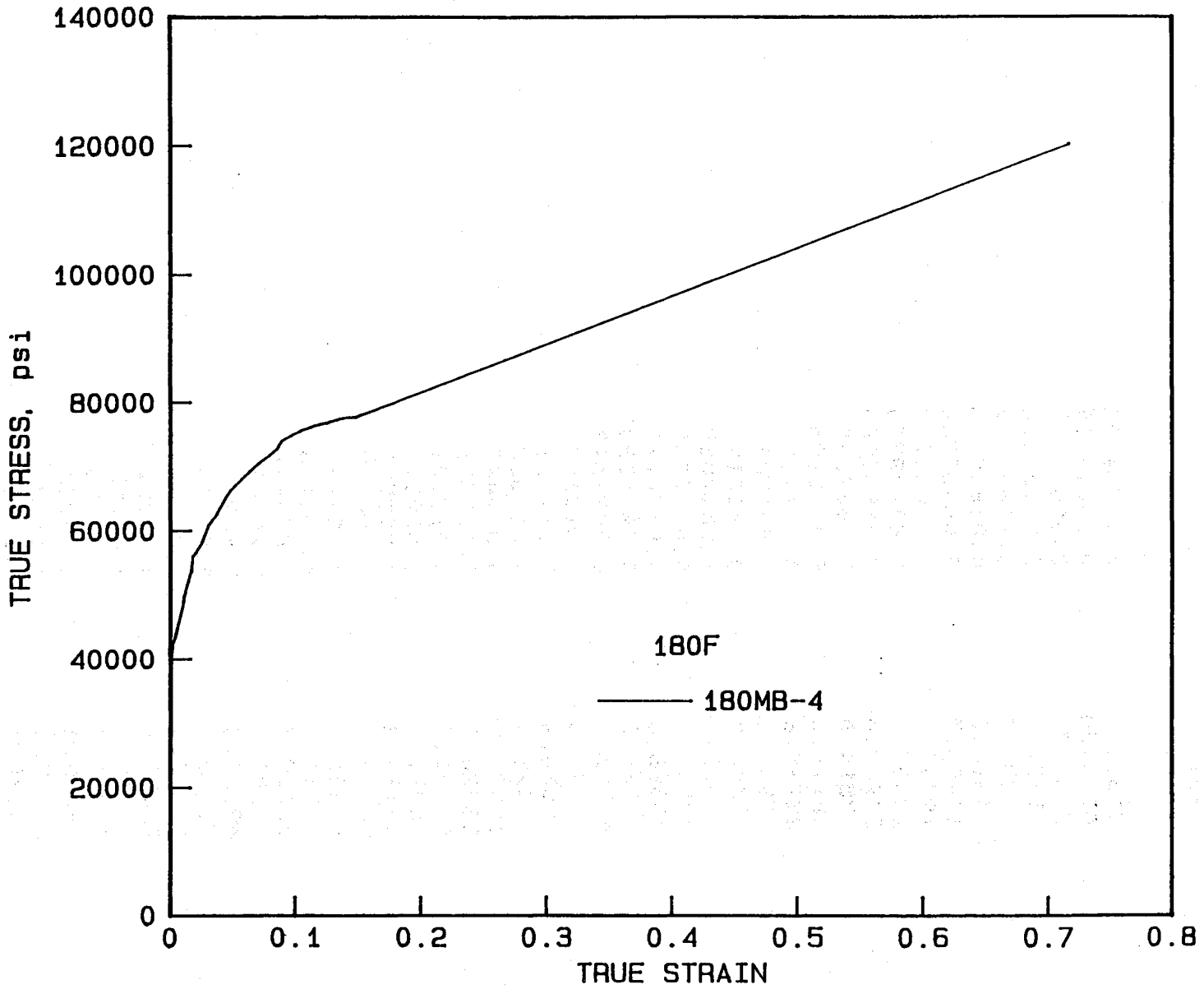
140000
120000
100000
80000
60000
40000
20000
0
TRUE STRESS, psi
0
0.1
0.2
0.3
0.4
0.5
0.6
0.7
0.8
TRUE STRAIN
180F
180MB-4

Specimen No. 180mb-4

True Stress, psi	Strain
0	0
2184.4	5.9998e-05
4550.34	0.00014999
7265.75	0.00023997
9569.91	0.00029996
12382.4	0.00040992
14616.3	0.00048988
16906.5	0.00055984
19700	0.00065978
22057	0.00073973
24968.4	0.00083965
27514.5	0.00093956
30116.6	0.0010195
32785.6	0.0011194
35333	0.0012093
38003.5	0.0013191
40428.1	0.0014889
42531	0.0027961
43808.8	0.0050174
45238.7	0.0064293
46702.6	0.0083649
48749.3	0.010693
49856.6	0.011513
51420.4	0.013587
53375.3	0.016493
53626.3	0.017329
56021.5	0.018626
56478	0.020312
58180.2	0.025551
60847.6	0.030917
62441.4	0.037199
64561	0.043136
66289.5	0.048447
67992.6	0.057089
69218.5	0.06396
70458.1	0.070831
71669.4	0.079412
72675.4	0.085719
73950.9	0.089521
74774.7	0.096854
75455.8	0.10368
76105.5	0.11226
76521.8	0.1192
76780.9	0.12632
77267.5	0.13339
77621.1	0.14172
77633.7	0.14868
120200	0.71725

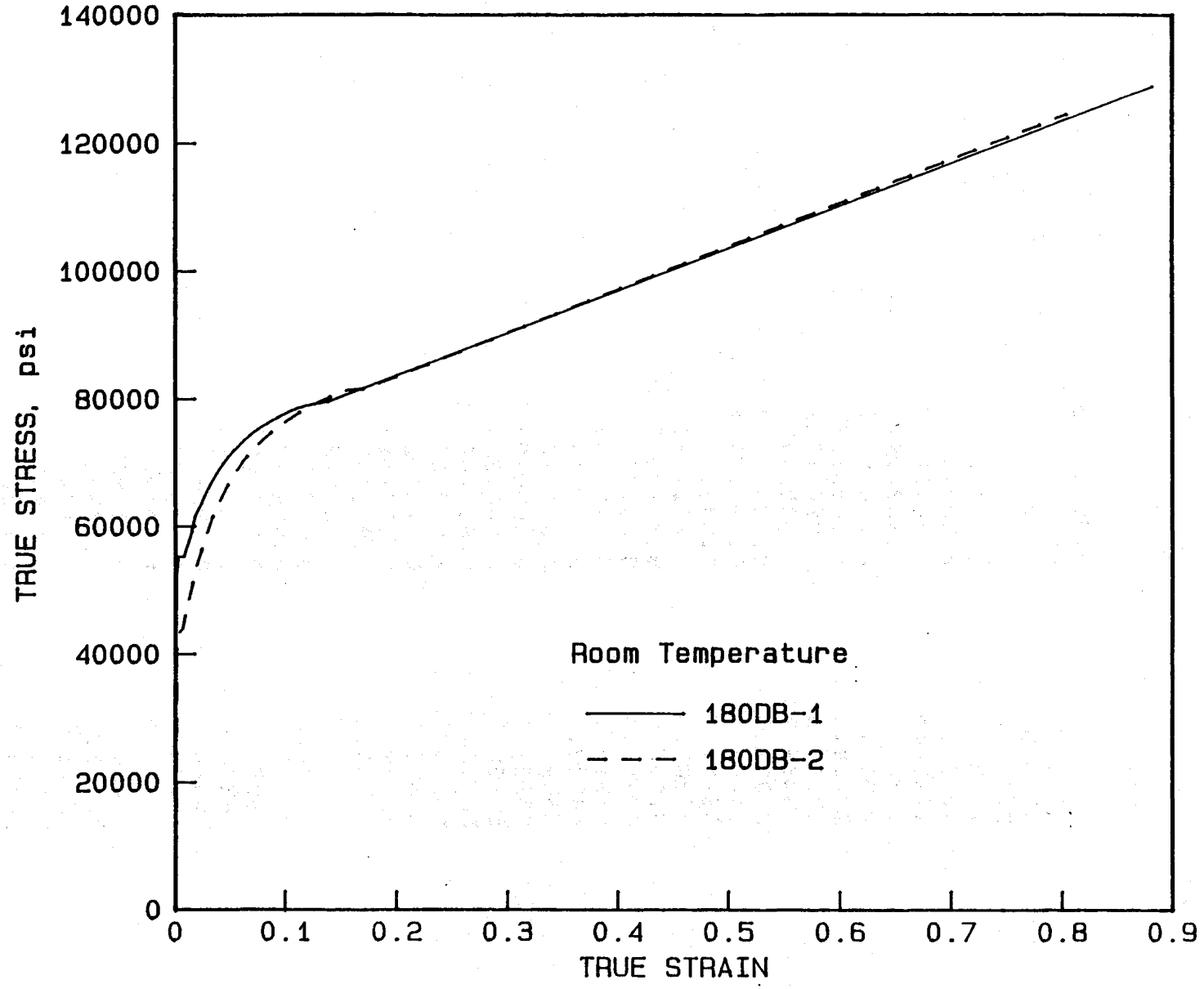
140000
120000
100000
80000
60000
40000
20000
0
TRUE STRESS, psi
0
0.1
0.2
0.3
0.4
0.5
0.6
0.7
0.8
0.9
TRUE STRAIN
Room Temperature
180DB-1
180DB-2

Specimen No. 180db-1

True Stress, psi	Strain
0	8.9996e-05
2360.96	0
4805.36	2e-05
7344.74	1e-05
10054.4	5.9998e-05
12551.1	0.00013999
15424.5	0.00020998
17968	0.00029996
20517.4	0.00039992
23250.6	0.00051987
25612.8	0.00061981
28469.7	0.00074972
31021.2	0.00084964
34006.1	0.00095954
36619.7	0.0010594
39289.6	0.0011593
41965.9	0.0012692
44642.6	0.001379
47319.5	0.0014789
50058.5	0.0015887
53068.2	0.001988
55239.4	0.0034939
55188.3	0.0081269
56913.8	0.011444
58818.5	0.014987
61632.9	0.018792
63409.7	0.023961
65845.8	0.030141
68129.7	0.037546
69827.1	0.043739
71733.8	0.052592
73037.3	0.060201
74243.6	0.067752
75312.8	0.075479
76148.4	0.083606
77071.9	0.092761
77820	0.10098
78435.6	0.10885
78816.5	0.11587
79178.2	0.12407
79480.5	0.13226
79632.1	0.13928
128900	0.88212

Specimen No. 180db-2

True Stress, psi	Strain
0	1e-05
2343.42	1e-05
4828.5	1e-05
7311.02	7.9997e-05
9733.57	0.00015999
12359.9	0.00025997
14793.5	0.00033994
17273.7	0.0004499
19942.1	0.00054985
22671.7	0.00063979
25031	0.00071974
27950.1	0.00082966
30432.8	0.00092957
33042.9	0.0010295
35898.1	0.0011493
38388.7	0.0012892
41019.1	0.0019681
43278.2	0.0038625
43984.8	0.0073033
46099.1	0.0098018
48434	0.012818
50465.3	0.015775
53398.5	0.019038
55819.3	0.023482
58038.4	0.027693
61255.4	0.034227
63552.6	0.039807
65957.6	0.046655
68029.8	0.053683
70163.6	0.061988
71657.3	0.069293
73283.9	0.078164
74647.7	0.086911
75873.7	0.09581
76961.2	0.1049
77851.7	0.11275
78794	0.12186
79483	0.12984
80233.4	0.13924
80820.4	0.14726
81367.8	0.15546
81568.6	0.16378
81597.7	0.17223
124500	0.80406

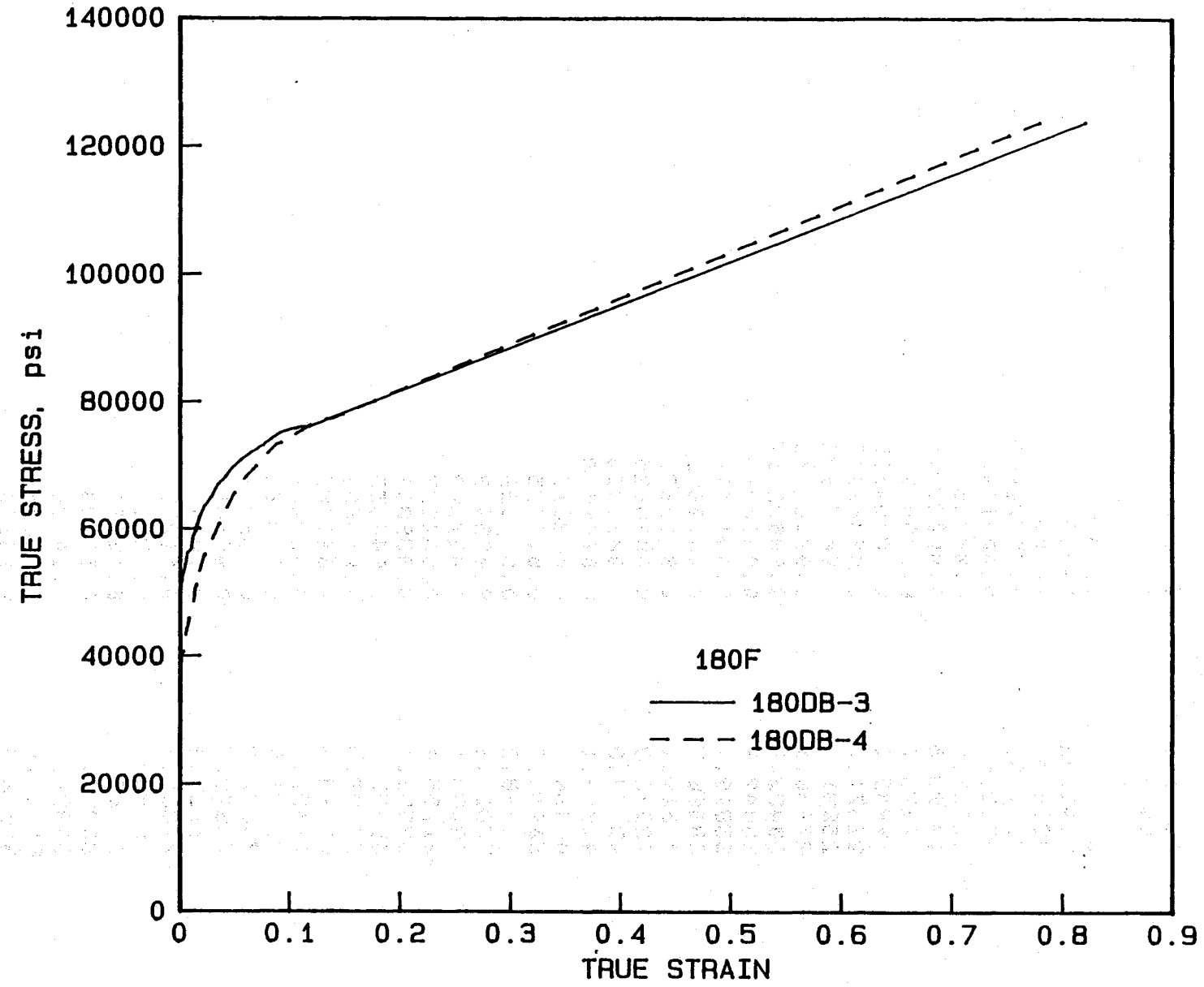
140000
120000
100000
80000
60000
40000
20000
0
TRUE STRESS, psi
0
0.1
0.2
0.3
0.4
0.5
0.6
0.7
0.8
0.9
TRUE STRAIN
180F
180DB-3
180DB-4

Specimen No. 180db-3

True Stress, psi	Strain
0	0.00022997
2327.98	3e-05
4698.07	1e-05
7049.85	0
9667.56	1e-05
12026	0
14582.7	1e-05
16941.2	2e-05
19550.1	8.9996e-05
22220.1	0.00013999
24641.4	0.00020998
27495.8	0.00029996
29978.6	0.00034994
32528.5	0.00042991
35139.3	0.00048988
37746.2	0.00057983
40419.6	0.00065978
43094.1	0.00075971
45830.6	0.00086962
48506.3	0.00096953
51088.9	0.0011294
52642.1	0.0026066
54427	0.0054352
56206.1	0.0070848
56803.7	0.010406
58761.8	0.012264
59723	0.014583
60507.6	0.015617
61793	0.018036
63461.6	0.022319
64978.3	0.028879
66939.2	0.034749
68209.4	0.041823
69589.2	0.047961
70789.6	0.055151
71745	0.062505
72614.6	0.070039
73209	0.075942
74197.3	0.083376
75097.8	0.090983
75562.9	0.097898
75871.5	0.10494
76095.2	0.11087
76128.7	0.11805
123800	0.82087

Specimen No. 180db-4

True Stress, psi	Strain
0	8.9996e-05
2279.65	1e-05
4562.9	2e-05
6953.33	1e-05
9571.12	2e-05
12021.1	2e-05
14644.6	6.9998e-05
17442	0.00016999
19797.2	0.00023997
22346.3	0.00032995
24829.6	0.00040992
27441.2	0.00052986
30052.7	0.00061981
32787.6	0.00072973
35523.1	0.00083965
38011.6	0.0009995
40403.9	0.0017784
41025.8	0.0047786
43563.6	0.005833
45157.9	0.0079582
46930.8	0.0098315
48170.6	0.010841
48510	0.01265
50796.1	0.014386
51245.3	0.015706
53324.6	0.016454
53154.3	0.018115
55532.3	0.021801
57294.3	0.027177
58811.6	0.030781
60751.6	0.035975
62490.2	0.041056
65138.8	0.048409
66704.5	0.054299
68185.4	0.060295
69402	0.066958
70833.6	0.074922
72019	0.08075
73300.8	0.087736
73785.3	0.095083
74704.7	0.10368
75534.1	0.11096
76249.9	0.11814
76951.2	0.12504
77265.8	0.13212
77401.9	0.13915
123800	0.7792

NRC FORM 335 (2-84) NRCM 1102, 3201, 3202

U.S. NUCLEAR REGULATORY COMMISSION

BIBLIOGRAPHIC DATA SHEET

SEE INSTRUCTIONS ON THE REVERSE.

1. REPORT NUMBER (Assigned by TIDC, add Vol. No., if any)
NUREG-1179, Vol. 2

2. TITLE AND SUBTITLE
Rupture of Model 48Y UF_6 Cylinder and Release of Uranium Hexafluoride
Cylinder Overfill, March 12-13, 1986
Investigation of a Failed UF_6 Shipping Cylinder

3. LEAVE BLANK

4. DATE REPORT COMPLETED
MONTH: May YEAR: 1986

5. AUTHOR(S)
R. Dale Smith, Charles L. Cain, Justin T. Long, Gary F. Sanborn

6. DATE REPORT ISSUED
MONTH: June YEAR: 1986

7. PERFORMING ORGANIZATION NAME AND MAILING ADDRESS (Include Zip Code)
U.S. Nuclear Regulatory Commission
Washington, DC 20555

8. PROJECT/TASK/WORK UNIT NUMBER

9. FIN OR GRANT NUMBER

10. SPONSORING ORGANIZATION NAME AND MAILING ADDRESS (Include Zip Code)
Same as 7, above.

11a. TYPE OF REPORT
Investigation Report

b. PERIOD COVERED (Inclusive dates)

12. SUPPLEMENTARY NOTES

13. ABSTRACT (200 words or less)

NUREG-1179, Volume 1, reported on the rupture of a Model 48Y uranium hexafluoride (UF_6) cylinder and the subsequent release of UF_6. At the time of publication, a detailed metallurgical examination of the damaged cylinder was under way and results were not available.

Subsequent to the publication of Volume 1, a second incident occurred at the Sequoyah Fuels Corporation facility. On March 13, 1986, a Model 48X cylinder was overfilled during a special one-time draining procedure; however, no release of UF_6 occurred. An Augmented Investigation Team investigated this second incident.

This report, NUREG-1179, Volume 2, presents the findings made by the Augmented Investigation Team of the March 13 incident and the report of the detailed metallurgical examination conducted by Battelle Columbus Division of the cylinder damaged on January 4, 1986.

14. DOCUMENT ANALYSIS - a. KEYWORDS/DESCRIPTORS
uranium
uranium hexafluoride
cylinder rupture
metallurgical examination
cylinder overfill

b. IDENTIFIERS/OPEN-ENDED TERMS

15. AVAILABILITY STATEMENT
Unlimited

16. SECURITY CLASSIFICATION
(This page) Unclassified
(This report) Unclassified

17. NUMBER OF PAGES

18. PRICE

UNITED STATES
NUCLEAR REGULATORY COMMISSION
WASHINGTON, D.C. 20555

SPECIAL FOURTH-CLASS RATE
POSTAGE & FEES PAID
USNRC
WASH. D.C.
PERMIT No. G-67